

NPS-57Va73071A

NAVAL POSTGRADUATE SCHOOL

//

Monterey, California



DESIGN REPORT OF HYBRID COMPRESSOR

AND

ASSOCIATED TEST RIG

by

M. H. Vavra

July 1973

Approved for public release; distribution unlimited.

NAVAL POSTGRADUATE SCHOOL
Monterey, California

Rear Admiral M. B. Freeman, USN
Superintendent

M. U. Clauser
Provost

ABSTRACT:

This report presents the aerodynamic calculations and describes the mechanical features of a test rig that has been designed at the Turbo-propulsion Laboratory, Department of Aeronautics, for research work on a special type of centrifugal compressor. This so-called Hybrid compressor consists of a centrifugal rotor with 180° flow deflection in the meridional plane followed by an axial flow diffuser. The report establishes a method to predict the off-design performance of the subject compressor, which can be applied also to conventional centrifugal compressors. Extensive use is made of modern programmable calculators, and programs are presented to show the effectiveness of these tools in engineering endeavors.

This work was supported by:

Navy Department
Naval Air Systems Command, Code 330C
AIRTASK No. A3303300/186B/3F41432301

TABLE OF CONTENTS

	INTRODUCTION	Page 1
I.	AERODYNAMIC DESIGN	2
	1. Impeller	2
	2. Inducer	6
	3. Diffusor	11
II.	DESIGN POINT PERFORMANCE	21
	1. Rotor	21
	2. Diffusor	24
	3. Flow Straightener and Discharge Duct	30
	4. Compressor Performance at Design Point	35
III.	OFF-DESIGN POINT PERFORMANCE	41
	1. General	41
	2. Rotor Performance	41
	3. Diffusor Performance	44
	4. Compressor Off-Design Performance	46
IV.	DRIVE TURBINE	49
	1. General	49
	2. Off-Design Turbine Performance	49
V.	MECHANICAL DESIGN	52
	1. Rotor	52
	2. Maximum Obtainable Pressure Ratios	54
	3. General Description of Test Rig	56
	REFERENCES	61
	TABLES (see list, page v.)	63
	FIGURES (see list, page vi.)	77
	APPENDIX A: Basic Elements for Advanced Design of Radial-Flow Compressors	110
	APPENDIX B: Manufacturing Drawings	153
	Dwg. 2103-A: Rotor Attachment	154
	" 2107 : Turbine Blade Profile	155
	" 2108-1: Turbine Rotors	156
	" 2109 : Turbine Stators	157
	" 2140 : Nozzle Casing	158
	" 2158 : Inlet Throttle Valve Assembly	159

Dwg. 2159	:	Control Valve Actuator	160
" 2164-1	:	Inlet Plenum	161
" 2203	:	Impeller of Hybrid Compressor	162
" 2204	:	Inducer of Hybrid Compressor	163
" 2205	:	Wheel Attachment	164
" 2207	:	Stator Casing	165
" 2208	:	Diffusor Sleeve	166
" 2209	:	Diffusor Blade Holders and Spacers	167
" 2210-1	:	Diffusor Blades Type A1	168
" 2210-2	:	" " " A2	169
" 2210-3	:	" " " B1	170
" 2210-4	:	" " " B2	171
" 2212	:	Shroud Support	172
" 2213	:	Shroud	173
" 2214-2	:	Inlet Casing	174
" 2215	:	Labyrinths	175
" 2216	:	Nozzle Frame	176
" 2222	:	Test Compressor Assembly	177
" 2223	:	Installation of Hybrid Compressor Test Rig	178
APPENDIX C: Losses in Radial Compressor Wheels			179
APPENDIX D: Calculating Programs for Monroe Model 1655/6 and Model 1880-20 Programmable Calculators:			195
Program No. 102: Flow Rate through Radial Compressor for Given Conditions at Discharge			196
Program No. 103: Determination of Pressure Ratio for Given Isentropic Flow Function for Different γ .			204
Program No. 104: Inlet Conditions of Radial Compressor with Axial Inlet Flow			211
Program No. 105: Relation between Rotor Efficiencies and Velocity Ratio of Radial Compressor Impeller			218
Program No. 106: Conditions at Discharge of Impeller of Radial Compressor			224
Program No. 108: Mass Flow Rate at Inducer Inlet as Function of V_{10}/a_0			231
Program No. 109: Flow Conditions after Cascade for Given Inlet Conditions, Flow Deflections and Total Pressure Loss Coefficient			238

Program No. 110: Calculation of Curve $r/a = \theta^{-b}$ with Zero Curvature at One Point and $\delta_{MAX} = 90^\circ$	248
Program No. 517: Off-Design Performance of Hybrid Compressor	251

LIST OF TABLES

	page
I. Flow, Blade, and Incidence Angles at Inducer Leading Edge	64
II. Loss Coefficients of First Blade Row of Diffusor	65
III. Design Values of First Blade Rows of Diffusors A and B	66
IV. Loss Coefficients of Second Blade Row of Diffusor	67
V. Design Values of Second Blade Rows of Diffusors A and B	68
VI. Determination of Diffusor Profile Data	69
VII. Flow Properties in Diffusor	70
VIII. Flow Conditions in Flow Straightener and Discharge Duct	71
IX. Estimated Compressor Performance at Design Point	72
X. Performance of Centrifugal Compressor Rotor (2 sheets)	73
XI. Calculated Performance of Hybrid Compressor at 16,666 rpm	75
XII. Calculated Performance of Hybrid Compressor at 12,018 rpm	76

LIST OF FIGURES

	page
1. Hybrid Compressor (Symbols and Stations)	78
2. Determination of Rotor and Hub Contours for Specified Blade Tip Contour	79
3. Conditions at Leading Edge of Inducer	80
4. Blade Angles of Straight Inducer Blades	81
5. Properties of Elliptical Inducer Blade Surface	82
6. Secondary Loss Coefficient of Ref. 6	83
7. Overall Loss Coefficients of First Diffusor Row	84
8. Overall Loss Coefficients of Second Diffusor Row	85
9. Diffusor Blade Data	86
10. Determination of Flow Conditions after Diffusor Row	87
11. Conditions in Flow Straightener and Discharge Duct	88
12. Rotor Dimensions	89
13. Polytropic Rotor Efficiency as Function of Flow Angle β_{10} at Inducer Tip Radius and Speed Ratio U_2/a_0	90
14. Arc Length of Parabolic Mean Camber Line of Inducer Blade ...	91
15. Flow Angle β_{10}^* for U_2/a_0 and M_{W1} ...	92
16. Velocity Distributions at Inducer Tip at Different Incidence Angles	93
17. Compressor Performance at $U_2/a_0 = 0.83$	94
18. Meridian Curve $r/a = \theta^{-b}$ with $\delta_m = \pi/2$	95
19. Relationship between y_0/x_0 , $x_0 k_m$ and y_0/x_0 for Meridian Curve of Fig. 18	96
20. Scale Drawing of Meridian Contours with $r/a = \theta^{-b}$ of Impeller of Fig. 12 ...	97
21. Dimensionless Mass Flow Rate $(\dot{m})^*$ as Function of Flow Function φ_1 of Fig. 17 ...	98
22. Polytropic Rotor Efficiency η_{RP} and Mach Number M_{W1} ... from Figs. 21 and 15 ...	99

23.	Polytropic Rotor Efficiency η_{RP} and Mach Number M_{W1} as Function of Flow Angle from Fig. 21 ... and Fig. 13...	100
24.	Adiabatic Rotor Efficiency η_R as Function of Mach Number M_{W1} , Peripheral Speed Ratio U_2/a_0 , and Incidence Angle i' ...	101
25.	Adiabatic Rotor Efficiency as Function of M_{W1} and i' of Fig. 24 ...	102
26.	Velocity Coefficient Ψ and Incidence Angle i' of Hybrid Compressor Rotor as Function of Deceleration Ratio W_2/W_{10} ...	103
27.	Assumed Change of Diffusor Pressure Loss Coefficient Y_t with Incidence Angle i	104
28.	Calculated Performance of Hybrid Compressor Operating in Test Rig	105
29.	Predicted Performance of Drive Turbine	106
30.	Predicted Turbine Performance	107
31.	Stress Distribution in Hybrid Rotor	108
32.	Blade Stresses of Hybrid Rotor	109

INTRODUCTION

The idea of arranging an axial diffuser after a special centrifugal compressor rotor that turns the flow by 180° instead of 90° , as in conventional machines, has been conceived by Mr. George Derderian, Naval Air Systems Command, Code AIR-53622B. For this so-called Hybrid compressor concept, he was awarded U. S. Patent 3, 365, 892 dated January 30, 1968.

To verify the conditions that exist after a Hybrid impeller, and to investigate whether it is possible to convert the kinetic energy of the flow after such a rotor into useful pressure rise with acceptable efficiency, a research project was started at the Turbopropulsion Laboratory, NPS, which was funded by the Naval Air Systems Command, under: AIRTASK A3303300/186B/3F41432301.

The present report gives the particulars of the design that led to the manufacture of the test rig which is now operative and being used to carry out the afore-mentioned research work.

The project was supervised by Mr. K. H. Guttmann, AIR-330C, who has been extremely helpful in all phases of the program. The author is deeply grateful to Mr. Guttmann for the patience, understanding and considerateness which he received during a lengthy period of personal misfortune which delayed the research program and the completion of this report.

I. AERODYNAMIC DESIGN

1. Impeller

Because of its peculiar design the rotor of the Hybrid compressor of Fig. 1 is highly stressed. (See Section V.1) Therefore, it must have meridional blades at the discharge to eliminate additional blade bending stresses. Ahead of the rotor the absolute inlet velocity will be axial everywhere. Hence it is possible to establish the rotor dimensions with the method of Ref. 1 which is enclosed as Appendix A. The corresponding dimensions of the Hybrid rotor are shown in Fig. 1.

The symbols used in the following are identical with those listed in Appendix A. For easier reference, the figures and equations of Appendix A are denoted by Fig. A and Eq. A Thus, Fig. A(3) is figure 3, and Eq. A II(4) is equation II(14) of Table II of Appendix A.

A parametric study indicated that optimum conditions were obtained for the following design values (see Fig. 1):

$$\beta_{10} = 55^\circ$$

$$\alpha_2 = 65^\circ$$

$$R_{10}/R_2 = 0.55$$

$$R_{1i}/R_2 = 0.18$$

The relatively small angle β_{10} of 55° is necessary to be able to limit the ratio R_{10}/R_2 to 0.55 and to obtain a sufficiently high flow rate so that the diffuser blade height b_2 does not become too small. For values of R_{10}/R_2 larger than 0.55 the meridional flow channel would also have very large curvatures at the blade tip contour of the Hybrid rotor. This would produce large radial velocity gradients at the rotor discharge. The choice of $\alpha_2 = 65^\circ$ was predicated by the permissible loading of the axial diffuser blade rows, and the large losses that occur if α_2 is

larger than 65° . A radius ratio $R_{1i}/R_2 = 0.18$ of the hub at the inducer inlet was chosen to be able to arrange 17 rotor blades with a thickness of about 0.125 inches. With smaller ratios R_{1i}/R_2 it is not possible to have 17 blades and it would then be necessary to design the impeller with splitter vanes, a feature which did not seem to be warranted for the present tests.

Preliminary investigation also showed that the peripheral rotor speed U_2 at the mean discharge radius R_2 of Fig. 1 should not exceed about 800 ft/s because of critical speed considerations if the rotor is made of aluminum.

For air with $\gamma = c_p/c_v = 1.4$ and a gas constant $R_G = 53.35$ (ft-lb)/(lbm, $^\circ R$), the velocity of sound a_0 at an assumed total inlet temperature $T_0 = 520^\circ R$ is

$$a_0 = \sqrt{g \gamma R_G T_0} = 1117.85 \text{ ft/s}$$

giving a ratio

$$U_2/a_0 = 0.7156$$

From Eq. A II(4) the Mach number M_{W1} of the relative velocity at the outer radius R_{1o} of the rotor inlet eye is then

$$M_{W1} = \left[\frac{\sin^2 \beta_{1o}}{\left(\frac{R_{1o}}{R_2} \frac{U_2}{a_0} \right)^2} - \frac{\gamma - 1}{2} \cos^2 \beta_{1o} \right]^{-\frac{1}{2}} = 0.4842 \quad (1)$$

For a weight flow rate $\dot{w} = \dot{m} g$ (lbm/s) there is from Eq. A II(9)

$$\pi R_2^2 k_{B1} = \frac{\dot{w}}{P_0} \sqrt{\frac{R_G T_0}{g}} (11.7944) \quad (2)$$

Figure A(3a) shows that the so-called slip factor μ depends of the number of rotor blades Z_R , the ratio R_{1o}/R_2 , the rotor efficiency η_R , and the flow coefficient ϕ_2 . Minor corrections for μ must be applied if

the tip clearance ratio δ/b_2 differs from 0.05 (see Fig. A(3b)) and if the flow in the rotor is turned by less than 90° in the meridian plane (see Fig. A(3c)). However, no data for μ are available if this turning is 180° as in the present wheel, and for this reason the slip factor is taken as that of a standard centrifugal compressor wheel with $\epsilon = 90^\circ$.

In accordance with Eq. A II(6) the flow coefficient φ_2 depends on μ . For a chosen value $\mu = 0.86$ there is

$$\varphi_2' = (0.86)(\cot 65^\circ) = 0.401$$

For an assumed rotor efficiency $\eta_R = 0.86$, $Z_R = 17$, and $R_{10}/R_2 = 0.55$, by extrapolating Fig. A(3a) to higher values of φ_2 , there is $\mu = 0.847$.

Hence, $\varphi_2 = 0.395$, and the slip factor for this velocity ratio is about 0.85, giving a final value $\varphi_2 = 0.3964$. For $\mu = 0.85$, from Eq. A II(5),

$$\frac{W_2}{W_{10}} = 0.6312 \quad (3)$$

Appendix A discusses the different possibilities to express the frictional losses in radial wheels. From Eq. A(25)

$$C = 0.7200$$

and from Eq. A(27) the so-called wheel efficiency η_W for $\eta_R = 0.86$ is

$$\eta_W = 0.4999$$

With this value and Eq. 3, the velocity ratio ψ of Eq. A (21) is

$$\psi = \frac{W_2}{W_{2is}} = 0.7548$$

With these data the rotor dimensions at the discharge are obtained from Eq. A II(11)

$$\pi R_2^2 \frac{b_2}{R_2} k_{B2} = \frac{\dot{W}}{P_0} \sqrt{\frac{R_G T_0}{g}} \quad (1.2739) \quad (4)$$

Hence, with Eq. 2

$$\frac{b_2}{R_2} \frac{k_{B2}}{k_{B1}} = \frac{1.2739}{11.7944} = 0.1080$$

The restriction factor k_{B1} at the inlet eye due to boundary layer growth is assumed to be 0.98, and $k_{B2} \approx 0.954$,

Thus

$$\frac{b_2}{R_2} = 0.1109 \quad (5)$$

In accordance with Fig. A(16) this ratio is acceptable.

The mean radius R_2 is chosen as 5.5 in., primarily to be able to drive the impeller by an available turbine and to mount the compressor to this item. Then the rotative speed N for $U_2 = 800$ ft/s is

$$N = \frac{800}{\frac{\pi R_2}{30 \cdot 12}} = \frac{(800)(360)}{\pi(5.5)} = 16,666 \text{ rpm}$$

The basic compressor dimensions in inches are then:

$$D_2 = 2 R_2 = 11.0$$

$$D_{10} = 2 R_{10} = 6.05$$

$$D_{1i} = 2 R_{1i} = 1.98$$

$$b_2 = 0.61$$

The radial overlaps δ of Fig. 1 at the impeller discharge are chosen to be 0.025 in., so that the blade height b_2' at the wheel discharge equals

$$b_2' = 0.56 \text{ in.}$$

Drawing 2222 of Appendix B shows the design of the Hybrid compressor. Details of the impeller and the inducer are given in Dwgs. 2203 and 2304. The meridional channel of the wheel was laid out by assuming a blade tip contour with the smallest possible curvature changes between R_{10} and the discharge. Drawings 2203 and 2204 show that such a contour could be

obtained with a two adjoining circular arcs with radii of 1.666 and 1.02 inches. By assuming that the meridional flow areas, without the restriction due to the blades, change linearly with the distance l along the tip contour from A_1 at the inlet to A_2' at the impeller discharge the meridional channel could be laid out with the method explained in Fig. 2. As shown in Dwgs. 2203 and 2204 the hub contour thus obtained could be approximated by four adjoining circular arcs whose radii decrease from the rotor inlet to the rotor discharge. The clearance between the blade tips and the adjoining casing of Dwg. 2213 is everywhere equal to 0.025 inch.

2. Inducer

Although some designers propose that the leading edges of the inducer blading have to be so arranged that particular incidence angles occur, it is shown in Ref. 2 that the correct incidence angles are obtained if the blockage because of the blade thickness is taken into account in the design. Figure 3 shows the conditions at the inducer entrance where V_1 , W_1 , β_1 are the flow properties just ahead of the inducer leading edges. In particular, the relative flow angle β_{10} at the radius R_{10} is equal to 55° . At an arbitrary radius R_1 the blade spacing is

$$S = \frac{2 \pi R_1}{Z_R} \quad (6)$$

Because of the blade thickness t or its projected thickness t_u in peripheral direction, the axial component V_1' of the flow after entering the inducer is

$$V_1' = V_1 \frac{S}{S - t_u} \quad (7)$$

giving a flow angle β_1' of

$$\beta_1' = \tan^{-1} \left(\frac{\omega R_1}{V_1'} \right) = \beta_B \quad (8)$$

If the blade has this angle β_1' at the leading edge there occurs an effective positive incidence angle

$$i = \beta_1 - \beta_1' = \beta_1 - \beta_B \quad (9)$$

Although in actuality the projected blade width is then $t_u' = t / \cos \beta_1'$ it is sufficiently accurate to take $t_u = t / \cos \beta_1$ because of the small values of i , and because the blade leading edge will actually be profiled as shown by the dotted contours of Fig. 3. For the same reason the thickness t is taken as 0.10 in., although the blade thickness t farther downstream is actually 0.125 in.. With these assumptions the blade angle $\beta_B = \beta_1'$ at the leading edge can be determined from Eqs. 6 to 8, or

$$\tan \beta_B = \frac{\omega R_1}{V_1} \left(1 - \frac{t_u}{s} \right) = \frac{\omega R_1}{V_1} \left(1 - \frac{t Z_R}{\cos \beta_1 \cdot 2 \pi R_1} \right)$$

Assuming V_1 to be constant along R_1 , and from the condition that at R_{10}

$$\tan \beta_{10} = \frac{\omega R_{10}}{V_1} = \tan 55^\circ$$

there is with $R_{10} = 3.025$ in.

$$\tan \beta_1 = \frac{R_1}{R_{10}} \tan 55^\circ = \frac{R_1}{3.025} \tan 55^\circ$$

and

$$\tan \beta_B = \tan \beta_1 \left[1 - \frac{(0.1)(17)}{\cos \beta_1 \cdot 2 \pi R_1} \right]$$

Table I gives the angles β_1 , β_B and the incidence angles i along the radius R_1 at the inducer inlet.

To be able to machine the impeller with simple means, it is assumed that its blade surfaces consist of generatrices that are everywhere parallel

to the radius at the inducer discharge where the blades must adjoin the radial impeller blades. As shown in Fig. 4, the camber line of the inducer blades can then be specified by a single function $y = f(x)$. At a point P the blade surface has the angle γ , where $\tan \gamma = dy/dx$. This angle, however, is the angle in planes A-A which are perpendicular to the radius at station Q, where the inducer blades line up with the impeller blades. To obtain the actual blade angle β_B at a radius R_1 the blade surface must be intersected with a cylinder of radius R_1 . For a point $P(x,y)$ of the blade surface the blade angle β_B at the radius R_1 is from Fig. 4

$$\tan \beta_B = \frac{dy}{\cos \theta \, dx} = \frac{\tan \gamma}{\cos \theta}$$

However

$$\cos \theta = \frac{\sqrt{R_1^2 - y^2}}{R_1}$$

Thus

$$\tan \beta_B = \frac{\tan \gamma}{\sqrt{1 - (y/R_1)^2}} = \frac{dy/dx}{\sqrt{1 - (y/R_1)^2}} \quad (10)$$

A function $y = f(x)$ for the blade surface will now be established such that the blade angles β_B of Table I can be obtained along the radius R_1 by varying the axial length x of the inducer blades, as indicated in Fig. 3. In particular, the camber line of the inducer blades is chosen to be an ellipse. In accordance with Fig. 5

$$y = b - \frac{b}{a} \sqrt{a^2 - x^2} \quad (11)$$

where $2a$ and $2b$ are the lengths of the major and minor axes of the ellipse, respectively. From Eq. 11

$$\frac{dy}{dx} = \tan \gamma = \frac{b}{a} \frac{x}{\sqrt{a^2 - x^2}} \quad (12)$$

Referring to Fig. 3, the values of "a" and "b" will be determined by specifying the conditions at stations C and D at the radii $R_{10} = 3.025$ in. and $R_{1i} = 0.99$ in. where, in accordance with Table I, the flow angles β_B must be 50.32° , and 18.08° , respectively. As shown in Fig. 3, it is assumed also that the axial lengths x of the inducer blades are 1.8 in. at C and 1.255 in. at D. These data are sufficient to determine the values of "a" and "b". However if Eqs. 11 and 12 are introduced into Eq. 10, one obtains fourth-order equations which cannot be solved with simple means. For this reason a method of successive approximations is used by assuming values for the angles γ_T and γ_H of Fig. 5 at R_{10} and R_{1i} and calculating the corresponding angles β_B by means of Eq. 10. Let, in accordance with Fig. 5,

$$x_T = 1.8 = \ell$$

$$x_H = 1.255 = \zeta \ell = (0.697) \ell$$

Then, from Eq. 12, with $c = b/a$,

$$\tan^2 \gamma_T = \frac{c^2}{(a/\ell)^2 - 1}$$

$$\tan^2 \gamma_H = \frac{\zeta^2 c^2}{(a/\ell)^2 - \zeta^2}$$

giving

$$\left(\frac{a}{\ell}\right)^2 = \frac{\zeta^2 (\tan^2 \gamma_T - \tan^2 \gamma_H)}{\zeta^2 \tan^2 \gamma_T - \tan^2 \gamma_H} \quad (13)$$

$$c^2 = \left(\frac{b/\ell}{a/\ell}\right)^2 = \frac{(1 - \zeta^2) \tan^2 \gamma_T \tan^2 \gamma_H}{\zeta^2 \tan^2 \gamma_T - \tan^2 \gamma_H} \quad (14)$$

Successive approximations of γ_T and γ_H established the following final values:

$$\gamma_T = 49.964^\circ; \tan \gamma_T = 1.1902$$

$$\gamma_H = 17.817^\circ; \tan \gamma_H = 0.3214$$

For these angles, from Eqs. 13 and 14,

$$\frac{a}{\ell} = 1.04442; a = 1.8799$$

$$\frac{b}{\ell} = 0.37460; b = 0.6743$$

and, by Eq. 11

$$\frac{y}{\ell} = 0.37460 - 0.35867 \sqrt{1.09081 - (x/\ell)^2} \quad (15)$$

For $x = \ell$ at $R_{10} = 3.025$,

$$y = 0.47973$$

and for $x = (0.697)\ell$ at $R = 0.99$,

$$y = 0.1721$$

With these values, from Eq. 10, at $R_{10} = 3.025$,

$$\tan \beta_{Bo} = \frac{1.1902}{\sqrt{1 - (0.47973/3.025)^2}} = 1.20545$$

and, at $R_{1i} = 0.99$,

$$\tan \beta_{Bi} = \frac{0.3214}{\sqrt{1 - (0.1721/0.99)^2}} = 0.32637$$

Table I shows that these angles coincide very closely with the required blade angles at these radii.

All blade angles β_B of Table I at the different radii R_1 can be obtained with the blade surface that is given by Eq. 15, for a particular change of the distance x of Figs. 3 and 5 with the radius R_1 . This

relationship between x and R_1 must be determined with an iterative method. For chosen values of x there can be determined y and dy/dx from Eqs. 15 and 12. These values introduced into Eq. 10, for the radius R_1 under consideration, give the value of β_B . If the blade angle thus determined differs from the required blade angle of Table I, the distance x must be varied until the correct angle is obtained. Drawing 2204 gives the values of $z = 1.8 - x$ vs. R_1 that were obtained in this manner for the blade surface of Eq. 15 whose coordinates are listed also in Dwg. 2204.

With this design the inducer can be fabricated from a forging by first machining the tip contour of the blades and the surface of revolution of the leading edges that is given by z vs. R . Then the blade passages can be produced by an end-mill that is moved in x and y directions, and along the radius, to produce the hub contour. However, with the described design the axis of the end-mill need not be tilted to produce the correct inlet blade angles.

3. Diffusor

The diffusor is arranged in a cylindrical annulus downstream of the impeller discharge, having the mean radius $R_2 = 5.5$ in., and a radial height $b_2 = 0.61$ inches. Ahead of the diffusor at station (2) the flow properties are obtained with the relations of Table A I. From Eq. A I(7), and the data established earlier,

$$\frac{T_2}{T_0} = 1.08402$$

From Eq. A I (8)

$$\frac{T_2'}{T_0} = 1.07013$$

From Eq. A I (6)

$$\frac{T_{t2}}{T_0} = 1.17411$$

From Eq. A I (20)

$$\frac{p_2}{p_0} = 1.2677$$

and from Eq. A I (19)

$$\frac{P_{t2}}{P_0} = 1.6764$$

The Mach number M_{V2} of the velocity V_2 ahead of the diffuser is from Eq. A II(6)

$$M_{V2} = 0.6446$$

for the chosen flow angle

$$\alpha_2 = 65^\circ$$

A preliminary analysis showed that a minimum of two diffuser blade rows is necessary to produce an acceptable diffuser efficiency. These rows are designed in the same manner as bladings of axial-flow compressors by using the method of Ref. 3. In the following, station (3) is after the first diffuser blade row and station (4) is located after the second diffuser row, as shown in Fig. 1.

Neglecting the change of the through-flow velocity because of the density increase from station (2) to station (3) the diffusion factor D of the first diffuser blade row is

$$D = 1 - \frac{\cos \alpha_2}{\cos \alpha_3} + \frac{(\tan \alpha_2 - \tan \alpha_3)}{2 \sigma} \cos \alpha_2 \quad (16)$$

where α_3 is the average flow angle at station (3) and σ the cascade solidity defined by

$$\sigma = \frac{\text{blade chord}}{\text{blade spacing}} = \frac{c}{s}$$

For different deflections $\Delta \alpha = \alpha_2 - \alpha_3$ and σ it is possible therefore to evaluate D from Eq. 16. The losses increase with increasing values of D. For the first diffuser blade row these losses can be expressed by the total pressure loss coefficient Y_t defined by

$$Y_t = \frac{\Delta P}{P_{t2} - p_2} = \frac{P_{t2} - P_{t3}}{P_{t2} - p_2} \quad (17)$$

where ΔP is the loss in total pressure in the blade row, and P_{t2} , p_2 , the total and static pressure, respectively, ahead of the cascade. Reference 4 shows that Y of a stator blade row with a discharge angle α_3 , diffusion factor D, and solidity σ can be calculated from

$$Y = \frac{2 \sigma}{\cos \alpha_3} \left[0.0004 + 0.0639(D + 0.1)^{2.91} + 0.057D^{2.02} (1 - \lambda)^{3.77} \right] \quad (18)$$

The factor λ is defined by

$$\lambda = \frac{R - R_H}{R_T - R_H} \quad (19)$$

where R is the radius at which Y is to be determined, and R_T , R_H are the tip and hub radii, respectively, of the blading. Since $1 - \lambda = 1$ at R_H , and $1 - \lambda = 0$ at R_T , the loss coefficient Y of Eq. 18 is higher at the hub than at the tip, if the other quantities in Eq. 18 do not vary radically along R. Equation 18 may give a realistic description of the loss variation in radial direction if the blade heights are large with respect to their chords, as for instance in axial compressors for jet engines. In such compressors the stator blades are attached at the tip and they usually have a clearance at the hub to prevent rubbing with the rotor assembly. The NASA calculating procedure of Refs. 3 or 4 does not separate the overall blade loss into profile losses, secondary or end losses, and tip clearance

losses. End and tip clearance losses depend on the ratio of blade height and chord and on the ratio of blade gap to blade height, respectively, and it is evident from Eq. 18 that these quantities do not influence the overall loss coefficient of the NASA design procedure. In the cascades to be determined the blade gap is zero but the ratio of blade height and chord, or b_2/c , is quite small compared with the values in jet engine compressors, and the end losses will be very much larger than those in stator cascades of such machines. It is assumed therefore that Eq. 18 for the mid-span, or for $\lambda = 0.5$, establishes the profile loss coefficients Y_p only, or

$$Y_p = \frac{2\sigma}{\cos \alpha_3} \left[0.004 + 0.0639(D + 0.1)^{2.91} + 0.0042 D^{2.02} \right] \quad (20)$$

To this profile loss coefficient will be added the so-called secondary loss coefficient Y_s to give the total loss coefficient Y_t , such that

$$Y_t = Y_p + Y_s = \frac{P_{t2} - P_{t3}}{P_{t2} - P_2} \quad (21)$$

Eq. 13(76) of Ref. 5, p. 380, gives the so-called induced drag coefficient C_{Di} of axial-flow cascades where the first part is the drag coefficient C_{DS} due to secondary flow effects, whereas the second part is due to tip clearance losses. This part is taken to be zero because no radial blade gaps δ exist in the present diffuser configuration. Hence

$$C_{DS} = 0.04 C_L^2 \sigma \frac{s}{h} \quad (22)$$

where the blade height h equals b_2 . The lift coefficient C_L is equal to (see Eq. 13(14), Ref. 5, p. 337)

$$C_L = \frac{2}{\sigma} (\tan \alpha_2 - \tan \alpha_3) \cos \alpha_\infty \quad (23)$$

The angle α_∞ is obtained from

$$\tan \alpha_{\infty} = \frac{\tan \alpha_2 + \tan \alpha_3}{2} \quad (24)$$

Equation 13(11) of Ref. 5 relates the drag coefficient to the total pressure loss coefficient ζ which, in the present application, would be defined by

$$\zeta = \frac{\Delta P}{P_{t3} - p_3}$$

It must be noted that ζ relates the drop in total pressure to the discharge conditions of a cascade. Then, since

$$Y_s \equiv \frac{\Delta P}{P_{t2} - p_2}$$

there is with Eqs. 22, 23, and 24

$$Y_s' = 0.16 \frac{s}{h} \cos^2 \alpha_2 \left[\tan \alpha_2 - \tan \alpha_3 \right]^2 \sqrt{1 + \frac{1}{4} [\tan \alpha_2 + \tan \alpha_3]^2} \quad (25)$$

since $1/\cos \alpha_{\infty} = \sqrt{1 + \tan^2 \alpha_{\infty}}$ The secondary loss coefficient of Eq. 25 is denoted by Y_s' to distinguish it from a secondary loss coefficient Y_s'' that has been proposed in Ref. 6. In Ref. 6 it is stated that the ratio $Y_s''/(Y_p + Y_s'') = Y_s''/Y_t''$ is a unique function of $\Delta\alpha(c/h)$, where $\Delta\alpha$ is the flow deflection in radians, and c/h the ratio of blade chord and blade height. This relationship is shown in Fig. 6. For known values of Y_p and Y_s''/Y_t'' there are

$$Y_s'' = Y_p \frac{(Y_s''/Y_t'')}{1 - (Y_s''/Y_t'')} \quad (26)$$

and

$$Y_t'' = \frac{Y_p}{1 - (Y_s''/Y_t'')} \quad (27)$$

The losses in the diffuser blade rows will be determined with Eq. 25 as well as with Eq. 26 for purposes of comparison. These two methods are

based on different models and concepts. It can be noted that for given flow angles the secondary losses of Eq. 25 are primarily a function of the ratio of blade spacing and blade height, whereas with the method of Ref. 6, or Eq. 26, they are depending mainly on the ratio of blade chord and blade height. Evidently, if Eq. 25 is used, one obtains different cascade arrangements for a specified total loss than if Eq. 26 is applied, and this situation is indicative of the present state of ignorance about secondary flows in general. A survey of the available analytical methods for the determination of secondary flow effects is given in Ref. 7.

As shown in Dwgs. 2202 and 2210-1, the diffuser blades will have a circular platform with a threaded cylindrical extension to attach them to the blade holders, which are shown as item 1 in Dwg. 2209. This design has been adopted to be able to change the blade stagger angle in the diffuser cascades if, because of the irregular flow conditions at the impeller discharge, the average flow angle α_2 differs from the design value of 65° . This diffuser blade attachment requires however, that each blade row does not have more than 38 blades. For $Z = 38$, the blade spacing s at the mean radius $R_2 = 5.5$ in. becomes

$$s = \frac{2 \pi R_2}{Z} = 0.9094 \text{ in.}$$

and

$$\frac{s}{h} = \frac{s}{b_2} = \frac{0.9094}{0.61} = 1.4908 \quad (28)$$

For particular values of $\sigma = c/s$,

$$\frac{c}{h} = \sigma \frac{s}{h} = \sigma(1.4908) \quad (29)$$

For $\Delta\alpha$ in degrees, the variable $\Delta\alpha(c/h)$ of Fig. 6 is,

$$\Delta \alpha (c/h) = \Delta \alpha^\circ \frac{\pi}{180} \sigma (1.4908) = \frac{2.602}{100} \sigma \Delta \alpha^\circ \quad (30)$$

Table II shows the diffusion factor D , the profile losses Y_p , and the overall loss coefficients Y_t' and Y_t'' as functions of solidity for flow deflections $\Delta \alpha = 10, 12$ and 14° in the first blade row of the diffuser. The quantities Y_t' and Y_t'' are also plotted in Fig. 7.

Although it is desirable to have the highest possible flow deflection $\Delta \alpha$ in the first diffuser blade row, the general level of the losses as evidenced by Fig. 7, and the non-uniform and non-steady flow conditions at the impeller exit, make it advisable to limit $\Delta \alpha$ to 12° . For this deflection the data of Fig. 7 show that the solidity should be about unity to obtain loss coefficients Y_t that are smaller than about 0.12. Experience with diffusers of centrifugal compressors seems to indicate however that, in spite of the results of Fig. 7, more favorable conditions may be obtained for higher solidities, primarily because of the afore-mentioned irregular flow properties at the rotor discharge. At higher solidities the diffuser blades form channels with better guidance of the flow than if the solidity were low. These channels will act as flow straighteners which can equalize the flow irregularities with smaller flow separations than those which might occur in low-solidity cascades where the diffusion factors and the blade loadings are higher. It is likely then that the performance of the second diffuser blade row, and possibly that of the whole diffuser, is better than if the solidity of the first row is small. In general, the writer is of the opinion that the secondary losses do not increase as radically with the flow deflection $\Delta \alpha$ and the solidity σ as obtained by Ref. 6.

For these reasons it was decided to build two sets of diffusers. In one, denoted by A, the solidity of the first row was chosen as 1.6. In

another, which is denoted by B, the first row has a solidity of 0.95. The deflections $\Delta\alpha$ have been chosen as 12° for both first rows of A and B. However, since the effects due to the non-steady impeller exit flows cannot be evaluated, the performance of these cascades will be determined with the loss coefficients of Fig. 7. The design criteria of the two first diffuser blade rows are listed in Table III, which also gives the values of the chosen maximum blade thickness.

The flow angle α_3 ahead of the second diffuser blade row is then $65 - 12 = 53^\circ$. Theoretically, the highest pressure recovery would be obtained in the diffuser if this angle could be reduced to zero in the second row. It can be seen, however, that the blade loadings and the losses would become excessive for such deflections. Preliminary investigations showed that the deflections $\Delta\alpha = \alpha_3 - \alpha_4$ cannot exceed about 26° to 38° at reasonable loss coefficients, so that after the diffuser the flow angles α_4 will be between 27° and 15° . Even though the kinetic energy of these whirl components of the discharge flow at station (4) cannot be converted into pressure rise, the overall efficiency of the compressor will be better than the one obtainable if it were tried to reduce the flow angle α_4 to zero.

Because it is intended to orient the blades of the second row in such a manner that they form a so-called tandem foil arrangement with the blades of the first row, the second diffuser row must also have 38 blades. Thus, its geometrical properties are likewise given by Eqs. 28, 29, and 30. The profile losses Y_p of the second row of diffuser blades can be determined by Eq. 20 if α_3 is replaced by α_4 . The diffusion factors of these rows are obtained by Eq. 16, replacing α_2 by α_3 and α_3 by α_4 . The overall loss coefficient Y_t is, similarly to Eq. 17,

$$Y_t = \frac{P_{t3} - P_{t4}}{P_{t3} - P_3} \quad (31)$$

The secondary flow loss coefficients Y_s will be determined by Eq. 26, replacing α_2 by α_3 , and α_3 by $\alpha_4 = \alpha_3 - \Delta\alpha$, and also with the method proposed in Ref. 6 by using the curve of Fig. 6. The results for different solidities and deflections $\Delta\alpha$ are listed in Table IV and plotted in Fig. 8.

Figure 8 shows that the overall losses increase very radically with solidity if the secondary flow losses are calculated in accordance with Ref. 6. If Eq. 25 is used however to determine Y_s , the overall losses Y_t' are almost constant for different values of σ , in fact they have a minimum for solidities of about unity. The data of Fig. 8 for Y_t'' ; that is, using Y_s'' of Ref. 6, suggest that with solidities much smaller than unity a diffuser with very low losses could be designed. However, not only would the blade chords be excessively small in such cascades, but the writer also believes that because of the high blade loading the flow would be too severely separated to make possible the small losses that Ref. 6 predicts. If in contrast to this opinion, the method of Ref. 6 should prove to give the correct values of Y_s'' , a cascade with solidity of 1.6, which was chosen for blade row A1, would have excessive losses. It was decided, therefore, to design two second row diffuser cascades also. Both rows will have a deflection $\Delta\alpha = \alpha_3 - \alpha_4 = 32^\circ$ to keep the losses within acceptable limits, independent of whether the one or the other prediction method gives the correct loss coefficients. The so-called row A2 will be designed for $\sigma = 1.4$, and for row B2 the solidity is chosen as unity. If Eq. 25 predicts the secondary losses properly, both cascades should have about equal losses. On the other hand, if Ref. 6 gives realistic secondary losses, row A2 would be greatly inferior to row B2. Although it will be

possible to arrange row A2 or B2 after either of the two first rows A1 or B1, for calculating purposes the so-called diffuser A is supposed to consist of rows A1 and A2 and diffuser B of rows B1 and B2. The design parameters of the second diffuser blade rows are listed in Table V.

The blade profiles and their orientation in the cascade are determined with the method of Ref. 3. The necessary calculating steps are described in paragraph 8 of Ref. 8. The basic thickness distribution of the profiles is shown in Fig. 13 of Ref. 8. Except for slight modifications near the leading edge this distribution corresponds to that of a British C-4 profile. The camber line of the profiles is a circular arc with camber angle φ . For known values of φ and thickness ratios t/c the profile coordinates are obtained with the relations of Fig. 14 of Ref. 8.

Figure 9 shows the attitude of a blade in a diffuser cascade and explains the symbols that are used for the profile calculations in Table VI. By using the method of Ref. 3 one often obtains excessively large incidence angles. As seen from Table VI this situation occurs for row A1 where $i = +4.312^\circ$, for row B1 where $i = -2.95$, and for row B2 where $i = -7.002^\circ$. For these rows, incidence angles i^* of $+2^\circ$, -1° , and -2° , respectively, are chosen, and the corresponding camber angles φ^* and the stagger angles γ^* are calculated with the values of $d\delta/di$ of Fig. 177 of Ref. 3. Table VI also lists the drawings of Appendix B where the different blade profiles and their coordinates are shown. From these drawings the angles $\Delta\gamma$ of Fig. 9 were determined graphically and were used to establish the stagger angles γ' that are necessary for the installation of the blades in the blade holders of Dwg. 2209.

II. DESIGN POINT PERFORMANCE

1. Rotor

For a chosen total temperature $T_0 = 520^\circ\text{R}$ at the compressor inlet, and for $U_2/a_0 = 0.7156$, $M_{w1} = 0.4842$ (see Eq. 1), the static temperature T_1 , and the static pressure p_1 at the inlet eye of the impeller are obtained from Eqs. A I (5) and A I (18), or

$$\frac{T_1}{T_0} = 0.9848$$

$$\frac{p_1}{p_0} = 0.9478$$

The absolute value of the total pressure P_0 at the impeller inlet is as yet unknown because in the test rig the compressor operates as an exhaustor. Drawing 2223 shows that the air entering the compressor is expanded in a throttle valve to a pressure below atmospheric pressure. From a plenum chamber (Dwg. 2164-1), where the kinetic energy of the flow through the throttle valve openings is destroyed by a system of adjustable screens, the air enters the suction pipe through a profiled orifice. This suction pipe with an inner diameter of 18 inches has a length of about 18 feet, so that non-uniformities of the flow which have not been removed in the plenum chamber will be equalized ahead of the flow measuring nozzle of Dwg. 2216. This nozzle has a diameter of 5.38 inches, hence its flow area is only about 9 percent of the cross sectional area of the suction pipe. The large acceleration of the flow in the nozzle will produce a uniform flow at its discharge. Drawing 2222 shows the location of the flow nozzle with respect to the compressor inlet. Drawing 2202 shows that provisions have been made in the nozzle casing (Dwg. 2140) to carry out flow surveys ahead of the 7 in. diameter duct ahead of the impeller by

means of Pitot probes.

Drawing 2222 shows that a honeycomb flow straightener is arranged after the diffuser blade rows to remove the whirl components of the flow at this station, and that the air is then discharged into the atmosphere. This arrangement has been adopted for simplicity of the design, since it does not require a scroll or a complicated collector after the compressor from where the flow is discharged into the atmosphere through a throttling valve. Moreover, with this arrangement the driving power of the compressor is lower than with a test set-up where the inlet flow of the compressor is at atmospheric pressure. However, the total inlet pressure P_0 , which is equal to the total pressure in the 7 in. diameter inlet duct, depends on the pressure ratio that is produced by the compressor. If, as shown in Fig. 1, the conditions at the exit of the discharge duct, arranged after the annular flow straightener, are denoted by the subscript (6), the static pressure p_6 must be equal to the ambient atmospheric pressure P_{atm} , or

$$P_0 = P_{atm} \frac{1}{(p_6/P_0)} \quad (32)$$

Hence it is necessary to determine the pressure ratio p_6/P_0 to obtain P_0 . Evidently, p_6/P_0 depends on the pressure drops in rotor, diffuser and flow straightener which will be evaluated in Section II.3.

The weight flow rate \dot{w} through the compressor can be determined from Eq. 2. For the assumed blockage factor $k_{B1} = 0.98$, and since $R_2 = 5.5$ inches,

$$\frac{\dot{w}}{P_0} \sqrt{\frac{R_G T_0}{g}} = \frac{\pi R_2^2 k_{B1}}{11.7944} = 7.8963 \text{ (in.}^2\text{)} \quad (33)$$

With $R_G = 53.35 \text{ (ft-lb)/(lbm, } ^\circ\text{R)}$, $g = 32.174 \text{ ft/s}^2$, $T_0 = 520^\circ \text{ R}$,

$$\dot{w} = 0.2689 \quad P_0 \quad (\text{lbm/s}) \quad (34)$$

In Eqs. 33 and 34, P_0 is the absolute total inlet pressure in psia.

In the rotor the total temperature of the fluid is increased from T_0 to T_{t2} . For an adiabatic process the energy increase due to this temperature rise is equal to the energy per unit flow rate that the rotor must transmit to the fluid. Hence, the power HP required to drive the rotor is, exclusive of bearing and other mechanical losses,

$$\text{HP} = \dot{w} c_p (T_{t2} - T_0) \frac{1}{550} \quad (\text{HP}) \quad (34a)$$

With

$$c_p = R_G \frac{\gamma}{\gamma - 1} \quad (\text{ft-lb})/(\text{lbm}, ^\circ\text{R})$$

and Eq. 33

$$\text{HP} = \frac{7.8963}{550} \frac{\gamma}{\gamma - 1} P_0 \sqrt{g R_G T_0} \left(\frac{T_{t2}}{T_0} - 1 \right)$$

For $\gamma = 1.4$, and since $T_{t2}/T_0 = 1.17411$,

$$\frac{\text{HP}}{P_0 \sqrt{g R_G T_0}} = \frac{8.7489}{(10^3)} \quad (35)$$

For $T_0 = 520^\circ \text{R}$, $\gamma = 1.4$, $R_G = 53.35$, there is also,

$$\text{HP} = 8.2656 P_0 \quad (\text{HP}) \quad (36)$$

In Eqs. 35 and 36 the pressure P_0 must be in psia.

The following data at the rotor discharge were obtained earlier:

$$\frac{T_2}{T_0} = 1.08402$$

$$\frac{p_2}{P_0} = 1.2677$$

$$\frac{P_{t2}}{P_0} = 1.6764$$

$$M_{V2} = \frac{V_2}{a_2} = 0.6446$$

With $T_0 = 520^\circ\text{R}$, or $a_0 = 1117.85 \text{ ft/s}$, the velocity of sound a_2 at the rotor discharge is

$$a_2 = a_0 \sqrt{T_2/T_0} = 1163.86 \quad \text{ft/s}$$

and

$$V_2 = 750.23 \quad \text{ft/s}$$

This average velocity at the rotor exit has an average flow angle $\alpha_2 = 65^\circ$.

2. Diffusor

The total pressure P_{t3} after the first diffusor blade row is obtained from Eq. 21, or

$$\frac{P_{t3}}{P_0} = (1 - Y_t) \frac{P_{t2}}{P_0} + Y_t \frac{P_2}{P_0} \quad (37)$$

where the pressure loss coefficients Y_t of the rows A1 and B1 are listed in Table III. At station (3), after the first diffusor row, the velocity V_3 has an average flow angle $\alpha_3 = 53^\circ$. Although the annular flow areas are equal at the station (2) and (3), the boundary layer growth in the blade row will make the effective flow area smaller at (3) than at (2). At station (2) a restriction factor $k_{B2} = 0.954$ has been assumed earlier to establish the diffusor annulus, or

$$A_2 = k_{B2} A_{\text{geom}}$$

where A_{geom} is the cross-sectional area of the annulus. At station (3) it is assumed that the effective flow area A_3 is

$$A_3 = k_{B3} A_{\text{geom}}$$

and $k_{B3} = 0.92$ by assumption.

The flow conditions at station (3) must be determined analytically for the flow area A_3 , the flow angle α_3 , and the total pressure P_{t3} , by using the energy equation, the equation of motion, and the equation of continuity. The energy equation for an assumed adiabatic process of a steady flow gives

$$T_{t3} = T_{t2}$$

In fact, the same total temperature will occur at stations (4), (5) and (6), if the flow processes are adiabatic.

Since the conditions after the second diffuser row at station (4) must be established with the same approach as those at station (3), a calculating procedure will be developed with the symbols of Fig. 10. Figure 10a shows a diffuser cascade in an annulus. The effective flow areas are $A_e = k_{Be} A_{geom}$ and $A_d = k_{Bd} A_{geom}$ at entrance and discharge, respectively. The average axial components V_{ea} and V_{da} that are uniform over A_e and A_d , respectively are

$$V_{ea} = V_e \cos \alpha_e$$

$$V_{da} = V_d \cos \alpha_d$$

A section through the blading of the diffuser row is shown in Fig. 10b, and Fig. 10c depicts the thermodynamic process between entrance and discharge in an entropy diagram. From the equation of motion

$$T_{te} = T_{td} = T_e + \frac{V_e^2}{2 g c_p} = T_d + \frac{V_d^2}{2 g c_p} \quad (38)$$

From the equation of continuity, with $\rho = p/(g R_G T)$

$$A_d V_d \cos \alpha_d \frac{p_d}{R_G T_d} = A_e V_e \cos \alpha_e \frac{p_e}{R_G T_e} \quad (39)$$

With $A_e/A_d = k_{Be}/k_{Bd}$, Eq. 39 can be rewritten as

$$\frac{V_d}{\sqrt{g \gamma R_G T_d}} = \frac{k_{Be}}{k_{Bd}} \frac{\cos \alpha_e}{\cos \alpha_d} \frac{(p_e/P_0)}{\sqrt{(T_e/T_0)}} \frac{V_e}{\sqrt{g \gamma R_G T_e}} \frac{\sqrt{(T_d/T_0)}}{(p_d/P_0)} \quad (40)$$

With the Mach numbers

$$M_d = \frac{V_d}{\sqrt{g \gamma R_G T_d}} \quad (41)$$

$$M_e = \frac{V_e}{\sqrt{g \gamma R_G T_e}} \quad (42)$$

and

$$K = \frac{k_{Be}}{k_{Bd}} \frac{\cos \alpha_e}{\cos \alpha_d} \frac{p_e/P_0}{\sqrt{(T_e/T_0)}} M_e \quad (43)$$

which is a constant for known entrance conditions and area ratios, there is from Eq. 40,

$$M_d = K \frac{\sqrt{(T_d/T_0)}}{(p_d/P_0)} \quad (44)$$

From Fig. 10c at the entropy s_d , from Eq. 38,

$$\frac{T_{td}}{T_d} = \frac{T_{te}}{T_d} = 1 + \frac{\gamma - 1}{2} M_d^2$$

and

$$\frac{p_{td}}{p_d} = \left(1 + \frac{\gamma - 1}{2} M_d^2\right)^{\gamma/(\gamma - 1)}$$

From these relations

$$\frac{T_d}{T_0} = \frac{T_{te}/T_0}{1 + \frac{\gamma - 1}{2} M_d^2} \quad (45)$$

and

$$\frac{p_d}{P_0} = \frac{P_{td}/P_0}{(1 + \frac{\gamma - 1}{2} M_d^2)^{\gamma/(\gamma - 1)}} \quad (46)$$

where, similar to Eq. 37, with the pressure loss coefficient Y_t of the blade row,

$$\frac{P_{td}}{P_0} = (1 - Y_t) \frac{P_{te}}{P_0} + Y_t \frac{p_e}{P_0} \quad (47)$$

Because of their exponential expressions it is not possible to substitute Eqs. 45 and 46 into Eq. 44 to obtain a closed solution for M_d . It is necessary to choose values of M_d , say M_d^* , to calculate T_d/T_0 and p_d/P_0 from Eqs. 45 and 46. These quantities are then used in Eq. 44 to determine the Mach number M_d . If M_d differs from M_d^* , other values of M_d^* must be chosen until agreement is reached. With the final value of $M_d = M_d^*$ it is possible to calculate the ratios T_d/T_0 and p_d/P_0 with Eqs. 45 and 46, and the velocity V_d is obtained from Eq. 41, or

$$V_d = M_d a_0 \sqrt{(T_d/T_0)} \quad (48)$$

This iterative calculating process has been carried out for the rows A1 and B1, for both overall loss coefficients Y_t' and Y_t'' that are listed in Table III. In Table VII where the final data are presented, the columns designated by A1' and A1'' give the performances of blade row A1 for the overall loss coefficients Y_t' and Y_t'' , respectively, of Table III. A similar designation is used for the performance of blade row B1, for the losses Y_t' and Y_t'' . With the flow conditions thus determined at (3), the flow properties at station (4), after the second diffuser blade row, can be calculated with the same method. These calculations are also carried out with both loss coefficients Y_t' and Y_t'' of Table V. The

quantity K of Eq. 43 is determined for $k_{Be} = k_{B3} = 0.92$ and $k_{Bd} = k_{B4} = 0.88$. The flow angles α_3 and α_4 are 53° and 21° , respectively, in accordance with Table VI.

The calculations of the flow conditions after the diffuser blade rows are quite lengthy and have to be carried out with great precision. On the other hand they do not warrant the use of a high-speed digital computer for which a rather elaborate program would have to be set up to perform the necessary iterations automatically. For the debugging of such a program several tries would probably be necessary until results could be obtained. However, for evaluations of the type discussed above, in fact for most calculations of this report, modern electronic and programmable display calculators are admirably suited. The Monroe Model 1655 with Card Reader CR-1 used at the Turbo-Propulsion Laboratory has proved to be an extremely valuable tool, and the writer believes that such calculators will completely revolutionize analytical engineering approaches. Libraries of programs for a variety of engineering calculations are already available, and programs for particular tasks can be established with great ease. Since most calculators, specifically the Monroe Model 1655, have provisions to verify and debug programs with a step by step procedure, program errors can be detected and corrected without delay by the programmer himself, without having to go to the trouble of submitting several modified programs as is necessary in most central computer facilities. At present, many high-speed computers are used for programs that do not really need the small access time and the large storage capacity of modern systems, and the use of programmable calculators will make available more time for those calculations that can be solved only by high-speed machines. Conversely the engineer or student is relieved of many routine calculations, without having to worry about inaccuracies and errors, and he obtains

results when needed during the progress of his work. Thus more time is available for creative efforts where the formulation of a problem is more important than the manipulation of numbers that is necessary for its solution.

To show the possibilities that exist in solving engineering problems with the Monroe 1655 calculator, some of the programs used for the calculations for this report are enclosed in Appendix D. Each program consists of a description, an operating instruction, and a listing of the program steps with their codes. The serial numbers of these programs refer to the private program library of the writer. The data of Table VII for the conditions after the two diffuser blade rows have been obtained with Program No. 109.

Appendix D also contains a more elaborate calculating program that requires the use of the Monroe calculator Model 1880 which is an advanced and more expensive machine with larger memory capacity.

The pressure ratios P_{t4}/P_0 of Table VII will be used to determine the so-called total-to-total compressor efficiency η_{t4} . For an isentropic compression from the total inlet pressure P_0 and the total inlet temperature T_0 to the total discharge pressure P_{t4} , the rise in total temperature ΔT_{tis} equals

$$\Delta T_{tis} = T_0 \left[(P_{t4}/P_0)^{(\gamma - 1)/\gamma} - 1 \right]$$

Since this temperature rise is proportional to the theoretical energy input per unit mass flow rate, and because for the actual process the energy per unit mass flow rate necessary to drive the rotor is proportional to $T_{t4} - T_0$, which equals $T_{t2} - T_0$, the compressor efficiency η_{t4} is

$$\eta_{t4} = \frac{(P_{t4}/P_0)^{(\gamma - 1)/\gamma} - 1}{(T_{t2}/T_0) - 1} \quad (49)$$

The compressor efficiencies η_{t4} are given also in Table VII. If the secondary flow losses are calculated in accordance with Eq. 25, an efficiency of 81.5% is obtained for the compressor with diffuser A, whereas if the losses for this configuration are determined with the method of Ref. 6 the efficiency is 78.9% only. The calculated compressor efficiencies with diffuser B are 82.3% and 82.8%, respectively, with the two methods.

It would appear, therefore, that higher efficiencies can be reached with diffuser B than with diffuser A. However, for the reason mentioned earlier, it may be that more favorable conditions can be obtained with the high-solidity diffuser A. Moreover, the performance calculations cannot take account of the radial velocity gradients or the non-steady flow at the rotor discharge, and it is because of these uncertainties that tests must be carried out to verify which diffuser configuration gives the best performance.

3. Flow Straightener and Discharge Duct

The flow conditions in the flow straightener and the discharge duct of Fig. 11a can be determined with approximate methods since the Mach numbers of the flow are small. At station (4), at the diffuser discharge, the velocity V_4 has the angle $\alpha_4 = 21^\circ$ with the axial direction. The peripheral component $V_4 \sin \alpha_4$ will be destroyed as the flow enters the axial flow straightener. This element consists of a honeycomb with hexagonal channels that have a spacing of 0.125 inch, a wall thickness of about 0.002 to 0.003 inch, and an axial length of 1.38 inch. As shown in Dwg. 2212, twelve honeycomb segments are arranged in an annulus between spacers that are 0.25 inches thick. On assuming that the flow leaving the diffuser does not diverge in radial direction, the velocity V_s in the channels of the flow straightener is with the symbols of Fig. 11a, neglecting density

changes,

$$V_4 \sqrt{2 \pi R_2 b_2} = V_S \left[\sqrt{2 \pi R_2 b_2} - (12)(0.25) b_2 \right] \left(\frac{0.123}{0.125} \right)$$

where the fraction 0.123/0.125 is the blockage due to the wall thickness of the honeycomb straightener. With $V_{4a} = V_4 \cos 21^\circ = 0.933 V_4$, $R_2 = 5.5$,

$$V_S = V_4 \cos 21^\circ \frac{(0.125/0.123)}{1 - \frac{(12)(0.25)}{2 \pi (5.5)}} = 1.039 V_4 \quad (50)$$

As shown in Fig. 11a, it is supposed that after the honeycomb the flow will diverge radially to a height $b_5 = 0.65$ in. at station (5). Hence the velocity V_5 is assumed to be

$$V_5 = \frac{b_2}{b_5} V_{4a} = \frac{0.61}{0.65} (0.933) V_4 = 0.8764 V_4 \quad (51)$$

Because the discharge duct between stations (5) and (6) is not a properly designed diffuser it will be assumed that the flow will follow the dash-dotted boundaries of Fig. 11a. Neglecting the change in density from (5) to (6), the velocity V_6 is then

$$V_6 = V_5 \frac{2 \pi (5.5)(0.65)}{2 \pi (6.2)(0.70)} = 0.824 V_5 = 0.722 V_4$$

Figure 11b shows the flow process between stations (4) and (6) in an entropy diagram. If the flow is adiabatic the total temperature T_t is everywhere constant, equal to $T_{t4} = T_{t2}$. From the diffuser discharge at (4) to the entrance of the honeycomb the velocity V_4 is reduced to V_{4a} at the constant static pressure p_4 . This process is associated with an increase in entropy from s_4 to s_4' , reducing the total pressure from P_{t4} to P_{t4}' . The velocity is then increased from V_{4a} to V_S at station (4') just inside the entrance to the flow straightener. If this acceleration is isentropic the pressure p_4 is reduced to p_4' . With the symbols of Fig. 11b,

$$T_{4}^{*} = T_{4} + \frac{V_{4}^2 - V_{4a}^2}{2 g c_p}$$

Since $C_p = R_G \gamma / (\gamma - 1)$, and $V_{4a} = V_4 \cos \alpha_4$,

$$\frac{T_{4}^{*}}{T_0} = \frac{T_4}{T_0} + \frac{\gamma - 1}{2} \left(\frac{V_4 \sin \alpha_4}{a_0} \right)^2 \quad (53)$$

where $a_0 = 1117.85 \text{ ft/s}$ and $\alpha_4 = 21^\circ$. Further,

$$\frac{P_{t4}'}{P_0} = \frac{P_4}{P_0} \left(\frac{T_{t2}/T_0}{T_{4}^{*}/T_0} \right)^{\gamma/(\gamma - 1)} \quad (54)$$

The velocity increase from V_{4a} to V_S at the entropy s_4' reduces the static temperature from T_{4}^{*} to T_{4}' , where

$$T_{4}' = T_{t2} - \frac{V_S^2}{2 g c_p}$$

or, with Eq. 50,

$$\frac{T_{4}'}{T_0} = \frac{T_{t2}}{T_0} - \frac{\gamma - 1}{2} \left(\frac{1.039 V_4}{a_0} \right)^2 \quad (55)$$

Also

$$\frac{P_{4}'}{P_{t4}'} = \left(\frac{T_{4}'}{T_{t2}} \right)^{\gamma/(\gamma - 1)}$$

and

$$\frac{P_{4}'}{P_0} = \frac{P_{t4}'}{P_0} \left(\frac{T_{4}'/T_0}{T_{t2}/T_0} \right)^{\gamma/(\gamma - 1)} \quad (56)$$

The loss in total pressure $\Delta P_S = P_{t4}' - P_{t4}''$ in the honeycomb will be determined with the frictional coefficient f of flows in pipes, or

$$\Delta P_S = \left(\frac{L}{d_h}\right) f \frac{\rho}{2} V_S^2 \quad (57)$$

The hydraulic diameter d_h of the flow channels in the honeycomb straightener is 0.123 in., and $L = 1.38$ in. The factor f depends on the Reynolds number

$$R_e = \frac{V_S d_h}{\nu}$$

Table VII shows that the velocities V_4 do not differ greatly, hence R_e can be determined for an average value $V_4 = 330$ ft/s. Moreover the average ratio T_4/T_0 is about 1.157, and the pressure p_4 is nearly equal to the atmospheric pressure. For $T_4 = (1.157)(520) = 602^\circ$ R, and $p_4 = 14.7$ psia, there is $\nu = 1.97(10^{-4})$ ft/s². Hence, with Eq. 50,

$$R_e = \frac{(1.039)(330)(0.123/12)}{1.97(10^{-4})} = 1.78(10^4)$$

From Ref. 9 for smooth surfaces, $f = 0.0265$, and by Eq. 57

$$\Delta P_S = \frac{(1.38)}{(0.123)} (0.0265) \frac{\rho}{2} V_S^2 = 0.3 \frac{\rho}{2} V_S^2$$

At the low Mach numbers of the flow, there is approximately

$$\frac{\rho}{2} V_S^2 = P_{t4}' - p_4'$$

or

$$\frac{P_{t4}'}{P_0} = 0.7 \frac{P_{t4}'}{P_0} + 0.3 \frac{p_4'}{P_0} \quad (58)$$

From Fig. 11b, and Eq. 56 the static pressure p_4'' is then obtained from

$$\frac{p_4''}{P_0} = \left(\frac{P_{t4}''/P_0}{P_{t4}'/P_0}\right) \left(\frac{p_4'}{P_0}\right) \quad (59)$$

The reduction of the velocity from V_S to V_5 is supposed to occur at the static pressure p_4'' , hence $p_5 = p_4''$, as indicated in Fig. 11b. The static temperature T_5 is with Eq. 51,

$$\frac{T_5}{T_0} = \frac{T_{t2}}{T_0} - \frac{\gamma - 1}{2} \left(\frac{0.8764 V_4}{a_0} \right)^2 \quad (60)$$

and the pressure ratio P_{t5}/P_0 is

$$\frac{P_{t5}}{P_0} = \frac{p_4''}{P_0} \left(\frac{T_{t2}/T_0}{T_5/T_0} \right)^{\gamma/(\gamma - 1)} \quad (61)$$

The loss in the discharge duct between stations (5) and (6) is assumed to be

$$P_{t6} - P_{t5} = (0.4)(P_{t5} - p_5)$$

Thus, with $p_5 = p_4''$

$$\frac{P_{t6}}{P_0} = 0.6 \frac{P_{t5}}{P_0} + 0.4 \frac{p_4''}{P_0} \quad (62)$$

With Eq. 52

$$\frac{T_6}{T_0} = \frac{T_{t2}}{T_0} - \frac{\gamma - 1}{2} \left(\frac{0.722 V_4}{a_0} \right)^2 \quad (63)$$

and

$$\frac{p_6}{P_0} = \frac{P_{t6}}{P_0} \left(\frac{T_6/T_0}{T_{t2}/T_0} \right)^{\gamma/(\gamma - 1)} \quad (64)$$

For the data at the diffuser discharge (station (4)) of Table VII the conditions of state in the flow straightener and the discharge duct have been calculated with the above relations. The results are summarized in Table VIII. As discussed earlier, the static pressure p_6 at the exit of the duct will equal the atmospheric pressure. If this ambient pressure

P_{atm} is taken as 14.7 psia, the total pressure P_0 at the compressor inlet is obtained from Eq. 32. The last line of Table VIII gives these pressures for diffusers A and B and the two different losses which were taken into account for their performance prediction.

4. Compressor Performance at Design Point

The weight flow rate \dot{w} and the driving power of the compressor can be determined from Eqs. 34 and 36 for the values of P_0 from Table VIII. The pressures thus obtained are for a total inlet temperature $T_0 = 520^\circ \text{R}$ and a speed of rotation $N = 16,666 \text{ rpm}$. Of interest is also the torque M that is necessary to turn the compressor, which equals

$$M = \frac{\text{HP}(550)}{\omega} = \frac{\text{HP}(550)}{\pi N/30} \quad (\text{ft-lb}) \quad (65)$$

With Eq. 34, and $N = 16,666 \text{ rpm}$

$$M = 2.6045 P_0 \quad (\text{ft-lb})$$

or

$$M = 31.2554 P_0 \quad (\text{in-lb}) \quad (65)$$

where P_0 must be in psia. In Table IX the compressor performance data for the design point at $N = 16,666 \text{ rpm}$ and $T_0 = 520^\circ \text{R}$ are summarized. Also given are the pressure ratios P_{t4}/P_0 and p_6/P_0 , and the efficiencies η_{t4} with the two diffusers A and B, for the two methods used for the determination of their secondary flow losses.

It is evident from Appendix A (Ref. 1), and the calculations of this report, that U_2/a_0 , $\gamma = c_p/c_v$, and the flow angles are the prime variables that establish the performance of a particular compressor, in fact of all designs which are geometrically similar. Except for possible changes in the loss coefficients which will be discussed later, the pressure ratio P_{t4}/P_0 of these machines will be equal if U_2/a_0 , γ , and the flow angles

are equal. This situation occurs because the density ratios of the fluid and the Mach numbers of the flow remain constant at particular stations in the compressors, which makes it possible to maintain the same flow angles with respect to the bladings. From Eq. A II(9) it is seen that the dimensionless mass flow rate $(\dot{m})^*$ defined by

$$(\dot{m})^* = \frac{(\dot{w}/g) \sqrt{g R_g T_0}}{\pi R_2^2 P_0} \quad (66)$$

must be constant at these conditions. From Eq. 35 and Eq. A I(6) it is apparent that the dimensionless power $(HP)^*$, defined by

$$(HP)^* = \frac{(HP)(550)}{\pi R_2^2 P_0 \sqrt{g R_g T_0}} \quad (67)$$

is invariant also for similar machines that operate at the same values U_2/a_0 and γ , and produce the same pressure ratio P_{t4}/P_0 .

Since $\omega = U_2/R_2$, the moment of Eq. 65 becomes with Eq. 67, and

$$a_0 = \sqrt{\gamma g T_G T_0},$$

$$M = \pi R_2^3 P_0 \frac{(HP)^*}{(U_2/a_0) \sqrt{\gamma}} \quad (68)$$

Hence, similar to Eqs. 66 and 67 the so-called dimensionless moment $(M)^*$ will be defined as

$$(M)^* = \frac{M}{\pi R_2^3 P_0} \quad (69)$$

which is constant also for the conditions at which $(\dot{m})^*$ and $(HP)^*$ do not change.

Obviously the dimensionless quantities of Eqs. 66, 67, and 69 have equal magnitudes in any consistent system of units for geometrically

similar compressors that operate at the same values of U_2/a_0 , γ , and P_{t4}/P_0 , independent of their size and the magnitudes of P_0 and T_0 . However, the losses in these machines do not depend only on the angles and the Mach numbers but also on the Reynolds numbers of the flow. That the Mach numbers remain constant at fixed values U_2/a_0 , γ , and flow angles, independent of the magnitudes of T_0 and P_0 , is shown by Eqs. A II(4) and A II(6). The flow angles, and therefore the blade incidence angles, remain equal at particular stations because the ratios T/T_0 and P/P_0 , which establish the density ratios ρ/ρ_0 , are also not affected by T_0 and P_0 . The Reynolds number R_e at a particular station, where the velocity V exists at p and T , can be expressed by

$$R_e = \frac{V R_2}{\mu_v} \rho$$

since, for geometrically similar compressors, the dimensions of all flow channels are constant fractions of the mean compressor radius R_2 . If M_V is the Mach number of V , or $V = M_V \sqrt{\gamma g R_G T}$, and, since $\rho = p/(g R_G T)$, there is also

$$R_e = \left[\frac{P_0 R_2}{\mu_v \sqrt{g R_G T_0}} \right] \left(\frac{(P/P_0) M_V \sqrt{\gamma}}{\sqrt{(T/T_0)}} \right) \quad (70)$$

Since the dynamic viscosity μ_v has the dimension $(\text{lb-s})/\text{ft}^2$ in the system of units used in this report, the term in the square bracket is dimensionless. This is necessary because the term in the round bracket and R_e are dimensionless also.

Whereas, for reasons discussed earlier, the expression in the round bracket is constant for all geometrically similar compressors operating at particular values of U_2/a_0 , P_{t4}/P_0 and γ , independent of P_0 and T_0 , the term in the square bracket depends on the compressor size, the gas properties,

and the magnitudes of P_0 and T_0 . Experience has shown, however, that the influence of Reynolds number on losses in turbomachines is quite small, and that large increases of the losses occur only below some critical value of R_e which is usually reached only at very low pressures or with small dimensions. For most gases the dynamic viscosities increase slightly with temperature but the absolute magnitudes of μ_v do not vary greatly for different gases. Most diatomic gases such as N_2 , O_2 , H_2 , CO , and also air, have values of γ of about 1.4 at ambient temperature, and the ratio of the viscosities of the heaviest of these gases (O_2) and the lightest one (H_2) is only about 2. A change in Reynolds number by a factor of two has a very small influence on the losses, except near the above-mentioned critical value of R_e .

This discussion shows that geometrically similar compressors that operate with gases that have the same specific heat ratio will have almost equal values of $(\dot{m})^*$, $(HP)^*$, and $(M)^*$ at particular values of U_2/a_0 and P_{t4}/P_0 , if the Reynolds numbers are sufficiently high. Evidently the efficiencies of the compressors at these operating conditions will then also be nearly equal, irrespective of the molecular weight of the gas and the magnitudes of inlet pressure and inlet temperature. The quantities $(\dot{m})^*$, $(HP)^*$ and $(M)^*$ are shown in Table IX for the ratio $U_2/a_0 = 0.7156$.

For a particular compressor operating with a particular gas, the dimensionless quantities of Eqs. 66, 67, and 69 can be simplified by introducing the ratios

$$\theta_C = \frac{T_0}{T_{REF}} \quad (71)$$

and

$$\delta_C = \frac{P_0}{P_{REF}} \quad (72)$$

where T_{REF} and P_{REF} are usually taken as $518.4^{\circ} R$ and 14.7 psia. The subscript C was introduced to differentiate these ratios from similar ones that later on are used for the performance calculations of the drive turbine.

With Eq. 71, the ratio U_2/a_0 is also

$$\frac{U_2}{a_0} = \frac{(\pi/30) N R_2}{\sqrt{g \gamma R_G \theta_C T_{REF}}}$$

Hence in a compressor that handles a specific gas, equal values of U_2/a_0 are obtained for equal ratios $N/\sqrt{\theta_C}$. Thus,

$$N_{REF} = N/\sqrt{\theta_C} \quad (\text{rpm}) \quad (73)$$

will be called the referred speed of the compressor. Similarly, from Eq. 66, the so-called referred weight flow rate is defined by

$$\dot{w}_{REF} = \frac{\dot{w} \sqrt{\theta_C}}{\delta_C} \quad (\text{lbm/s}) \quad (74)$$

From Eq. 67 the referred power is

$$(\text{HP})_{REF} = \frac{\text{HP}}{\delta_C \sqrt{\theta_C}} \quad (\text{HP}) \quad (75)$$

and from Eq. 69 the so-called referred torque becomes

$$M_{REF} = \frac{M}{\delta_C} \quad (\text{ft-lb}) \text{ or } (\text{in-lb}) \quad (76)$$

On the basis of the previous discussion it can be stated that a compressor designed for and operated with a particular fluid will have the same pressure ratio at the same values of N_{REF} and \dot{w}_{REF} independent of the absolute magnitudes of P_0 and T_0 , provided that the possible variations of Reynolds number have a minor effect on the losses in the bladings of

the machine. Then the referred power required by the compressor will also be a unique function of $N/\sqrt{\theta_C}$ and $\dot{w} \sqrt{\theta_C}/\delta_C$, indicating that its efficiency is only depending on these two variables also. The main disadvantage of the so-called referred parameters is that they are not dimensionless, and that they cannot be used to compare the operating performance of different machines with each other, as it is possible with the earlier defined non-dimensional quantities.

The referred operating parameters of Eqs. 73 to 76 for the design point are given in Table IX.

III. OFF-DESIGN POINT PERFORMANCE

1. General

Because the Hybrid compressor operates as an exhaustor in the test rig it is of interest to know its performance at pressure ratios and speed other than those for the design point. If the pressure ratio is smaller than the design value, the pressure P_0 will be higher and since the weight flow rate, and the driving power are proportional to P_0 , it is likely that the maximum power occurs at pressure ratios lower than the values at the design point.

2. Rotor Performance

Prime variables for the rotor performance are the peripheral speed ratio U_2/a_0 and the absolute discharge angle α_2 . If particular values of these quantities are chosen and if the slip factor μ and the velocity ratio ψ were known it would be possible to determine the dimensionless mass flow rate through the wheel by means of Eq. A II(11). These calculations can be carried out by means of program 102 of Appendix D, which also establishes the ratios T_2/T_0 and p_2/P_0 for the assumed values of μ and ψ . Actually, program 102 determines the quantities:

$$\frac{\dot{w} \sqrt{(R_G/g) T_0}}{P_0} = (\dot{m})^* \pi R_2^2 \quad (77)$$

$$\phi_2 = \frac{\dot{w} \sqrt{(R_G/g) T_0}}{A_2 k_{B2} P_0} = \frac{\dot{w} \sqrt{(R_G/g) T_0}}{2\pi R_2 b_2 k_{B2} P_0} \quad (78)$$

and

$$\phi_1 = \frac{\dot{w} \sqrt{(R_G/g) T_0}}{A_1 k_{B1} P_0} = \frac{\dot{w} \sqrt{(R_G/g) T_0}}{\pi (R_{10}^2 - R_{1i}^2) k_{B1} P_0} \quad (79)$$

for chosen blockage factors k_{B1} and k_{B2} .

The dimensionless flow function ϕ_1 of Eq. 79 can be used to establish the ratio of the static pressure p_1 and P_0 , since P_0 is identical with the total pressure P_{t1} at station (1), with the relation

$$\phi_1 = \sqrt{\frac{2\gamma}{\gamma - 1} \left[(p_1/P_0)^{2/\gamma} - (p_1/P_0)^{(\gamma + 1)/\gamma} \right]} \quad (80)$$

Since for known values of ϕ_1 and γ , it is not possible to calculate p_1/P_0 in closed form, the calculating program 103 of Ref. D has been set up to determine p_1/P_0 with an iterative process.

Program 104 of Appendix D can then be used to determine the flow properties at the inducer inlet with the relations of Appendix A which are listed in the program description. This program gives T_1/T_0 , V_1/a_0 , W_{10}/a_0 , and the quantities M_{W1} and i' . The latter is the incidence angle at the outer inlet radius R_{10} if blockage due to inducer blade thickness is taken into account.

Appendix C analyzes available test data of losses in centrifugal compressor rotors, and shows that Fig. 24 can be used for the present off-design calculations. From Fig. 24 the rotor efficiencies η_R are obtained as functions of i' and M_{W1} . The efficiency η_R is defined by Eq. A (12). With Eqs. A II(5), A (27), and A (21) it is possible to calculate the velocity ratio $\psi = W_2/W_{2is}$ which is used for the performance calculations with the method of Appendix A. This conversion can be carried out with program 105 of Appendix D. The wheel efficiency η_W of Eq. A (15) and the deceleration ratio W_2/W_{10} are outputs of this program also. The value of ψ thus obtained should coincide with that initially assumed for use in program 102, and ψ must be iterated by successive approximations till agreement is reached.

For the design point the slip factor $\mu = \mu_d = 0.85$ has been determined from Fig. A (3a) for the given rotor dimensions, the assumed rotor

efficiency $\eta_R = 0.86$, and the design flow coefficient $\varphi_2 = \varphi_{2d} = 0.3964$. Experience shows that Fig. A (3a) cannot be used to establish μ at off-design conditions. Most theoretical analyses predict that the slip factor for rotors with radial blades at the discharge remains constant if the flow coefficient and η_R change. As shown in Ref. 13, and by other authors, this condition does not occur in actuality. For the present calculations the conclusion reached in Ref. 13 is applied, namely, that the relative flow angle β_2 of Fig. 1 at the rotor exit remains constant at all operating conditions. Then, by Fig. 1

$$\tan \beta_2 = U_2 \frac{(1 - \mu)}{V_{m2}} = \frac{1 - \mu}{\varphi_2}$$

For the design point with μ_d and φ_{2d} , and for $\beta_2 = \beta_{2d}$

$$\frac{1 - \mu}{\varphi_2} = \frac{1 - \mu_d}{\varphi_{2d}}$$

and, since

$$\varphi_2 = \mu \cot \alpha_2$$

there is

$$\mu = \frac{1}{1 + \frac{1 - \mu_d}{\varphi_{2d}} \cot \alpha_2} \quad (81)$$

Then, for $\mu_d = 0.85$ and $\varphi_{2d} = 0.3964$

$$\mu = \frac{1}{1 + (0.3784) \cot \alpha_2} \quad (82)$$

Sheets 1 and 2 of Table X give the final results of the rotor performance for speed ratios $U_2/a_0 = 0.7156$ and $U_2/a_0 = 0.516$, respectively, obtained with the procedure outlined above. As pointed out earlier, a value of $\psi = \psi_j$ has to be assumed (line 7 of Table X) and must be changed until it and the value ψ calculated by program 105 (line 22 of Table X) coincide.

Table X only gives the final value of ψ_j for each chosen angle α_2 , the intermediate results of the iterations in ψ have not been listed. The curves of Fig. 25 are identical with those of Fig. 24 which were used to obtain the rotor efficiencies η_R as functions of M_{W1} and i' for the calculations in Table X. In Fig. 25 the rotor efficiencies η_R of Table X are plotted vs. M_{W1} and i' to show the location of the curves $U_1/a_0 = 0.7156$ and $U_1/a_0 = 0.516$ in relation to the other curves $U_1/a_0 = \text{constant}$ which were actually disregarded in establishing η_R for the calculations of Table X. It can be noticed that the two curves $U_1/a_0 = \text{constant}$, that could be drawn through the data points of Table X, are similar to the dashed curves of Figs. 24 and 25 but have somewhat different slopes.

A far more interesting representation of the data of Table X is given in Fig. 26 where the velocity coefficients ψ and the incidence angles i' are shown as function of the deceleration ratio W_2/W_{10} of the relative velocities in the rotor. As expected, the velocity coefficients ψ decrease with decreasing ratios W_2/W_{10} , and if W_2/W_{10} approaches unity the values of ψ seem to reach an asymptotic value which is higher at the lower velocity ratio U_1/a_0 because of the lower Mach number of the flow. Figure 26 also shows that the incidence angles decrease almost linearly with W_2/W_{10} . In the writer's opinion losses of centrifugal compressors rotors should be presented in the manner of Fig. 26. Data of this nature for different impellers would enable the engineer to arrive at optimum designs and make it possible to establish off-design performance maps with greater accuracy than with the rotor efficiencies η_R .

3. Diffusor Performance

To determine the compressor performance for the rotor data of Table X the conditions in the diffusor must be evaluated also. Experience shows that the pressure loss coefficient Y_t of a decelerating axial

cascade varies with incidence angle and inlet Mach number. Limited information is however available in the literature about these influences. Figure 27 has been established on the basis of Fig. 130 of Ref. 3, but these data are educated guesses at best, although they are representative of observed behavior. In particular, the solid curve will be used for $U_2/a_0 = 0.7156$ and the dashed curve for $U_2/a_0 = 0.516$, for the range of the Mach numbers indicated. Because of the approximate nature of these curves it is sufficient to treat the two diffuser rows together. At the design point the total pressure loss coefficient of rows A_1' and A_2' of diffuser A' is from Table VII

$$Y_t = (Y_t)_{i_0} \frac{P_{t2}/P_0 - P_{t4}/P_0}{P_{t2}/P_0 - P_2/P_0} = \frac{1.6764 - 1.5910}{1.6764 - 1.2677} = 0.2089$$

This loss coefficient is supposed to occur at the design incidence angle $i = i_0 = +2^\circ$ of the first diffuser blade row A_1 in accordance with Table VI. At other incidence angles

$$i = \alpha_2 - 63^\circ$$

the pressure loss coefficients Y_t are taken as

$$Y_t = 0.2089 \left[Y_t / (Y_t)_{i_0} \right]$$

where the ratio in the square bracket is read from Fig. 27.

Reference 3 shows that the deviation angle δ is almost constant if the incidence angle of the flow of a particular cascade changes. Thus, the discharge flow angle of a cascade is nearly constant. This general phenomenon is evident also from Fig. 14 (7) of Ref. 5. Because of the approximate nature of the present investigation it is permissible, therefore, to assume that the flow angle after the second diffuser row A_2 is

constant, equal to $\alpha_4 = 21^\circ$, irrespective of incidence angle and Mach number of diffuser row A_1 (see Table VI).

The calculating method of program 109 of Appendix D will be used to establish the conditions of state of the fluid after the diffuser for the data of Table X. It is assumed that the blockage factors at inlet and exit of the diffuser are those at the design point, or

$$k_{Be} = k_{B2} = 0.954$$

$$k_{Bd} = k_{B4} = 0.88$$

The quantity K of Eq. D 109(2) is then, with $A_4 = A_2$, $\alpha_4 = 21^\circ$, and

$$M_2 = M_{V2}$$

$$K = 1.161218 \cos \alpha_2 \frac{p_2/p_0}{\sqrt{T_2/T_0}} M_2$$

The Mach number M_4 and the velocity V_4 must be obtained with the iterative procedure outlined in program 109.

The processes in the flow straightener and discharge duct, illustrated in Figs. 11a and 11b, are determined with Eqs. 50 to 64. The objective of this procedure is to obtain the pressure ratio p_6/p_0 . Since p_6 is equal to the ambient pressure, or 14.7 psia, these calculations establish the value of the total pressure P_0 ahead of the compressor rotor. It is assumed that the total temperature T_0 equals 520°R .

4. Compressor Off-Design Performance

From line 8 of Table X there are known the ratios $\dot{w}\sqrt{(R_G/g)T_0}/P_0$. Hence the flow rate \dot{w} in lbm/s is obtained from

$$\dot{w} = 0.034055 \frac{\dot{w}\sqrt{(R_G/g)T_0}}{P_0} P_0 \text{ (lbm/s)} \quad (83)$$

for $R_G = 53.35 \text{ (lb-ft)/(lbm, } ^\circ\text{R)}$, $g = 32.174 \text{ ft/s}^2$, and $T_0 = 520^\circ\text{R}$, if P_0 is introduced in psia. The drive power of the compressor is, from Eq. 34a,

$$HP = 176.54 \dot{w} [(T_{t2}/T_0) - 1] \text{ (HP)} \quad (84)$$

where T_{t2}/T_0 is known from line 23 of Table X.

The total-to-total efficiency η_{t4} of Eq. 49 can be determined for the pressure ratio P_{t4}/P_0 that is obtained by the calculations. For $T_0 = 520^\circ\text{R}$, and $R_2 = 5.5 \text{ in.}$, the speed N of the compressor is

$$N = 23290.21 (U_2/a_0) \text{ (rpm)} \quad (85)$$

These calculations have been performed with program 517 on a Monroe Model 1880-22 scientific programmable printing calculator. Program 517 contains the earlier mentioned program 109. With this advanced calculator the whole calculating procedure can be carried out without the need of introducing several programs as would have been necessary with Monroe Model 1556, which is limited to 256 program steps and seven active memory registers. Program 517 which is described in Appendix D requires 557 program steps and 40 data storage registers.

The results of the calculations for the data of Table X are listed in Table XI for the design velocity ratio $U_2/a_0 = 0.7156$ and in Table XII for $U_2/a_0 = 0.516$. The data of these tables are direct print-outs of the Model 1880 calculator.

The data at the design speed of 16,666 rpm and for $\alpha_2 = 65^\circ$ (Table XI) should coincide with the values of Table IX. It can be noted that the agreement is good, hence, it can be concluded that no arithmetic errors were made in the calculations.

Figure 28 is a graph of the data of Tables XI and XII. As expected, the driving power is higher at flow rates larger than that of the design point. It is necessary therefore to run the compressor with a turbine that is capable of producing at least 130 HP at 16,666 rpm, although only about 83 HP are required at the design point conditions. It can also be seen

from Fig. 28 that the calculated optimum compressor efficiencies at 12,018 and 16,666 rpm are nearly equal, namely, 81.35% at the lower and 81.49% at the higher speed. It seems possible, therefore, to obtain a good measure of the maximum compressor efficiency with tests at speeds lower than design, say, at about 13,000 to 14,000 rpm.

The data points in Fig. 28 at the lowest flow rates are for $\alpha_2 = 73^\circ$ at both speeds. As indicated in Fig. 25 these points lie on the curve labeled "surge limit." At $\alpha_2 = 73^\circ$ the diffuser incidence angle i is 10° . By Fig. 27 the ratio $Y_t/(Y_t)_0$ for $i = 10^\circ$ is 1.90 for $U_2/a_0 = 0.7156$ and 1.22 for $U_2/a_0 = 0.516$. A frequently applied rule assumes that an axial blade row stalls if the loss is twice that at the design incidence angle. If this condition were to hold for the tandem row of the present diffuser, it could be stated that compressor surge is due to rotor stall at both speed ratios. The surge limit indicated in Fig. 28 holds for this premise.

IV. DRIVE TURBINE

1. General

An available test stand for investigations of transonic axial compressor wheels is driven by a dual-flow air turbine with 50 percent reaction which is illustrated in Dwg. 2222 of Appendix B. The rotors of this turbine are shown in Dwg. 2108-1 and the guide vanes in Dwg. 2109. The blades of rotor and stator are identical with the profiles of Dwg. 2107, but to avoid wake interferences the stator row has 31 and the rotor 32 blades. The two parallel stages are designed for the following conditions

$$P_{t0}/p_2 = 2.8 \text{ for } p_2 = p_{AMB} = 14.7 \text{ psia}$$

$$T_{t0} = 640 \text{ }^{\circ}\text{R}$$

$$\dot{w} = 10.85 \text{ lbm/s}$$

$$\text{HP} = 485 \text{ HP}$$

$$N = 30,500 \text{ rpm}$$

where P_{t0} and T_{t0} are total inlet pressure and total inlet temperature, respectively, and p_2 the static discharge pressure.

To be determined are the pressure ratio, inlet temperatures, and weight flow rates for turbine powers of 130 HP at 16,666 rpm, and 60 HP at 12,018 rpm.

2. Off-Design Turbine Performance

These calculations were performed by Prof. E. Macchi during his stay as Visiting Professor at NPS. Use was made of the computer program of Ref. 14 which treats the three-dimensional flow in a turbine stage by taking account of streamline curvatures and slopes, as well as energy and entropy gradients. In Ref. 14 it is possible to select one of five loss correlation methods that are included in the program. For the present

investigation the method of Traupel (Ref. 15) has been applied, since it was found to give good performance predictions for 50 percent reaction turbines. The results of these calculations are presented in Fig. 29, showing referred flow rate $\dot{w}\sqrt{\theta_T}/\delta_T$, and referred power $HP/(\delta_T \sqrt{\theta_T})$ as function of the referred speed $N/\sqrt{\theta_T}$ for different turbine pressure ratios. There are:

$$\delta_T = P_{t0}/14.7$$

$$\theta_T = T_{t0}/518.4$$

If the ambient pressure is assumed to be 14.7 psia the turbine pressure ratio P_{t0}/p_2 equals δ_T .

For ease of operation it will be endeavored to run the turbine at the lowest possible inlet temperature T_{t0} . A lower limit is given by the condensation or icing of the water vapor in the operating air which has nearly 100 percent relative humidity. It will therefore be assumed that the static turbine discharge temperature T_2 shall not be less than 45° F or 505° R. The off-design calculations showed that the total-to-static turbine efficiency η_s does not exceed about 81% in the range of operating conditions for the Hybrid compressor. The temperature T_2 is obtained from

$$T_2 = T_{t0} \left\{ 1 - \eta_s \left[1 - (1/\delta_T)^{(\gamma - 1)/\gamma} \right] \right\} \quad (86)$$

For $T_2 = 505^\circ \text{ R}$ and $\eta_s = 0.81$ the temperature T_{t0} can therefore be determined for different values of δ_T and $\gamma = 1.4$. Thus, the ratios $\theta_T = T_{t0}/518.4$ are known as functions of δ_T . For a particular speed N , or ratio $N/\sqrt{\theta_T}$, the referred turbine parameters are then obtained from Fig. 29 for the three values of δ_T . The results are listed in the following table:

N (rpm)	16,666			12,018		
δ_T	1.4	1.8	2.2	1.4	1.8	2.2
T_{t0} ($^{\circ}$ R) (Eq. 86)	545.5	577.3	603.6	545.5	557.3	603.6
$\theta_T = T_{t0}/518.4$	1.05227	1.11360	1.16439	1.05227	1.11360	1.16439
$N/\sqrt{\theta_T}$	16,247	15,793	15,445	11,716	11,388	11,137
$\frac{\dot{w}\sqrt{\theta_T}}{\delta_T}$ (Fig. 29)	3.65	4.18	4.30	3.72	4.27	4.36
$\frac{HP}{\delta_T\sqrt{\theta_T}}$ (Fig. 29)	48.5	89.1	111.8	46.8	81.0	97.2
\dot{w} (lbm/s)	4.98	7.13	8.77	5.08	7.28	8.89
HP	69.6	169.2	265.4	67.2	153.8	230.7

From the plot of these data in Fig. 30 it can be seen that the turbine is capable of producing 130 HP at 16,666 rpm with a pressure ratio of 1.64 at a flow rate of 6.4 lbm/s. The inlet temperature must be about 105 $^{\circ}$ F. At the lower speed of 12,018 rpm a power of 60 HP is produced at a pressure ratio of 1.37 for a flow rate of 4.85 lbm/s with a turbine inlet temperature of 82 $^{\circ}$ F.

The air supply system of the Turbopropulsion Laboratory is capable of producing these inlet conditions and no difficulty is expected to drive the compressor at all possible operating conditions.

V. MECHANICAL DESIGN

1. Rotor

An investigation of the stresses in the Hybrid rotor has been carried out to determine its maximum operating speed. As evident from Dwg. 2203 of Appendix B the outer rim of the rotor will produce bending stresses which will be reduced, in part, by the restraint of the radial blades. In Ref. 16 the stresses were calculated by ignoring these bending stresses and the support by the blades. Referred to the outer rotor radius $R_o = 5.94$ inch the maximum stress σ_{\max} was determined to be

$$\sigma_{\max} = 0.53 \rho \omega^2 R_o^2$$

where ρ is the density of the rotor material.

For aluminum alloy AL-7079 with $\rho = 2.616 (10^{-4})$ lb s²/in.⁴, there is at $N = 17,000$ rpm

$$\rho \omega^2 R_o^2 = 29,252 \text{ psi}$$

and

$$\sigma_{\max} = 15,504 \text{ psi}$$

With a correction factor of about 1.25, to allow for the inaccuracies of the model used for the calculation, the design stress σ_d was taken as

$$\sigma_d = 1.25 \sigma_{\max} = 19,380 \text{ psi}$$

Aluminum alloy Al-7079-T6 was chosen as material. In forged condition this alloy has a 0.2% yield stress of 73 kpsi, and an ultimate stress of 83 kpsi.

During his stay at NPS as Visiting Assistant Professor, Dr. W. Schlachter undertook a more accurate stress analysis with the method of Ref. 17 which is discussed also in Ref. 18. This method takes account of the bending moments that occur in non-symmetrical disks with radial blades. Although the forces and moments produced by the blade elements are evaluated properly, these

effects are later distributed evenly along the periphery to obtain axisymmetric conditions. Thus the rotor is supposed to have an infinite number of blades which have the same effect as the actual number of blades. In spite of its complexity the method of Ref. 17 gives doubtful results in the vicinity of the outer radius of the Hybrid rotor, and finite-element methods should actually be employed to give more accurate conditions.

Figure 31 shows the dimensionless stresses $\sigma/(\rho\omega^2 R_o^2)$ in the disk in radial and peripheral directions. In Fig. 31 the shape of the Hybrid rotor is shown also to indicate that the plotted stress ratios exist on either the outer or the inner disk contour, which are designated by A and B, respectively. Evidently, high stresses occur at a radius ratio $R/R_o = 0.7$ where the disk has its smallest thickness. On contour A the disk is in compression and on contour B it is in tension. This is indicative of the bending moment that must occur at this station.

The highest stress occurs at the radius R_o on the inner contour B of the rotor but it has the nature of a stress concentration which, in ductile materials, will be reduced considerably by local plastic deformations if the yield stress is exceeded. For this reason ductile materials have to be used for rotors to equalize stress peaks. From Fig. 31 it can be concluded that a maximum stress of about $0.60 (\rho\omega^2 R_o^2)$ can be used as a design criterion for the Hybrid rotor if it is made of a material with good ductility.

This criterion seems to be invalidated by Fig. 32 which shows the blade stresses at the tip, and at the base where they adjoin the disk. These stations are designated as contours D and C, respectively, of the rotor which is shown in Fig. 32, also. However, the high stress ratio at the blade tips at a radius ratio $R_D/R_o = 0.7$ is clearly a local condition which will be reduced by plastic yielding if the material has good

ductility. Drawing 2203 of Appendix B shows that the blades of the rotor have a thickness of 0.125 inch. If this thickness were increased to 0.16 inches the blade tip stress ratio could be reduced from 2 to about 1.22 without loss in efficiency. However, the writer believes that even with the thin blades the rotor is capable of operating at 17,000 rpm without danger. For a stress ratio of 0.6, the maximum stress σ_{\max} is

$$\sigma_{\max} = 17,500 \text{ psi}$$

If a maximum design stress of 55 kpsi is taken for AL-7075-T6, or about 75 percent of its 0.2% yield stress (73 kpsi), the maximum rotor speed could be

$$N_{\max} = 17,000 \sqrt{\frac{55,000}{17,500}} = 30,100 \text{ rpm}$$

A design speed of 17,000 rpm was used because of the critical speed of the rotor assembly. For the overhung arrangement of Dwg. 2222, where the shaft is supported by ball bearings with 30 mm bore, and for an aluminum rotor that weighs about 19.5 lb, the critical speeds are:

$$N_{CI} = 21,620 \text{ rpm}$$

and

$$N_{CII} = 66,230 \text{ rpm}$$

These speeds were obtained without taking account of the flexibility of the bearing supports. Thus, the decision was made to limit the operating speed to 17,000 rpm or about 78 percent of the first critical shaft speed.

2. Maximum Obtainable Pressure Ratios

It is of interest to evaluate what pressure ratio could be produced by the Hybrid compressor if it were rotating at 30,100 instead of at 16,666 rpm. The peripheral speed ratio U_2/a_0 for a total inlet temperature $T_0 = 520^\circ \text{ R}$ could then be increased from 0.7156 to

$$(U_2/a_0)_{\max} = 1.2924$$

From Eq. A II(3)

$$\frac{P_{t4}}{P_0} = \left[1 + (\gamma - 1) \mu \eta_c (U_2/a_0)^2 \right]^{\gamma/(\gamma - 1)} \quad (87)$$

For an assumed efficiency $\eta_c = 0.8$, and $\gamma = 1.4$, $\mu = 0.85$,

$$\left(\frac{P_{t4}}{P_0} \right)_{\max} = 3.71$$

At this pressure ratio the static temperature T_2 at the rotor exit is from Eq. A I(7), for $T_0 = 520^\circ \text{ R}$,

$$(T_2)_{\max} = 662.5^\circ \text{ R} = 202.5^\circ \text{ F}$$

This temperature is somewhat high for aluminum alloys since their physical properties are reduced considerably at higher temperatures. At 300° F , for instance, the 0.2% yield strength of AL-7075-T6 is reduced from 73 kpsi (at room temperature) to 22 kpsi.

Titanium alloy 6AL-4V would be a better rotor material for the higher speeds. At a temperature of about 300° F the 0.2% yield strength of a forging with an elongation of 13 percent is about 130 kpsi. For a design stress of 75 percent of this yield strength, or

$$\sigma_{\max} = 97,500 \text{ psi}$$

and

$$\sigma_{\max} = 0.6 (\rho \omega^2 R_o^2)$$

there is with

$$\rho = 4.144 (10^{-4}) \text{ lb s}^2/\text{in.}^4$$

$$N_{\max} = \frac{30}{\pi} \omega = \frac{30}{\pi} \sqrt{\frac{\sigma_{\max}}{(0.6) \rho R_o^2}} = 31,835 \text{ rpm}$$

Then

$$U_2/a_0 = 1.3669$$

From Eq. 87 the pressure ratio at this speed ratio is, for $\eta_c = .80$,
 $\gamma = 1.4$, $\mu = 0.85$,

$$\frac{P_{t4}}{P_0} = 4.213$$

at a temperature T_2 of

$$T_2 = 679.4^\circ \text{ R} = 219.4^\circ \text{ F}$$

These calculations indicate that pressure ratios larger than about 4.2 can be reached only in a Hybrid compressor of the design proposed here, if spin tests show that stress ratios $\sigma_{\max}/(\rho \omega^2 R_o^2)$ higher than 0.6 are permissible, or that the ratio of 75 percent of design and yield stress is too conservative.

3. General Description of Test Rig

Drawing No. 2222 of Appendix B shows that the compressor shaft is supported by two matched pairs of high-precision ball bearings. The rotor assembly is held together by a central tie-bolt which is prevented from turning by prongs in the quill shaft that connects the compressor to the drive turbine. At the compressor end of the assembly, a steel attachment, shown in Dwg. 2103-A, pre-loads the inner races of the ball bearings and serves as support for the aluminum rotor. To ensure that the rotor remains concentric with the shaft, even if it increases its diameter by centrifugal stresses, four matched bushings (part 2103-2) are inserted in holes in the rotor collar and part 2103-1, that are drilled and reamed together. These bushings center the rotor and transmit the torque. The maximum torque is about 605 in.-lb at 160 HP and 16,666 rpm. The cross-sectional area of one bushing (0.25 OD, 0.196 ID) is 0.0189 in.^2 . The shear force acting at the

diameter of 3.2 in., where the rotor rests on the steel disk (part 2103-1) is $605 / (2 \times 3.2) = 94.5$ lb if all bushings carry equal loads. Thus the shear stress per bushing is $94.5 / 0.0189 = 5000$ psi. The bushings are of Steel AISI 4340, hardened to 360 Brinell, to obtain a yield strength of about 160 kpsi. Hence the allowable shear stress is 80,000 psi and it is possible for one bushing to transmit the whole torque without danger.

The axial thrust exerted by the impeller is eliminated by the rotating balance piston near the quill shaft. The ball bearings at this shaft end are floating but they are supported by flexures which are equipped with strain gages. Calibrations of the assembly with known applied axial forces will indicate how much thrust is acting on the bearings. The read-out of the strain gages is displayed in the control room so that the balance air pressure can be adjusted for minimum thrust acting on the bearings. Because of its symmetrical design the drive turbine will not produce any axial thrust. The bearings are oil-mist lubricated, and the temperature of each outer race of the eight bearings is measured by a thermocouple which can be read in the control room also.

The diffuser blades are attached to blade holders (Part 1 of Dwg. 2209) by nuts and lock washers. Hence their stagger angles can be varied. These blade holders are inserted in a casing (Part 4 of Dwg. 2208). A number of spacer rings (see Dwg. 2209) were manufactured to be able to locate the diffuser blade rows at different distances from the rotor discharge. It is possible also to rotate the blade holders with respect to each other. With this arrangement it is possible to produce different arrangements of tandem blade rows. Part 4 of Dwg. 2208 is bolted to a casing (Part 1 of Dwg. 2207) on one side and to the shroud support of Dwg. 2212 on the other. To this support is attached the rotor shroud (Part 1 of Dwg. 2213) to form the floating stator assembly whose functions

are described in the next paragraph. Honeycomb flow straighteners are arranged between the fins of the shroud support.

At the design point the total temperature of the air passing through the compressor will increase by about 90° R. Hence a temperature error of one degree will result in a change of the calculated efficiency of about 1.2 points. Errors of temperature measurements of one degree easily occur in high speed flows, especially if they are non-steady. It was therefore decided to make arrangements for direct torque measurements. As shown in Dwg. 2222 the so-called floating stator assembly, consisting of the diffuser vanes, the flow straightener, the rotor shroud, and an outer casing, is supported by two special Kaydon ball bearings. The flow ahead of the inducer is in axial direction and the flow straightener after the diffuser will produce an axial discharge velocity. Then, the moment exerted on the rotor must be equal and opposite to the moment acting on the above-mentioned assembly. This moment is measured by flexures with strain gages (Part 4 of Dwg. 2215) which are calibrated against known torques, that are applied with a lever and known weights.

This arrangement requires labyrinth seals at the inner and outer diameters of the shroud of Dwg. 2213. These labyrinths are shown in Dwg. 2215. For radial clearances of 0.015 inch a leakage flow of about 0.012 lbm/s will pass through the inner labyrinth with 6.4 inch ID, from the region inside the shroud to the inducer inlet. This quantity is about 0.4 percent of the design flow rate. Through the outer labyrinth with an OD of 9.48 inch, however, a leakage flow of 0.064 lbm/s will occur from the opening after the flow straightener to the region inside the shroud. To maintain the required pressure between the labyrinths, an air flow of $0.064 - 0.012 = 0.054$ lbs/s has to be vented from this region. For this reason the inlet casing, shown in Dwg. 2214-2, is hollow and is connected

by four 1 inch tubes to openings in the 18 inch suction pipe ahead of the flow measuring nozzle.

The measuring nozzle has a diameter of 5.375 inches and is formed of epoxy as shown in Dwg. 2222, with parts of the contour machined in the nozzle frame of Dwg. 2216. The shape of the nozzle conforms to the norms of VDI measuring orifices. A nozzle with a diameter of 5.375 inches will produce a pressure difference of about 20 inches of water for the measuring of the design flow rate of 2.7 lbm/s.

Drawing 2223 shows the general installation of the compressor test rig in Test Cell 2 of the Turbopropulsion Laboratory. Air supplied from a multi-stage axial compressor with a drive power of 1250 HP passes through a remote-controlled butterfly valve to the drive turbine. In case of runaway conditions, which could be caused by a compressor blade failure, the turbine air can be blown directly to the atmosphere through an emergency bypass valve.

The compressor air flow is controlled by the inlet throttle valve of Dwg. 2158. It consists of a fixed and a rotating plate that have the same arrangement of holes. The maximum flow area is 158 in.², corresponding to the area of a pipe of about 14 inch ID. The rotating plate is supported by ball bearings and can be moved with the oil pressure actuator of Dwg. 2159. This actuator can produce a force of about 1700^{lb} ± 1700 lb for an oil pressure of 400 psi. It is controlled from the control room by a reversible electric motor of less than 1/10 HP. The actuator is inherently stable and maintains the same position irrespective of the force applied to it, provided it is less than about 2000 lb.

After the throttling valve the velocity of the air is destroyed in the plenum chamber of Dwg. 2164-1. It is equipped with six perforated plates, with 43 percent free opening, which can be located at arbitrary positions

along the axis of the plenum. A contoured plastic nozzle guides the flow into the 18 inch diameter suction pipes, which contain the measuring nozzle.

REFERENCES

1. Vavra, M. H., "Basic Elements for Advanced Design of Radial Flow Compressors", Article 6 of AGARD Lecture Series No. 39 on Advanced Compressors, Technical Editing and Reproduction Ltd., London, June 1970. (Enclosed as Appendix A)
2. Stiefel, W., "Theoretical and Experimental Research on Limit Loading of Radial Compressors" Part II, Course Note 53b, Von Karman Institute for Fluid Dynamics, Rhode-Saint-Genese, Belgium, March 1965.
3. Lieblein, S., "Experimental Flow in Two-Dimensional Cascades", Chapter VI of "Aerodynamic Design of Axial-Flow Compressors", Edited by I. A. Johnson and R. O. Bullock, NASA SP-36, Washington, D.C., 1965.
4. Steinke, R. J., and Crouse, J. E., "Analytical Studies of Aspect Ratio and Curvature Variations for Axial-Flow Compressor Inlet Stages under High Loading", NASA TN D-3959, May 1967.
5. Vavra, M. H., "Aerothermodynamics and Flow in Turbomachines," John Wiley & Sons, New York 1960.
6. Griepentrog, H., "Secondary Flow Losses in Axial Compressors", Article 5 of AGARD Lecture Series No. 39 on Advanced Compressors, Technical Editing and Reproduction Ltd., London, June 1970.
7. Woods, J. R. Jr., "The Analytical Treatment of Secondary Flows and Associated Losses in Axial-Flow Turbomachines", Report NPS-57W071121A, Naval Postgraduate School, Monterey, California, December 1971.
8. Vavra, M. H., "Aerodynamic Design of Symmetrical Blading for Three-Stage Axial Flow Compressor Test Rig" Report NPS-57VA70091A, Naval Postgraduate School, Monterey, California, September 1970.

9. Giles, R. V., "Fluid Mechanics and Hydraulics" 2nd. Ed., p. 257,
Schaum Publishing Co., New York, 1962.
10. Linsi, U., "Experiments on the Radial Compressors of Turbochargers"
Brown Boveri Review, Vol. 52, No. 3, pp. 161/170, March 1965.
11. Meldahl, A., "The Separation of Impeller and Diffusor Losses in
Radial Blowers" Brown Boveri Review, Vol. 28, No. 8/9, pp. 203/206,
Aug./Sept. 1941.
12. Traupel, W. "Die Theorie der Stroemung durch Radialmaschinen", p. 100,
G. Braun, Karlsruhe, 1962.
13. Stahler, A. F., "The Slip Factor of a Radial Bladed Centrifugal
Compressor", ASME Paper 64-GTP-1, March 1965.
14. Macchi, E., "Computer Program for Prediction of Axial Flow Turbine
Performance", Report NPS-57MA70081A, Naval Postgraduate School,
Monterey, California, August 1970.
15. Traupel, W., "Thermische Turbomaschinen", Vol. 1, pp. 269/298, Springer
Verlag, Berlin, 1958.
16. Griepentrog, H., "Calculation of Hybrid Compressor", Encl. 3 of Progress
Report, February 1970, on "Research in Hybrid Compressor Concept",
Naval Postgraduate School, Monterey, California. AIR TASK A330536
O/551B/OF32432302
17. Schilhansl, M. J., "Stress Analysis of Radial-Flow Rotor", Trans.
ASME J. of Engg. for Power, January 1962 pp. 124-130.
18. Vavra, M. H., "Mechanical Problems in Radial Turbines", Short Course
March 1968, Part C, p. C14/C26, Von Karman Institute for Fluid
Dynamics, Rhode-Saint-Genese, Belgium.

TABLES

TABLE I: Flow, Blade, and Incidence Angles
at Inducer Leading Edge

R_1 (in.)	β_1 ($^\circ$)	β_B ($^\circ$)	$\tan \beta_B$	$i=\beta_1-\beta_B$ ($^\circ$)
3.025	55	50.32	1.20545	4.68
2.8	52.89	47.99	1.11016	4.90
2.6	50.83	45.71	1.02525	5.12
2.4	48.57	43.23	0.94024	5.34
2.2	46.09	40.51	0.85449	5.58
2.0	43.36	37.54	0.76852	5.82
1.8	40.36	34.30	0.68216	6.06
1.6	37.07	30.76	0.59530	6.31
1.5	35.30	28.88	0.55166	6.42
1.4	33.46	26.92	0.50784	6.54
1.3	31.54	24.88	0.46388	6.66
1.2	29.53	22.77	0.41973	6.76
1.1	27.44	20.57	0.37538	6.87
1.023	25.78	18.83	0.34111	6.95
1.00	25.27	18.30	0.33085	6.97
0.99	25.05	18.08	0.32639	6.97

TABLE II: Loss Coefficients of First Blade

Row of Diffusor

$\Delta\alpha$	$\sigma =$	0.8	1.0	1.2	1.4	1.6	1.8
10°	D	0.4524	0.4146	0.3893	0.3713	0.3578	0.3473
	Y_P	0.0452	0.0486	0.0527	0.0572	0.0619	0.0668
	Y_t'	0.0900	0.0934	0.0975	0.1020	0.1067	0.1116
	Y_t''	0.0680	0.0788	0.0902	0.1031	0.1169	0.1323
12°	D	0.5137	0.4705	0.4417	0.4211	0.4057	0.3937
	Y_P	0.0545	0.0578	0.0620	0.0666	0.0716	0.0768
	Y_t'	0.1116	0.1148	0.1190	0.1236	0.1286	0.1338
	Y_t''	0.0873	0.0988	0.1127	0.1289	0.1470	0.1669
14°	D	0.5687	0.5207	0.4886	0.4657	0.4485	0.4352
	Y_P	0.0639	0.0670	0.0711	0.0760	0.0812	0.0857
	Y_t'	0.1332	0.1362	0.1403	0.1452	0.1504	0.1549
	Y_t''	0.1069	0.1207	0.1376	0.1569	0.1788	0.2017

$\Delta\alpha = \alpha_2 - \alpha_3 = 65^\circ - \alpha_3 = \text{Flow Deflection}$

$\sigma = \text{Solidity} = (\text{Blade Chord/Blade Spacing})$

D = Diffusion Factor (Eq. 16)

Y_P = Profile Loss Coefficient (Eq. 20)

$Y_t' = Y_P + Y_s' = \text{Overall Loss Coefficient}$

$Y_t'' = Y_P + Y_s'' = \text{Overall Loss Coefficient (Eq. 27)}$

$Y_s' = \text{Secondary Flow Loss Coefficient (Eq. 25)}$

$Y_s'' = \text{Secondary Flow Loss Coefficient (Eq. 26 with}$

Y_s''/Y_t'' from Fig. 6)

TABLE III: Design Values of First Blade Rows
of Diffusors A and B

Diffusor	A	B
Diffusor Blade Row Designation	A ₁	B ₁
Flow Deflection $\Delta\alpha^{\circ} = \alpha_2 - \alpha_3$	12	12
Number of Blades	38	38
Solidity σ	1.6	0.95
Diffusion Factor D	0.4057	0.4796
Profile Loss Coefficient Y_p	0.0716	0.0569
Total Loss Coefficient Y_t'	0.1286	0.1139
Total Loss Coefficient Y_t''	0.1470	0.0958
Blade Chord c (in.)	1.455	0.864
Maximum Blade Thickness t (in.)	0.090	0.085
Thickness Ratio t/c	0.062	0.098

TABLE IV: Loss Coefficients of Second
Blade Row of Diffusor

$\Delta\alpha$	$\sigma =$	0.8	1.0	1.2	1.4	1.6	1.8
26°	D	0.6321	0.5706	0.5296	0.5003	0.4783	0.4612
	Y_P	0.0565	0.0568	0.0587	0.0613	0.0644	0.0678
	Y_t'	0.1349	0.1352	0.1371	0.1397	0.1428	0.1462
	Y_t''	0.1201	0.1354	0.1553	0.1793	0.2077	0.2387
32°	D	0.7101	0.6392	0.5919	0.5581	0.5327	0.5130
	Y_P	0.0698	0.0690	0.0703	0.0726	0.0755	0.0789
	Y_t'	0.1709	0.1702	0.1714	0.1737	0.1767	0.1801
	Y_t''	0.1654	0.1856	0.2129	0.2461	0.2906	0.3432
38°	D	0.7753	0.6956	0.6425	0.6046	0.5761	0.5540
	Y_P	0.0826	0.0805	0.0810	0.0829	0.0856	0.0889
	Y_t'	0.2066	0.2044	0.2049	0.2068	0.2095	0.2128
	Y_t''	0.2135	0.2439	0.2811	0.3288	0.3926	0.4677

$\Delta\alpha = \alpha_3 - \alpha_4 = 53^\circ - \alpha_4 = \text{Flow Deflection}$

$\sigma = \text{Solidity} = (\text{Blade Chord/Blade Spacing})$

D = Diffusion Factor (Eq. 16 with $\alpha_2 = \alpha_3$, $\alpha_3 = \alpha_4$)

Y_P = Profile Loss Coefficient (Eq. 26 with $\alpha_3 = \alpha_4$)

$Y_t' = Y_P + Y_s' = \text{Overall Loss Coefficient}$

$Y_t'' = Y_P + Y_s'' = \text{Overall Loss Coefficient}$

$Y_s' = \text{Secondary Flow Loss Coefficient (Eq. 25 with}$

$\alpha_2 = \alpha_3, \alpha_3 = \alpha_4)$

$Y_s'' = \text{Secondary Flow Loss Coefficient (Eq. 26 with}$

Y_s''/Y_t'' from Fig. 6)

TABLE V: Design Values of Second Blade
Rows of Diffusors A and B

Diffusor	A	B
Diffusor Blade Row Designation	A2	B2
Flow Deflection $\Delta\alpha^{\circ} = \alpha_3 - \alpha_4$	32	32
Number of Blades	38	38
Solidity σ	1.4	1.0
Diffusion Factor D	0.5581	0.6392
Profile Loss Coefficient Y_p	0.0726	0.0690
Total Loss Coefficient Y_t'	0.1737	0.1702
Total Loss Coefficient Y_t''	0.2461	0.1856
Blade Chord c (in.)	1.275	0.910
Maximum Blade Thickness t (in.)	0.090	0.085
Thickness Ratio t/c	0.070	0.093

TABLE VI: Determination of Diffusor Profile Data
(For Symbols see Fig. 9)

Diffusor Blade Row	A1	B1	A2	B2
$\alpha_e(^{\circ})$	65	65	53	53
$\Delta\alpha(^{\circ})$	12	12	32	32
$\alpha_d(^{\circ})$	53	53	21	21
σ	1.6	0.95	1.4	1.0
t/c	0.062	0.098	0.07	0.093
From Ref. 3				
$\left\{ \begin{array}{l} (k_i)_{sh} \\ (k_\delta)_{sh} \\ (i_0)_{10} \\ (\delta_0)_{10} \\ m \\ n \\ (k_i)_t \\ (k_\delta)_t \end{array} \right.$	$\left\{ \begin{array}{l} 1.1 \\ 1.1 \\ 7.85^{\circ} \\ 3.22^{\circ} \\ 0.245 \\ -0.197 \\ 0.79 \\ 0.545 \end{array} \right.$	$\left\{ \begin{array}{l} 1.1 \\ 1.1 \\ 4.55^{\circ} \\ 2.05^{\circ} \\ 0.338 \\ -0.293 \\ 0.99 \\ 0.925 \end{array} \right.$	$\left\{ \begin{array}{l} 1.1 \\ 1.1 \\ 5.80^{\circ} \\ 1.40^{\circ} \\ 0.231 \\ -0.140 \\ 0.845 \\ 0.630 \end{array} \right.$	$\left\{ \begin{array}{l} 1.1 \\ 1.1 \\ 4.10^{\circ} \\ 1.80^{\circ} \\ 0.300 \\ -0.195 \\ 0.970 \\ 0.955 \end{array} \right.$
$i_0 = (i_0)_{10}(k_i)_t(k_i)_{sh}$	6.822°	4.955°	5.391°	4.375°
$\delta_0 = (\delta_0)_{10}(k_\delta)_t(k_\delta)_{sh}$	1.930°	2.086°	0.97°	1.891°
$\varphi = (\Delta\alpha - i_0 + \delta_0)/(1 - m + n)$	12.738°	24.74°	43.846°	58.447°
$i = i_0 + n\varphi$	4.312°	-2.95°	-0.747°	-7.022°
$\delta = \delta_0 + m\varphi$	5.051°	10.50°	11.098°	19.425°
$\gamma = \alpha_e - \varphi/2 - i$	54.319	54.922	31.824	30.798
Chosen incidence i^*	$+2^{\circ}$	-1°	$0^{\circ}45'$	-2°
From Ref. 3: $(d\delta/di)$	0.04	0.13	--	0.085
$\varphi^* = \varphi - (i^* - i)(1 - d\delta/di)$	14.957	23.613	43.846	53.852
$\gamma^* = \alpha_e - \varphi^*/2 - i^*$	$55^{\circ}31'$	$54^{\circ}11'$	$31^{\circ}50'$	$28^{\circ}04'$
Profile coordinates:	Dwg 2210-1	Dwg 2210-3	Dwg 2210-2	Dwg 2210-4
$\Delta\gamma$	$0^{\circ}39'$	$1^{\circ}09'$	0°	$0^{\circ}06'$
$\gamma' = \gamma + \Delta\gamma$ or $\gamma^* + \Delta\gamma$	$56^{\circ}10'$	$55^{\circ}20'$	$31^{\circ}50'$	$28^{\circ}10'$

TABLE VII: Flow Properties in Diffusor

Blade Row	A1'	A1''	B1'	B1''
P_{t2}/P_0	————	1.6764	————	
$T_{t2}/T_0 = T_{t3}/T_0 = T_{t4}/T_0$	————	1.17411	————	
P_2/P_0	————	1.2677	————	
T_2/T_0	————	1.08402	————	
K (Eq. 43)	————	0.571523	————	
Y_t (Table III)	0.1286	0.1470	0.1139	0.0958
P_{t3}/P_0 (Eq. 47)	1.6238	1.6163	1.6298	1.6372
M_3^* (chosen)	0.4240	0.4265	0.4220	0.4196
T_3/T_0 (Eq. 45)	1.13336	1.13290	1.13373	1.13417
P_3/P_0 (Eq. 46)	1.4350	1.4263	1.4419	1.4505
M_3 (Eq. 44)	0.4240	0.4265	0.4220	0.4196
V_3 (ft/s) (Eq. 48)	504.6	507.7	502.3	499.5
Blade Row	A2'	A2''	B2'	B2''
K (Eq. 43)	0.385168	0.385168	0.385132	0.385150
Y_t (Table V)	0.1737	0.2461	0.1702	0.1856
P_{t4}/P_0 (Eq. 47)	1.5910	1.5695	1.5978	1.6025
M_4^* (chosen)	0.2743	0.2784	0.2730	0.2722
T_4/T_0 (Eq. 45)	1.15670	1.15618	1.15686	1.15670
P_4/P_0 (Eq. 46)	1.5100	1.4872	1.5172	1.5221
M_4 (Eq. 44)	0.2743	0.2785	0.2730	0.2722
V_4 (ft/s) (Eq. 48)	329.8	334.7	328.2	327.2
η_{t4} (Eq. 49)	81.5%	78.9%	82.3%	82.8%

TABLE VIII: Flow Conditions in Flow Straightener
and Discharge Duct

(See Fig. 11 for Symbols and Location of Stations)

Diffusor	A'	A''	B'	B''
V_4 (ft/s) } P_{t4}/P_0 } p_4/P_0 } T_4/T_0 }	329.8	334.6	328.2	327.2
From Table VII	1.5910	1.5696	1.5979	1.6026
	1.5100	1.4873	1.5172	1.5222
	1.15670	1.15619	1.15686	1.15698
$V_4/a_0 = V_4/(1117.85)$	0.2950	0.2993	0.2936	0.2927
T_4^*/T_0 (Eq. 53)	1.15893	1.15849	1.15907	1.15918
P_{t4}'/P_0 (Eq. 54)	1.5803	1.5587	1.5872	1.5919
T_4'/T_0 (Eq. 55)	1.15532	1.15477	1.15550	1.15561
p_4'/P_0 (Eq. 56)	1.4935	1.4706	1.5009	1.5059
P_{t4}''/P_0 (Eq. 58)	1.5543	1.5323	1.5613	1.5661
p_4''/P_0 (Eq. 59)	1.4689	1.4457	1.4764	1.4814
T_5/T_0 (Eq. 60)	1.16074	1.16035	1.16087	1.16095
P_{t5}/P_0 (Eq. 61)	1.5290	1.5066	1.5362	1.5410
P_{t6}/P_0 (Eq. 62)	1.5050	1.4822	1.5123	1.5172
T_6/T_0 (Eq. 63)	1.16503	1.16477	1.16512	1.16518
p_6/P_0 (Eq. 64)	1.4647	1.4414	1.4721	1.4772
$P_0 = \frac{14.7}{(p_6/P_0)}$ (psia)	10.036	10.198	9.985	9.951

TABLE IX: Estimated Compressor Performance

at Design Point ($N = 16,666$ rpm, $T_0 = 520^\circ\text{R}$)

Diffusor	A'	A''	B'	B''
P_{t4}/P_0 (Table VII)	1.5910	1.5696	1.5979	1.6026
η_{t4} (Table VII)	81.5%	78.9%	82.3%	82.8%
P_6/P_0 (Table VIII)	1.4647	1.4414	1.4721	1.4772
P_0 (Table VIII), (psia)	10.036	10.198	9.985	9.951
\dot{w} (Eq. 34), (lbm/s)	2.698	2.742	2.685	2.676
HP (Eq. 36), (HP)	83.0	84.3	82.5	82.2
M (Eq. 65), (in.-lb)	313.7	318.7	312.1	311.0
U_2/a_0	———— 0.7156 ————			
$(\dot{m})^*$ (Eq. 66)	———— 0.08309 ————			
(HP)* (Eq. 67)	———— 0.05063 ————			
(M)* (Eq. 69)	———— 0.05980 ————			
$\theta_c = 520/518.4$	———— 1.0031 ————			
$\delta_c = P_0/14.7$	0.6827	0.6937	0.6792	0.6769
N_{REF} (Eq. 73), (rpm)	———— 16,642 ————			
\dot{w}_{REF} (Eq. 74), (lbm/s)	———— 3.9591 ————			
(HP) _{REF} (Eq. 75), (HP)	———— 121.317 ————			
M_{REF} (Eq. 76), (in.-lb)	———— 459.45 ————			

TABLE X (SHEET 1 OF 2) PERFORMANCE OF CENTRIFUGAL COMPRESSOR ROTOR (MONROE 1655/6)

TABLE X (SHEET 1 OF 2) PERFORMANCE OF CENTRIFUGAL COMPRESSOR ROTOR

(MONROE CALCULATOR 1655/6)

ROTOR DIMENSIONS:

γ of Fluid = 1.4		$A_2 = 21.0801$	(in^2)	$A_1 = 25.6685$	(in^2)	$R_1/R_2 = 0.55$	$\beta_g = 50.32$	$(^\circ)$	$k = 0.8599$
SELECTED PARAMETERS	U_2/a_0	1	←	—	0.7156	—	—	—	—
	α_2	2	65	58	54	67	71	73	—
	k_{B2}	3	←	—	0.954	—	—	—	—
	k_{B1}	4	←	—	0.980	—	—	—	—
Eq. 82 ITERATION OF ψ	ω	5	.85	.8088	.7844	.8616	.8847	.8963	—
	No. = j	6	DESIGN POINT	FINAL	FINAL	FINAL	FINAL	FINAL	—
	ψ_j	7	.7548	.788	.781	.717	.6686	.548	—
	$\dot{\omega} \sqrt{(R_G/g) T_0/P_0}$	8	7.892 906	8.717 619	9.622 001	10.461 233	6.705 048	5.462 317	—
PROGR. 102	ϕ_2	9	.392 478	.433 488	.478 458	.520 190	.333 412	.302 747	.271 616
	ϕ_1	10	.313 769	.346 554	.382 506	.415 869	.266 548	.242 032	.217 145
	P_1/P_0	11	.947 862	.935 492	.919 985	.903 564	.955 697	.969 728	.975 796
	T_1/T_0	12	.984 817	.981 128	.976 454	.971 442	.987 136	.991 256	.993 024
PROGR. 104	\dot{V}_1/a_0	13	.275 522	.307 180	.343 120	.377 877	.253 608	.231 421	.209 096
	\dot{W}_{10}/a_0	14	.480 435	.499 264	.522 146	.545 615	.468 212	.456 577	.445 675
	$\beta_{10} (^\circ)$	15	55.006	52.029	48.918	46.166	57.204	59.545	62.020
	$\beta_{10}' (^\circ)$	16	50.851	47.772	44.606	41.849	53.154	55.636	58.291
FIG. 24	M_{W1}	17	.4841	.5040	.5284	.5536	.4712	.4590	.4476
	$i' (^\circ)$	18	+0.531	-2.548	-5.713	-8.471	+2.834	+5.316	+7.971
	η_R	19	.86	.8574	.80	.7396	.8514	.8373	.8187
	\dot{W}_2/\dot{W}_{10}	20	.6312	.6783	.7405	.7991	.5976	.5617	.5229
PROGR. 105	η_2	21	.4999	.4789	.2198	-.1250	.4747	.4300	.3699
	ψ	22	.7548	.7878	.7802	.7817	.7170	.6686	.6116
	T_{t2}/T_0	23	1.174 108	1.170 524	1.165 669	1.160 671	1.176 484	1.178 860	1.181 216
	P_{t2}/P_0	24	1.676 382	1.657 610	1.605 044	1.554 246	1.683 471	1.687 492	1.688 961
PROGR. 100	T_2/T_0	25	1.084 022	1.079 476	1.072 513	1.064 392	1.086 156	1.089 263	1.091 551
	P_2/P_0	26	1.267 734	1.248 524	1.199 174	1.147 873	1.275 311	1.279 641	1.281 213
	M_{v2}	27	.6446	.6494	.6590	.6725	.6425	.6409	.6413

TABLE X (SHEET 2 OF 2) PERFORMANCE OF CENTRIFUGAL COMPRESSOR ROTOR
(MONROE CALCULATOR 1655/6)
ROTOR DIMENSIONS:

Y of Fluid = 1.4		$A_2 = 21.0801$	(in^2)	$A_1 = 25.6685$	(in^2)	$R_{10}/R_2 = 0.55$	$\beta_R = 50.32$	$(^\circ)$	$k = 0.8599$
SELECTED PARAMETERS	U_2/a_0	1	←			0.516			→
	α_2	2	65		54	50	67	71	73
	k_{B2}	3	←			0.954			→
	k_{B1}	4	←			0.98			→
EC. 82 ITERATION OF ψ	u	5	.85		.7844	.7590	.8616	.8847	.8963
	No. = j	6	FINAL	FINAL	FINAL	FINAL	FINAL	FINAL	FINAL
	ψ_j	7	.1546		.8351	.840	.7111	.612	.554
PROGR. 102	$\dot{W}/(R_g/g)T_0/P_0$	8	5.265 458	5.875 178	6.653 236	8.099 555	4.881 731	4.070 451	3.660 138
	ϕ_2	9	.262 822	.292 146	.330 835	.402 754	.242 746	.202 405	.182 002
	ϕ_1	10	.210 114	.233 558	.264 488	.321 984	.194 065	.161 814	.145 503
	P_1/P_0	11	.977 378	.971 878	.963 604	.944 912	.980 773	.986 719	.989 292
PROGR. 103	T_1/T_0	12	.993 483	.991 883	.989 463	.983 941	.994 468	.996 187	.996 929
	V_1/a_0	13	.180 505	.201 455	.229 532	.283 366	.166 305	.152 213	.123 921
	W_{10}/a_0	14	.336 340	.348 033	.365 003	.401 047	.328 937	.322 042	.309 676
	$\beta_{10} (^\circ)$	15	57.542	54.631	51.035	45.044	59.630	64.057	66.411
FIG. 24	$\beta_{10}' (^\circ)$	16	53.511	50.460	46.755	40.735	55.727	60.500	63.079
	M_{W1}	17	.3374	.3494	.3669	.4043	.3298	.3162	.3101
	$i' (^\circ)$	18	+ 3.191	+ 0.14	- 3.565	- 9.584	+ 5.407	+ 10.180	+ 12.759
	η_R	19	.856	.86	.86	.7680	.8428	.8164	.8006
PROGR. 105	W_2/W_{10}	20	.6502	.7017	.7639	.8220	.6134	.5742	.4882
	η_W	21	.4465	.4371	.3914	.1176	.4102	.3813	.2936
	ψ	22	.7547	.7955	.8350	.8381	.7111	.6655	.5541
	T_{12}/T_0	23	1.090 552	1.088 663	1.086 139	1.083 540	1.091 762	1.094 223	1.095 458
PROGR. 106	P_{12}/P_0	24	1.321 177	1.315 198	1.305 222	1.287 029	1.323 813	1.327 759	1.329 071
	T_2/T_0	25	1.043 687	1.041 323	1.037 703	1.033 481	1.045 108	1.047 602	1.048 680
	P_2/P_0	26	1.133 514	1.125 676	1.112 604	1.090 658	1.136 169	1.140 082	1.140 810
	M_{V2}	27	.473 705	.476 767	.483 096	.492 128	.472 442	.471 802	.472 264

TABLE XI CALCULATED PERFORMANCE OF HYBRID COMPRESSOR AT 16,666RPM

$$T_0 = 520^\circ\text{R} ; P_0 = 14.7/(p_6/P_0) \text{ (psia)}$$

U_2/a_0	0.7156	0.7156	0.7156	0.7156
α_2	65.0000	62.0000	58.0000	54.0000
P_{t4}/P_0	1.5910	1.5722	1.5135	1.4235
P_4/P_0	1.5100	1.4708	1.3825	1.2527
T_4/T_0	1.1567	1.1485	1.1359	1.1190
M_{V4}	0.2743	0.3100	0.3620	0.4313
V_4/a_0	0.2951	0.3322	0.3858	0.4562
P_{t4}'/P_0	1.5803	1.5586	1.4958	1.4000
P_4'/P_0	1.4935	1.4504	1.3563	1.2193
P_{t4}''/P_0	1.5543	1.5262	1.4539	1.3458
P_4''/P_0	1.4689	1.4202	1.3184	1.1720
P_{t5}/P_0	1.5290	1.4946	1.4131	1.2924
P_{t6}/P_0	1.5050	1.4648	1.3752	1.2443
P_6/P_0	1.4646	1.4151	1.3122	1.1647
P_0 (psia)	10.0367	10.3883	11.2026	12.6209
\dot{w} (lbm/s)	2.6978	3.0841	3.6709	4.4963
HP	82.9226	92.8442	107.3626	127.5371
N (rpm)	16,666.	16,666.	16,666.	16,666.
η_T	0.8149	0.8093	0.7587	0.6607

U_2/a_0	0.7156	0.7156	0.7156	0.7156
α_2	67.0000	69.0000	71.0000	73.0000
P_{t4}/P_0	1.5982	1.5997	1.5816	1.5264
P_4/P_0	1.5295	1.5423	1.5339	1.4867
T_4/T_0	1.1618	1.1666	1.1709	1.1747
M_{V4}	0.2513	0.2292	0.2096	0.1943
V_4/a_0	0.2709	0.2475	0.2268	0.2106
P_{t4}'/P_0	1.5892	1.5922	1.5754	1.5212
P_4'/P_0	1.5155	1.5306	1.5242	1.4786
P_{t4}''/P_0	1.5671	1.5737	1.5600	1.5084
P_4''/P_0	1.4944	1.5128	1.5093	1.4661
P_{t5}/P_0	1.5457	1.5558	1.5452	1.4961
P_{t6}/P_0	1.5252	1.5386	1.5308	1.4841
P_6/P_0	1.4907	1.5096	1.5066	1.4639
P_0 (psia)	9.8609	9.7375	9.7569	10.0417
\dot{w} (lbm/s)	2.4541	2.2235	2.0230	1.8680
HP	76.4618	70.2088	64.7194	60.5433
N (rpm)	16,666.	16,666.	16,666.	16,666.
η_T	0.8123	0.8032	0.7723	0.6995

TABLE XII CALCULATED PERFORMANCE OF HYBRID COMPRESSOR AT 12,018 RPM

$$T_0 = 520^{\circ}\text{R} ; P_0 = 14.7/(p_6/P_0) \text{ (psia)}$$

U_2/a_0	0.5160	0.5160	0.5160	0.5160	0.516
α_2	65.0000	62.0000	58.0000	54.0000	50.000
P_{t4}/P_0	1.2824	1.2756	1.2642	1.2362	1.193
P_4/P_0	1.2414	1.2243	1.1969	1.1501	1.083
T_4/T_0	1.0805	1.0760	1.0693	1.0614	1.051
M_{V4}	0.2160	0.2429	0.2805	0.3228	0.374
V_4/a_0	0.2245	0.2520	0.2901	0.3326	0.383
P_{t4}'/P_0	1.2771	1.2689	1.2553	1.2246	1.178
P_4'/P_0	1.2330	1.2138	1.1833	1.1327	1.061
P_{t4}''/P_0	1.2639	1.2523	1.2337	1.1971	1.143
P_4''/P_0	1.2203	1.1980	1.1630	1.1072	1.029
P_{t5}/P_0	1.2511	1.2364	1.2127	1.1702	1.108
P_{t6}/P_0	1.2388	1.2210	1.1928	1.1450	1.077
P_6/P_0	1.2180	1.1952	1.1595	1.1029	1.024
P_0 (psia)	12.0689	12.2989	12.6784	13.3279	14.348
\dot{w} (lbm/s)	2.1724	2.4608	2.8726	3.3517	3.957
HP	34.7276	38.5173	43.6842	49.4315	56.478
N (rpm)	12,018.	12,018.	12,018.	12,018.	12,018
η_T	0.8135	0.8123	0.8042	0.7475	0.639

U_2/a_0	0.5160	0.5160	0.5160	0.5160	
α_2	67.0000	69.0000	71.0000	73.0000	
P_{t4}/P_0	1.2846	1.2870	1.2870	1.2811	
P_4/P_0	1.2498	1.2579	1.2630	1.2617	
T_4/T_0	1.0832	1.0859	1.0884	1.0907	
M_{V4}	0.1984	0.1810	0.1641	0.1479	
V_4/a_0	0.2065	0.1887	0.1712	0.1544	
P_{t4}'/P_0	1.2801	1.2832	1.2839	1.2786	
P_4'/P_0	1.2427	1.2519	1.2581	1.2577	
P_{t4}''/P_0	1.2689	1.2738	1.2761	1.2723	
P_4''/P_0	1.2318	1.2427	1.2505	1.2515	
P_{t5}/P_0	1.2580	1.2647	1.2687	1.2663	
P_{t6}/P_0	1.2475	1.2559	1.2614	1.2604	
P_6/P_0	1.2299	1.2411	1.2491	1.2504	
P_0 (psia)	11.9526	11.8448	11.7683	11.7565	
\dot{w} (lbm/s)	1.9871	1.8064	1.6313	1.4654	
HP	32.1903	29.6570	27.1356	24.6953	
N (rpm)	12,018.	12,018.	12,018.	12,018.	
η_T	0.8084	0.8037	0.7933	0.7683	

FIGURES

FIG. 1 HYBRID COMPRESSOR (SYMBOLS AND STATIONS)
(NOT TO SCALE)

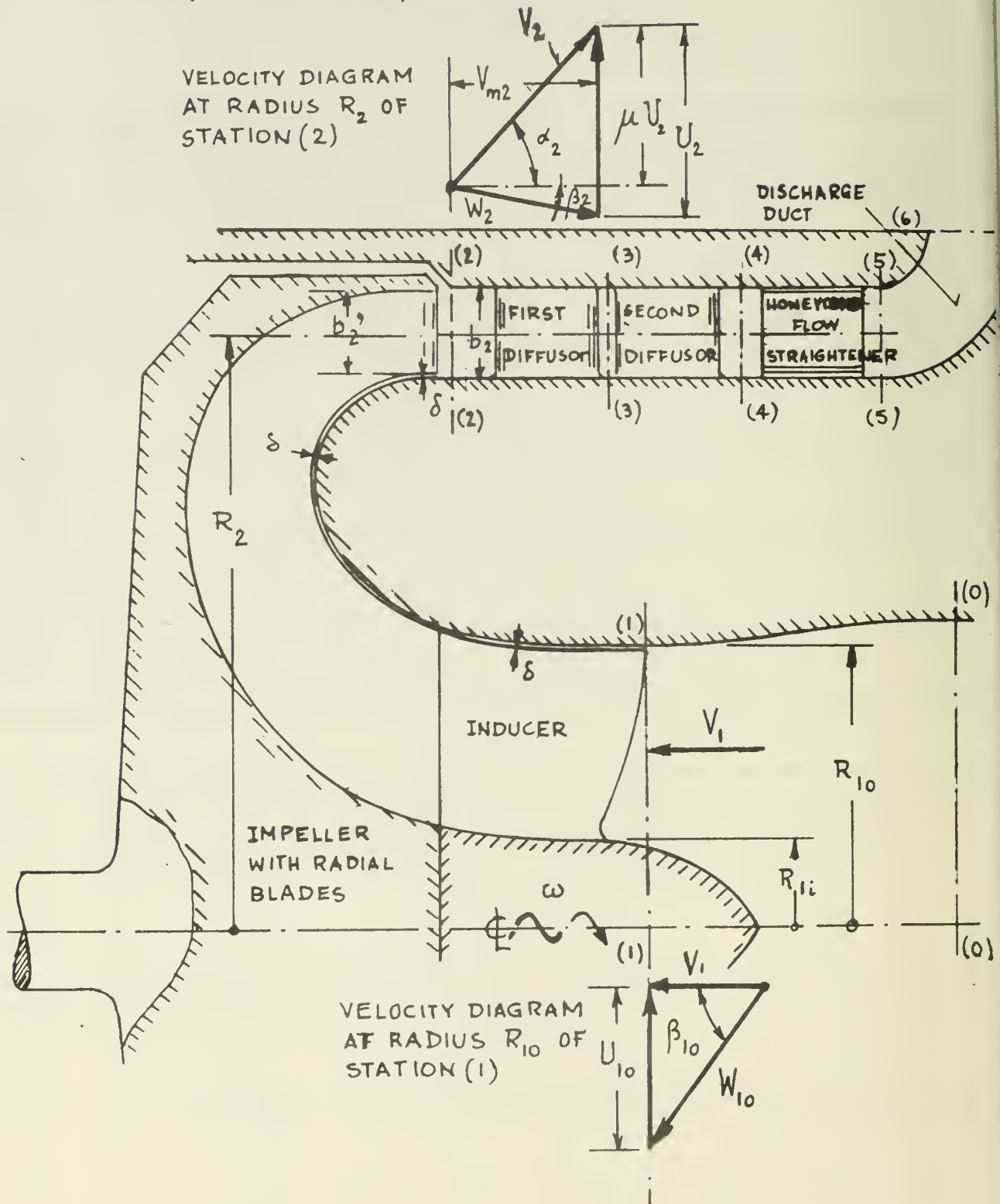
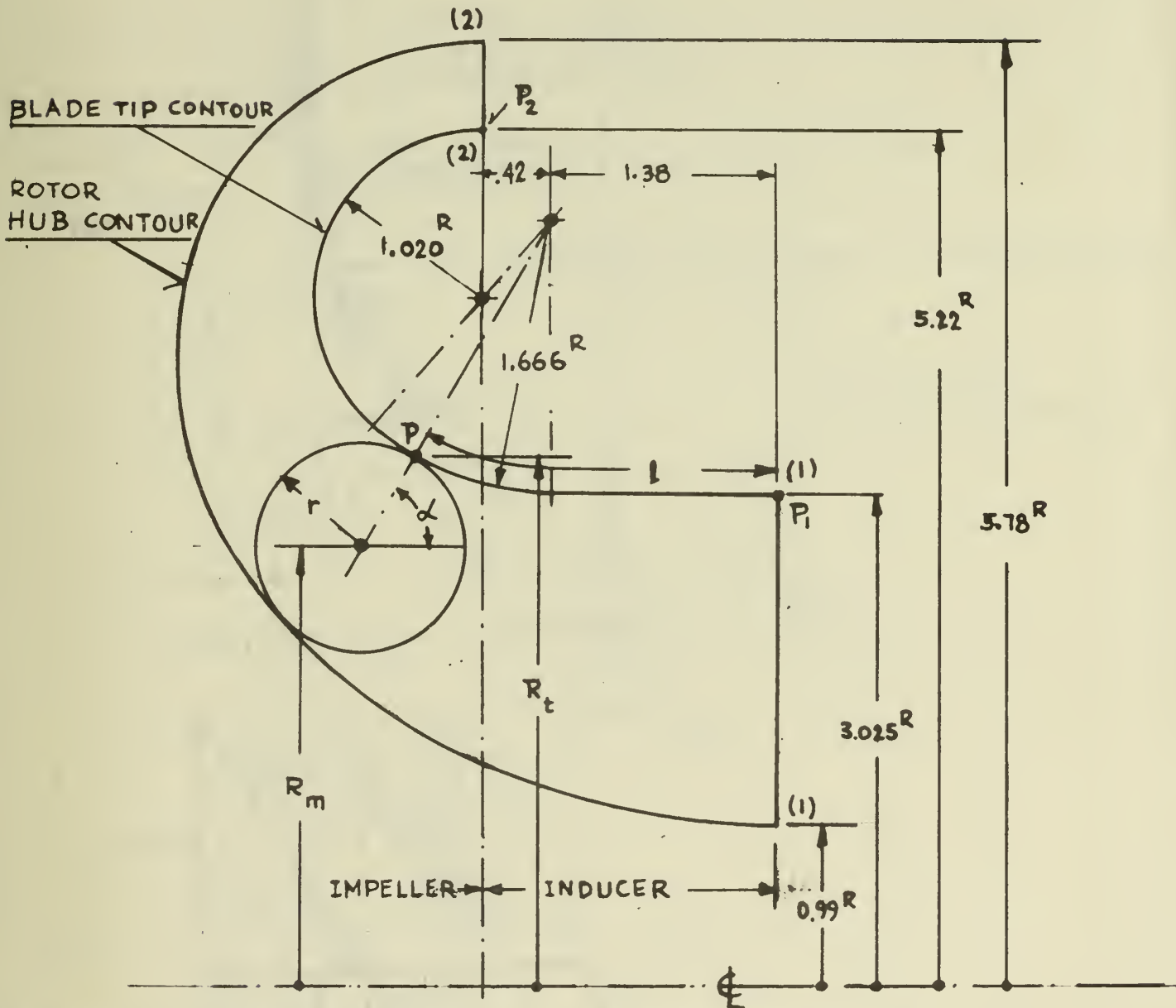


FIG. 2 DETERMINATION OF ROTOR HUB CONTOUR
FOR SPECIFIED BLADE TIP CONTOUR
(TO SCALE)



A_1 = ANNULUS AREA AT (1)-(1) ; A_2 = ANNULUS AREA AT (2)-(2)

AT POINT P: l = LENGTH OF TIP CONTOUR FROM P_1 TO P

l_0 = LENGTH OF TIP CONTOUR FROM P_1 TO P_2

$$A = 2\pi R_m r = A_1 - (A_1 - A_2) \frac{l}{l_0}$$

$$R_m = R_t - r \sin \alpha$$

$$r = \frac{R_t}{2 \sin \alpha} - \sqrt{\left(\frac{R_t}{2 \sin \alpha} \right)^2 - \frac{A_1 - (A_1 - A_2)(l/l_0)}{4\pi \sin \alpha}}$$

FIG. 3 CONDITIONS AT LEADING EDGE OF INDUCER

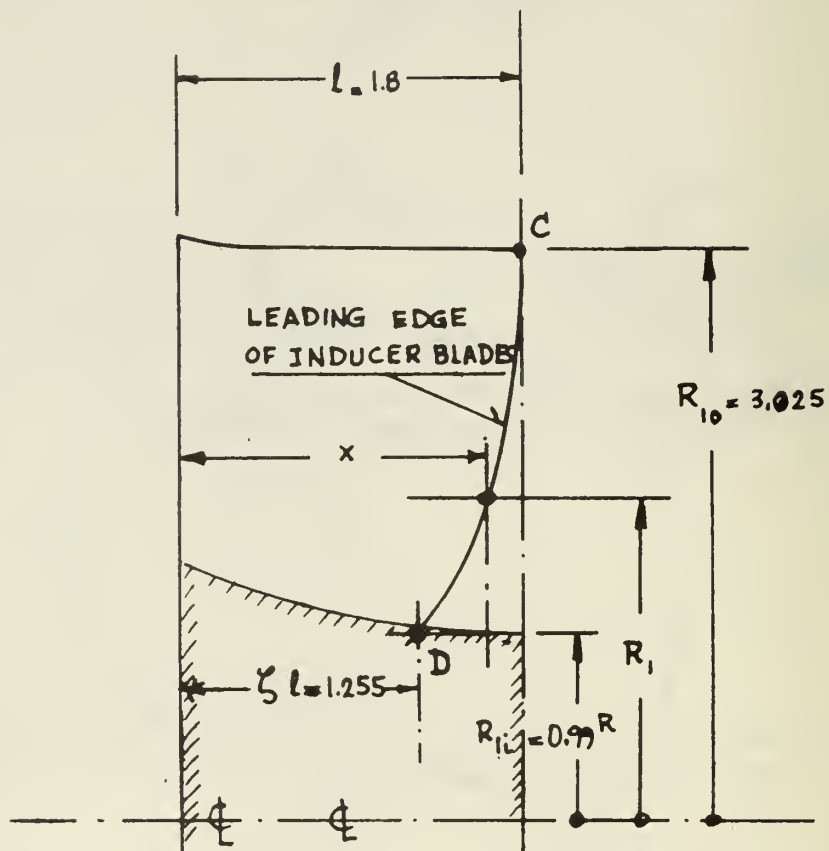


FIG. 3a MERIDIONAL CROSS-SECTION

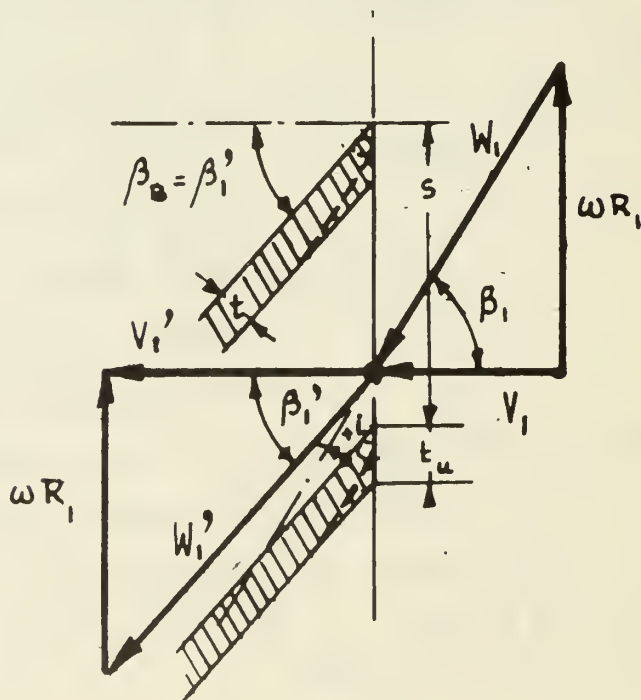
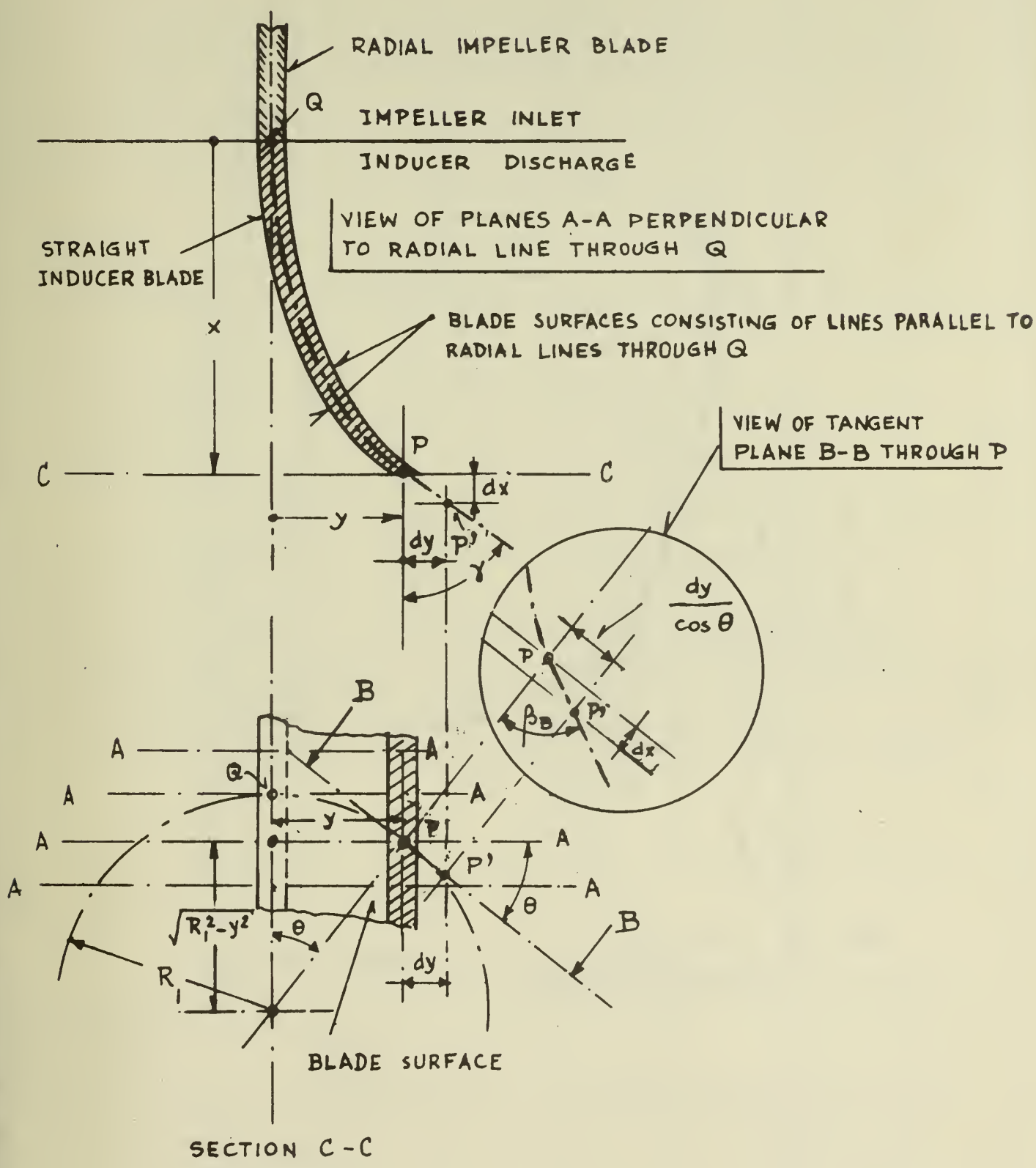


FIG. 3b CONDITIONS AT RADIUS R_1

FIG. 4 BLADE ANGLES OF STRAIGHT INDUCER BLADES



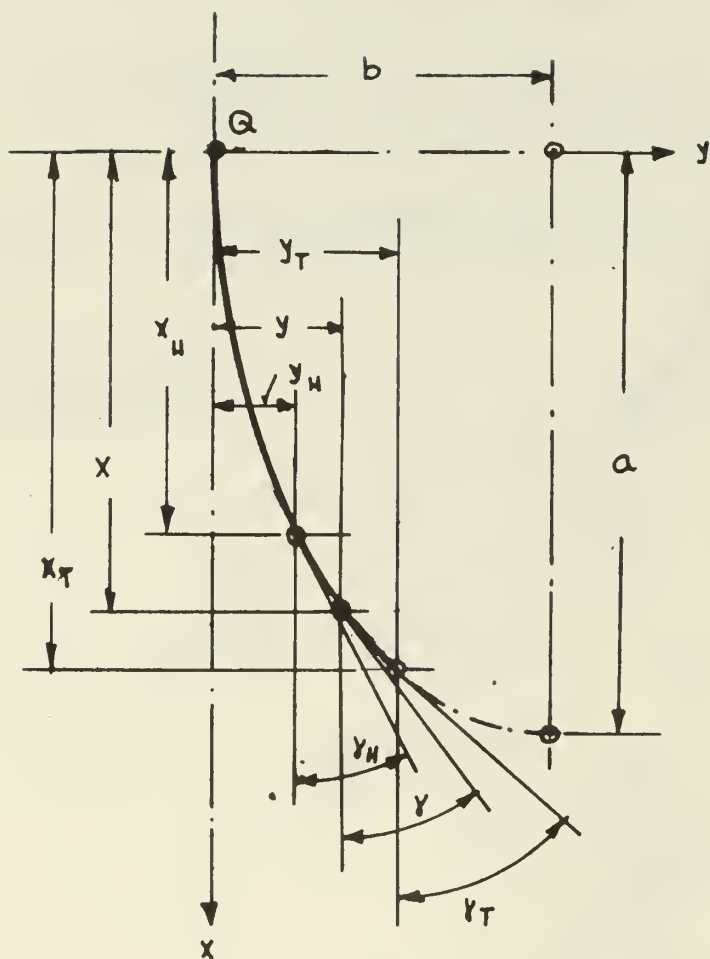


FIG. 5 PROPERTIES OF ELLIPTICAL INDUCER
BLADE SURFACE

FIG. 6 SECONDARY LOSS COEFFICIENT OF REF. 6
 γ_s'' - SECONDARY LOSS COEFFICIENT, γ_t'' - TOTAL LOSS COEFFICIENT
 $\Delta\alpha$ - FLOW DEFLECTION (RADIAN)
 c - BLADE CHORD, h - BLADE HEIGHT

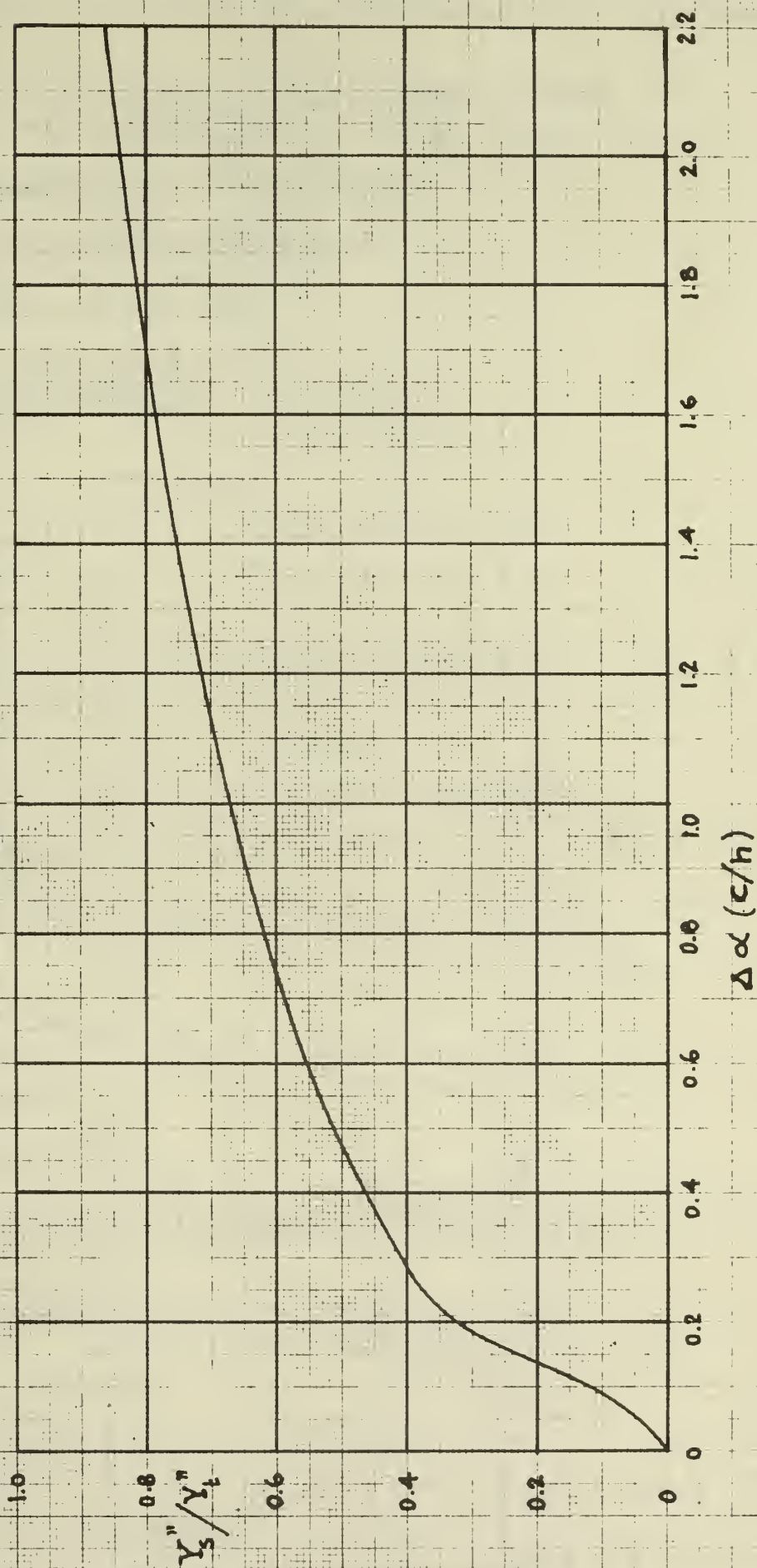


FIG. 7 OVERALL LOSS COEFFICIENTS Y_t' , Y_t'' OF FIRST DIFFUSOR ROW

Y_t' WITH SECONDARY FLOW LOSSES OF EQ. 26
 Y_t'' WITH SECONDARY FLOW LOSSES FROM FIG. 6
 $\Delta\alpha = \alpha_2 - \alpha_3 = 65^\circ - \alpha_3$
 $\sigma = \frac{\text{BLADE CHORD}}{\text{BLADE SPACING}}$

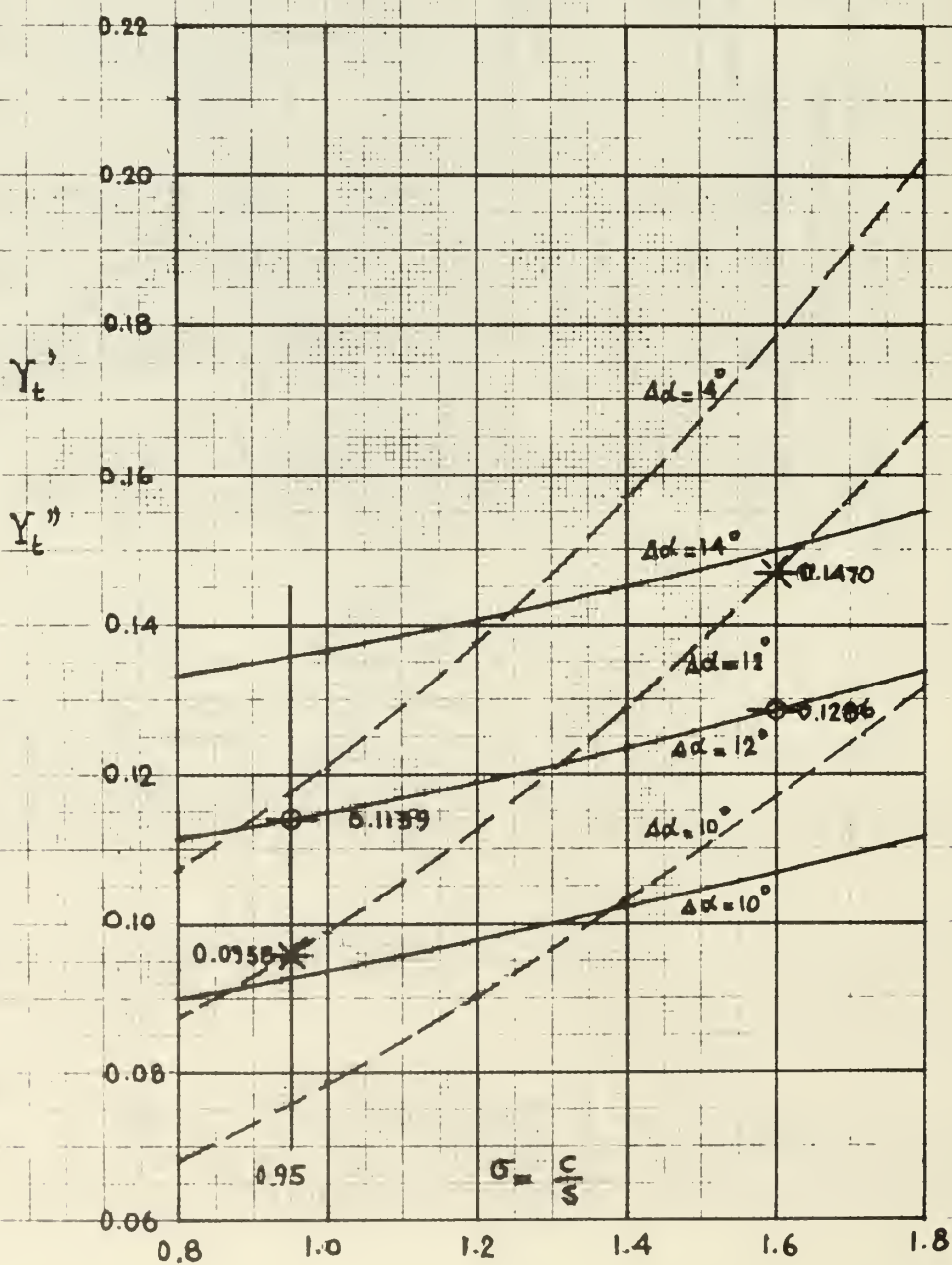


FIG. 8 OVERALL LOSS COEFFICIENTS Y_t' , Y_t'' OF SECOND DIFFUSOR ROW

—— Y_t' WITH SECONDARY FLOW LOSSES OF EQ. 26
 - - - Y_t'' WITH SECONDARY FLOW LOSSES FROM FIG. 6

$$\Delta\alpha = \alpha_3 - \alpha_4 = 53^\circ - \alpha_4$$

$$\sigma = \frac{\text{BLADE CHORD}}{\text{BLADE SPACING}}$$

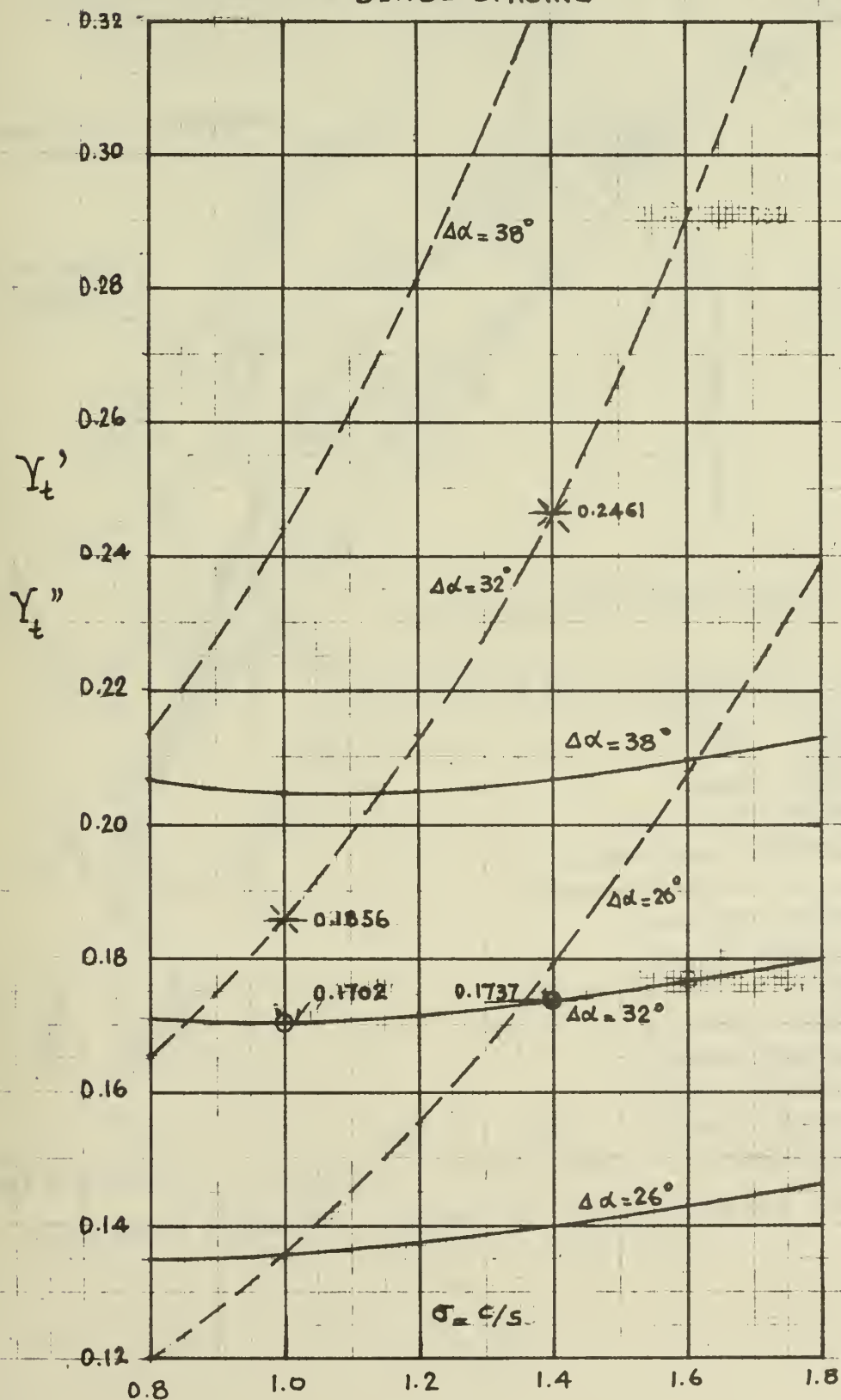
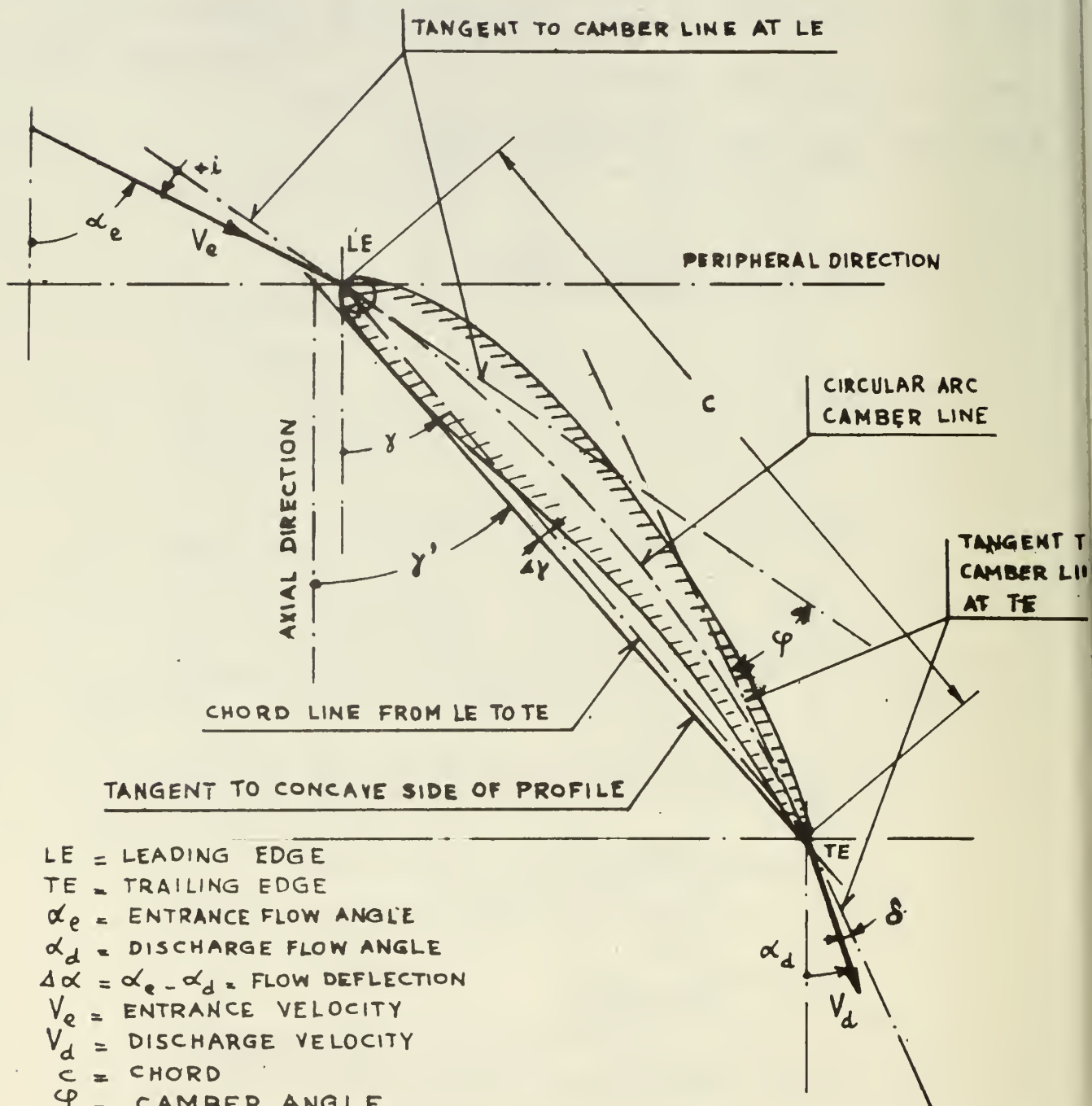


FIG. 9 DIFFUSOR BLADE DATA



LE = LEADING EDGE
 TE = TRAILING EDGE
 α_e = ENTRANCE FLOW ANGLE
 α_d = DISCHARGE FLOW ANGLE
 $\Delta\alpha = \alpha_e - \alpha_d$ = FLOW DEFLECTION

V_e = ENTRANCE VELOCITY
 V_d = DISCHARGE VELOCITY

c = CHORD

ϕ = CAMBER ANGLE

i = INCIDENCE ANGLE

δ = DEVIATION ANGLE

γ = STAGGER ANGLE = $\alpha_e - i - \phi/2$

$\Delta\gamma$ = ANGLE BETWEEN CHORD LINE AND TANGENT TO CONCAVE PROFILE SIDE

$\gamma' = \gamma + \Delta\gamma$ = STAGGER ANGLE OF TANGENT TO CONCAVE PROFILE SIDE

FIG. 10 DETERMINATION OF FLOW CONDITIONS AFTER DIFFUSOR ROW

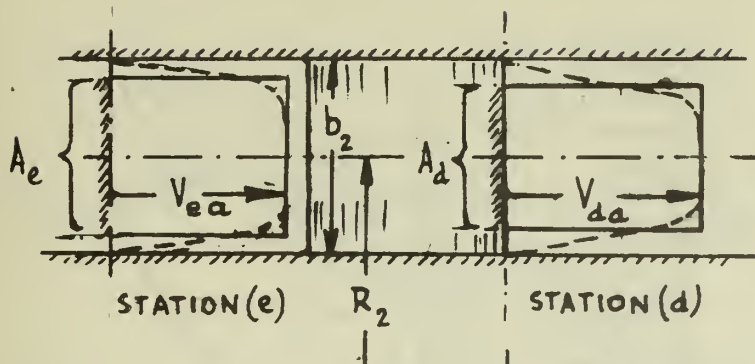


FIG. 10a. MERIDIONAL SECTION

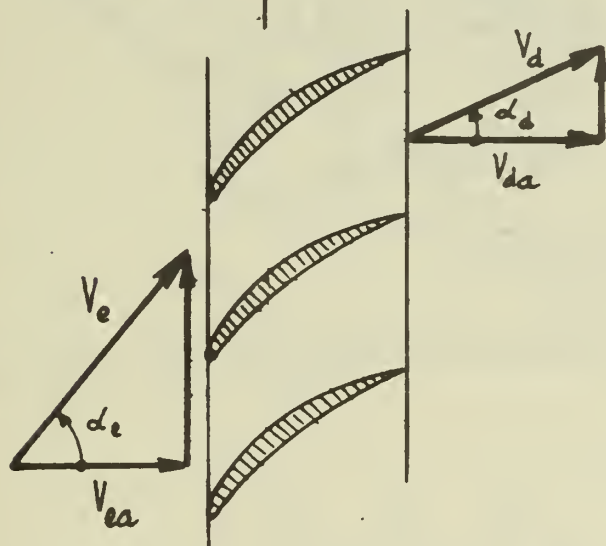


FIG. 10b. DEVELOPED CASCADE AT RADIUS R_2

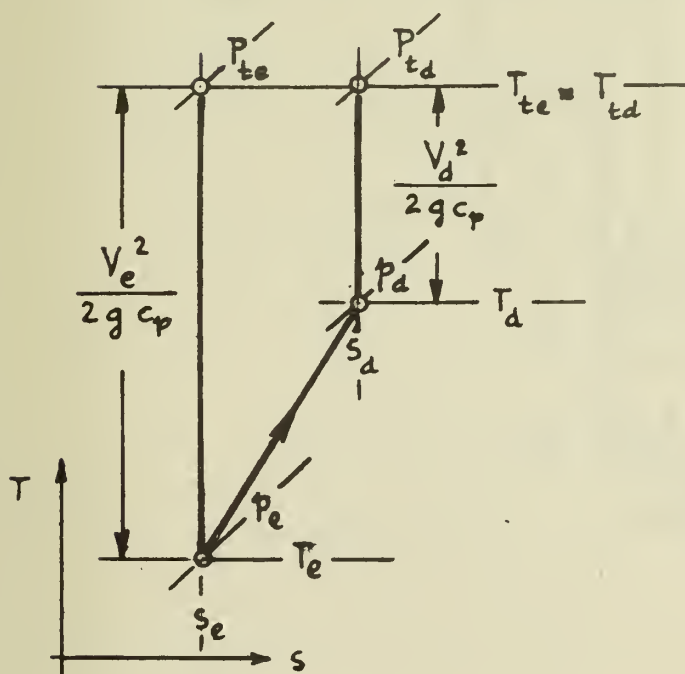


FIG 10c. PROCESS IN ENTROPY DIAGRAM

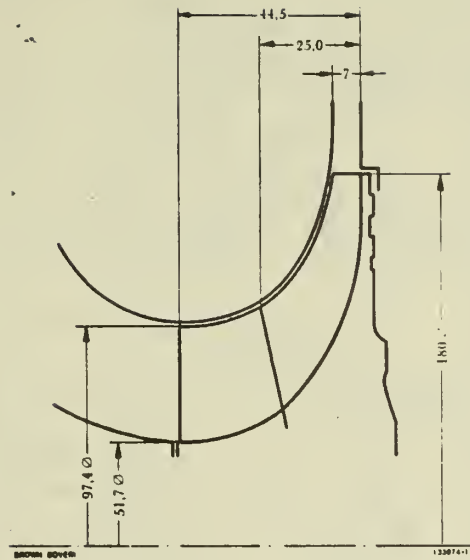


FIG. 12 ROTOR DIMENSIONS

Fig. 12 is identical with Fig. 2 of Ref. 10
(Dimensions are in millimeters)

$$R_{10}/R_2 = 97.4/180 = 0.541$$

$$R_{1i}/R_2 = 51.7/180 = 0.287$$

$$b_2/R_2 = 7/90 = 0.078$$

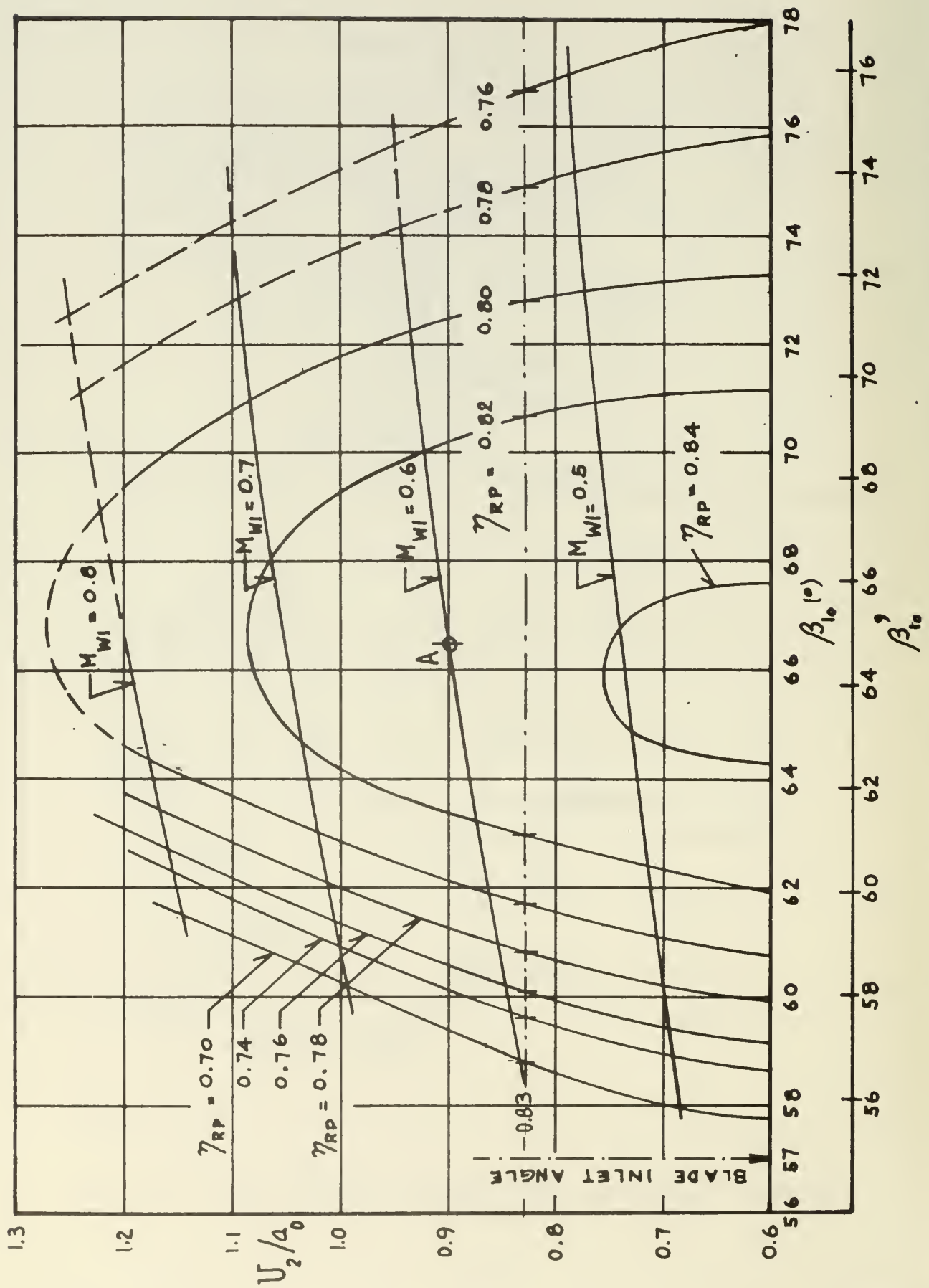
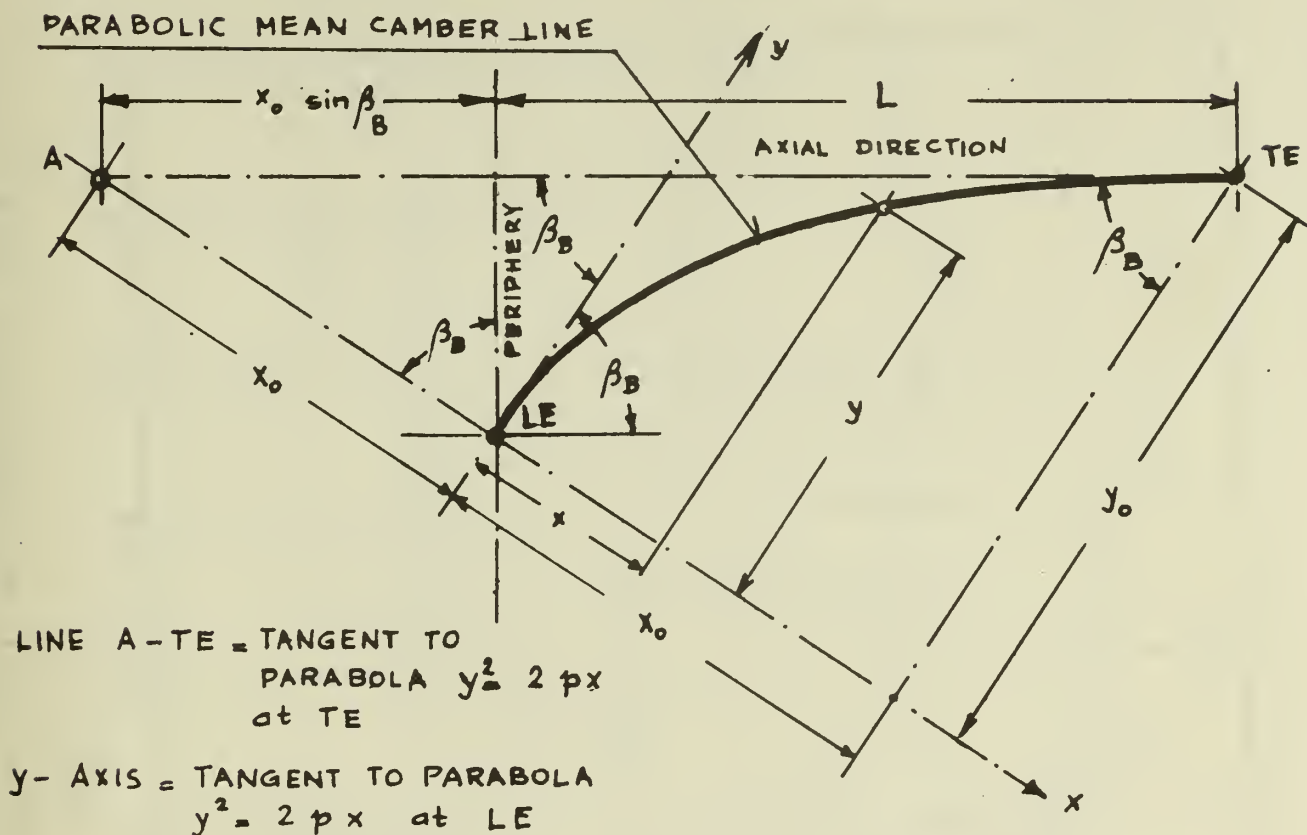


FIG. 13 POLYTROPIC ROTOR EFFICIENCY η_{RP} AS FUNCTION OF FLOW ANGLE β_{10} AT INDUCER TIP RADIUS AND SPEED RATIO U_2/a_0 . (ADAPTED FROM FIG. 4 OF REF. 10)

FIG. 14. ARC LENGTH OF PARABOLIC MEAN CAMBER LINE OF INDUCER BLADE OF AXIAL LENGTH L AND BLADE ANGLE β_B AT LEADING EDGE LE



$$\tan \beta_B = \frac{2x_0}{y_0}$$

$$\rightarrow y_0 = 2x_0 \cot \beta_B$$

$$p = \frac{y_0^2}{2x_0} = 2x_0 \cot^2 \beta_B$$

$$(x_0 \sin \beta_B + L) \sin \beta_B = 2x_0 \rightarrow x_0 = \frac{L}{(2/\sin \beta_B) - \sin \beta_B}$$

$$p = \frac{2L \cot^2 \beta_B}{(2/\sin \beta_B) - \sin \beta_B}$$

m = ARC LENGTH OF CAMBER LINE FROM LE TO TE

$$m = \frac{p}{2} \left\{ \sqrt{\frac{2x_0}{p} \left(1 + \frac{2x_0}{p}\right)} + \ln \left(\sqrt{\frac{2x_0}{p}} + \sqrt{\left(1 + \frac{2x_0}{p}\right)} \right) \right\}$$

EXAMPLE : $\beta_B = 57^\circ$, $L = 19.5$

$$x_0 = 12.61 \quad y_0 = 16.38 \quad p = 10.64 \quad m = 21.51$$

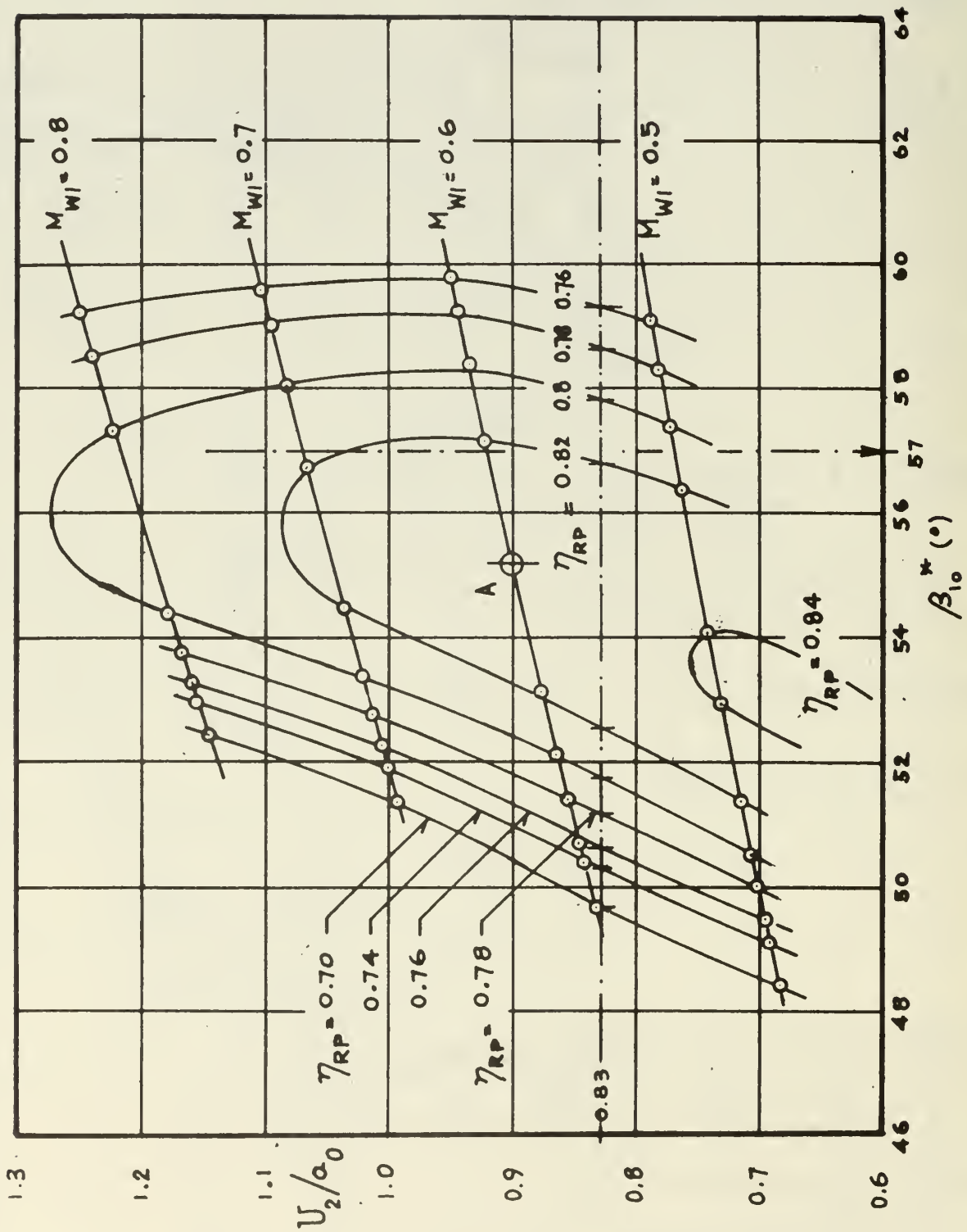


FIG. 15 FLOW ANGLE β_{10}^* CALCULATED FROM EQ.C(4) FOR VALUES OF U_2/a_0 AND M_{WI} OF FIG. 13 FOR $R_{10}/R_2 = 97.4/180 = 0.541$ IN ACCORDANCE WITH FIG. 12

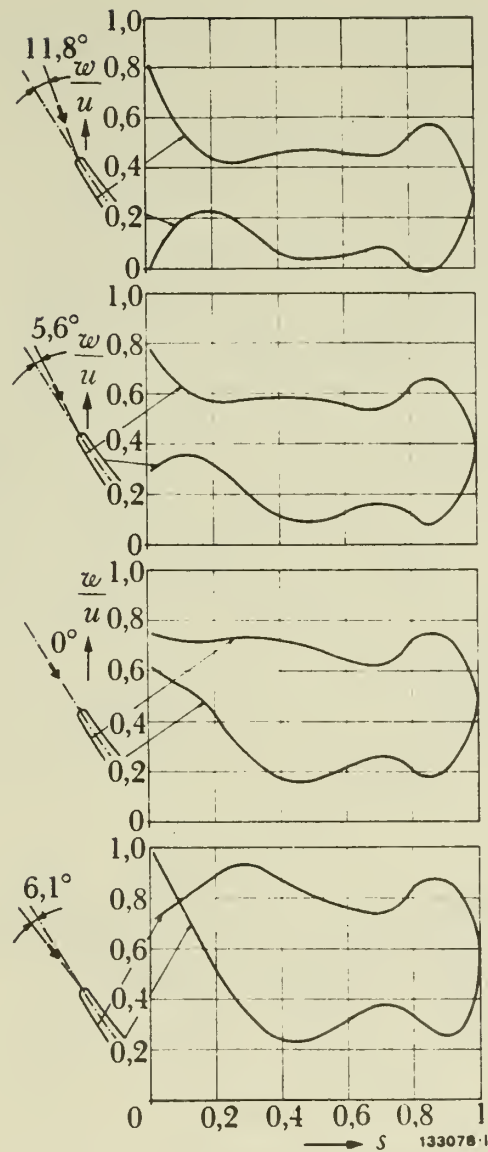


FIG. 16 VELOCITY DISTRIBUTIONS AT INDUCER TIP AT DIFFERENT INCIDENCE ANGLES

w = Relative velocity on blade surface

u = Peripheral speed

s = Distance along parabolic camber line of inducer

(Fig. 16 is identical with Fig. 5 of Ref. 10 and presents velocity distributions that are calculated by ignoring blade thickness, compressibility effects, and friction)

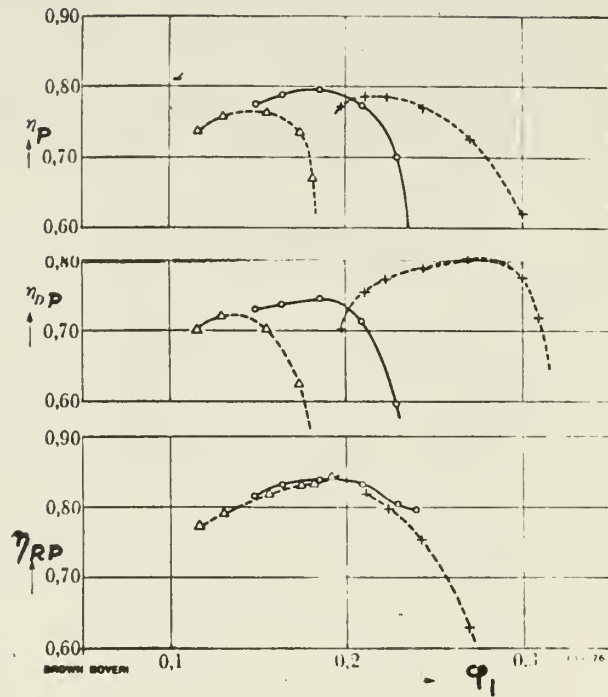


FIG. 17 COMPRESSOR PERFORMANCE AT $U_2/a_0 = 0.83$ OF ROTOR OF FIG. 12 WITH THREE DIFFERENT DIFFUSORS
(Adapted from Fig. 3 of Ref. 10)

η_{RP} = Polytropic Rotor Efficiency

η_{DP} = Polytropic Diffusor Efficiency

η_P = Polytropic Compressor Efficiency

$\phi_1 = Q_1 / (U_2 R_2^2)$

Q_1 = Volume Flow Rate at Inducer Inlet

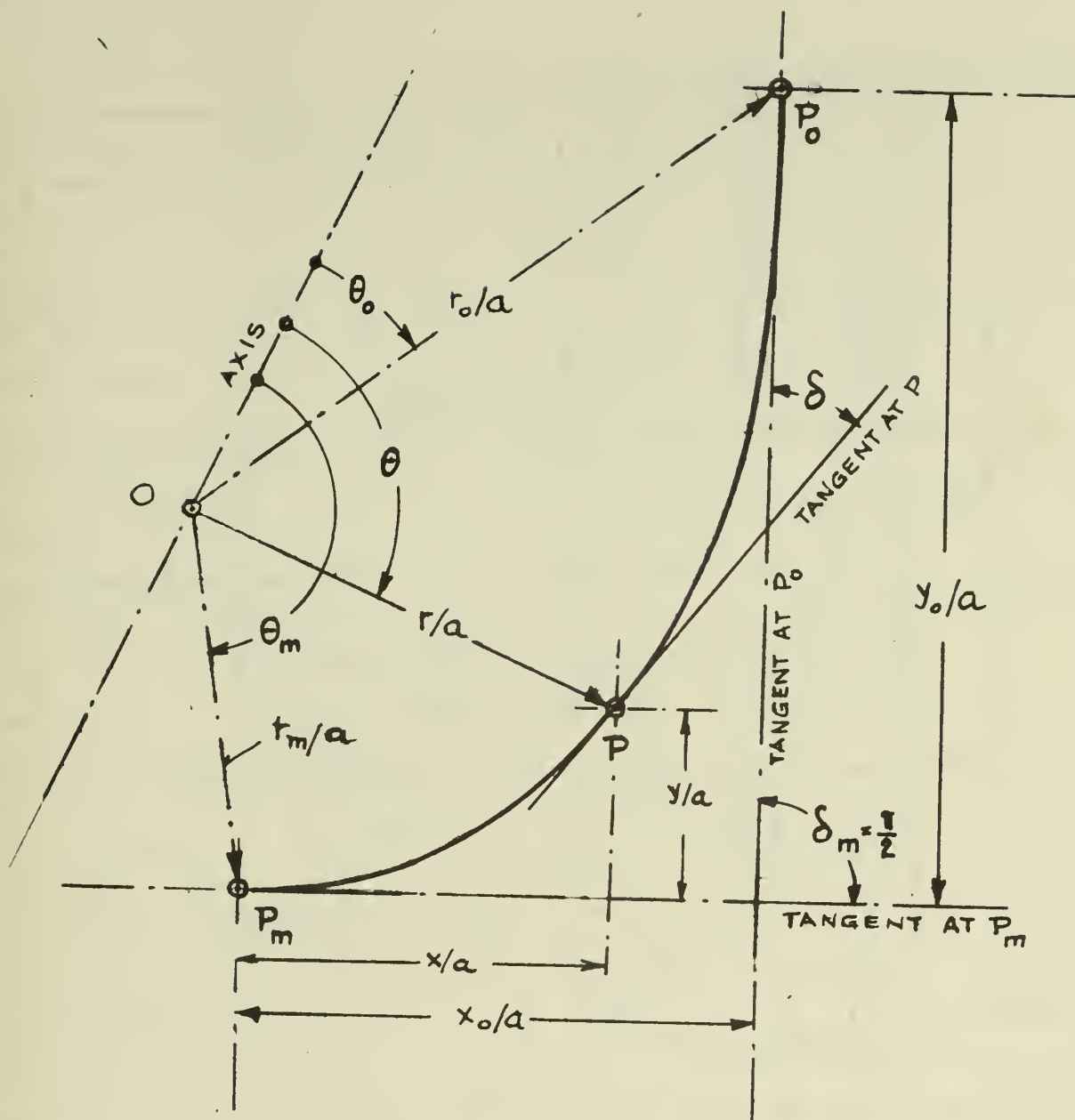


FIG. 18 MERIDIAN CURVE $r/a = \theta^{-b}$ with $\delta_m = \pi/2$

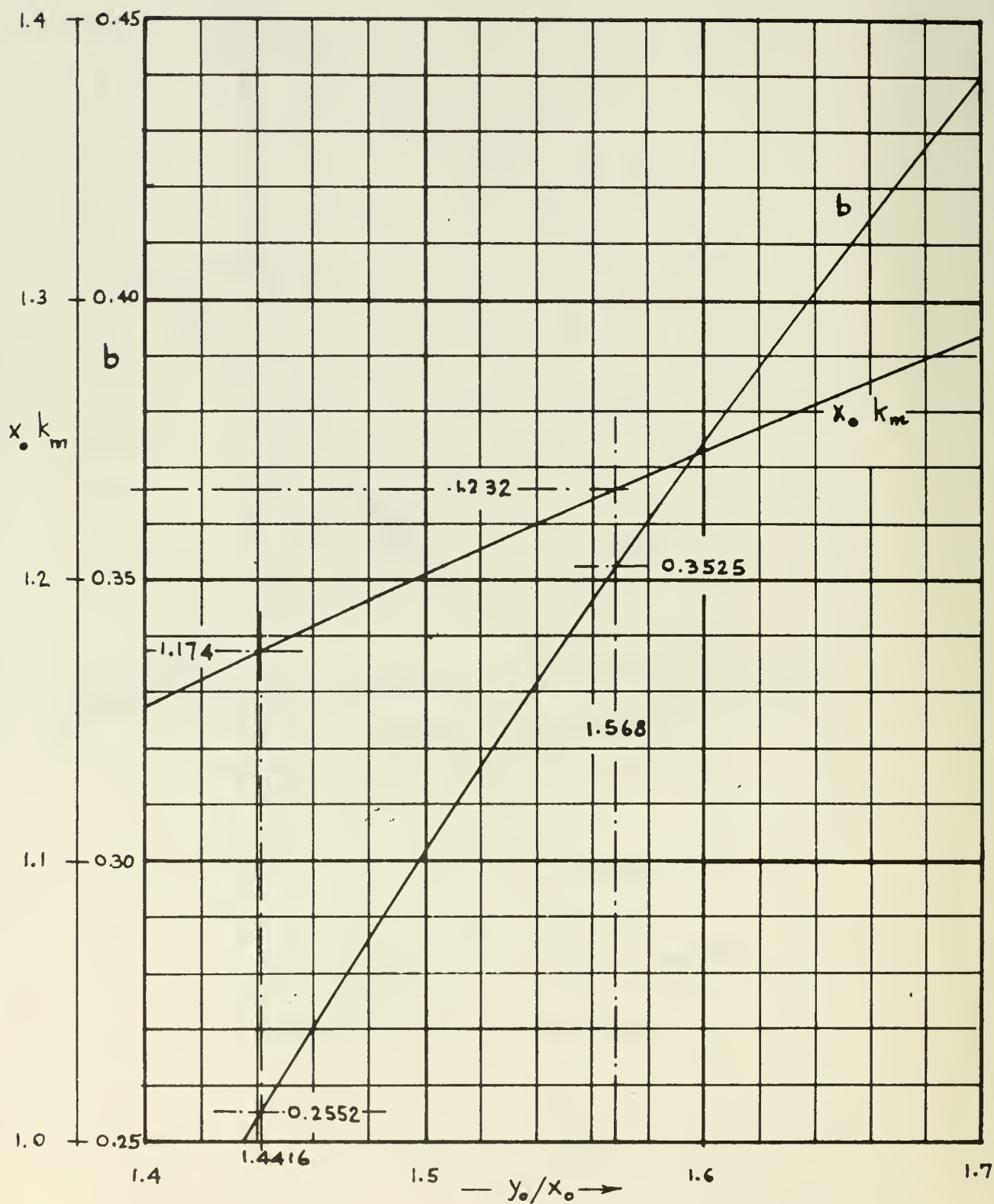


FIG. 19 RELATIONSHIP BETWEEN y_o/x_o , $x_o k_m$ AND y_o/x_o FOR MERIDIAN CURVE OF FIG. 18 CALCULATED WITH PROGRAM No. 110 OF APPENDIX D

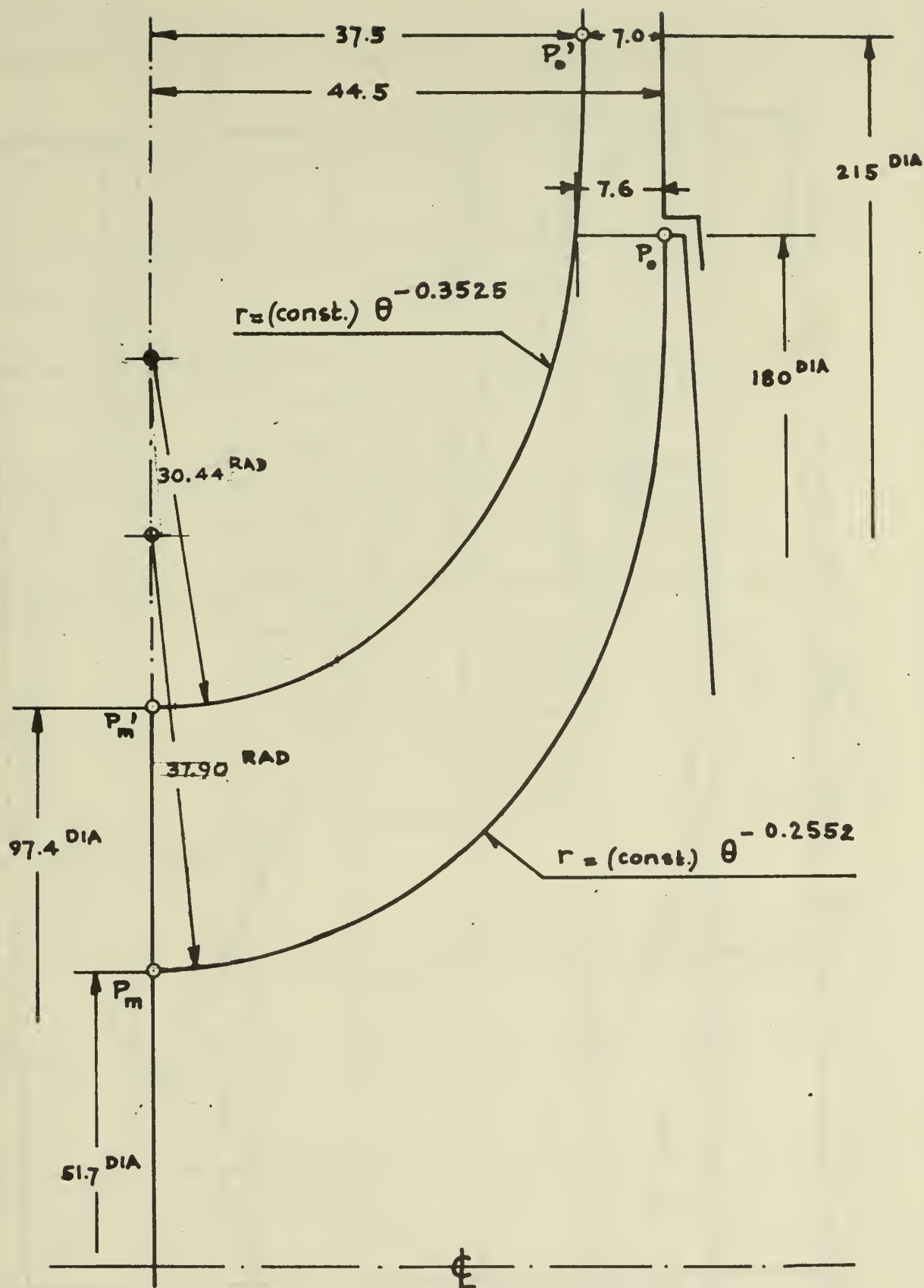


FIG. 20 SCALE DRAWING (2:1) OF MERIDIAN CONTOURS WITH $r/a = \theta^{-b}$ OF IMPELLER
 OF FIG. 12 THROUGH POINTS P_o , P_m , P_o' , P_m' .
 (Dimensions are in Millimeters)

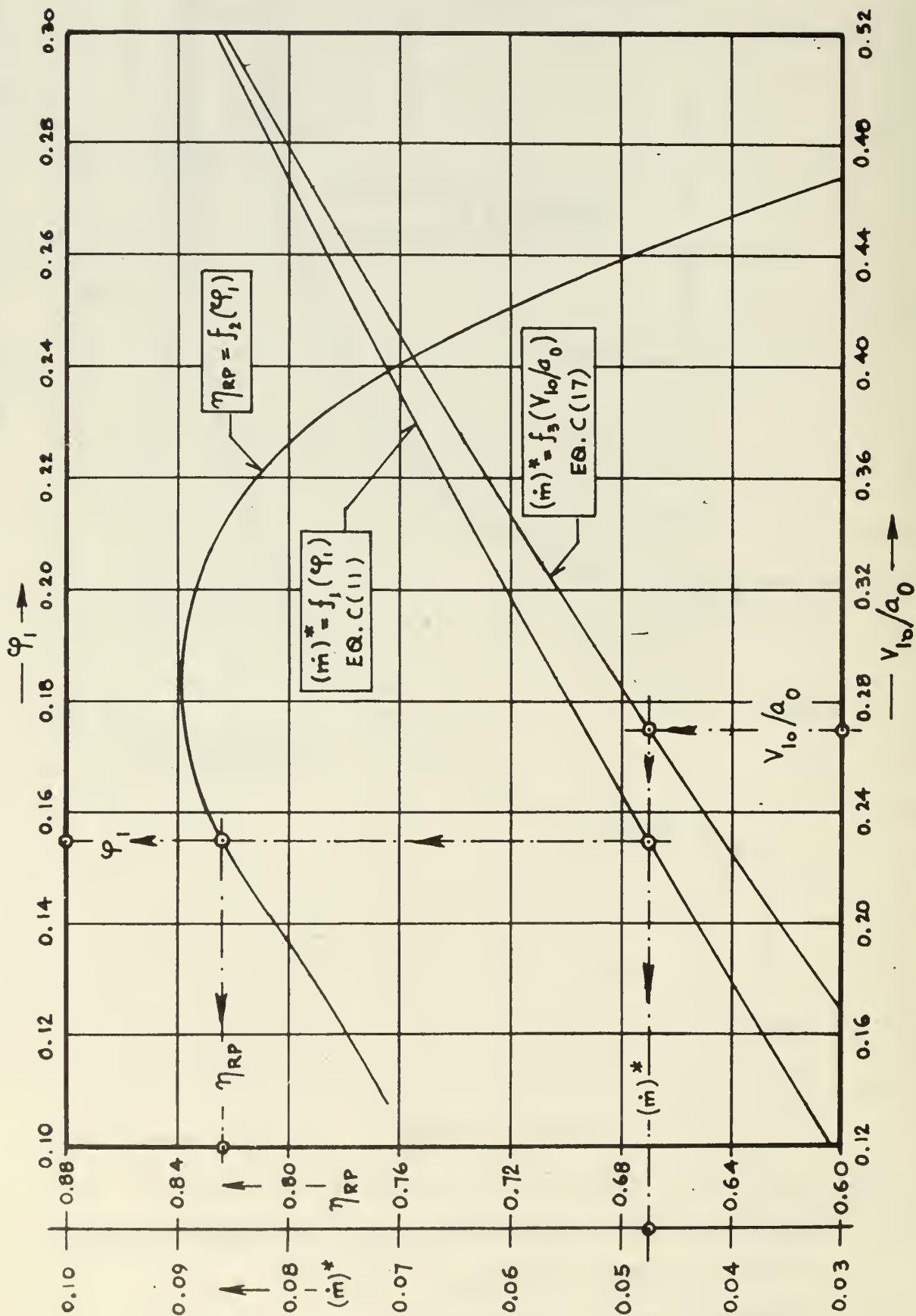


FIG. 21 DIMENSIONLESS MASS FLOW RATE $(\dot{m})^*$ AS FUNCTIONS OF FLOW FUNCTION φ_1 OF FIG. 17, AND V_{10}/a_0 CALCULATED FROM EQ. C(17), WITH POLYTROPIC ROTOR EFFICIENCY η_{RP} FROM FIG. 17 FOR $U/a_0 = 0.83$.

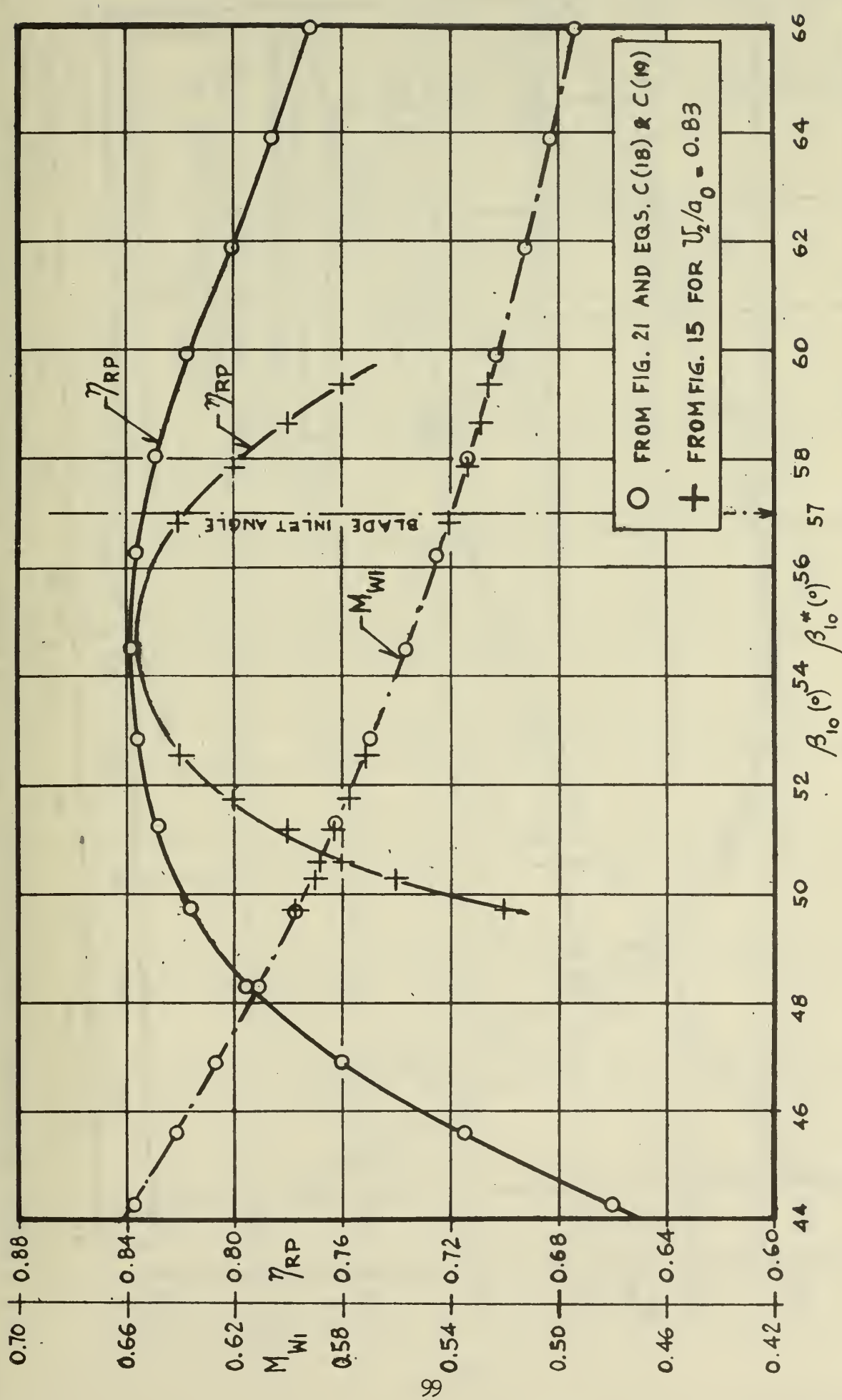


FIG. 22 POLYTROPIC ROTOR EFFICIENCY η_{RP} AND MACH NUMBER M_{w1} FROM FIGS. 21 AND 15, AS FUNCTIONS OF FLOW ANGLE β_{10} , FOR $U_2/a_0 = 0.83$

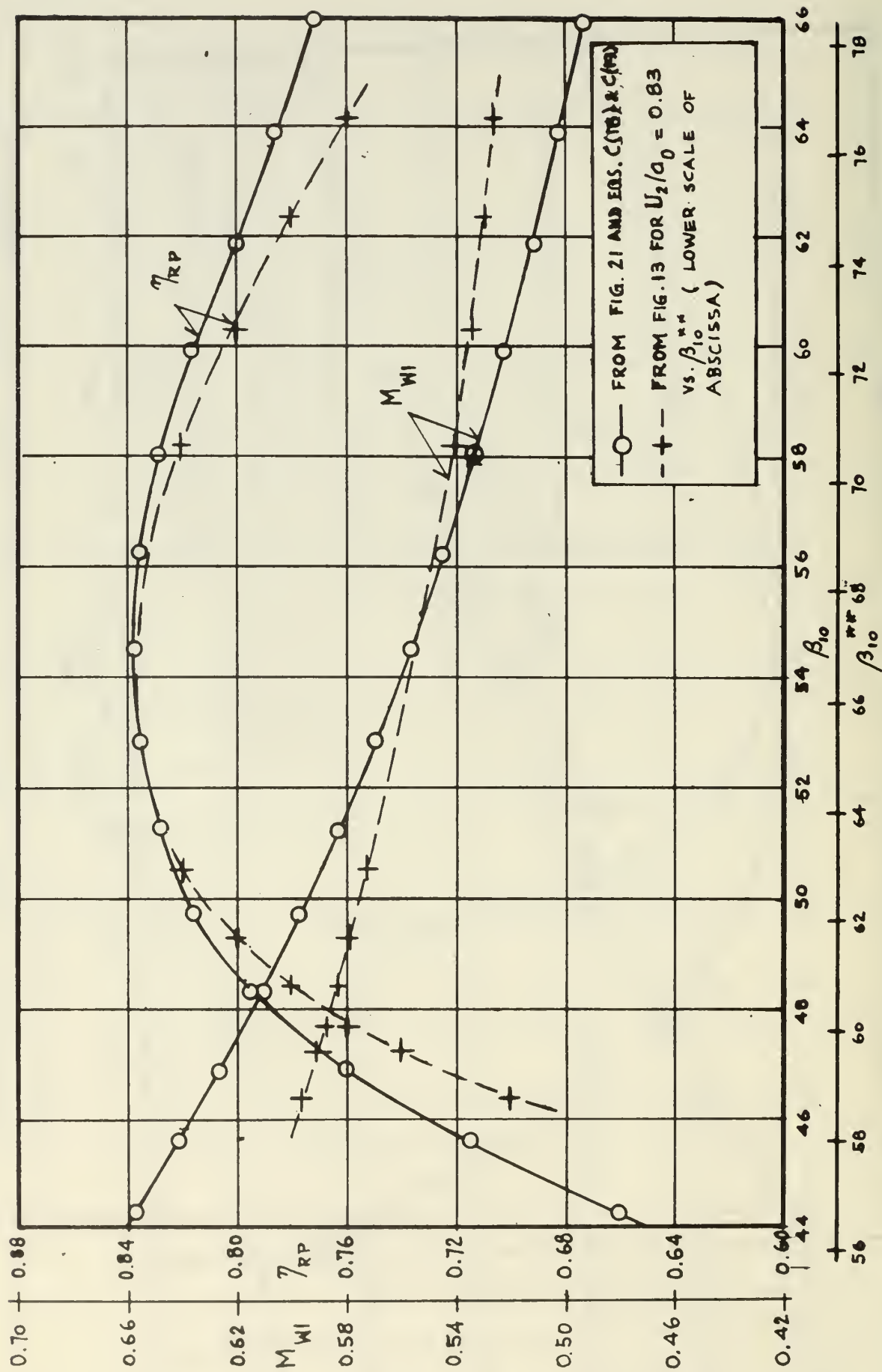


FIG. 23 POLYTROPIC ROTOR EFFICIENCY η_{RP} AND MACH NUMBER M_{WI} AS FUNCTION OF FLOW ANGLE FROM FIG. 21

(UPPER SCALE FOR β_{10}) AND FIG. 13 FOR $U_2/a_0 = 0.83$ (LOWER SCALE FOR β_{10})

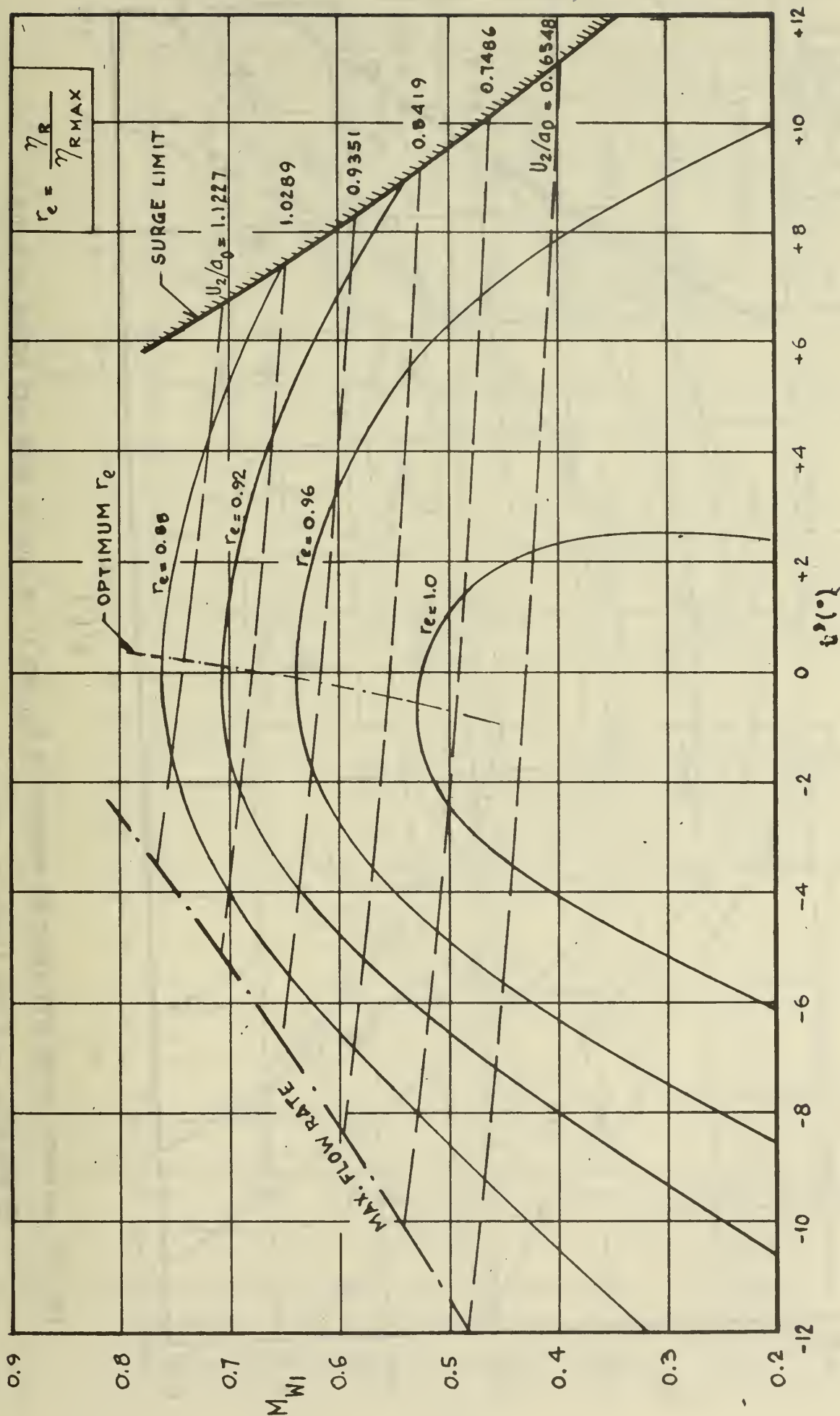


FIG. 24 ADIABATIC ROTOR EFFICIENCY η_R AS FUNCTION OF MACH NUMBER M_{WL} , PERIPHERAL SPEED RATIO U_2/a_0 , AND INCIDENCE ANGLE i' (ADAPTED FROM FIG. 23b OF REF. 2)

-- Curves for $U_2/a_0 = \text{constant}$
 η_{RMAX} = Maximum Adiabatic Rotor Efficiency

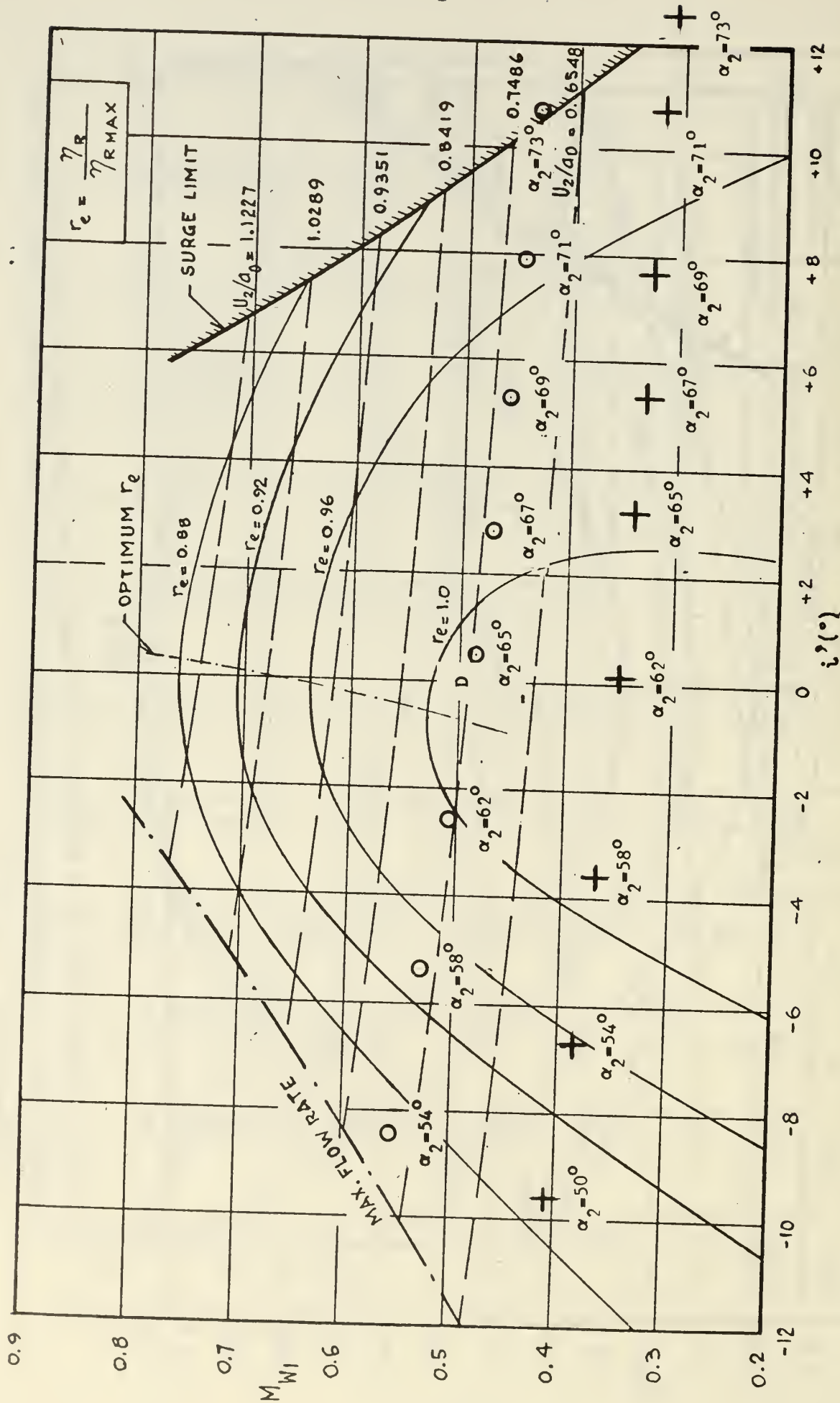


FIG. 25 ADIABATIC ROTOR EFFICIENCY AS FUNCTION OF M_{W1} AND i' OF FIG. 24 WITH DATA POINTS OF TABLE X

\odot FOR $U_2/a_0 = 0.7156$ (TABLE X, SHEET 1)

$+$ FOR $U_2/a_0 = 0.516$ (TABLE X, SHEET 2)

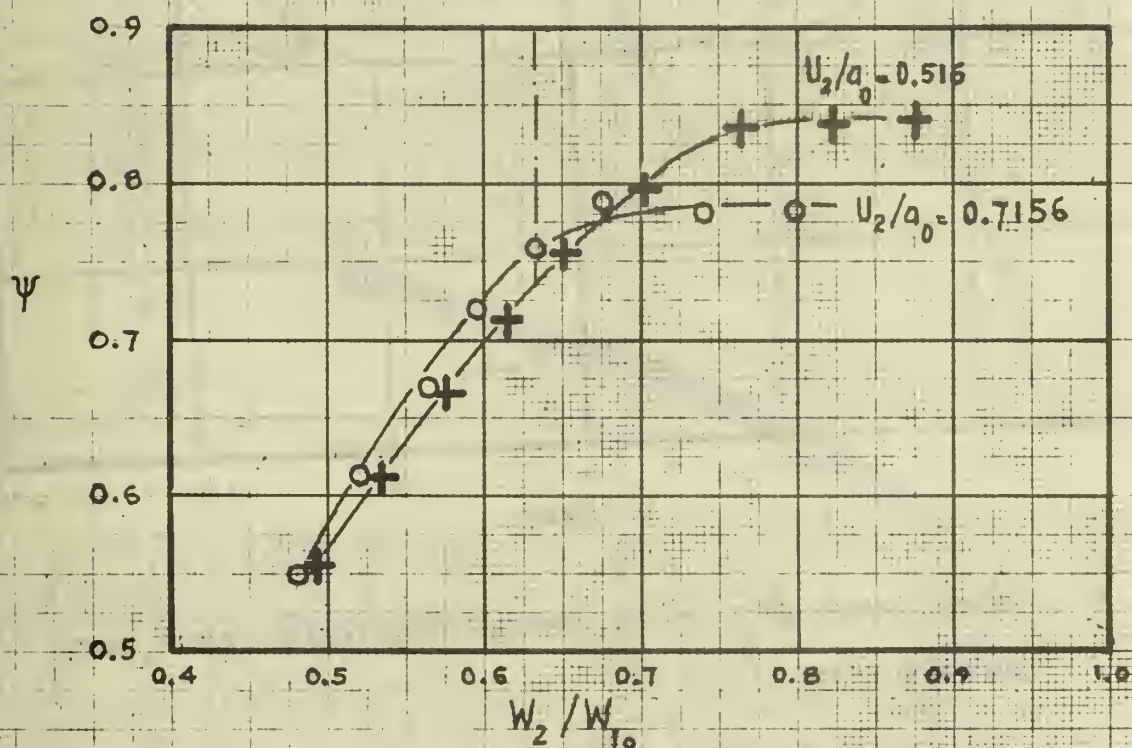
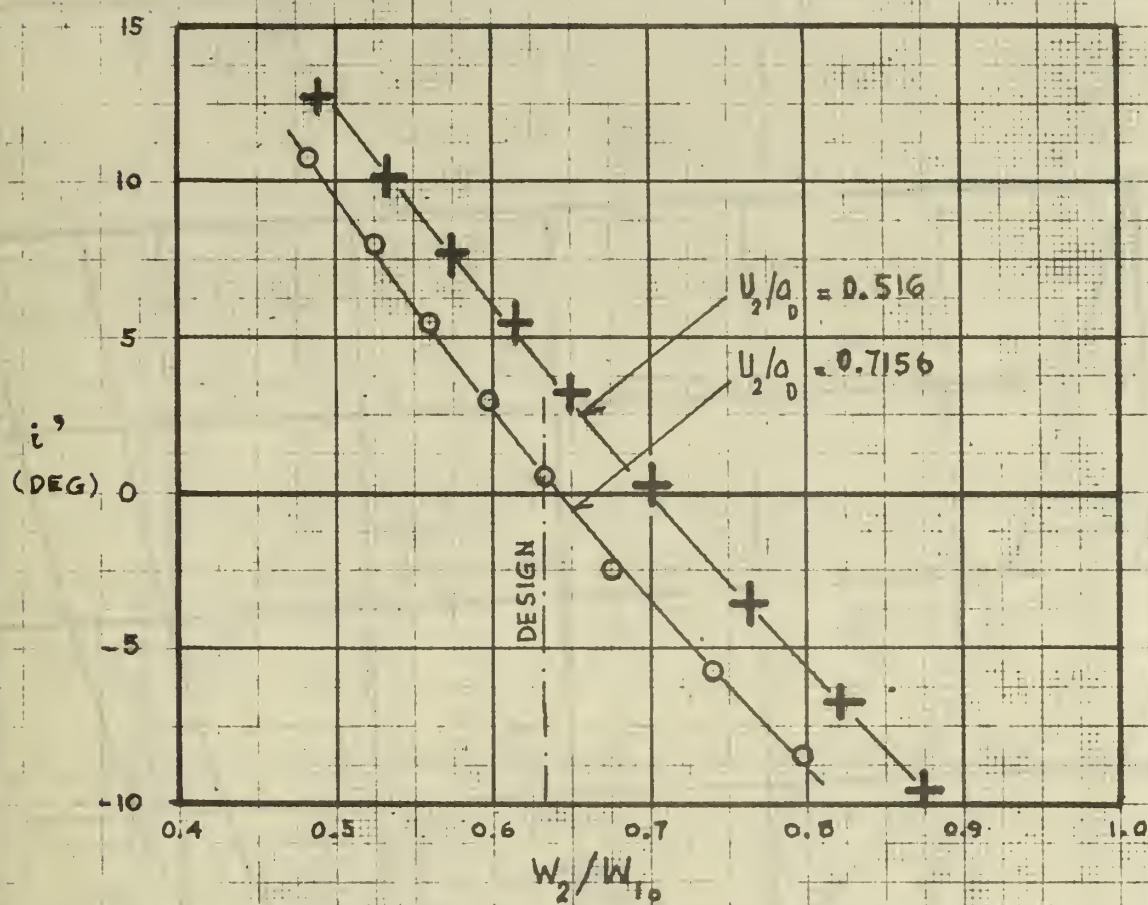


FIG. 26 VELOCITY COEFFICIENT ψ AND INCIDENCE ANGLE i' OF HYBRID COMPRESSOR ROTOR AS FUNCTION OF DECELERATION RATIO W_2/W_{10} OF RELATIVE VELOCITIES FROM DATA OF TABLE X

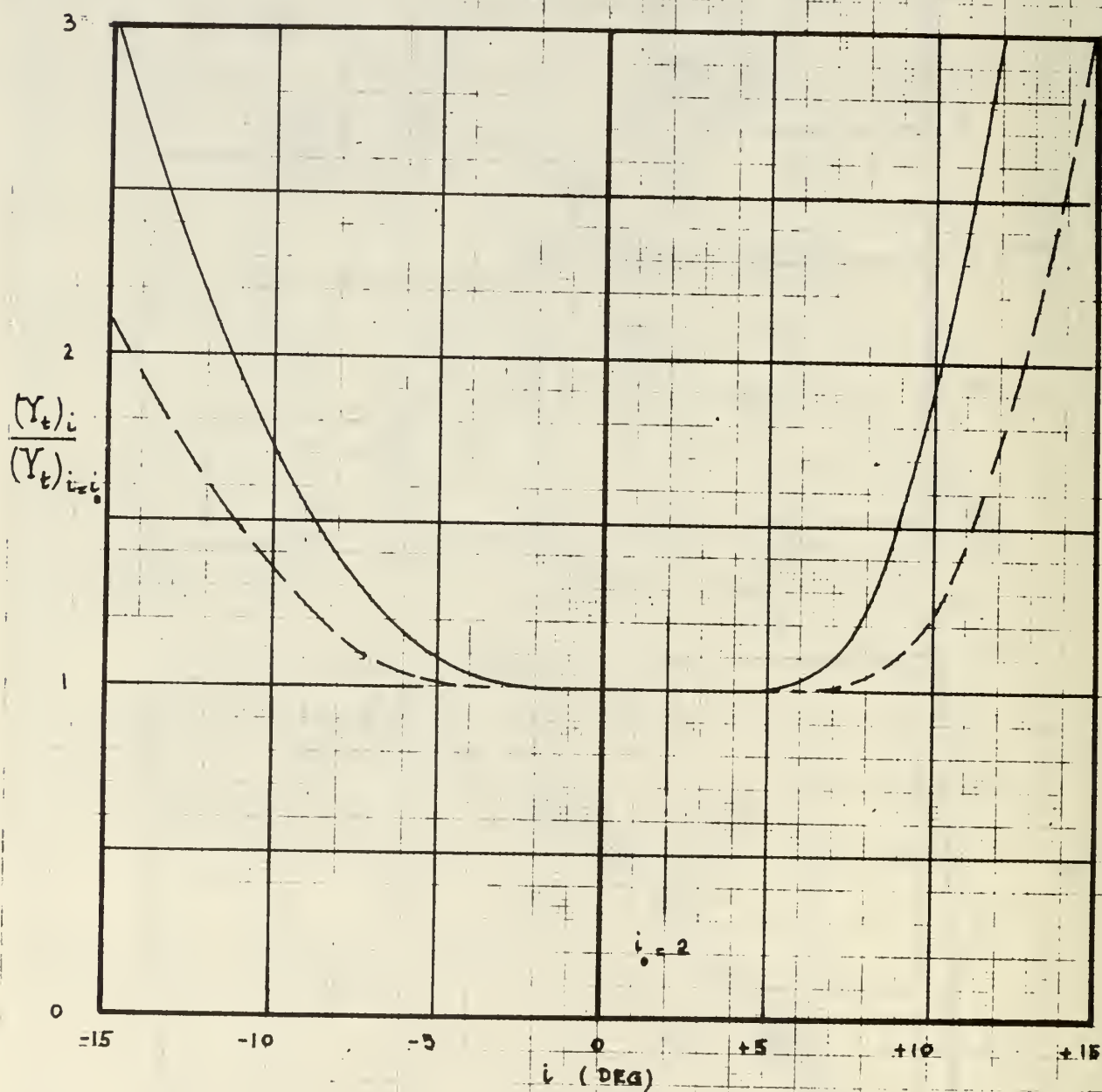
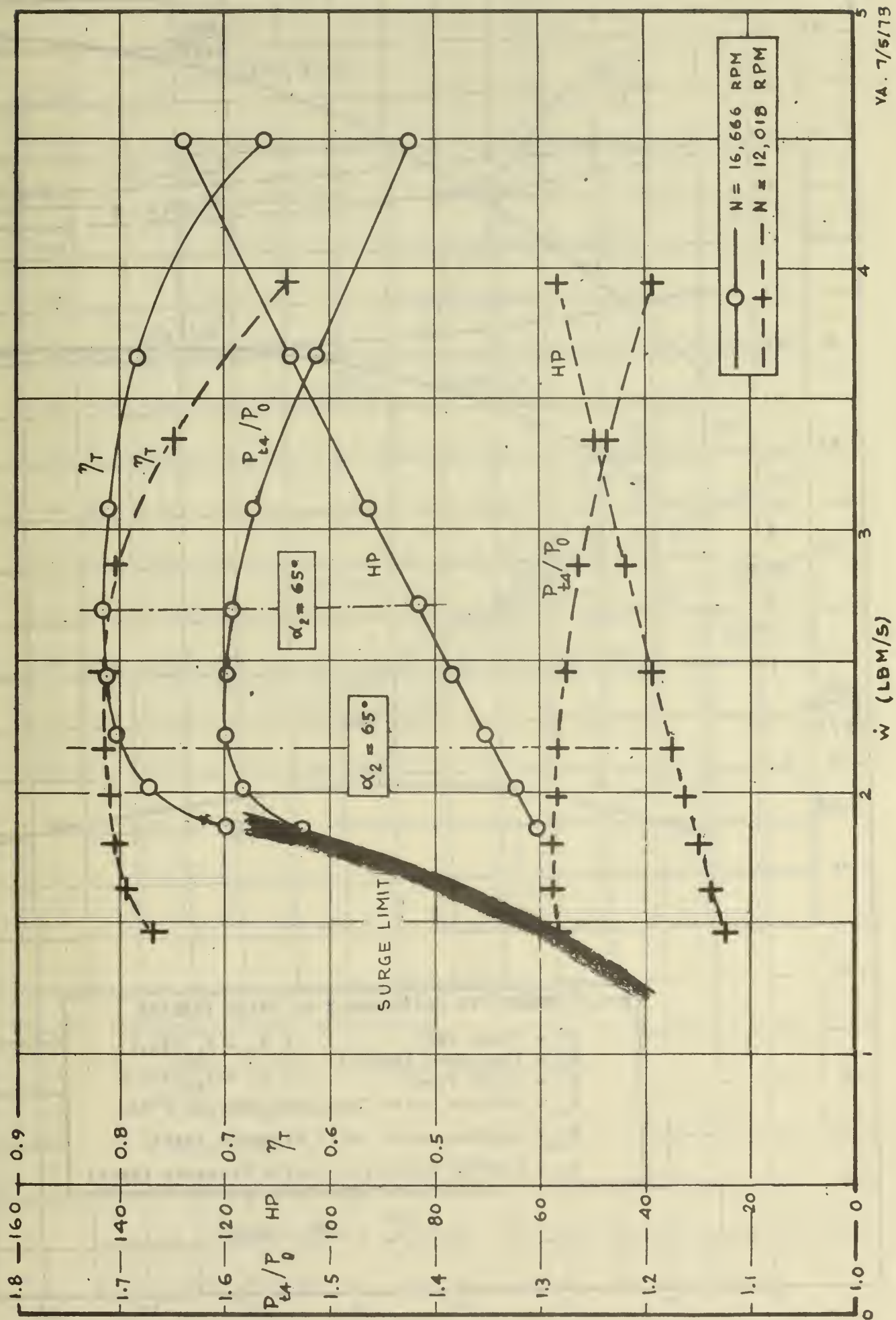


FIG. 27 ASSUMED CHANGE OF DIFFUSOR PRESSURE LOSS COEFFICIENT Y_t WITH INCIDENCE ANGLE i

— $U_2/a_0 = 0.7156$; $0.641 \leq M_{V2} \leq 0.672$

- - - $U_2/a_0 = 0.516$; $0.472 \leq M_{V2} \leq 0.504$

P_{t4}/P_0 = Pressure Ratio; HP = Drive Power; \dot{W}_T = Total-Total Efficiency; \dot{W} = Flow Rate; N = Speed



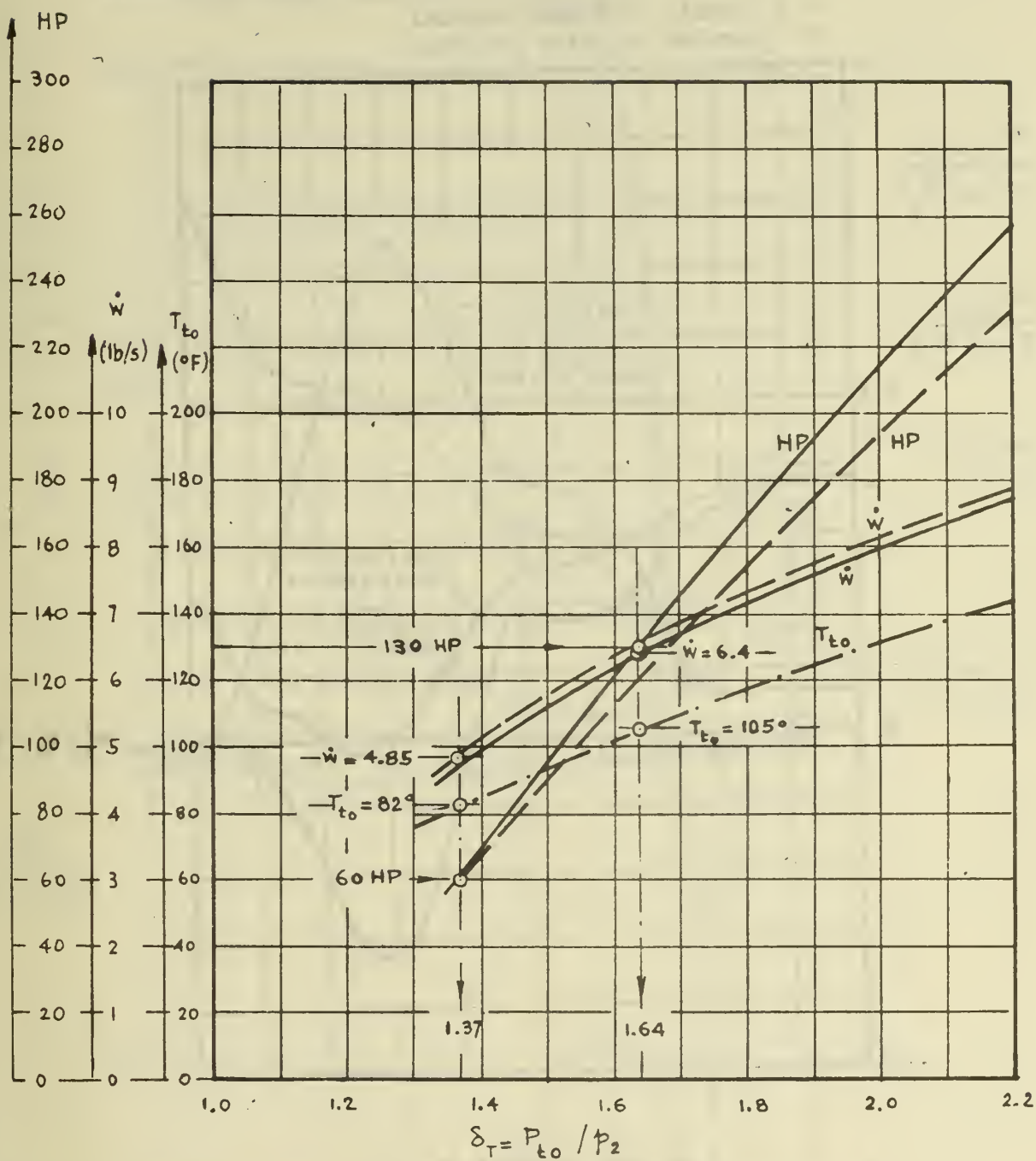


FIG. 30 PREDICTED TURBINE PERFORMANCE

$\delta_T = P_{t0}/p_2$ = Total-to-Static Pressure Ratio

\dot{W} = Flow Rate (lbm/s)

HP = Horse Power

T_{t0} = Turbine Inlet Temperature ($^\circ$ F)

— $N = 16,666$ rpm

- - - $N = 12,018$ rpm

FIG. 31 STRESS DISTRIBUTION IN HYBRID ROTOR
(Method of Schilhansl, Ref. 17)

σ_{RADIAL} = Radial Stress; σ_{HOOP} = Tangential Stress

ρ = Density of Blade Material

ω = Angular Velocity of Rotor

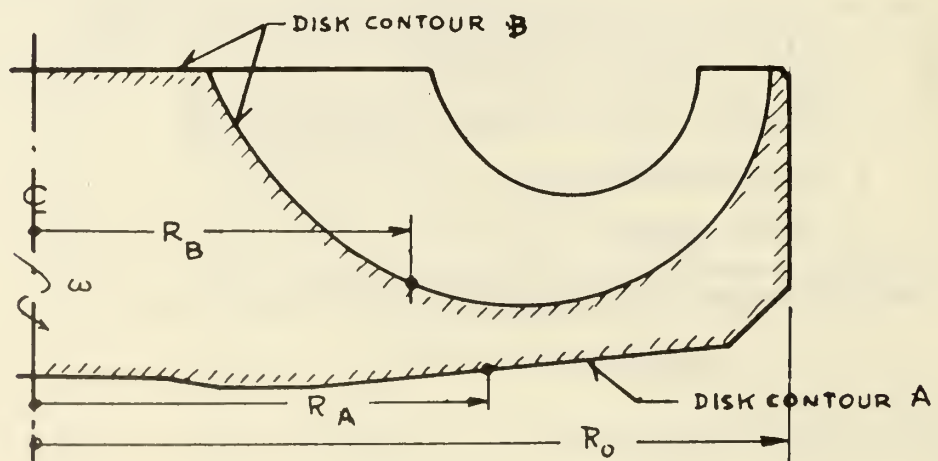
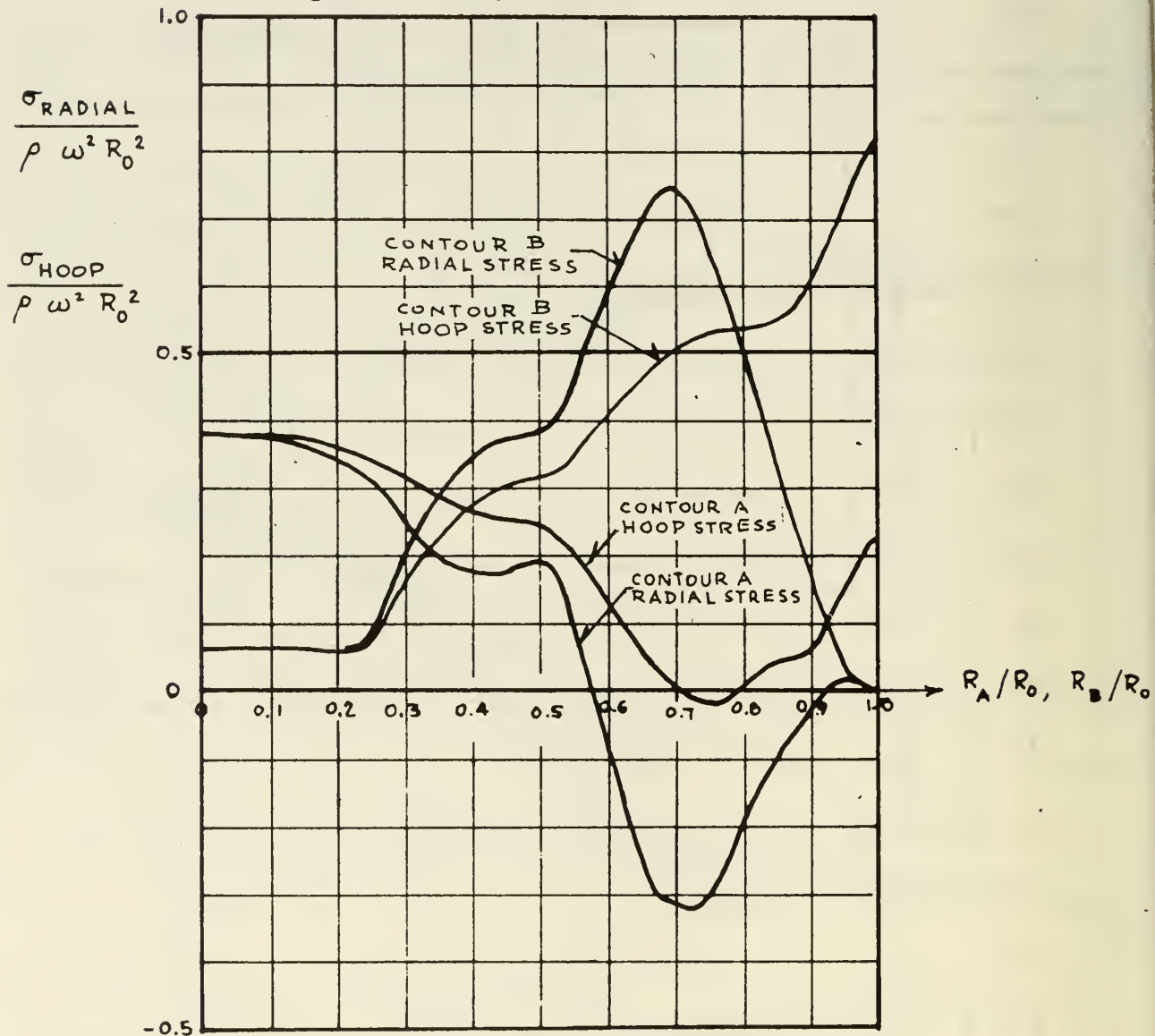
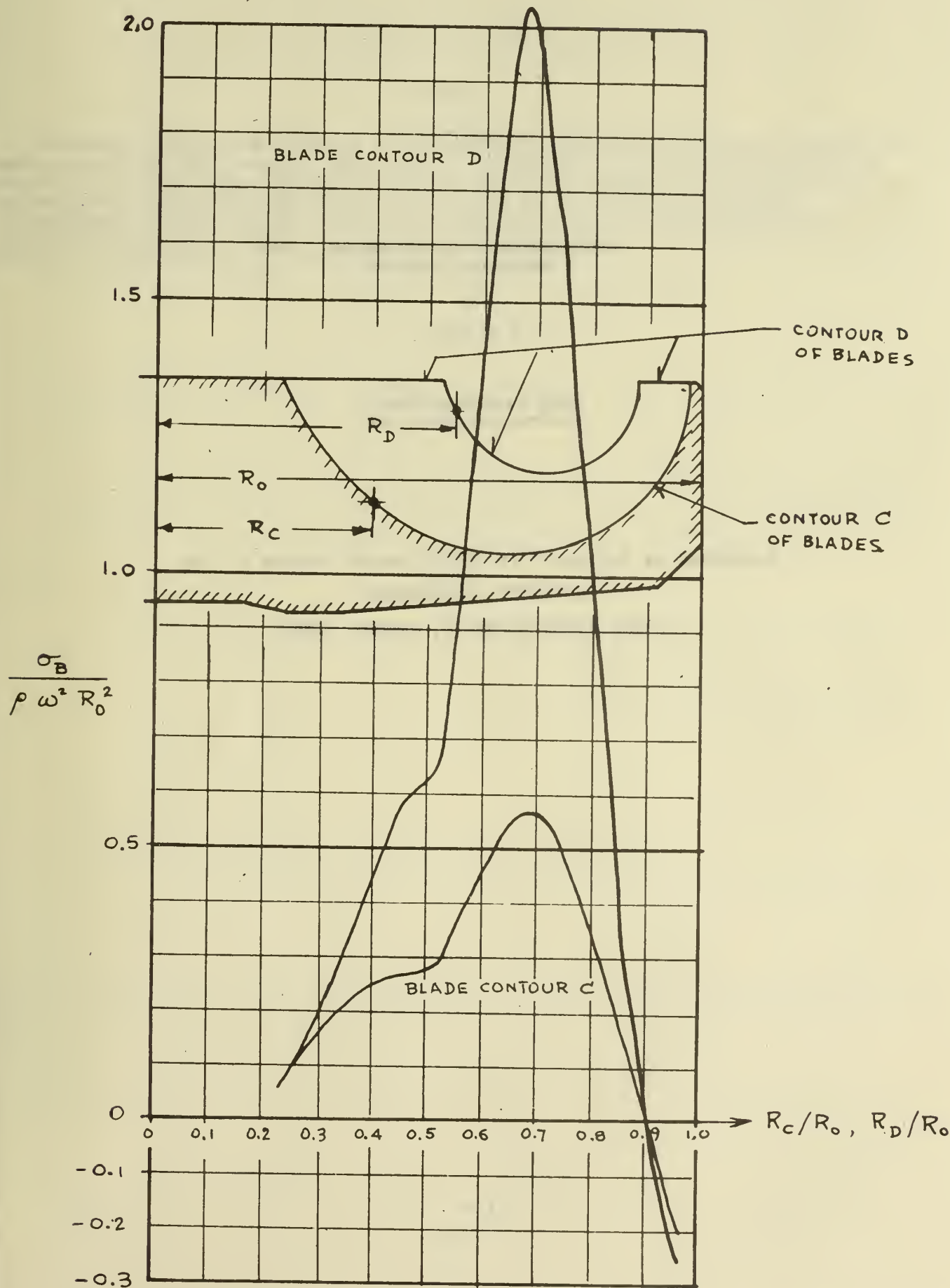


FIG. 32 BLADE STRESSES OF HYBRID ROTOR

(Method of Schilhansl, Ref. 17)

σ_B = Blade Stress

(For other symbols, see Fig. 31)



APPENDIX A

BASIC ELEMENTS FOR ADVANCED DESIGNS
OF RADIAL-FLOW COMPRESSORS

by

M. H. Vavra

Naval Postgraduate School
Monterey, California 93940

Published as Article 6 in AGARD Lecture Series No. 39

"ADVANCED COMPRESSORS"

NATO, AGARD-LS-39-70, London 1970

SUMMARY

Dimensionless parameters are presented for the design of compressors with axial inlet velocities and radial blades at the rotor discharge. These parameters take account of the compressibility of the flow and hold for arbitrary fluids. They permit to evaluate the effect of changes of the design variables on the conditions of state of the fluid at different locations, and on the geometry of the design. Loss relationships are discussed and their effects on performance are shown. The design parameters are compared with the so-called specific speed criteria to show that the latter do not satisfy the laws of similarity if compressibility effects are taken into account.

BASIC ELEMENTS FOR ADVANCED DESIGN OF RADIAL-FLOW COMPRESSORS

M. H. Vavra

1. INTRODUCTION

Under consideration are high-speed centrifugal compressors with rotors of the type shown in Fig. 1 that have radial blades at the discharge and where the absolute inlet velocities are in axial direction. With a straight annular inlet duct these inlet velocities will be uniform between the radii R_{1i} and R_{1o} of the impeller eye. For a particular relative flow angle β_{1o} and the relative velocity W_{1o} at R_{1o} , there is then known the peripheral speed U_{1o} , which, for chosen radius ratios R_2/R_{1o} , establishes the peripheral rotor speed U_2 at R_2 . The average relative velocity W_2 at the discharge of a rotor with radial blades is not radial, but has an average angle β_2 . With the slip factor μ there is

$$\beta_2 = \tan^{-1} \frac{(1-\mu) U_2}{V_{m2}} \quad (1)$$

where V_{m2} is the average meridional velocity at the rotor discharge. Equation 1 is a consequence of the definition of the slip factor

$$\mu = \frac{V_{u2}}{U_2} \quad (2)$$

For a simplified analysis of the compressor performance that assumes uniform conditions at the rotor discharge not only in peripheral but also in axial direction, across the blade width b_2 , and for axial absolute velocities V_1 at the rotor inlet, the specific work ΔH_w necessary to drive the compressor is from moment of momentum consideration, for an assumed adiabatic process,

$$\Delta H_w = \mu U_2^2 \quad \left(\frac{\text{ft-lb}}{\text{slug}} \right) \quad (3)$$

For a perfect gas with $\gamma = c_p/c_v = \text{constant}$, the actual rise in total temperature ΔT_w in the rotor is

$$\Delta T_w = \frac{\Delta H_w}{c_p} = \frac{\mu U_2^2}{c_p}$$

With the gas constant R_G there is

$$c_p = R_G \frac{\gamma}{\gamma-1} \quad (4)$$

Let

$$a_0 = \sqrt{\gamma R_G T_{t1}} = \sqrt{\gamma R_G T_0} \quad (5)$$

be the velocity of sound at the total inlet temperature $T_{t1} = T_0$. Then

$$\frac{\Delta T_w}{T_0} = \mu (\gamma-1) \left(\frac{U_2}{a_0} \right)^2 \quad (6)$$

For an isentropic compression process from the total inlet pressure $P_0 = P_{t0} = P_{t1}$ to the discharge pressure P_{t4} , the necessary work required would be $c_p \Delta T_{is}$, where

$$\Delta T_{is} = T_0 \left[\left(\frac{P_{t4}}{P_0} \right)^{\frac{\gamma-1}{\gamma}} - 1 \right] \quad (7)$$

The compressor efficiency η_c is defined by

$$\eta_c = \frac{\Delta T_{is}}{\Delta T_w} = \frac{\left(\frac{P_{t4}}{P_0} \right)^{\frac{\gamma-1}{\gamma}} - 1}{\mu (\gamma-1) \left(\frac{U_2}{a_0} \right)^2} \quad (8)$$

For a particular design the following data are usually prescribed:

\dot{m}	-	mass flow rate (slug/s)
P_0	-	total inlet pressure (psia)
T_0	-	total inlet temperature ($^{\circ}\text{R}$)
P_{t4}	-	discharge pressure (psia)
γ	-	ratio of specific heats c_p and c_v
R_G	-	gas constant ($\frac{\text{ft-lb}}{\text{slug} \cdot ^{\circ}\text{R}}$)

With the indicated units, which are frequently used for engineering purposes, a quantity of mass is in slugs which is derived from the chosen units of force, length, and time. However, the relations which are going to be established hold for any consistent system of units, hence also for one where the primary units are mass, length and time, and where forces are in derived units.

For the given conditions there are to be found the following data for an optimum design:

U_2	-	peripheral rotor speed at R_2
b_2/R_2	-	<u>ratio of axial impeller width at discharge</u> outer radius of impeller
R_{10}/R_2	-	<u>outer radius at rotor inlet</u> outer radius of impeller
R_{11}/R_{10}	-	<u>inner radius at rotor inlet</u> outer radius at rotor inlet
ω	-	angular velocity of impeller (radians/s)
β_{10}	-	relative flow angle at R_{10}
α_2	-	absolute flow angle at R_2
R_3/R_2	-	<u>radius at inlet lip of diffuser blades</u> outer radius of impeller
R_4/R_2	-	<u>radius at discharge of diffuser</u> outer radius of impeller

Important design criteria are also:

$$M_{W1} = \frac{W_{10}}{a_1} - \text{Mach number of relative velocity } W_{10} \text{ at outer radius } R_{10} \text{ at impeller inlet}$$

$$M_{V2} = \frac{V_2}{a_2} - \text{Mach number of absolute velocity } V_2 \text{ at impeller discharge}$$

Mechanical and fluid dynamics considerations impose design limits of:

- U_2 , because of permissible rotor stresses
- R_{10}/R_2 , which cannot exceed about 0.70 to 0.75 to obtain an outer rotor contour with acceptably small curvatures in the meridinal plane
- R_{11}/R_{10} , which, if too small, does not permit the arrangement of a sufficiently large number of rotor blades Z_R with reasonable thickness
- β_{10} , which cannot be larger than about 70° for manufacturing reasons
- b_2/R_2 , which cannot be smaller than certain limits to obtain good efficiencies
- α_2 , which cannot exceed 70° to 80° because of manufacturing reasons and because of poor diffuser performance, especially if M_{V2} is larger than unity.

2. COMPRESSION PROCESS

Figure 2 is a temperature-entropy diagram showing the thermodynamic process in the compressor of Fig. 1. The temperature differences in Fig. 2 correspond roughly to the velocities of the triangles of Fig. 1 to obtain a realistic representation. Since by Eq. 6 the work input ΔT_w is also $\Delta T_w = \mu (U_2^2/c_p)$, the temperature rise $T_2 - T_1$ in the rotor is roughly one-half of ΔT_w . Later on the so-called degree of reaction r^* will be introduced to determine this ratio more precisely.

Station (1) in Fig. 2 corresponds to the static condition at the rotor inlet, given by the static pressure p_1 and the static temperature T_1 . The total pressure and total temperature at this station are $P_{t1} = P_0$ and $T_{t1} = T_0$. For the isentropic process between (0) and (1).

$$\frac{T_{t1}}{T_1} = \frac{T_0}{T_1} = 1 + \frac{\gamma-1}{2} M_{V1}^2 \quad (9)$$

and

$$\frac{p_{t1}}{p_1} = \frac{p_0}{p_1} = \left(\frac{T_0}{T_1}\right)^{\frac{\gamma}{\gamma-1}}$$

where

$$M_{V1} = \frac{V_1}{a_1} = \frac{V_1}{[\gamma R_G T_1]^{\frac{1}{2}}}$$

is the Mach number of the absolute velocity V_1 at the rotor inlet.

The conditions of state at all locations can be expressed with the parameters U_2/a_0 , R_{10}/R_2 , M_{W1} , β_{10} , α_2 , μ , and loss coefficients that establish the entropy increments between the different stations, if it is assumed that the flow process along the outer contour of the rotor between the radii R_{10} and R_2 is representative of the rotor flow in general. The later assumption is made because the relative velocity W_1 and the relative flow angle β_1 are higher at R_{10} than at other radii R_1 . Hence along the outer rotor contour from R_{10} to R_2 there occur the highest deceleration ratio W_{10}/W_2 and the largest flow deflection $\Delta\beta = \beta_{10} + \beta_2$. Moreover since the path travelled by a fluid particle along the outer rotor contour is shorter than that travelled by a particle entering at other radii R_1 , the conditions along the outer rotor contour will establish design limitations and have a critical influence on the rotor losses.

With the chosen parameters, Eq. 9 can be rewritten

$$\frac{T_1}{T_0} = \frac{1}{1 + \frac{\gamma-1}{2} M_{W1}^2 \cos^2 \beta_{10}}$$

This formula is also given by Eq. I(5) of Table I. This table has been arranged to list the pertinent relations for the determination of the flow properties in the compressor for ready reference. In the following only the main steps will be indicated that led to these formulas without going into the details of their derivations. Some of the equations, for instance Eq. I(6), can be obtained directly from Fig. 2. It can be noted that all temperatures are given as multiples of the total inlet temperature $T_0 = T_{t1}$, and pressures are listed as ratios with respect to $p_0 = p_{t1}$. The static temperature T_2 of the rotor discharge [Eq. I(7)] is equal to the difference of the total temperature T_{t2} at the rotor exit and $V_2^2/2c_p$, where V_2 is given by Eq. I(3). The temperature T_2' is necessary to calculate the pressure ratio p_2/p_0 by Eq. I(20). Evidently T_2' depends on the entropy increase $s_2 - s_1$ in the rotor.

The process between stations (1) and (2) from the rotor inlet to its discharge can be formulated by

$$T_1 - \frac{W_{10}^2}{2c_p} - \frac{U_{10}^2}{2c_p} = T_2 + \frac{W_2^2}{2c_p} - \frac{U_2^2}{2c_p} \quad (10)$$

which is a fundamental relation obtained from the energy equation for steady, adiabatic flows along streamlines in rotors, as shown in Art. 7.5 of Ref. 1.

The following discussion uses a relation which is obtained from Eq. 10 for incompressible flows (See Eq. 7(44) of Ref. 1). At a particular radius R along the outer rotor contour where the peripheral and relative velocities are U and W , respectively, the static pressure p is

$$p = p_1 + \frac{\rho}{2} (U^2 - U_{10}^2) + \frac{\rho}{2} (W_{10}^2 - W^2) - \Delta p_f \quad (11)$$

where ρ is the constant mass density of the fluid, and Δp_f the pressure loss due to frictional effects in the rotor. At the rotor inlet, where $U = U_{10}$ and $W = W_{10}$, the static pressure is evidently equal to p_1 , the static pressure in the absolute flow just ahead of the rotor at R_{10} . Equation 11 shows that, independently of the values of W and Δp_f , there will always occur a pressure increase $\rho/2(U^2 - U_{10}^2)$ if a fluid particle moves from R_{10} to R . An additional pressure rise is produced by decelerating the relative velocity from W_{10} to W . A flow that moves in a direction where the static pressure increases is more susceptible to separations than an accelerated flow, but the frictional pressure loss between neighboring stations is proportional to the dynamic head $(\rho/2) W^2$ in both flows. In view of Eq. 11 however there exist differences between flows that pass through stationary channels and those in rotating impellers. If a relative flow is decelerated in a rotating channel, whose distance from the axis of rotation increases in flow direction, it will not necessarily separate even though it moves against rapidly increasing static pressures, provided these pressure gradients are produced by the centrifugal force field and not by large reductions in relative velocity. If the same static pressure rise would have to be produced in a stationary channel of the same length as the rotating one, the deceleration of the flow per unit length would very likely become excessive and could be associated with considerably increased losses because of flow separations. On the other hand, if it were possible to ignore the effects due to Coriolis accelerations, it could be stated that the pressure losses in a stationary and in a rotating channel of equal length and shape would have to be equal for the same velocity heads and equal flow decelerations, except for influences due to Reynolds number differences. Moreover, for different velocity heads the pressure losses would be directly proportional to the velocity heads at corresponding locations in the two channels. However if the respective performance of the two channels were evaluated by a loss coefficient ζ_R that relates the frictional pressure drop Δp_f to the actual static pressure rise in the channel, its value would be lower for the rotating channel than for the stationary one because of the additional pressure rise $(\rho/2)(U^2 - U_{10}^2)$. The performance of the channels can be compared only by means of a loss coefficient ζ_W that is defined as the ratio of the pressure drop Δp_f and

the pressure rise $(\rho/2)(W_{10}^2 - W_1^2)$ due to the flow deceleration, irrespective of whether additional pressure rise is produced by the centrifugal force field or not.

These elementary considerations have not been presented here to imply that the loss coefficients ζ_W in a rotating and in a stationary channel of the same geometry are equal. In Ref. 1, Art. 8.5, it is shown that flows in stationary and rotating channels have fundamental differences as far as their rotational characteristics are concerned, and consequences of these conditions are described in Arts. 10.5 and 12.2 of Ref. 1. The intent of the above discussion is to draw attention to the fact that frequently used formulations for the efficiency of impellers for centrifugal turbines and compressors cannot serve as a measure for the performance of these rotors, and that some of the separation criteria applied to flows in centrifugal rotors have no physical meaning.

A commonly used definition for the efficiency of a centrifugal compressor rotor is

$$\eta_R = \frac{T_2' - T_1}{T_2 - T_1} \quad (12)$$

The significance of the temperatures is evident from Fig. 2. Equation 12 holds for the compressible flow of fluids with a constant value of $\gamma = c_p/c_v$. Similar to the preceding discussion that dealt with incompressible flows, part of the temperature rise in the rotor is due to the increase in peripheral speed from station (1) to station (2). Equation 10, rewritten as

$$T_2 - T_1 = \frac{U_2^2 - U_{10}^2}{2c_p} + \frac{W_{10}^2 - W_2^2}{2c_p} = T_u - T_1 + \frac{W_{10}^2 - W_2^2}{2c_p} \quad (13)$$

shows that the static temperature rise $T_u - T_1$ due to the centrifugal force field is equal to the first term on the right-hand side of Eq. 13. It occurs in rotors with and without flow losses, hence it is independent of the entropy increase $s_2 - s_1$. Thus the compression corresponding to $(U_2^2 - U_{10}^2)/2c_p$ occurs along the isentropic line $s_1 = \text{constant}$ from T_1 to T_u , from station (1) to station (u) in Fig. 2, producing the static pressure rise $p_u - p_1$, where

$$\frac{p_u}{p_1} = \left(\frac{T_u}{T_1}\right)^{\frac{\gamma}{\gamma-1}} = \left(1 + \frac{(U_2^2 - U_{10}^2)}{2c_p T_1}\right)^{\frac{\gamma}{\gamma-1}} = \left(1 + \frac{\gamma-1}{2} \frac{U_2^2 - U_{10}^2}{\gamma R_G T_1}\right)^{\frac{\gamma}{\gamma-1}}$$

The deceleration of the relative velocity from W_{10} to W_2 produces the temperature rise

$$T_2 - T_u = \frac{W_{10}^2 - W_2^2}{2c_p} \quad (14)$$

with an entropy increase from s_1 to s_2 , due to the flow losses, which in turn affect the pressure rise $p_2 - p_u$. The efficiency of the process from (u) to (2) can be defined by the so-called wheel efficiency η_W

$$\eta_W = \frac{T_2' - T_u}{T_2 - T_u} = \frac{T_2' - T_u}{(W_{10}^2 - W_2^2)/2c_p} \quad (15)$$

giving

$$\frac{T_2'}{T_u} = \eta_W \frac{T_2}{T_u} + 1 - \eta_W$$

and

$$\frac{p_2}{p_u} = \left(\frac{T_2'}{T_u}\right)^{\frac{\gamma}{\gamma-1}}$$

From a fluid dynamics view point only the efficiency η_W is a measure for the quality of the rotor performance. In particular, low measured values of η_W are indications for the existence of flow separations, although η_W will be affected also by the tip clearance losses, the so-called scrubbing losses produced by the rotating blades in the wall boundary layer at the fixed shroud, and the mixing losses after the rotor. However, low efficiencies η_W are only partly reflected in the rotor efficiency η_R of Eq 12 because of the temperature rise $T_u - T_1$ which is produced without entropy increases. If the entropy diagram of Fig. 2 were to represent the actual conditions in the compressor of Fig. 1, there would be, by measuring the temperature differences in Fig. 2,

$$\eta_R = 0.84$$

and

$$\eta_W = 0.57$$

Although the value of $\eta_R = 0.84$ seems to indicate that the flow in the rotor is reasonably good, the low value of $\eta_W = 0.57$ shows clearly that it should be possible to improve the rotor considerably with a redesign. Such improvement should be undertaken not only to increase the overall efficiency of the compressor by reducing the entropy rise $s_2 - s_1$ in the rotor, but also to produce more uniform flow conditions at the

rotor discharge since it might then be possible to reduce the diffuser losses also.

The process in the rotor that involves the relative velocity changes can be considered also from a different view point. Equation 10 may be written as

$$T_E = T_1 + \frac{W_{10}^2}{2 c_p} + \frac{U_2^2 - U_{10}^2}{2 c_p} = T_u + \frac{W_{10}^2}{2 c_p} = T_2 + \frac{W_2^2}{2 c_p} \quad (16)$$

where T_E is the so-called equivalent total temperature of the rotor flow. Equation 16 has the same form as the energy equation for an adiabatic process of an absolute flow if T_E is replaced by the constant absolute total temperature T_t and W_2 by the absolute velocity V . The temperature T_E is constant for a process in a particular rotor having a fixed radius ratio R_{10}/R_2 and turning at a specified speed. Thus, for given inlet conditions, Eq. 16 can be used also for an isentropic process along $s_1 = \text{constant}$ from (u) to (2') to give, in accordance with Fig. 2,

$$T_E = T_2' + \frac{W_{2is}^2}{2 c_p} \quad (17)$$

for the same pressure rise $p_2 - p_u$ as produced by the process with friction, and W_{2is} is the theoretical velocity available at the pressure p_2 . In turbine calculations it is customary to express the rotor losses by so-called velocity coefficients ψ

$$\psi = \frac{W_2}{W_{2is}} \quad (18)$$

If this formulation is used for compressors also, there is from Eq. 17,

$$T_2' = T_E - \frac{1}{\psi} \frac{W_2^2}{2 c_p} \quad (19)$$

Introduced into Eq. 15

$$\eta_W = \frac{\frac{W_{10}^2}{2} - \frac{W_2^2}{2}}{\frac{W_{10}^2}{2} - \frac{W_2^2}{2}} = \frac{1 - \frac{1}{2} \left(\frac{W_2}{W_{10}} \right)^2}{1 - \left(\frac{W_2}{W_{10}} \right)^2} \quad (20)$$

or

$$\psi = \frac{W_2/W_{10}}{\left[1 - \eta_W + \eta_W \left(\frac{W_2}{W_{10}} \right)^2 \right]^{1/2}} \quad (21)$$

The reason for introducing ψ as an alternate for η_W is that η_W equals $-\infty$ for the special condition where $W_2 = W_{10}$, or $T_2 = T_u$. In this case, and if W_2 is larger than W_{10} , the velocity coefficient ψ can however still be applied. On the other hand, for usual designs where W_2 is smaller than W_{10} , the velocity coefficient is not a good measure for the rotor performance since ψ can be increased by simply making the velocity W_2 smaller, and it is then more appropriate to use the wheel efficiency η_W for the loss evaluation. Since the same difficulties in expressing the losses occur in turbines also, an additional formulation is sometimes used which establishes the drop in total pressure that is associated with the entropy increase $s_2 - s_1$. For radial compressor rotors these formulation are either

$$Y_1 = \frac{P_{E1} - P_{E2}}{P_{E1} - P_u} \quad (22)$$

or

$$Y_2 = \frac{P_{E1} - P_{E2}}{P_{E2} - P_2} \quad (23)$$

depending on whether the pressure drop $P_{E1} - P_{E2}$ is referred to the inlet or the exit conditions. Although these total pressure loss coefficients are useful at small Mach numbers, or for incompressible flows where $P_{E1} - P_u = (\rho/2) W_{10}^2$ and $P_{E2} - P_2 = (\rho/2) W_2^2$, it can be shown that the corresponding coefficients which relate the losses to the kinetic energy of the flow (in the same manner as η_W of Eq. 15, or ψ of Eq. 18) become smaller for constant values of Y_1 or Y_2 if the Mach number of the inlet or discharge flow increases.² Although the actual energy losses tend to increase with increasing flow Mach numbers, an indiscriminate application of Eqs. 22 or 23 with values of Y from low-speed tests can be used as a wrong argument that the opposite is true.

To simplify the relations for the determination of the conditions of state in the compressor the velocity coefficients ψ will be used in the equations of Table I. To compare two rotors with different radius ratios and different deceleration ratios W_2/W_{10} , the efficiency η_W of Eq. 15 should be used as a

measure for their performance. Equations 20 and 21 relate ψ and η_W to each other. Paragraph 5 contains a discussion that deals with the magnitudes of η_W . With the formulas of Table I it is possible also to establish a relation for the determination of η_W for known values of η_R of Eq. 12, or vice versa. From

$$\eta_R = \frac{\eta_W \left[\left(\frac{W_{10}}{U_2} \right)^2 - \left(\frac{W_2}{U_2} \right)^2 \right] + 1 - \left(\frac{R_{10}}{R_2} \right)^2}{\left(\frac{W_{10}}{U_2} \right)^2 - \left(\frac{W_2}{U_2} \right)^2 + 1 - \left(\frac{R_{10}}{R_2} \right)^2} \quad (24)$$

and with

$$C = \frac{1 - \left(\frac{R_{10}}{R_2} \right)^2}{\left(\frac{R_{10}}{R_2} \right)^2 \cot^2 \beta_{10} + 2\mu \left(1 - \frac{\mu}{2 \sin^2 \alpha_2} \right)} \quad (25)$$

there are

$$\eta_R = \eta_W + C (1 - \eta_W) \quad (26)$$

and

$$\eta_W = \frac{\eta_R - C}{1 - C} \quad (27)$$

High performance compressors with high pressure ratios cannot be equipped with diffusors that are circular cascades with airfoil shaped blades. Figure 1 is a realistic sketch of a high speed compressor operating with an average discharge velocity V_2 that is supersonic. To obtain reasonably large axial blade widths b_2 as well as acceptable shapes of the meridional rotor contours, it is necessary to resort to large angles α_2 at the rotor discharge. At large angles α_2 , practical considerations dictate a limited number of diffuser channels, say, about 8 to 10 for angles α_2 of about 75° , and the permissible diffusion in these individual channels produces configurations similar to that depicted in Fig. 1. One of the most critical problem areas is the design of the flow passages from the rotor discharge to the entrance of the diffuser channels proper. The absolute flow leaving the rotor is not only non-uniform but also non-steady, because the relative velocity at the rotor discharge must by necessity vary between the suction and the pressure sides of the rotor blades at R_2 . Designs where the radius R_3 is very much larger than the outer rotor radius R_2 , or compressors with vaneless diffuser for large angles α_2 , were found to be inferior to machines with small radial gaps $R_3 - R_2$, especially for high subsonic or supersonic velocities V_2 . If it were not for the excessive noise the diffuser lips would preferably be arranged even closer to R_2 as shown in Fig. 1.

Theoretical attempts were made in Refs. 3 and 4 to evaluate the losses in the space between R_2 and R_3 , and in vaneless diffusers, that are due to mixing and frictional effects. The results of these investigations do not agree with reality if M_{V2} and/or α_2 are large. These inconsistencies are due to the assumption that equal flow angles are supposed to occur across the axial width b_2 of the flow channel after the rotor, a condition which is created by assuming that the frictional forces along the walls act equally on all particles between them. In actuality the flow angles α (measured with respect to the radial direction) decrease radically in the wall boundary layers in the direction from the mid-section of the channel toward the wall. The particles inside the boundary layers then move more rapidly to larger radii into zones of higher pressure than those outside of the boundary layers and very easily cause flow separations from the walls, thereby impairing the effectiveness of such diffusers.

In the writer's opinion it is incorrect to state that in efficient diffusers the vanes must not be too close to the impeller, or that the velocity at their entrance must be subsonic in all cases. For the reason mentioned above, it is equally wrong to maintain that vaneless diffusers must be arranged for supersonic absolute velocities at the rotor discharge.

Because of the inability to separate the losses that exist between the radii R_2 and R_4 of Fig. 1 an overall diffuser efficiency η_D will be introduced. With the symbols of Fig. 2

$$\eta_D = \frac{T_{t4}' - T_2}{T_{t4} - T_2} \quad (28)$$

where

$$T_{t4} - T_2 = \frac{V_2^2 - V_4^2}{2 c_p} \quad (29)$$

The velocity V_4 exists at the diffuser discharge at the radius R_4 , and is taken as

$$V_4 = \lambda V_2 \quad (30)$$

With small values of λ the radius ratios R_4/R_2 become large because of the limited amount of diffusion that is possible per unit length in flow direction to avoid separations in the diffuser channels. Values of λ of about 0.20 to 0.30 are common to limit R_4/R_2 to about 2. With designs of the type shown in Fig. 1 the kinetic energy $V_4^2/2 c_p$ cannot be converted into pressure rise, since the flow from the individual diffusers is dumped into a receiver surrounding them. As indicated by station (d) in Fig. 2 the total pressure P_{t4} at the compressor discharge is then equal to the static pressure p_4 at the diffuser exit, and

the total temperature at the compressor discharge is $T_{t4} = T_{t2}$ for adiabatic processes. The dumping of the kinetic energy $V_4^2/2 c_p$ is reflected in the overall diffuser efficiency η_D^* between rotor and compressor discharge

$$\eta_D^* = \eta_D (1 - \lambda^2) \quad (40)$$

Diffuser design criteria and approximate methods to evaluate the diffuser losses are given in paragraph 5.

Since

$$T_4 = T_{t2} - \frac{V_4^2}{2 c_p} = T_{t4} - \lambda^2 \frac{V_2^2}{2 c_p}$$

and with Eq. 28 there is then obtained the temperature T_4 , as given by Eq. I(11) of Table I. The pressure $p_4 = p_{t4}$ is determined from

$$\frac{p_4}{p_2} = \left(\frac{T_4}{T_2} \right)^{\frac{\gamma}{\gamma-1}}$$

for the isentropic process along the line $s_2 = \text{constant}$. Because the isentropic temperature differences between lines of constant pressure are proportional to the initial temperatures of the processes, there is, with the symbols of Fig. 2,

$$\frac{T_4'' - T_2'}{T_4' - T_2} = \frac{T_2'}{T_2}$$

and

$$\frac{T_4''}{T_0} = \frac{(T_4'/T_0)(T_2'/T_0)}{T_2/T_0}$$

As shown in Table I the ratio T_4''/T_0 can be expressed by Eq. I(13) which has the form

$$\frac{T_4''}{T_0} = \frac{1 + A(X_1 + A X_2)}{1 + A B} \quad (41)$$

where X_1 and X_2 are given by Eqs. I(14) and I(15), and

$$A = (\gamma-1) \mu \left(\frac{U_2}{a_0} \right)^2 \quad (42)$$

$$B = 1 - \frac{\mu}{2 \sin^2 \alpha_2} \quad (43)$$

The temperature rise ΔT_{is} for an isentropic compression from the total conditions P_0, T_0 at the compressor inlet, to the discharge pressure p_{t4} is, with Eq. 41,

$$\frac{\Delta T_{is}}{T_0} = \frac{T_4''}{T_0} - 1 = \frac{A[X_1 - B + A X_2]}{1 + A B} \quad (44)$$

Eq. 44 is identical with Eq. I(16) of Table I.

As shown in Table I the pressures at the different stations can be determined from the established temperatures by using the pressure-temperature relation for isentropic processes of perfect gases.

3. PERFORMANCE AND DESIGN PARAMETERS

The overall compressor efficiency defined by Eq. 8 is, with Eqs. 6, 42, and 44,

$$\eta_c = \frac{\Delta T_{is}}{\Delta T_w} = \frac{X_1 - B + A X_2}{1 + A B}$$

With Eqs. 42 and 43 the above relation establishes Eq. II(1) of Table II. This table lists the equations necessary to determine the performance and the geometry of the compressor. Only the principal steps that led to the equations of Table II are described in the following, the details of the derivations are omitted. The symbols of Table II are those of Figs. 1 and 2, with additional ones that are defined in this paragraph.

The degree of reaction r^* is defined as the ratio of the isentropic temperature rise $T_2' - T_0$ in the rotor to that corresponding to the pressure ratio P_{t4}/P_0 . Equation II(2) of Table II shows that for $\eta_c = 1$ and $\psi = 1$, the degree of reaction is

$$r^* = r_o^* = \left[1 - \frac{\mu}{2 \sin^2 \alpha_2} \right]$$

For a slip factor $\mu = 0.85$, r_o^* changes from about 0.544 to 0.433 if the angle α_2 is reduced from 75° to 60° . For low degrees of reaction a large part of the overall pressure rise must be produced in the diffuser. Since this energy conversion is associated with greater losses than the pressure rise produced in the rotor, high degrees of reaction are desirable. This condition is used in hydraulic pumps which usually have backward-bent rotor blades to produce most, if not all, of the pressure rise in the rotor. However, if such rotors were employed for light gases, such as air, the pressure rise would be too small for most applications, not only because of the reduced specific work input but also because such rotors would not be able to operate at high speeds on account of the high bending stresses in the blades. In rotors with radial blades it seems beneficial to use large angles α_2 to increase r^* . At a fixed peripheral speed U_2 the velocities V_2 decrease if α_2 is increased, but difficulties occur then because of the geometry of the passages from the wheel to the diffuser inlet. The deceleration ratio W_2/W_{10} becomes smaller also, as shown by Eq. II(5), and the increased losses caused by larger flow decelerations in the rotor may off-set the gain that would be obtained from the increased degree of reaction if other conditions would remain unchanged. The choice of these design parameters to obtain the best possible solution must usually be based on experience because of the interactions between rotor and diffuser that are greatly influenced by their designs.

The slip factor μ appears in most of the equations of Tables I and II. More has been written on this subject than on any other in the field of radial pumps and compressors, primarily because it is of great importance to know exactly how much energy a wheel will absorb. If wrong values of μ are used in a design the desired pressure ratio will not be obtained even though the expected efficiency is reached. Reference 7 is a recent paper where tests obtained with one particular wheel are compared with data obtained from experiments, and with slip factor formulas, by other authors. As is frequently the case in many studies on the subject, test data from a single wheel obtained at off-design conditions are used to establish design point data for other impellers. Moreover, the highest ratio U_2/a_0 was only about 0.51 in the tests of Ref. 7. The bibliography of Ref. 7 fails to mention the investigations of Refs. 5 and 6 which were undertaken at Daimler-Benz A. G. by systematically testing ten high-performance impellers of different shapes up to values of U_2/a_0 of about 1.1. In the writer's opinion, the data published in Refs. 5 and 6 are extremely valuable to the designer and the original curves of the article have been replotted in Fig. 3 to give wider publicity to this important contribution to the state of the art.

With the slip factor known from Fig. 3 the compressor efficiency of a particular design can be determined from Eq. II(1) for known losses. Equation II(3) is plotted in Fig. 4 for $\gamma = 1.4$, and different values of $\mu\eta_c$, to show the magnitudes of U_2/a_0 necessary to produce particular pressure ratios. For advanced gas turbine applications it would be desirable to operate at pressure ratios of between 8 and 10. For $\eta_c = 0.8$ and $\mu = 0.875$, Fig. 3 shows that values of U_2/a_0 of about 1.8 are necessary to reach this goal. Thus, at an inlet temperature of 60°F , where $a_0 = 1120 \text{ ft/s}$, the rotor of such a compressor has to operate with a peripheral speed U_2 of about 2000 ft/s, requiring special materials and careful rotor designs for the resulting high stresses.

By Eq. I(6) the rise of the total temperature in the compressor is $T_{t2} - T_0 = T_0(\gamma-1)\mu(U_2/a_0)^2 = 590^\circ\text{F}$, or about 600°F , for $\mu = 0.875$ and $T_0 = 520^\circ\text{R}$. Since the degree of reaction is around 0.5, the static temperature T_2 at the rotor discharge is then about $60 + 600/2 = 360^\circ\text{F}$. At this temperature, high-strength aluminum alloys have rupture stresses, and stresses for specified creep rates, which are less than one-half of the allowable stresses at room temperature. Hence it is necessary to use titanium alloys, for instance those with about 6 percent aluminum and 4 percent vanadium. At 360°F the design criterion for these materials is the yield stress since no appreciable creep effects occur even for operating times of 100,000 hours. Their 0.2 percent offset yield strength at 360°F is about 120 kpsi, with an ultimate strength of about 150 kpsi. As shown in chapter C of Ref. 8, the tangential stress in a non-supported ring of small radial thickness rotating with the peripheral speed U_2 is ρU_2^2 . For titanium with a specific gravity of 4.43, this value is about 240 kpsi at $U_2 = 2000 \text{ ft/s}$. Figures C.27 and C.29 of Ref. 8 show the so-called equivalent centrifugal stresses σ_e in rotors with radial blades as multiples of $\rho U_2^2 = \rho \omega^2 R_2^2$, for a design where the disk extends to the outer tip of the blades at R_2 , and another which has so-called scallops between the blades, similar to the rotor design shown in Fig. 1. Not counting the stress peaks at the central bore, which are more of the nature of stress concentrations that will be relieved by plastic deformations, because titanium has high ductility on account of its 20 percent elongation, the maximum stress ratios $\sigma_e/(\rho U_2^2)$ are about 0.25 and 0.16 for the rotors without and with scallops, respectively. Hence the maximum stresses at 2000 ft/s will be about 60 kpsi for one and about 40 kpsi for the other rotor. This discussion shows that compressor rotors operating at tip speeds of 2000 ft/s are feasible and that by arranging scallops, and using 75 percent of the 0.2 percent offset yield stress, or 90 kpsi, as design criterion, the maximum tip speed could be as high as 3000 ft/s or over 900 m/s. The latter speeds would give velocity ratios U_2/a_0 of about 2.68 at $T_0 = 60^\circ\text{F}$ and $\gamma = 1.4$. For $U_2/a_0 = 2.68$, $\mu = 0.85$, $\eta_c = 0.80$, pressure ratios P_{t4}/P_0 of about 43 could be reached in a single stage for gases with $\gamma = 1.4$. The extreme difficulties that would be associated with such a design, in particular those arising because of the large volume flow reductions, will not be discussed here. The intent of the fore-going deliberations is to show that pressure ratios in centrifugal compressors for air are not restricted because of rotor stresses.

Important advances are being made in nuclear gas turbines with helium as working fluid, as described in a recent article by Bammert and Bohm⁹. The main difficulties in the design of the turbomachines for this plant are the low pressure ratios that can be produced with helium in a conventional compressor stage, since the molecular weight of helium is only about 4 and $\gamma = 1.659$. At 60°F the velocity of sound in helium is 3275 ft/s. For a rotor with $U_2 = 3000 \text{ ft/s}$, a speed ratio $U_2/a_0 = 0.916$ would be obtained in a radial compressor. All velocities in the compressor would be subsonic and design point efficiencies of about $\eta_c = 0.85$ seem feasible. For $\mu = 0.90$, $\eta_c = 0.85$, $U_2/a_0 = 0.916$, at $\gamma = 1.659$, the resulting pressure ratio P_{t4}/P_0 would be 2.43 in accordance with Eq. 8.

In Ref. 9 a 25 MW_e closed-cycle helium gas turbine plant is described that operates with a turbine pressure ratio of 2.55. The pressure ratio of the compressors will have to be about 2.7 to overcome the pressure losses in the reactor and heat exchangers, of which no values are given in the paper. Reference 9 shows however that the plant has three axial compressors in series, each consisting of 9 stages. Since intercoolers are arranged between the three compressors each will produce a pressure ratio of about 1.4. If the three axial compressors were replaced by two single-stage radial compressors, of the type described with an intercooler between them, it would be possible to obtain an overall pressure ratio of about six which would be of advantage for the cycle. The writer does not want to minimize the difficulties that would be connected with the development of radial compressors and radial turbines for such applications, in addition to those connected with the bearings, seals and gear drives, but it is felt that they might be the ultimate solution for these highly interesting power plants.

Equation I(1) will be used in an example to show the influence of the diffuser losses on the compressor efficiency at different speed ratios U_2/a_0 , for absolute flow angles α_2 of 60° and 75° . The velocity coefficients ψ will be determined by assuming a wheel efficiency η_w of Eq. 15 of 0.7 for both impellers. Equations 21 and 24 were used to establish Fig. 5. The deceleration ratios W_2/W_{10} are 0.68 for $\alpha_2 = 60^\circ$ and 0.366 for $\alpha_2 = 75^\circ$ by Eq. I(5) for the data listed in Fig. 5. This difference makes the choice of equal efficiencies η_w for both cases somewhat dubious. It is seen from Fig. 5 that the rotor efficiencies η_R are 0.89 and 0.855 for $\alpha_2 = 60^\circ$ and $\alpha_2 = 75^\circ$, respectively. The corresponding values of ψ , which will be used in Eq. I(1), are 0.865 and 0.585. It is assumed further that the velocity V_4 at the diffuser discharge is $0.2 V_2$, or $\lambda = 0.2$, so that $\eta_D^* = 0.96 \eta_D$ by Eq. I(12). Figure 6 shows the large effect of the diffuser losses on the compressor efficiency. To obtain $\eta_c = 0.85$, the diffuser efficiency must be about 0.9 for all speed ratios U_2/a_0 . If η_D were 0.7 instead of 0.9, the compressor efficiency would only be 0.75. At $U_2/a_0 = 1.6$, this decreased diffuser efficiency would reduce the pressure ratio of the compressor from about 7 to 5.8, which in a gas turbine plant would produce a mismatch between turbine and compressor, with additional adverse effects on the thermal efficiency of the plant. Figure 6 shows also that the diffuser has a larger influence on η_c at the higher flow angle α_2 . On the other hand, the Mach number Mv_2 of the rotor discharge velocity will be lower at $\alpha_2 = 75^\circ$ than at $\alpha_2 = 60^\circ$. The respective values can be obtained from Eq. II(6) which has been represented in Fig. 7 for $\gamma = 1.4$. At $U_2/a_0 = 1.6$, the values of Mv_2 are 1.16 and 1.24 for α_2 of 75° and 60° , respectively, for the design parameters listed in Fig. 5.

Figure 7 shows that the Mach number Mv_2 becomes unity for values of U_2/a_0 between 1.1 and 1.3, depending on the choice of α_2 . From Fig. 8, which is a representation of Eq. II(4), it can be noted that for a speed ratio $U_2/a_0 = 1.2$ and at a radius ratio R_{10}/R_2 of about 0.67, which represents an average design value, the relative velocity W_{10} at the rotor inlet has a Mach number M_{W1} of about 0.9 at an inlet angle β_{10} of 65° . Figures 8 and 4 show that the Mach number M_{W1} for air compressors will not have to be larger than about 1.3 to produce pressure ratios up to about ten. Some sources state that no efficient inducers can be built for values of M_{W1} larger than 0.8 because of "shock losses". It seems to the writer that such statements are not different from those made some years ago, which predicted that it would be impossible for an airplane to break the "sonic barrier", or others which maintained that an axial compressor has to operate at subsonic velocities to be efficient. Advances in transonic axial-flow compressor stages have shown that human ingenuity can overcome these so-called barriers. Reference 10 is cited as an example, where a transonic boost stage ahead of the inlet of a centrifugal compressor is described, which produces a pressure ratio of 1.43 for air at an efficiency of 90 percent with a tip Mach number of 1.05.

The flow in an inducer of an impeller with radial blades is different from that in an axial-flow rotor. In the latter, particles that have been moving along the suction and the pressure sides of the blades are mixed at essentially constant static pressure after the trailing edges at the discharge, whereas no such mixing occurs in the flow channels where the inducer joins the radial blades of the impeller. Hence the pressure distributions along the walls of the inducer blades must be radically different from those along the surfaces of an axial rotor blade, and separation criteria that are based on the diffusion factor of axial cascades cannot be applied. Similar to the conditions in transonic axial stages the supersonic relative velocity at the tip of an inducer becomes sonic at a particular radius R_{1c} , and subsonic at radii R_{1x} smaller than R_{1c} . Denoting the Mach number of W_1 at R_{1x} by M_{1x} , and that at R_{10} by M_{W1} as previously defined, there is

$$\frac{R_{1x}}{R_{10}} = \frac{1}{\sin \beta_{10}} \left[\left(\frac{M_{1x}}{M_{W1}} \right)^2 + \sin^2 \beta_{10} - 1 \right]^{\frac{1}{2}} \quad (45)$$

Figure 10 shows the values of R_{1x}/R_{10} obtained from Eq. 45 for $M_{W1} = 1.3$, at different relative flow angles β_{10} at the inducer tip, and for particular values of the Mach number M_{1x} . This graph is presented to show that it is non-sensical to state that M_{W1} cannot exceed particular values without specifying at what angle β_{10} and at what ratio R_{1i}/R_{10} this limitation holds. Whereas at $\beta_{10} = 75^\circ$ a Mach number of unity occurs at $R_{1x}/R_{10} = 0.75$, the whole inlet annulus will have supersonic relative velocities at $\beta_{10} = 50^\circ$, for the same Mach number $M_{W1} = 1.3$ at the tip. Moreover, if at $\beta_{10} = 75^\circ$ the hub/tip ratio R_{1i}/R_{10} of the inlet eye is 0.75 in one machine and, say, 0.3 in another the losses due to compressibility effects will certainly be different. Figure 10 also shows the Mach numbers M_{v1} of the absolute velocity V_1 ahead of the impeller which, as indicated earlier, has been assumed to remain constant in radial direction. They have values of 0.336 and 0.919, respectively, for $\beta_{10} = 75^\circ$ and $\beta_{10} = 55^\circ$ at $M_{W1} = 1.3$, and it is inconceivable to the writer that the losses will remain constant independent of M_{v1} . Clearly, if M_{v1} becomes larger than unity very special conditions occur since the flow in the annulus becomes choked at $M_{v1} = 1$ as has been discussed in Art. 9.9 of Ref. 1. Some of the peculiarities associated with cascades at supersonic inlet velocities are mentioned in Art. 9.10 of the same reference.

The writer believes that the, by now, almost classical view points of flows through turbomachines have outlived their usefulness. They may even be a hindrance for future developments and if accepted without questioning, may prevent original thinking and could make people believe that all problems have been or will be solved by their use. This classical method assumes that the fluid particles in a turbomachine move on axisymmetric stream surfaces of shapes which are either assumed a priori, or obtained

by simplified theoretical methods. Further, it is assumed that the flow through a turbomachine can be replaced by the flows through a multiplicity of annular channels bounded by neighboring stream surfaces, which are closely spaced between the meridional contours of the flow channel of the machine at hub and tip. The stream surfaces are actually considered to be thin, solid walls that do not create disturbances, and it is assumed that the flows in these individual channels do not interact with each other. In each one of the channels there exists then a so-called quasi two-dimensional flow of the type described in Art. 12 of Ref. 1. The performances of the different cascades, which are now arranged in the various flow channels to produce the specified flow deflection, are taken to be those of two-dimensional cascades obtained either in cascade test rigs or by theoretical methods. With the latter, one can at best attempt a solution for the special relative flows W in rotors that satisfy the condition $\nabla \times \vec{W} = -2\vec{\omega}$; that is, where the curl of the velocity function is a constant, since $\vec{\omega}$ is the angular velocity vector of the rotor. Such flows are isentropic but can be compressible. However, disturbances due to shocks cannot occur. This condition limits the theoretical evaluation to flows where the local Mach numbers must be less than or, at the most, equal to unity. More general solutions of the so-called blade-to-blade problem on axisymmetric stream surfaces have not yet been obtained and are very difficult to formulate.

So-called quasi two-dimensional flows with $\nabla \times \vec{W} = -2\vec{\omega}$ are discussed in Art. 12 of Ref. 1. By introducing a stream function ψ there is obtained a second order partial differential equation of the form (see Eq. 12(9), p. 307, Ref. 1)

$$\frac{1}{R^2} \psi_{,\theta} + \psi_{,m} - \frac{1}{R^2} [(\ln \rho)_{,\theta}] \psi_{,\theta} + [(\ln R)_{,m} - [\ln(\Delta h \rho)]_{,m}] \psi_{,m} = -2(\Delta h) \rho \omega \sin \lambda \quad (46)$$

The commas denote partial differentiations with respect to the coordinates listed after them, where θ is the angle in peripheral direction and m the length along the generatrix of the stream surface. The mass density is denoted by ρ , R is the radius from the axis, Δh is the varying distance between neighboring stream surfaces, ω is the angular rotor velocity, and λ is the angle of the tangent to the generatrix with the axis of rotation. For $\lambda = 0$ the particles move on cylindrical stream surfaces, and $\lambda = 90^\circ$ covers flows in radial compressor wheels with stream surfaces that are planes perpendicular to the axis. For the latter case, and for conical stream surfaces, Eq. 46 has been solved by Stanitz for thin blades.³ For cascades with airfoil-shaped blades, that are arranged on an arbitrary surface of revolution, computer programs are described in Ref. 11 for solutions with relaxation methods that need high-speed computers with large storage capacities. As interesting and useful these theoretical attempts are, one must be critical to evaluate what they really produce in form of results, and whether or how these data will help to improve present designs, and to create the turbomachinery which is to be built in the future.

The mere fact that modern computers can solve differential equations with complicated boundary conditions which, hitherto, could not be tackled by hand calculations is no assurance that the results must be correct from a physical point of view. Computers can only perform mathematical manipulations as they are told to do, and no result is better than the assumptions that were used to formulate the problem that is solved by these apparently sophisticated, but inherently stupid, machines.

Two of the necessary boundary conditions for solving Eq. 46 with the programs of Ref. 11 require that the flows upstream and downstream of the blades are uniform, and that the flow angles at these stations be specified. These conditions imply that the tangential deflection through the cascade is known a priori, whereas in actuality the possible deflection depends on the attitude of the blades in the cascade and the upstream conditions only. Whereas in turbine cascades it is possible to calculate the discharge angle from the geometry of the cascade with approximate methods, such predictions are not possible in axial compressor cascades, in fact one of the major problems is to find out what the discharge angles are for imposed incidence angles. Actually then, Ref. 11 produces pressure distributions about blades for specified locations of the rear stagnation points, and if they have been chosen wrongly the pressure pattern will be wrong also. As in most theoretical cascade flow investigations the effects of upstream or downstream cascades cannot be taken into account; the row investigated constitutes in actuality a disturbance located between two flow fields that extend to infinity far upstream and far downstream without being disturbed by other cascades.

A major drawback of all methods that are based on Eq. 46 is however that the right-hand side of this relation becomes zero if either ω is zero, or if λ is zero. If the angular velocity is zero the cascade is stationary and instead of the pattern of the relative velocity W one deals with the absolute velocity V in a stator whose curl $\nabla \times \vec{V}$ is now zero because of the initial condition that $\nabla \times \vec{W} = -2\vec{\omega}$. The velocities V of such flows must be gradients of a potential function φ , and Eq. 46 can be modified to

$$\nabla_a^2 \varphi = \frac{\nabla \varphi}{a} \cdot \nabla \left(\frac{V^2}{2} \right) \quad (47)$$

where " a " is the variable velocity of sound at the different locations in the flow field. As before it is necessary that $M = V/a$ is everywhere smaller than unity. For incompressible flows, where the velocity of sound " a " is tending toward infinity, Eq. 47 reduces to Laplace's equation $\nabla^2 \varphi = 0$. Equation 47 is a partial differential equation of the Poisson type and the term on its right-hand side can be interpreted mathematically to be the result of sources in the flow field. Expressed differently, the curl of \vec{V} is zero, but its divergence $\nabla \cdot \vec{V}$ is not; which means that flow must be generated somewhere in the field, and sources judiciously arranged therein can take care of this situation. Reference 12 develops calculating methods that are based on this idea by using the principles of superposition, but again for assumed axisymmetric stream surfaces, namely, cones in particular.

It can be noticed also, that Eq. 46 changes into Eq. 47 if $\lambda = 0$; that is, if cylindrical stream surfaces are assumed to exist. Thus, as far as axial machines with cylindrical stream surfaces are concerned, the flow through a rotor is not different from the flow through a stator, if the cascades have the same geometries and if the flow angles of the relative and absolute flows are equal. On the other hand it can be proved without a shadow of a doubt, e.g., by Art. 8.5 of Ref. 1, that even isentropic relative flows in rotors must be fundamentally different in character from absolute flows. From Eq. 8(23) of Ref. 1 it can be seen clearly that the simplest relative flow must have $\nabla \times \vec{W} = -2\vec{\omega}$, and if Kelvin's theorem is extended to relative flows (Eq. 8(22) of Ref. 1), and applied to isentropic conditions, one sees that the change of the circulation Γ_R around a moving fluid curve C in a relative flow is not zero but equal to

$$\frac{d\Gamma_R}{dt} = -2 \oint_{(C)} d\vec{r}_R \cdot \vec{\omega} \times \vec{W} \quad (48)$$

In an absolute isentropic flow, however, the change of the circulation around a moving fluid is indeed zero. Equation 48 indicates that $d\Gamma_R/dt$ is zero only if the relative flow vectors \vec{W} are everywhere parallel with $\vec{\omega}$, hence parallel with the axis of rotation. Rotors of this type are not capable of changing the energy of fluids and have no practical interest. That the condition $\nabla \times \vec{W} = -2\vec{\omega}$ is not in conflict with Eq. 48 can be proved with simple means.

It can be stated therefore that the stream surfaces in a rotating cascade must differ from those that would occur if the same cascade were stationary. More precisely, the stream surface in a stationary cascade, whose flow satisfies $\nabla \times \vec{V} = 0$, must change to a pattern that satisfies $\nabla \times \vec{W} = -2\vec{\omega}$, and it is not possible that the relative flow in the rotating cascade has the same stream surfaces as the absolute flow. In particular, the relative stream surfaces cannot be axisymmetric, if those of the absolute have this character. More about these conditions has been described in Art. 10.5 of Ref. 1, but it is evident from the above discussion that results obtained by solving Eqs. 46 and 47 must be of approximate nature even for the idealized flows that are investigated, and they must be interpreted in the proper perspective of their initial assumptions.

Such results, or data from stationary cascade test rigs which basically are obtained with the same assumptions as those of the above-mentioned theories, are now used to establish the blading elements in the individual flow channels between the solid stream surfaces. The classical method consists in designing the actual blade surfaces through the profiles of these blade elements. The "solid" stream surfaces are then, so to say, removed and it is assumed that the originally calculated or assumed stream surfaces will also exist for the flow about these three-dimensional blades. It is quite clear that there are many possibilities of arranging an actual blading with the profile sections that are obtained from the flows through the individual flow channels, depending, for instance, on how the leading edge of the blade is arranged. In the inducer of Fig. 1 the leading edge of the blade could be pulled forward in flow direction to obtain a blade surface that is leaning more away from a meridional plane than if the leading edge were to slant backward, although at the different radii the blade angles would be exactly equal. Without a doubt these two blades would exert different forces on the flow, one could tend to push the flow toward the tip, the other toward the hub, and it is inconceivable that the flow pattern in the meridional channel would remain unchanged. In Ref. 2 (Table C-2, p. 26) an investigation dealing with the blading of an axial-flow machine has been carried out to check whether it is possible to build a rotor with a very large number of thin blades that produces the idealized relative flow with $\nabla \times \vec{W} = -2\vec{\omega}$ near its cylindrical hub. This flow condition establishes a particular change of the flow angle in radial direction, and requires that the blade surface consists of radial lines. Since for a large number of blades the flow and the blade angles must be identical, the last mentioned requirement establishes the change of the flow angle along the radius by itself. It can be seen that the two values differ, primarily because from $\nabla \times \vec{W} = -2\vec{\omega}$ the necessary blade angle change depends on the ratio of ω and the axial component of \vec{W} , whereas this is not the case for the other. Hence, it is evident that the condition $\nabla \times \vec{W} = -2\vec{\omega}$ cannot be maintained in a blading with a finite axial length, and that the actual blade shapes as a whole will have an influence on the flow through them. These examples show that the flow patterns in a machine can be influenced by particular arrangements of the profiles in direction of the blade height and that they will have a bearing on the meridional flow. The classical approach, so to say, linearizes the problem, and does not take account of the interactions that occur between the flows through the different elementary channels from the hub to the tip. It further tries to explain all phenomena with a two-dimensional model, at best with one on stream surfaces that are surfaces of revolution, and loses sight of the actual three-dimensional effects that occur in reality. These limiting view points seem to be particularly harmful if supersonic flows occur in a relative flow field where, as discussed earlier in connection with the inducer inlet, the absolute flow is subsonic. Stationary cascade test data cannot give a true picture of the conditions since they replace again the relative flows by an absolute flow between "solid" stream surfaces, where in particular the condition that the flow component perpendicular to the cascade axis, which is in reality the actual absolute flow, has no special significance. In a supersonic cascade test rig it will hardly be possible to determine cascade performance at different incidence angles nor establish design data for blades where only parts of the blades have supersonic velocities. For inducers of radial compressors which are followed by radial blades it does not seem possible to use cascade data with any degree of realism, and only experimental work with actual rotating wheels will show what detrimental effects high relative flow Mach numbers have on the performance.

There seem to exist a number of design variables that should be examined for supersonic inducers. The possibility of influencing the flow pattern near the tip by appropriate blade shapes to produce, say, greater mass flow rates per unit area near the hub, has been mentioned. These designs could be extended to produce swept-wing effects, similar to what has become the standard design of wings for high-speed airplanes. It is well known that in supersonic flows the velocity parallel with the leading edge of a swept-back wing with infinite span cannot produce variations in pressure, hence only the component of velocity perpendicular to the leading edge can create losses that are caused by compressibility effects. Peculiar conditions could however occur at the outer wall, if this principle were applied to the design of the inducer inlet edges, but it might be possible to obtain considerable improvements. The writer is surprised that such designs

have not been tried for axial compressor stages, especially for those with large blade heights. Swept-back blades would not necessarily have greatly increased bending stresses, since the maximum section modulus of an airfoil profile is a large multiple of the minimum modulus about the outer principal axis. If the centers of gravity of the profiles along the blade height were displaced backward along this axis of the hub profile, it should be possible to minimize the stresses that are caused by the additional bending moment about the other principal axis.

The writer believes that it is possible to build inducers at supersonic relative inlet velocities for absolute inlet Mach numbers M_{V1} of about 0.5 to 0.6 with good efficiency and minimum flow disturbances. Converging-diverging passages in the inducer seem unnecessary, especially if only part of the rotating channel has supersonic velocities. Leading edge radii must be as small as possible, but large enough to avoid damage by flutter, and great care must be taken to properly design the suction side of the blade to provide a good transition into the actual blade channel. It is not believed however that the blades must be designed for incidence angles if the proper blockage factor is used for the flow area calculations at the inlet. This statement contradicts the data of Ref. 13, where the optimum rotor efficiency η_R is shown to occur at positive incidence angles of about 10° at R_{10} for blade angles of 57° . The inlet channel ahead of the eye of the wheel that was tested, has curved meridional contours, hence the inlet velocity V_1 is not uniform from R_{11} to R_{10} . Although it is stated in Ref. 13 that the distribution of V_1 was determined by probes, slight inaccuracies of the measurements, or a location of the probe at some distance forward of the leading edges of the rotor could easily be responsible for these unusually large incidence angles. By means of theoretical methods, which are not described in detail, the velocity distributions along the inducer were determined also in Ref. 13 to verify the test data. However, as shown by Fig. 5 of Ref. 13, the inducer has simply been replaced by a cascade, since at its discharge the velocities on either sides of the blade are shown to be equal, a situation which cannot exist in reality, and which gives questionable value to the argumentation based on it.

Design criteria for the whole rotor passages from the inlet to the discharge are often given in terms of the deceleration ratio W_2/W_{10} of the relative rotor velocities. From earlier discussions with regard to rotor losses it is evident that not all losses in a rotating impeller depend exclusively on this ratio. They will also be greatly influenced by the performance of the inducer, in particular, on the velocity distribution that exists at the station where the inducer blades join the radial impeller blades. It is necessary to have a good appreciation of the complexities of flows in rotating impellers to avoid oversimplifications and the setting up of design criteria that are based on wrong models. An invaluable contribution to investigating the real flow phenomena in rotating impellers has been made by Fowler¹⁴, who actually measured the velocity distribution in the passages of a large compressor with probes from a platform inside the hub that was rotating with the wheel. Figure 11 has been adapted from a personal communication of Mr. Fowler to the writer. It shows the velocity profiles at seven cross sections of the rotor flow channel of an unshrouded wheel with radial blades at the discharge, when operating at a peripheral speed $U_2 = 17$ ft/s. The meridional flow channel has the smoothly changing contours used for modern designs. Plane 1 of Fig. 11 is at the inlet section of the inducer blades, extending from the leading edge of one blade to the back of a neighboring one, and the blades become radial near plane 3. The zones with reduced velocities at the blade tips that are due to the blade gap and the scrubbing effects along the outside wall, remain almost equal from plane 3 to the discharge plane 7. It is of interest to compare these measured velocity distributions with the theoretical solutions of Eq. 47 for radial blades and incompressible flows. The pattern of the streamlines obtained by Stanitz for a radial impeller with 20 blades is shown in Fig. 3.5.2 of Ref. 3. The velocities are inversely proportional to the distance between neighboring streamlines. The leading surface of a blade will be called the pressure side, the trailing surface of the same blade is its suction side. Hence the direction in a blade channel from the pressure side of one blade to the suction side of the neighboring one, is in direction of rotation of the wheel.

At the outer radius of the wheel ($R = 1$ in Fig. 3.5.2 of Ref. 3) the theoretical analysis predicts that the velocity in a blade channel increases in direction of rotation, whereas exactly the opposite trend is seen to occur in plane 7 of Fig. 11. However in planes 3 and 4, and to a lesser degree in plane 5, the measured velocity changes agree in the main with the theoretical ones which predict a velocity increase in direction of rotation at all radii. This situation occurs because the theoretical method shows, or is based on the assumption, that at radii smaller than about 70 percent of R_2 the relative velocities are everywhere radial. Then, as determined in Art. 10.6 of Ref. 1, and as shown in Fig. 10(5a), they will increase linearly with the angle along the periphery in direction of rotation. The measured reversal of this behavior, starting from plane 5 to the discharge plane 7, cannot be due to viscous effects only, which are neglected in the theoretical treatment, but must occur because of flow peculiarities that a simplified theory cannot take into account. In his personal communication to the writer, Mr. Fowler also remarked that the directions of the relative velocities at the discharge did not have as large a deviation from the radial direction as Fig. 3.5.3 of Ref. 3 shows. The measured flow distributions suggest that considerable mixing of the different flow strata must occur while they pass through the compressor and it is very unlikely that there exist axisymmetric surfaces. Reference 15 describes tests of single, straight diffusors that were arranged radially and rotated in the test rig of Ref. 14, to examine the effects of centrifugal and Coriolis forces on decelerated flows that move radially outward. Diffusors with different divergence angles were investigated, first while stationary and then while rotating. It was found that considerable differences occur if a diffusor is rotated. Static tests with a two-dimensional diffusor with an included angle of 10° showed the well-known peaked velocity distributions that occur for these angles. If rotating, the peaks flatten out and the flow becomes more stable. These results agree with the conclusions reached earlier about the beneficial effects of a centrifugal force field on decelerated flows, but they show also that boundary layers along rotating walls, where the fluid particles are also affected by Coriolis forces, exhibit different characteristics than those along stationary walls. Similar results have been obtained in Ref. 16 which describes tests of flows through a channel with constant cross section that is rotated about an axis. Because of these conditions, different separation criteria for boundary layers must be applied if they occur on stationary walls or on surfaces that rotate about an axis.

For this reason it is not possible to use conventional boundary layer theories as a means to find permissible deceleration ratio W_2/W_{10} for the relative flows in impellers, nor can attempts be successful that try to relate this ratio to the NASA diffusion factor, which has proved to be a satisfactory separation criterion for axial compressor bladings which have small flow deflections, hence, where the changes of the

Coriolis forces are small if the blading rotates. Much more fundamental work dealing with boundary layers on rotating walls and investigations with modern flow visualization methods must be carried out before it is possible to establish satisfactory design limits for flows in radial impellers. Recent endeavors that use holography with Pulse-Lasers for investigations of flows in rotating wheels might open entirely new ways to study actual flows in high-speed machines where the effects of centrifugal and Coriolis forces are large.

If the above-mentioned peculiarities of rotor flows are not taken into account one might come to the conclusion, as some sources do, that flow separations will occur in an impeller if W_2/W_{10} equals 0.6, and that a ratio of 0.62 should be used for design purposes to avoid excessive losses. Such values are obtained from analogies with stationary diffusers or oversimplified boundary layer considerations for, say, linearly changing velocities along a surface, as is the case on the suction side of a blade in an axial compressor cascade. Figure 9 is a diagram for the determination of the deceleration ratio W_2/W_{10} in accordance with Eq. II(5) of Table II. If, for instance, the limit for this ratio were set at 0.65, the discharge angle α_2 could not be larger than about 60° for a radius ratio R_{10}/R_2 of 0.7 and $\beta_{10} = 60^\circ$. For larger discharge angle α_2 the radius ratio R_{10}/R_2 would have to be decreased. Figure 12 is presented to show these conditions more precisely if the lower limit of W_2/W_{10} is assumed to equal 0.6 and if the slip factor μ is 0.85. For these conditions and at $\alpha_2 = 75^\circ$, the maximum radius ratio R_{10}/R_2 could not exceed 0.42 at a relative flow angle $\beta_{10} = 70^\circ$. Experience with high performance compressors shows however that impellers with radius ratio in accordance with the dashed curve have operated successfully. At $\alpha_2 = 75^\circ$, for instance, and at a radius ratio R_{10}/R_2 of 0.68 the deceleration ratio is of the order of 0.35 to 0.3, depending on β_{10} , as shown in Fig. 9 by following path "b" in the diagram. Therefore, if the deceleration ratio W_2/W_{10} is used as a preliminary design criterion it is permissible to apply minimum values of about 0.3 or even somewhat lower, say, about 0.26. A unique relationship between W_2/W_{10} and the wheel efficiency η_w cannot be established because of lack of test data but in Paragraph 5 some test results are plotted to show the order of magnitude of η_w . A correlation between W_2/W_{10} and η_w can probably never be obtained because of the additional rotor losses that depend on a number of additional factors.

For known values of M_{w1} , β_{10} , and U_2/a_0 it is possible to calculate the wheel radius R_2 with Eq. II(9) of Table II, if the ratio R_{11}/R_{10} were known. The quantity kb_1 is a blockage factor which is primarily depending on the number of inducer blades and their thickness at the inlet throat, although excessively thick boundary layers on the walls of the inlet annulus can affect kb_1 also. Evidently if U_2/a_0 is known the angular velocity ω is known also, if R_2 has been determined. However ω can be determined directly by Eq. II(10) of Table II, for known or chosen quantities M_{w1} and β_{10} . Eq. II(10) is useful to establish the necessary rotative speed to handle particular flow rates. If ω is given, because of the prime mover that drives the compressor, Eq. II(10) makes it possible to verify whether a particular flow rate can be handled at this speed. The ratio of axial blade width b_2 and R_2 is obtained by Eq. II(11). The blockage factor kb_2 is the ratio of the actual flow area at the wheel discharge and the area $2\pi R_2 b_2$, multiplied by an experience factor that depends on the boundary layer thickness on the side walls.

The necessary diffuser exit area A_4 at the radius R_4 is obtained from Eq. II(14) for specified values $\lambda = V_4/V_2$ and known efficiencies η_c . A blockage factor kb_4 takes account of the displacement thickness of the boundary layers which reduce the actual flow area at the discharge of the diffuser. Section x-x of Fig. 1 is taken to be either the throat of the diffuser where the flow is choked if the absolute velocity V_2 after the rotor is supersonic, or the entrance section of the actual diffuser if V_2 is subsonic. The necessary total flow area of all diffuser channels is denoted by A_x , and kb_x is again an area blockage factor. The area A_x can be determined for both cases if the ratio of the total pressures P_{tx} at station x and P_{t2} at the rotor discharge is known. Although P_{t2}/P_0 could be expressed by Eq. I(19) of Table I and then introduced into Eqs. II(13) and II(14), it is better to use these relations as listed, since it is possible to judge approximately what values the ratio P_{tx}/P_{t2} will have for particular diffuser designs. If V_2 is supersonic the throat area is obtained with the dimensionless critical flow function ϕ_c of Eq. II(14) which has a value $\phi_c = 0.6847$ for $\gamma = 1.4$. For subsonic velocities V_2 the diffuser inlet area can be determined only if the velocity V_x at station x is specified, by assuming a value $\xi = V_x/V_2$. Usually this ratio is taken to be about 1.02 to 1.05 because a slight acceleration between stations (2) and (x) will produce more uniform flow conditions at the diffuser inlet. For a chosen number of diffuser flow channels, usually arranged between parallel walls, the diffuser widths at inlet and discharge can be determined from A_x and A_4 , and the methods described in Paragraph 5 establish the necessary length of the diffuser channels. With this length and the chosen diffuser arrangement it is possible to establish the outer radius R_4 of the diffuser.

4. SIMILARITY CONSIDERATIONS

If effects due to gravity, surface tension, and heat conductivity can be ignored, which is permissible for most flows in turbomachines, the laws of dynamic similarity establish that flow processes of perfect gases in geometrically similar channels are equal in performance if the Reynolds numbers Re and the velocity ratios $V/\sqrt{R_g T}$ are respectively equal at corresponding stations in the channels. As derived for instance by Ackeret et. al., in Ref. 17, the latter condition can be expressed in terms of equal Mach numbers M , with the additional requirement that the fluids passing through the geometrically similar channels have equal specific heat ratios γ . Reference 17 shows also that the effects of different values of γ are small only if the Mach numbers are less than about 0.6. The reason is that gases with different heat ratios γ produce different relative changes in density if passing through a channel with particular area ratios. Hence the values $V/\sqrt{R_g T}$ cannot remain equal in geometrically similar channels.

Assuming then that gases with equal values of γ are considered only, and that the Reynolds numbers of the flows in the compressors to be compared are in a range where they can vary considerably without largely changing the frictional coefficients; that is, if they are moderately large and if the flow surfaces are rough, dynamic similarity is achieved in geometrically similar machines at equal Mach numbers.

In hydraulic machines, similarity considerations that are based on the so-called specific speed have been used with success and it will now be examined whether it is possible to apply this method also to the compressors considered here that operate at high speed ratios U_2/a_0 . Attempts to obtain design limits and to establish the optimum operating range of radial compressors with this means are described in Refs.

18 and 19. In both reference there is used the specific speed N_S (see Eq. III(1) of Table III)

$$N_S = \frac{N Q^{\frac{1}{2}}}{H_{1s}^{3/4}}$$

similar to the practice in hydraulic pump design. In the latter application, Q , which is the volume flow rate through the machine, is everywhere constant. In a compressor for gases however, where the volume flow rate will change considerably from inlet to discharge, a choice must be made whether Q at station (1), or at, say, station (2) is to be used in Eq. 50. In both references the quantity Q is taken to be the inlet flow rate Q_1 without giving reasons for this choice. As in Refs. 18 and 19, and as shown in Table III by Eq. III(1), the value of N_S depends on the system of units which is used. In the two cited references N_S has the dimension $\text{rpm ft}^{3/4} \text{ sec}^{-1/2}$, which is awkward for purposes of comparison with similar coefficients in other systems of units, and such formulations are not in keeping with the general and very desirable tendency to use dimensionless quantities throughout. For this reason it is more appropriate to use the dimensionless speed n_S , with units as defined by Eq. III(3) of Table III, which for particular conditions has the same value in all consistent systems of units. The quantity n_S is obtained by dividing the value of N_S in the given English units by 129.

Whereas Ref. 18 (Fig. 2.8) simply presents a graph showing a direct correlation of the efficiency of different compressor types with N_S , Ref. 19 uses the so-called specific diameter d_S as an additional parameter, which is defined by (see Eq. III(2) of Table III)

$$d_S = \frac{D H_{1s}^{1/4}}{Q_1^{1/2}}$$

This quantity is also not dimensionless. However Eq. III(4) defines a dimensionless specific diameter d_S that is obtained from d_S in English units by division with 0.42.

The coefficient ξ_1 of Eq. III(5) represents the ratio of the area of the flow annulus at the compressor inlet and the area πR_{10}^2 , where R_{10} is the outer radius of the rotor inlet eye. As shown in Table III the quantities n_S and d_S can be expressed also with the chosen parameters of Tables I and II, to obtain Eqs. III(6) and III(7). Both contain ξ_1 , so that this ratio can be obtained from either of these relations as shown by Eqs. III(8) and III(9). By equating these expressions there is obtained Eq. III(10), or

$$n_S d_S = \frac{2}{(\mu \eta_c)^{1/2}}$$

where μ is the slip factor and η_c the compressor efficiency. Since μ is a known quantity for a particular compressor design, and because η_c can be determined with Eq. II(1), the specific diameter d_S is directly related to n_S and there is no reason why both n_S and d_S should be specified for a design with radial blades. Equation III(11) shows that by specifying n_S there can be obtained the radius ratio R_{11}/R_{10} for particular values of β_{10} and R_{10}/R_2 which are usually chosen on the basis of other considerations, as explained earlier, Equations II(9) and II(10) of Table II, with the known ratios R_{11}/R_{10} , would then give directly the necessary radius R_2 or the angular velocity ω for given operating conditions. If the optimum efficiency of a compressor were a unique function of n_S , and if R_{11}/R_{10} and/or the other parameters could be adjusted to meet the optimum value, the designer would have a simple criterion for the optimization of compressors.

From Ref. 18 (Fig. 2.8, p. 38) it appears that radial compressors should have the best efficiency for values of N_S between 75 and 85, or for n_S between 0.58 and 0.66. Table III gives an example for design parameters that have been used successfully. In one case, a radius ratio R_{10}/R_2 of 0.56, in another a ratio $R_{10}/R_2 = 0.7$ was chosen. For the smaller value of R_{10}/R_2 it is not possible to design for $N_S = 80$, since the hub/tip ratio at the inlet becomes zero at $N_S = 71$. In an actual design of a compressor that had efficiencies higher than 80 percent, the hub/tip ratio at the inlet was about 0.46 for $R_{10}/R_2 = 0.56$, hence it operated at $N_S = 60$ and did not have the much lower efficiency predicted by Ref. 18. For the example in Table III with the higher ratio $R_{10}/R_2 = 0.7$ the ratio R_{11}/R_{10} becomes zero at $N_S = 99.4$, and an actual high-performance machine is known to the writer that has an inlet hub/tip ratio of 0.34, hence it operates at $n_S = 0.725$ or $N_S = 93.5$. Thus, the sharp optimum for N_S in Ref. 18 does not occur in reality and $N_S = 80$ or $n_S = 0.62$ is not a design criterion.

It is obvious from Eq. III(6) that all radial compressors have values of N_S between, say, 60 and 110. Lower and higher values would lead to impossible designs which would never be built anyway. The only merit of the specific speed is to find out whether a radial compressor can be built at all for given values of N , Q_1 , and H_{1s} . If N_S is outside the range of 60 to 110, and if the above-mentioned design conditions cannot be changed, another type of compressor has to be chosen. However, if the relations of Table II were applied, the same conclusions would also be reached immediately even if the specific speed concept had never been invented. In fact its use can also be dangerous if, as might be the case for the example of Table III with $R_{10}/R_2 = 0.56$, the designer would try to reach the highest possible N_S by making the radius ratio R_{11}/R_0 excessively small or choosing too high a value of R_{11}/R_0 to reduce N_S for $R_{10}/R_2 = 0.7$. The example also shows that large changes of R_{11}/R_{10} have a small influence of N_S except, near the maximum possible value of N_S where R_{11}/R_0 tends toward zero. Further, if $N_S = 80$ would be considered necessary, a large number of high-performance radial compressors would never have been built, much to the detriment of the development of these promising machines, where a better physical understanding of the complicated flow phenomena can still lead to considerably improved performance.

Unfortunately there always exists the tendency in engineering to try to set up simple rules or criteria which make it possible to judge whether or not a design is feasible, without having to go through the strenuous mental processes to try to understand the phenomena that actually occur and to relate them to the fundamental laws of nature. If our only task were to build the same machines over and over again, sometimes

a little smaller, all would be well with this kind of handbook engineering. However, if an engineer believes that improvements are possible, and if he reflects on what has happened during the past years he cannot doubt that this will be the case, he must not accept the barriers that have been set up by past experience, and be impressed by the achievements that have been made. With a critical mind he has to evaluate what is true and what is false with accepted methods, and his aim must be to try to understand, to search, and to improve. Too often engineers are handlers of formulas or recipes, and there is the tendency to accept their results as correct without much questioning, especially if they are ground out by a computer, without finding out what sort of basic principles and assumptions led to the numbers. In the near future our modern computers may well be the biggest obstacle to imaginative original thinking and the use of new concepts, since for every problem there will very soon exist some sort of a program that can show that everything is known, and that nothing new needs to be added. All one has to know is the necessary format for the input to obtain the desired result, in print, in graphs, even in drawings. The inventive and critical engineer however must take the trouble to find out how the program was established and what basic principles and assumption were made, and must then evaluate the obtained numbers in the light of these conditions.

The biggest objection to the specific speed criteria is however that they do not satisfy the laws of dynamic similarity, even not for the limiting conditions that were assumed earlier. Equation III(6) shows that N_s is independent of the pressure ratio that is produced by a compressor. If all factors in Eq. III(6) are equal for two compressors, they can have different values of U_2/a_0 and therefore widely different blade width b_2 at the rotor discharge. One compressor could operate with subsonic, the other with supersonic velocities at the diffuser inlet. Figure 13 is an adaptation of Fig. 4 of Ref. 19. The curves of constant efficiency $\eta_c = 0.7$ and $\eta_c = 0.8$ and the curves labeled $N_{W1} = 1.0$ and $N_{W1} = 1.2$ for P_{t4}/P_0 were taken from Ref. 19 and redrawn in a bigger scale. Although labeled as lines of constant Mach number in Ref. 19 the curves for $N_{W1} = \text{constant}$ are for constant ratios of relative inlet and critical velocity for the total inlet temperature. Equation III(14) of Table III shows how these ratios are related to the actual Mach numbers M_{W1} . Although the differences between N_{W1} and M_{W1} are small at low Mach numbers, the values of M_{W1} vary from 0.94 to 1.01 for $N_{W1} = 1.0$ if β_{10} changes from 50° to 75° . According to the author of Ref. 19 the curves for $N_{W1} = 1.0$ and 1.2 represent design limits for higher pressure ratios. It is stated that maximum efficiencies will occur for impellers with backward bent blades operating at specific speeds N_s between 90 and 130, and specific diameters D_s between 1.3 and 1.7. The straight lines labeled $\mu\eta_c = \text{constant}$ which the present writer drew into the original diagram of Ref. 19 represent Eq. III(10), and relate D_s to N_s for wheels with radial blades at the discharge. Average values for $\mu\eta_c$ for such impellers are 0.7, hence all radial compressor of this type must lie in the vicinity of this curve for $\mu\eta_c$ in Fig. 13. The points labeled (1) to (7) in Fig. 13 represent design points for some actual compressors known to the writer, operating with U_2/a_0 of about unity, and inlet Mach numbers of 0.9 and higher. It is of interest to note that all these points lie on the curve $\eta_c = 0.70$ of Ref. 19 whereas all compressors, even those having N_s -values between 60 and 70, have efficiencies of 80 percent and higher. This situation shows again that the specific speed concept is a highly unsatisfactory design criterion, especially for radially-bladed compressor wheels, since it is impossible to design such machines with operating points that fall inside the closed curve, labeled $\eta = 0.8$ in Fig. 13. It is pointed out in Ref. 19 that the data presented in its Fig. 4 were calculated on the basis of loss considerations. It can be concluded therefore that this loss evaluation is in error or unsuitable for compressors with rotors that have radial blades at the discharge.

What seems more crucial to the writer is the fact that on the basis of Fig. 4 of Ref. 19 (or Fig. 13 of the present article) one might come to the conclusion that it is not possible to build high-speed compressors of the type discussed here with high efficiencies, for instance, as required for gas turbines, and that further developments of these machines might not be undertaken because of "proof" that improvements are not possible. This is again a case which shows that an analysis is no better than its assumption. Since the specific speed has no real physical meaning, unlike the actual similarity parameters such as Reynolds number, Mach number and others, the writer deplores the tendency to express everything in flow machines with N_s , also phenomena on which N_s has really no primary influence. Because of the definition of N_s it is always possible to do so because either rotative speeds and flow velocities, or lengths, can be related to it, and since in all these expressions there then appears N_s in one form or another, depending on what simplifying assumptions were made, the reader is given to believe that N_s has a governing influence on the performance, and that manipulating N_s is all that needs to be done to create an optimum design. Everyone who has observed actual flows in turbomachines in test rigs, and has tried to understand the complexities of these processes will agree that nature just is not so simple that it can be explained by a set of convenient numbers.

5. LOSSES IN RADIAL COMPRESSORS

It has been stated earlier that the wheel efficiency η_w of Eq. 15 is the best measure for the quality of a rotor wheel. As indicated, a number of factors influence η_w , but it will be examined now whether the deceleration ratio W_2/W_{10} has an overriding effect on η_w , as has been suggested by some sources which state that W_2/W_{10} should not be smaller than about 0.6 to avoid flow separations. It has already been shown in Fig. 12 that such a limit cannot be used for compressors that operate at high speed ratios U_2/a_0 because the radius ratios R_{10}/R_2 become too small, and it is then not possible to handle the large changes in volume flow rate from rotor inlet to rotor discharge, that occur at high pressure ratios, with acceptable ratios of axial blade width b_2 and R_2 . The example of paragraph 6 demonstrates this condition clearly. If $W_2/W_{10} \geq 0.6$ were a realistic criterion, the losses in rotors with high speed ratios would be large and it would be difficult to obtain high efficiencies. Figure 14 is presented to show that many compressors have deceleration ratios that are smaller than 0.6 without a drastic decrease in η_w . The circles in Fig. 14 represent design point data of some of the compressors of Ref. 6, and others that are known to the writer. The points indicated by x and + were calculated from the data given in Ref. 13, and the curves drawn through them represent the change of η_w with operating conditions of a particular wheel at values of U_2/a_0 of 0.83 and 1.02, respectively. All data points are for impellers with radial blades at the rotor discharge, and all compressors operate at high speed ratios, having overall efficiencies in excess of 80 percent.

In contrast to the expected trend that η_w decreases with decreasing values of W_2/W_{10} , the opposite

could be deduced from Fig. 14, since wheel No. 1 with $W_2/W_{10} = 0.265$ has the highest efficiency $\eta_w = 0.77$. For each data point in Fig. 14 are also given the ratios R_{10}/R_2 , R_{11}/R_{10} , b_2/R_2 and $\Delta x/\Delta R$ of the rotor. The latter ratio establishes the general shape of the meridional channel and the values show that the contours of the meridional flow paths of all compressors must have small curvatures with the exception, maybe, of wheel No. 11. Definite reasons for the higher values of η_w in some designs cannot be given, probably because of the effect of the design of the inducers on the wheel performance. However, it is recognizable from Fig. 14 that high efficiencies η_w are reached either for high ratios R_{11}/R_{10} or high values of b_2/R_2 . The influence of R_{10}/R_2 seems small, although most good wheels have values of R_{10}/R_2 between 0.6 and 0.7. Large ratios R_{11}/R_{10} require high relative Mach numbers M_{w1} to pass the flow rate through the eye of the impeller, and high ratios b_2/R_2 are obtained if the absolute flow angles α_2 are large. For high values of M_{w1} the inducer becomes critical, and with large angles α_2 the design of the diffuser, especially the transition between wheel and diffuser throat, becomes a difficult task. It is felt that high performance compressors can be developed if more attention is given to these two problem areas.

From the curves in Fig. 14 it is quite evident that the range in which η_w remains constant for off-design operation becomes smaller the higher the speed ratio U_2/a_0 is, a condition which is, at least in part, responsible for the steeper characteristics of compressors operating at high speed ratios.

The ratio of b_2/R_2 also has an effect on the disk friction loss of an impeller. Assuming that the disk extends to the outer radius R_2 ; that is, if no scallops are arranged, a frictional moment M_{DF} acts on the back side of the impeller which can be determined by ²⁰

$$M_{DF} = c_M \rho_2 D_2^3 U_2^2 \quad (49)$$

where c_M depends on the Reynolds number

$$Re = \frac{U_2 D_2}{\nu} \quad (50)$$

and the axial gap δ_a between the rotating disk and the stationary wall. The influence of the ratio δ_a/R_2 , and the effect of disk roughness, which have been investigated by Refs. 21, 22, 23, and 24 are discussed in Ref. 8. Figure 15 has been established from the results of the quoted references, but experience has shown that the values of c_M can be a multiple of those of Fig. 15 if the flow in the region between the disk and the wall has radial velocity components pointing away from or toward the axis of the impeller. For compressors pumping ambient air the Reynolds number of Eq. 50 varies between about (10^6) and $3(10^7)$ for peripheral speeds between 1000 and 1600 ft/s, and rotor diameters between 3 and 20 inches. Although the average value of c_M from Fig. 15 is then about $1.5(10^{-4})$, it has been shown by experience that $c_M = 2.5(10^{-4})$ is more realistic for actual compressor wheels. For a mass flow rate \dot{m} the power absorbed by an impeller is $\dot{m} \mu U_2^2$ in accordance with Eq. 3, which is also equal to $M\omega$, where M is the driving moment, and

$$M = \frac{\dot{m} \mu U_2^2}{\omega} = \dot{m} R_2 \mu U_2$$

However

$$\dot{m} = 2 \pi R_2 b_2 k_{B2} \nu_{m2} \rho_2$$

and, with the relations of Table I,

$$M = 2\pi R_2^3 \left(\frac{b_2}{R_2}\right) k_{B2} \mu^2 U_2^3 \rho_2 \cot \alpha_2 \quad (51)$$

The total moment which has to be overcome by the driving source is then $M + M_{DF}$ and if the efficiency of the compressor is η_c , without taking the disk friction moment into account, the actual compressor efficiency η of the machine is $\xi_{DF} \eta_c$, and

$$\xi_{DF} = \frac{M}{M + M_{DF}} = \frac{1}{1 + (M_{DF}/M)}$$

Then by Eqs. 49 and 51

$$\xi_{DF} = \frac{1}{1 + \frac{(4/\pi) c_M \tan \alpha_2}{(b_2/R_2) \mu^2 k_{B2}}} \quad (52)$$

It can be noted that ξ_{DF} is independent of the mass density ρ_2 and R_2 since both M and M_{DF} are proportional to these quantities. Hence Eq. 51 holds for all impellers with radial blades the outer radius R_2 . Equation

52 is plotted in Fig. 16. This figure shows that with small ratios b_2/R_2 there can occur a considerable reduction in efficiency, which is the greater the larger the angle α_2 is. For $\alpha_2 = 75^\circ$ the ratio $(b_2/R_2) k_{p2} u^2$ should not be less than about 0.06 to limit ξ_{pF} to 0.98. Then, with $k_{p2} = 0.95$ and $u = 0.90$, the ratio of b_2/R_2 must not be smaller than 0.08 to avoid efficiency reductions because of disk friction moments.

Although the above limit for b_2/R_2 has been obtained by considering the frictional moment at the back side of the impeller, it is very probably that the so-called scrubbing loss of the blade tips at the outer contour of the meridional flow path produces frictional moments which are of similar nature and of the same order of magnitude as the disk friction moments. Moreover, as shown in Fig. 15 for the latter, these moments will also not be greatly influenced by the ratio of tip clearance and R_2 if it is of the order of 0.05, which constitutes a normal to lower limit for most designs. The scrubbing loss is similar to the loss due to disk friction because the boundary layer along the stationary outer wall is rotated by the blade tips. If the losses at the blade tip would be taken to be those due to the flow of the fluid from the pressure side to the pressure side of the blade across the blade clearance, it would be inconceivable that the reductions in compressor efficiency with increased tip clearance are as small as shown by the measurements of Ref. 25. The same behavior has been found in radial turbines⁸ where an increase of the ratio of tip clearance and axial blade width b from 4 percent to 10 percent produced practically no drop in efficiency, but if 10 percent was exceeded there occurred a radical efficiency reduction. The sudden drop beyond the 10 percent clearance ratio could occur because of massively increased leakage flows across the blade tips once they are outside the wall boundary layer.

Experience has also shown that the ratio of blade width b_2/R_2 should not be less than 8 percent. The value of c_m in Eq. 51 for the representation in Fig. 16 has actually been increased from the average value for disk friction ($\sim 1.5(10^{-4})$) to $2.5(10^{-4})$ to demonstrate that this limit is very likely due to the combined effects of disk friction and scrubbing loss. For this ratio of b_2/R_2 and for properly designed inducer sections of an impeller, with meridional contours having small and smoothly changing curvatures, it should be possible to obtain wheel efficiencies η_w of between 0.75 and 0.80 for $b_2/R_2 = 0.08$ if the ratios R_{11}/R_{10} are not less than about 0.5.

A large portion of the total losses in radial compressors occurs between the discharge of the wheel and the diffuser throat. The non-uniform distribution of the relative velocities at the rotor discharge produces a non-steady and greatly irregular absolute flow at this station which must be directed toward the diffuser inlet, preferably in a manner that provides uniform flow conditions at this station. If this uniformity is not achieved it is very unlikely that the diffuser proper can perform its function with minimum losses. Very limited data are available for the design of and the losses in these transition sections. Figure 17 shows a typical distribution of the static pressures along the side walls of such a diffuser inlet for a machine that has a value of M_{y2} of about 1.18. Firstly it is clear that the absolute flow is irregular, judging from the change of the pressures in peripheral direction at the wheel discharge. Secondly, the design of the diffuser inlet is not as good as it is desirable because fluid particles undergo compressions and expansions before they reach the diffuser throat. Moreover, Fig. 17 also shows the futility of trying to apply simplified calculating method for this part of the process in the compressor.

Of particular importance is the design of the leading edge of the diffuser blade since the slightest misorientation will produce major disturbances usually with the effect that the flow rate at which the compressor surges is too close to its design flow rate. This condition occurs if the mean angle of the lip section with respect to the radial direction is too large or too small, and since the optimum angle depends on the performance of the rotor, it is not possible to indicate exactly how the transition section must be designed. Experiences have made it obvious, however, that theoretical methods which prescribe a logarithmic spiral or other shapes for the curved part of the transition section overlook the fact that the flows to be handled are so far from being uniform that is almost impossible to obtain optimum solutions without extensive experimental work that investigate the performance of different shapes, not only with respect to optimum efficiency but also to obtain the necessary surge margin. One of the major problems with experiments however is the accurate measurement of the static pressures in these irregular flows. In most cases it is found that Pitot-static pressure probes with even the smallest possible tube diameters are sufficient to change the flow pattern, in fact they usually throw the compressor into surge if it is operating near the design point, so that one has to rely on static wall pressure taps to investigate the effectiveness of different designs. Schlieren pictures for supersonic conditions do also not give information that can be interpreted with ease because of the three-dimensional character of the flow, not to mention the difficulties associated with the arrangement of the necessary optical system. It is therefore quite difficult to measure the true average static pressure after a compressor wheel, and because of the uncertainties that arise if the average static wall pressures at R_2 is identified with it, the separation of the losses into those originating in the wheel, and those occurring in the transition section to the diffuser, is equally difficult. For this reason the evaluation of the actual wheel efficiency η_w may be associated with errors and this could be the reason why it is often impossible to correlate experimental data from different sources. Laser systems were mentioned earlier as an experimental tool to investigate flows in turbomachines, and if the so-called velocimeter, using two laser beams for the determination of the actual magnitude and direction of the velocity in the vicinity of a particular station has been perfected, this instrumentation would be the best possible means to observe the true flow patterns in machines, not only qualitatively but also quantitatively.

In accordance with a limited amount of test data with a compressor operating at $U_2/a_0 = 1.4$, with $M_{y2} = 1.18$, the approximate ratio of the total pressure P_{t2} at the rotor discharge and P_{tx} at the throat of the diffuser was found to be about 1.14, giving an efficiency of the transition section of 0.63. This efficiency is defined as the ratio of the actual static temperature rise to obtain sonic velocity at the throat to that of an isentropic compression for the same pressure ratio. The average discharge flow angle α_2 was about 75° . It seems however that the transition section of the compressor in question could be improved, so that the numbers given above represent only orders of magnitude and not values that cannot be improved.

Although a large number of tests have been carried out with subsonic diffusers by many sources, these data cannot be applied directly to the diffusers of compressors with high speed ratios, especially if the

Mach numbers at the diffuser inlet are close to unity. Moreover, it has almost become standard procedure to apply the so-called equivalent cone angle of straight, round diffusers to decelerating flow channels with other cross sections. This procedure converts the inlet and discharge flow areas of a diffuser with arbitrary cross sections into circular ones, either with equal areas or by means of the hydraulic diameter, and then determines the equivalent cone angle with these diameters and the actual length of the diffuser. Either of the two methods for the determination of the equivalent cone angle breaks down for particular designs, or gives results that are in disagreement with actual test data.

An attempt to establish a more rigorous calculating method for arbitrary channels has been made by Traupel²⁶, primarily for incompressible flows and approximations for the compressible case, but it is then suggested that the equivalent cone angle be used again as a criterion for the permissible deceleration. A different approach is possible, however, which has a minimum of simplifying assumption and has proved to be valid for diffusers of arbitrary geometry, even axisymmetric ones with curved meridian channels and annular cross sections, for instance those arranged after turbomachines to deflect the flow from the axial to the radial direction. The derivation and the use of the equations are given in Table IV. From the laws of conservation of momentum, mass, and energy, combined with the first law of thermodynamics, there is obtained Eq. IV(10) which relates the frictional heat Tds to the work necessary to overcome the action of the shear stresses along the channel walls. With the so-called referred mass flow rate \dot{m}_r at the diffuser inlet, which is a dimensionless quantity defined by Eq. IV(14), there is then obtained the principal equation IV(15). This equation is of the form $dX_1 = dX_2$, where dX_1 contains the properties of state p , p , and s , at the stations along the channel length, and dX_2 is depending only on the channel geometry and the skin friction coefficient c_f . Actually, for a given diffuser the variables in dX_1 are not independent of the changes of the channel geometry along its length L that occur in dX_2 . However, if one were to adjust the flow areas A and the wetted perimeter C of the sections between the inlet and the exit in such a manner that the thermodynamic process of the fluid in the channel would follow a polytropic law, it would be possible to integrate dX_1 independently from dX_2 since s , and p are then unique functions of the pressure p for a constant polytropic efficiency η_p or a constant loss coefficient $\zeta = 1 - \eta_p$. Conversely, if an average skin friction coefficient \bar{c}_f is introduced, the value of X_2 is obtained by integrating the quantity $d\Omega$ from diffuser inlet to diffuser discharge, establishing the so-called diffuser shape factor Ω which is identical with the value Φ of Ref. 26. The diffuser shape factor is a dimensionless quantity which depends only on the area and perimeter changes along the length L of the diffuser.

From the integration of dX_1 there is obtained the quantity X_1 as a unique function of the static pressure ratio in the diffuser, γ , and the polytropic loss coefficient ζ . For $\gamma = 1.4$ the function X_1 is plotted in Fig. 18 for different values of ζ , as function of the pressure ratio p_4/p_3 . Obviously the conditions of state change monotonously during the polytropic process from p_3 to p_4 in Fig. IV(2), and the function X_1 only holds for such changes. Hence if the area changes in the diffuser would be such that compressions in one part would be followed by expansions in another part, the function X_1 could not take care of the situation, since for an expansion the polytropic law established by Eq. IV(7) would produce an entropy decrease in violation of the second law of thermodynamics. However, even for smoothly changing areas in the diffuser, which it will have in any case, the thermodynamic process in the T - s diagram of Fig. IV(2) might not follow the isentropic line which is shown there, but one which curves either upward or downward from it. It must be recognized however that the value of the function X_1 will not be greatly changed by different distribution of p along L , similar to the integral of Tds which is about equal to $(T_3 + T_4)(s_4 - s_3)/2$ almost independent of how the process proceeds from station (3) to station (4), provided it goes along a smooth and fairly regular curve in the T - s diagram.

Moreover, the polytropic loss coefficient ζ is not assumed a priori, but adjusted to satisfy the equation of continuity at the diffuser discharge for a specified average skin friction coefficient. The necessary iteration to solve this problem is explained in Table IV. The method employs the dimensionless flow function Φ which is plotted in Fig. 18 also, with the ratio of total and static pressure that correspond to an isentropic process as variable. Blockage factors for the diffuser areas are introduced to take account of the boundary layer thickness.

For small pressure ratios p_4/p_3 ; that is, for low Mach numbers at the diffuser inlet, the method leads to relations that are identical with those commonly applied for the loss evaluation for incompressible diffuser flows. In particular, the average skin friction coefficient is equal to

$$\bar{c}_f = \frac{C_{PRI} - C_{PR}}{\Omega} \quad (53)$$

where C_{PRI} and C_{PR} are the so-called ideal and actual recovery factors, which express the increase in static pressure as percentage of the kinetic energy of the flow at the diffuser inlet. The quantity Ω is the diffuser shape factor defined by Eq. IV(19).

Figure 19 shows the skin friction coefficients \bar{c}_f obtained with Eq. 53 from the experimental data of Ref. 27 for two-dimensional diffusers. Except for the diffuser with $L_0/a_1 = 48$, which is unduly long, the data lie within a relatively small band, with the test data for a thin displacement thickness of the boundary layer at the inlet near its lower boundary. It is of interest to note that for large values of Ω the skin friction coefficients are very nearly equal to those of fully developed turbulent flows along moderately rough surfaces in pipes or along plates, as shown by Ref. 20 (p. 587, and p. 611). The results of Ref. 28 which were obtained, in part, at high subsonic speeds give values of \bar{c}_f that lie in the same band as in Fig. 19, indicating that the skin friction coefficients \bar{c}_f are directly related to Ω for different types of cross sections, and at speeds where compressibility effects cannot be disregarded.

This product is shown in Fig 20

From Eq. IV(18) of Table IV it is seen that X_2 is directly proportional to $\bar{c}_f \Omega$, for the same data points of Ref. 27 as plotted in Fig. 19. Hence it appears that a diffuser with a shape factor Ω equal to 10 represents an optimum solution. If Ω is smaller the efficiency decreases radically and for values of Ω larger than 10 a diffuser does not make full use of the possible adverse pressure gradient that a boundary layer can sustain without flow separations. The criterion $\Omega = 10$ has been used by the writer with

success for a number of diffuser designs, and a variety of different diffuser shapes is now being tested at NPGS to verify the validity of the criterion at high inlet velocities and with inlet flow distortions.

As shown also in Ref. 26, the shape factor of a round conical diffuser with inlet radius R_1 , length L , and the half-angle ϵ of its divergence is

$$\Omega = \frac{1}{2 \tan \epsilon} \left[1 - \frac{1}{(1 + 2(L/R_1) \tan \epsilon)^4} \right] \quad (54)$$

For conical diffusers where L is large with respect to R_1 , Eq. 54 gives a divergence angle of $2\epsilon = 50.45'$. The influence of the ratio L/R_1 is small if L/R_1 is larger than about 10. Two-dimensional straight diffusers with constant depth b , and widths a_1 at the inlet and a_2 at the discharge, determined by $a_2 = a_1 + 2 L \tan \epsilon$, where ϵ is again the half-angle of the channel, have shape factors

$$\Omega = \frac{L/a_1}{1 + 2(L/a_1) \tan \epsilon} \left[1 + \frac{1}{1 + 2(L/a_1) \tan \epsilon} + \frac{2 a_1}{b} \right] \quad (55)$$

If the diffuser of Fig. 17 had a ratio $a_1/b = 2.4$, the value of Ω for $\epsilon = 5^\circ$ and $L/a_1 = 10$, is about equal 22.4, which appears to be excessive. Hence the diffuser should have a divergence perpendicular to the plane of drawing also to increase b_1 at the inlet to b_2 at the discharge. For shapes of this type the expression of Eq. IV(19) for Ω leads to complicated integrals. However with a simple graphical integration for a half-angle of divergence of about 2° that produces a ratio $b_2/b_1 = 2.4$ with the widths a_1 and a_2 remaining unchanged, the diffuser form factor is reduced to about 11.2. A diffuser channel for this value of Ω for compressors is very likely very close to the optimum possible solution because of then non-uniform flow conditions that exist at its inlet.

Because of these disturbances, the values of $\Omega \bar{c}_f$ presented in Fig. 20 should also be increased, say, from 0.10 to about 0.15, or 0.20, for Ω of about 10. How these values affect the diffuser efficiency will be shown with a simplified approach of the diffuser design method of Table IV. It is assumed that the Mach number M_{V3} at the throat is unity, but the method is not restricted to this value. The flow function ϕ_3 of Eq. IV(22) is then equal to 0.6847 in accordance with Fig. 18, and $P_{t3}/P_3 = 1.8929$. From Eq. IV(28) for $M_{V3} = 1$, $\gamma = 1.4$,

$$\dot{m}_{r3} = (0.6847) (1.2)^3 = 1.1832$$

From Eq. IV(18)

$$X_2 = \frac{1.1832^2}{2} \bar{c}_f \Omega = 0.7 \bar{c}_f \Omega$$

Hence, $X_2 = 0.07$ for $\bar{c}_f \Omega = 0.1$, $X_2 = 0.14$ for $\bar{c}_f \Omega = 0.2$, and these values are equal to the values of the function X_1 which is plotted in Fig. 18. It will now be assumed that the area ratio A_3/A_4 of the diffuser is $1/6.6 = 0.151$ as is the case for the design of Fig. 17 with a half-angle of divergence of 2° to increase the depth b also. With blockage factors $k_{B3} = 0.96$ and $k_{B4} = 0.90$, by Eq. IV(29)

$$\phi_4 = (0.6847) (0.151) (0.96/0.9) (P_{t3}/P_{t4}) = 0.11 (P_{t3}/P_{t4})$$

Assuming that P_{t3}/P_{t4} is about 1.05, the value of ϕ_4 is 0.115. From the plot of ϕ vs P_t/P_t it can be seen that $\phi_4 = 0.115$, or slight changes of it on account of a wrongly chosen value of P_{t3}/P_{t4} , the value of P_{t4}/p_4 will not be higher than 1.02 because of the large change of ϕ with P_t/P_t close to unity. Then,

$$\frac{p_4}{P_3} = \frac{P_{t3}/P_3}{P_{t4}/P_4} \frac{P_{t4}}{P_{t3}} = \frac{1.8929}{1.02} \left(\frac{1}{1.05} \right) = 1.77$$

The approximate values of ζ can then be read from Fig. 18 at the intersection of the lines for the known values of X_1 and for $p_4/P_3 = 1.77$. For $\bar{c}_f \Omega = 0.1$, or $X_1 = 0.07$, there is $\zeta = 0.070$, and for $\bar{c}_f \Omega = 0.2$, or $X_1 = 0.14$, one finds $\zeta = 0.130$, giving approximate values of the diffuser efficiency of 0.93 and 0.87, respectively, without taking account of the reheat effects that are reflected in Eq. IV(35). The values of ζ thus obtained can then be used to determine the pressure ratio p_4/P_3 more precisely, by taking the pressure ratio P_{t3}/P_{t4} to be that obtained from Eq. IV(33) with the approximate pressure ratio $p_4/P_3 = 1.77$.

6. SAMPLE CALCULATIONS

To demonstrate the effectiveness of the developed performance parameters, and the help of the figures, the dimensions of an impeller for an air compressor with a pressure ratio of eight will be established for the following conditions:

$$\dot{m} = 2.5 \text{ lbm/s} = (2.5/32.174) \text{ slug/s}$$

$$P_0 = 14.7 \text{ psia}; T_0 = 520^\circ\text{R}$$

$$P_{t4}/P_0 = 8$$

$$R_G = 1716.48 \frac{\text{ft-lb}}{\text{slug, } ^\circ\text{R}}; \gamma = 1.4$$

From Eq. 5

$$a_0 = 1117.8 \text{ ft/s}$$

Assuming $\mu = 0.9$; $\eta_c = 0.82$, from Eq. II(3), or Fig. 4,

$$U_2/a_0 = 1.658$$

hence

$$U_2 = 1853.4 \text{ ft/s}$$

Figure 8 clearly shows that for U_2/a_0 and reasonable ratios R_{10}/R_2 the relative inlet velocity M_{w1} must be supersonic. For $M_{w1} = 1.15$ and $\beta_{10} = 70^\circ$ there is from Fig. 8, or Eq. II(4),

$$\frac{R_{10}}{R_2} = 0.642$$

Judging from Fig. 4 it is necessary to choose $\alpha_2 = 74^\circ$ to obtain a value of W_2/W_{10} of about 0.4. More precisely from Eq. II(5)

$$\frac{W_2}{W_{10}} = 0.405$$

For a chosen value of the wheel efficiency η_w of 0.7, there are from Eq. 21

$$\Psi = 0.629; \Psi^2 = 0.394$$

and the usual rotor efficiency η_R defined by Eq. 12, in accordance with Eq. 24, is

$$\eta_R = 0.88$$

With these values by Eq. II(9)

$$\left[1 - \left(\frac{R_{11}}{R_{10}}\right)^2\right] k_{B1} = \frac{\dot{m} \sqrt{R_G T_0}}{\pi R_2^2 P_0} \quad (5.7138)$$

and from Eq. II(11)

$$\frac{b_2}{R_2} k_{B2} = \frac{\dot{m} \sqrt{R_G T_0}}{\pi R_2^2 P_0} \quad (0.4127)$$

and, for approximate values $k_{B1} = 0.85$, $k_{B2} = 0.95$, by division of two above-listed relations,

$$\frac{b_2/R_2}{1 - (R_{11}/R_{10})^2} = 0.0646$$

Evidently this ratio holds for all compressors for the chosen conditions, irrespective of the flow rate and the inlet pressure. For chosen radius ratios R_{11}/R_{10} there are:

$R_{11}/R_{10} =$	0.2	0.3	0.4	0.5
$b_2/R_2 =$	0.062	0.059	0.054	0.048

All these ratios are too small to obtain the desired efficiency. They were obtained because R_{10}/R_2 was chosen too small and the angle β_{10} is too large, and both these values were taken to maintain a low Mach number M_{w1} . For a second try, let:

$$R_{10}/R_2 = 0.7; \beta_{10} = 60^\circ; \alpha_2 = 75^\circ$$

Then, from the inverse of Eq. II(4), expressing M_{w1} as function of R_{10}/R_2 and β_{10} ,

$$M_{w1} = 1.3198$$

From Eq. II(5)

$$\frac{W_2}{W_{10}} = 0.360$$

The latter value seems acceptable in view of Fig. 14, and by proper rotor dimensioning a wheel efficiency $\eta_w = 0.7$ should still be reached. By Eq. 21.

$$\psi = 0.576; \psi^2 = 0.332$$

By Eq. II(9)

$$\left[1 - \left(\frac{R_{11}}{R_{10}}\right)^2\right] k_{B1} = \frac{\sqrt{R_G T_0}}{\pi R_2^2 P_0} (3.7063)$$

and, from Eq. II(11)

$$\frac{b_2}{R_2} k_{B2} = \frac{\sqrt{R_G T_0}}{\pi R_2^2 P_0} (0.4494)$$

With $k_{B1} = 0.85$, $k_{B2} = 0.95$

$$\frac{b_2/R_2}{1 - (R_{11}/R_{10})^2} = 0.1074$$

For the chosen value $b_2/R_2 = 0.08$ the radius ratio R_{10}/R_2 can be 0.5, which makes it possible to design a meridional flow path that has an acceptable shape.

From the inlet conditions and the design flow rate:

$$\frac{\sqrt{R_G T_0}}{P_0} = \frac{2.5}{32.174} \frac{\sqrt{(1716.48)(520)}}{14.7} = 4.994 \text{ in.}^2$$

because the pressure P_0 was introduced in pound per sq. in.. Then, from the previous data,

$$\pi R_2^2 = \frac{(4.994)(3.7063)}{(1 - 0.25)(0.85)} = 29.034 \text{ in.}^2$$

Hence

$$R_2 = 3.04 \text{ in.}; D_2 = 6.08 \text{ in.}$$

$$R_{10} = 2.125 \text{ in.}; D_{10} = 4.25 \text{ in.}$$

$$R_{11} = 1.062 \text{ in.}; D_{11} = 2.125 \text{ in.}$$

$$b_2 = 0.243 \text{ in.}$$

For the chosen data, from Eq. II(6),

$$M_{v2} = 1.256$$

The rotative speed N can be determined from Eq. II(10), or directly from

$$N = \frac{30}{\pi} \omega = \frac{30}{\pi} \frac{U_2}{R_2} = \frac{(30)(1853.4)}{\pi(3.04/12)} = 69,860 \text{ rpm}$$

REFERENCES

1. Vavra, M. H. Aerothermodynamics and Flow in Turbomachines, Wiley Bros, New York, 1960.
2. Vavra, M. H. Axial Flow Turbines, Von Karman Institute for Fluid Dynamics, Lecture Series 15, pp. 99/100, April 1969.
3. Traupel, W. Die Theorie der Stroemung durch Radialmaschinen, Braun, Karlsruhe, 1962.
4. Johnston, J. P.
Dean, R. C., Jr. J. Engg. for Power, Trans. ASME, pp. 49-62, January 1966.
5. Stiefel, W. "Experimental Investigations on Radial Compressors ...", Course Note 53b, Von Karman Institute, March 1965.
6. Stiefel, W. "Untersuchung an Radialen Verdichterlauferen", AVA Forschungsbericht 63-01, Triebwerksaerodynamik der Turbomaschinen, Teil II, Goettingen, 1963.
7. Sakai, T.
Watanabe, I., et al. "On the Slip Factor of Centrifugal and Mixed-Flow Impellers", ASME Paper 67-WA/GT-10.
8. Vavra, M. H. "Radial Turbines", Part 4 of AGARD-VKI Lecture Series 6 on "Flow in Turbines", Von Karman Institute, March 1968.
9. Bammert, K.
Bohm, E. "Nuclear Plants with High-Temperature Reactor and Helium Turbine," ASME Paper 69-GT-43, March 1969.
10. Groh, F. W.
Robb, W. L. "High Efficiency Can Be Achieved in Small Size Transonic Compressor Rotors," SAE Paper 820C, January 1964.
11. Katsanis, T.
McNally, W. D. "Programs for Computation of Velocities and Streamlines on a Blade-to-Blade Surface of a Turbomachine" ASME Paper 69-GT-48, March 1969.
12. Jmbach, H. E. "Die Berechnung der kompressiblen, reibungsfreien Unterschallstroemung durch raumliche Gitter aus Schaufeln auch grosser Dicke und starker Woelbung" Mittlg No 8, Inst. Thermische Turbomaschinen, ETH, Juris Verlag, Zurich, 1964.
13. Linsi, U. Brown Boveri Review, Vol. 53, No. 3, p. 161, March 1965.
14. Fowler, H. S. "Some Measurements of the Flow Patterns in a Centrifugal Compressor Impeller," ASME Paper 65-WA/FTP-7, April 1965.
15. Fowler, H. S. "The Distribution and Stability of Flow in a Rotating Channel," ASME Paper 68-GT-1, March 1968.
16. Halleen, R. M.
Johnson, J. P. "The Influence of Rotation on Flow in a Long Rectangular Channel" Stanford University, Report MD-18, May 1967.
17. Ackeret, J.
Keller, C.
Salzmann, F. Schweizer Bauzeitung, No. 23, December 1934.
18. Shepherd, D. G. "Principles of Turbomachinery", Macmillan; New York, 1956.
19. Baljé, O. E. J. Engg for Power, Trans. ASME Series A, Vol. 84, No. 1, pp. 83-114, Jan 1962.
20. Schlichting, H. Boundary-Layer Theory, 6th ed., p. 606, McGraw-Hill, N. Y., 1968.
21. Daily, J. W.,
Nece, R. E. J. of Basic Engg., Trans. ASME, p. 217, March 1960.
22. Nece, R. E.
Daily, J. R. J. of Basic Engg., Trans. ASME, p. 553, Sept. 1960.
23. Pantel, K. Forschung, Vol. 16, p. 97, 1950.
24. Maroti, L. A.
Deak, G.
Kreith, F. J. of Basic Engg., Trans. ASME, p. 539, Sept. 1960.
25. Schmidt-Theuner, P.
Mattern, J. Brown Boveri Review, Vol. 55, No. 8, p. 453, 1968.

26. Traupel, W. Thermische Turbomaschinen, Bd. 1., p. 308, Springer, Berlin, 1962.
27. Waitman, B. A.
Reneau, L. R.
Kline, S. J. J. of Basic Engg., Trans. ASME, Vol. 83, Series D., No. 3, p. 349, Sept. 1961.
28. Sovran, G.
Klomp, E. D. "Experimentally Determined Optimum Geometries for Rectilinear Diffusers with Rectangular, Conical or Annular Cross Sections," Symposium on Fluid Mechanics of Internal Flow, General Motors Research Laboratories, Sept. 1965.

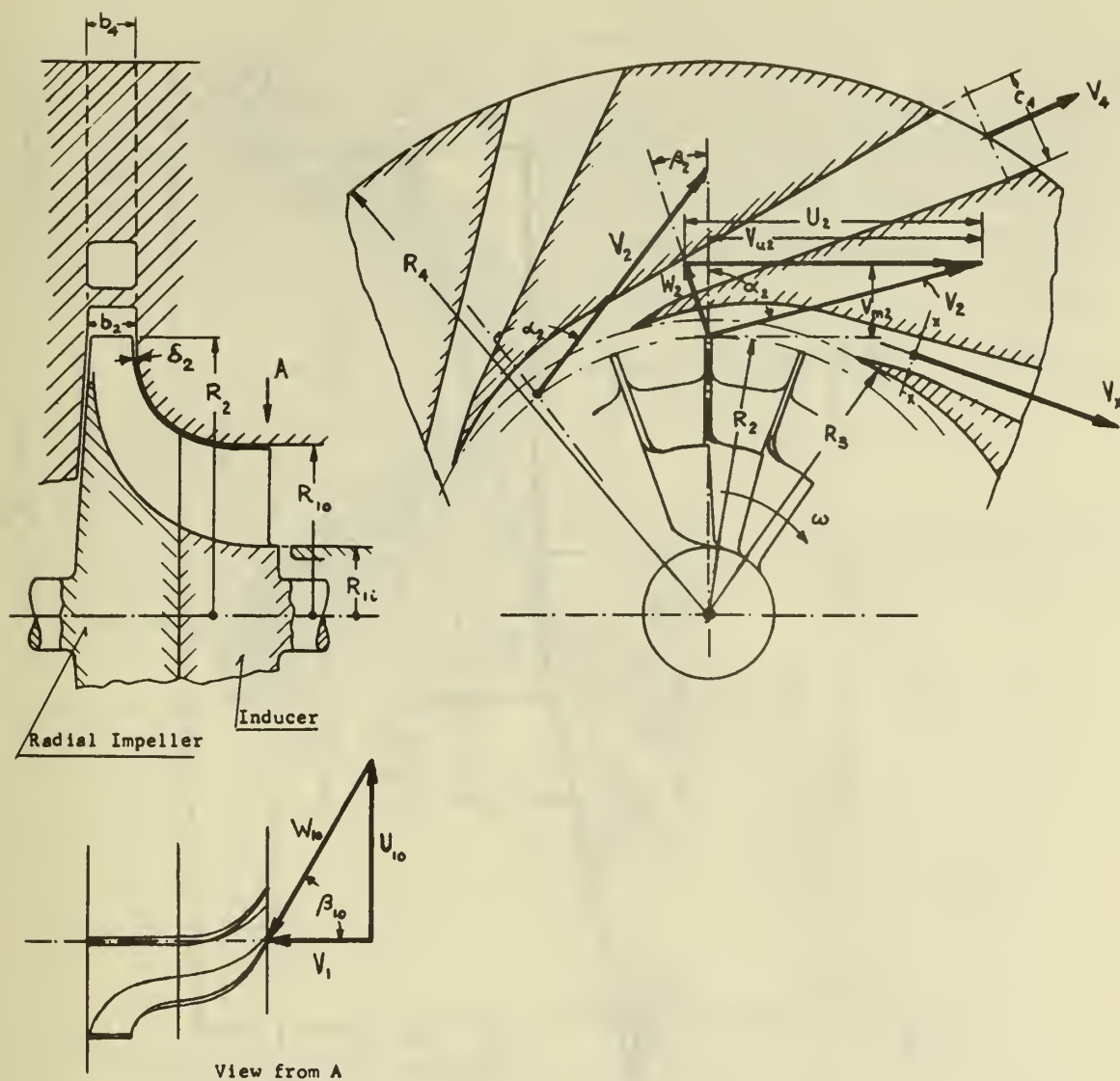


FIG. 1 RADIAL - FLOW COMPRESSOR

- R - Radius
 V - Absolute Velocity
 W - Relative Velocity
 U - Peripheral Speed
 α - Absolute Flow Angle
 β - Relative Flow Angle
 b - Axial Channel Width
 c - Height of Diffuser Channel

Subscripts:

- 1 - refers to rotor inlet
 2 - refers to rotor discharge
 3 - refers to inlet lip of diffuser blades
 x - refers to throat of diffuser channel
 4 - refers to discharge of diffuser channel
 m - refers to meridional direction
 u - refers to peripheral direction
 i - refers to inner radius at compressor inlet
 o - refers to outer radius at compressor inlet

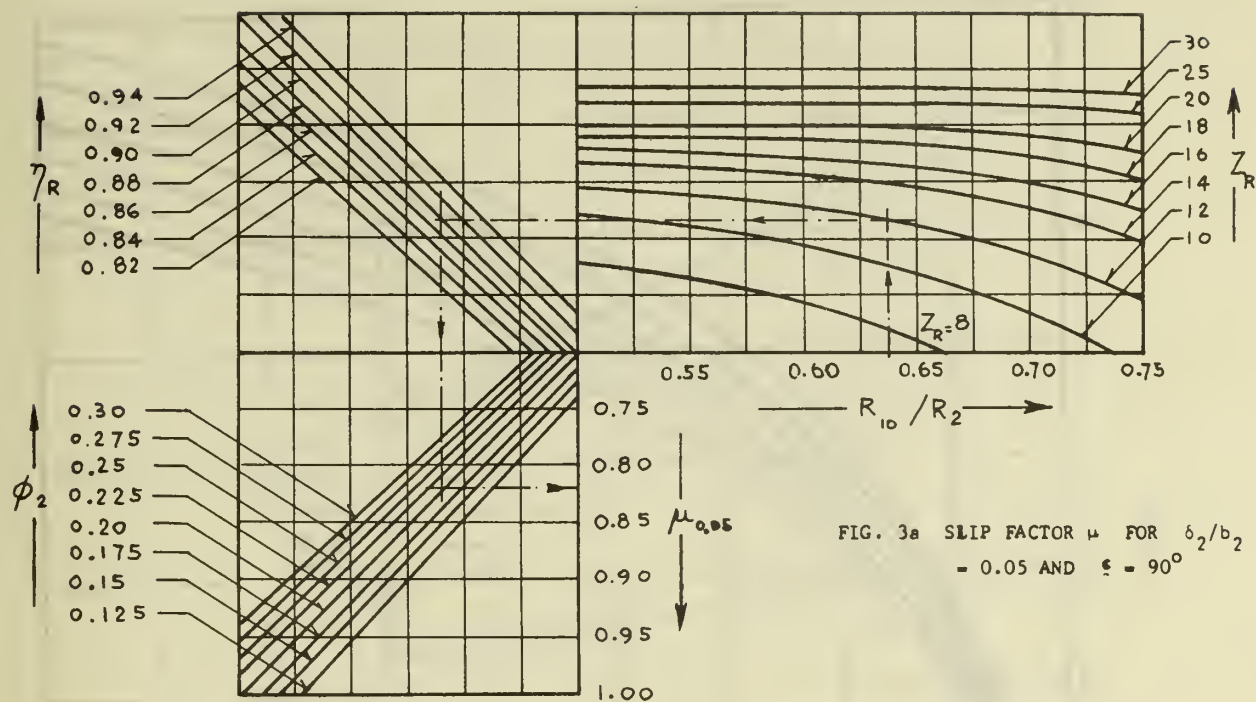


FIG. 3a SLIP FACTOR μ FOR $\delta_2/b_2 = 0.05$ AND $\epsilon = 90^\circ$

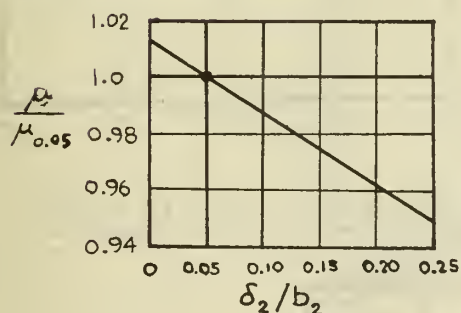


FIG. 3b CORRECTION FACTOR FOR RATIOS OF TIP CLEARANCE δ_2 AND AXIAL BLADE WIDTH b_2 DIFFERENT FROM 0.05

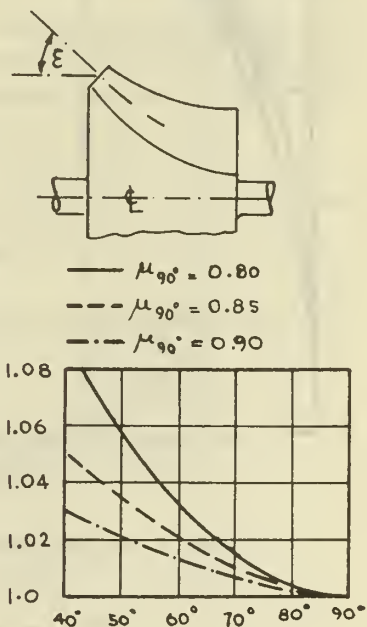


FIG. 3c CORRECTION FACTOR FOR MIXED-FLOW IMPELLERS

FIG. 3 SLIP FACTOR FOR RADIAL COMPRESSOR IMPELLERS WITH RADIAL BLADES AT DISCHARGE

(Figures were adapted from Refs. 5 and 6)

$$\phi_2 = \frac{v_{m2}}{U_2} \quad (\text{ see Eq. II(8) of Table II })$$

η_R - Rotor Efficiency (see Eq. 12)

Z_R - Number of Rotor Blades

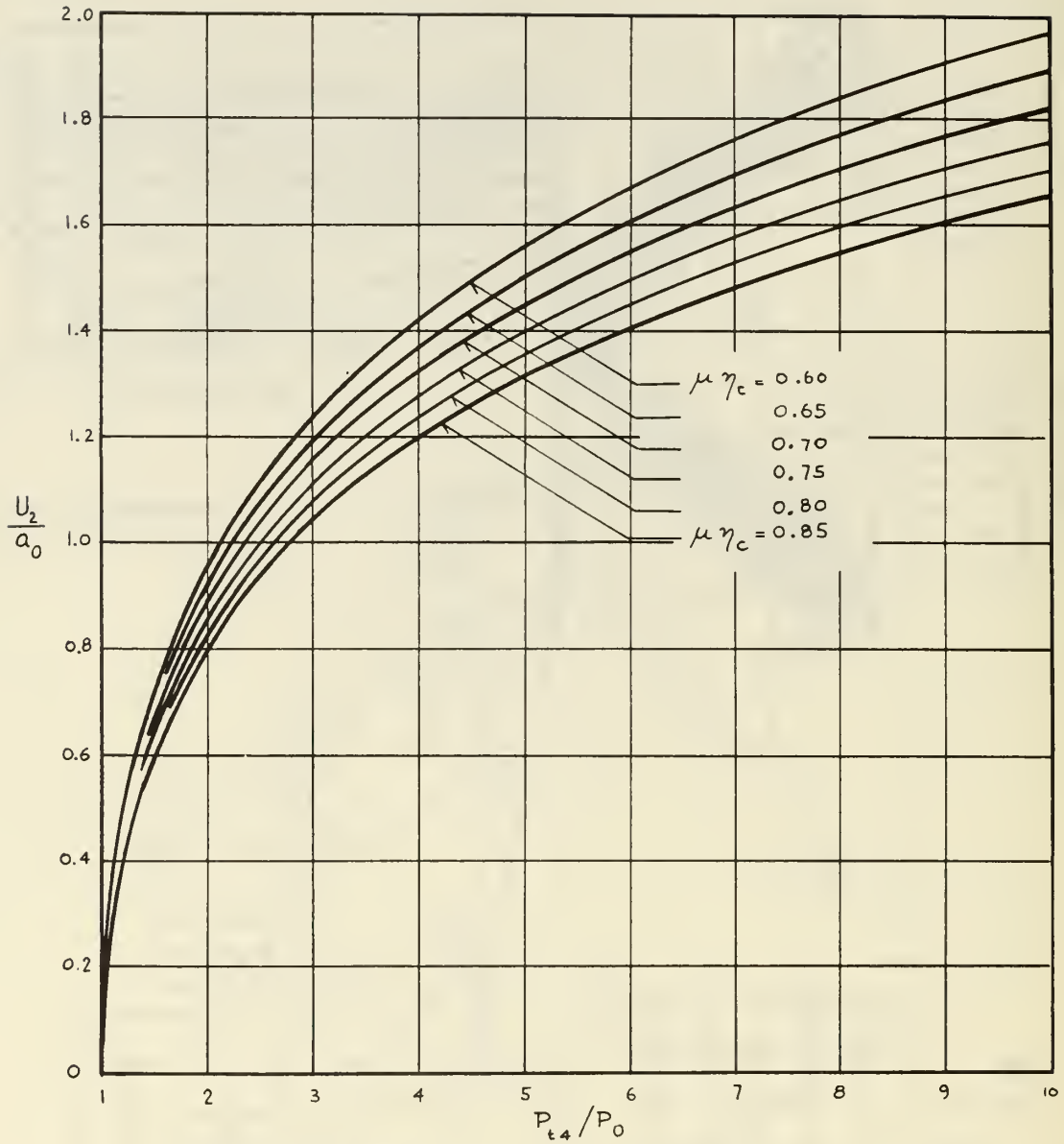


FIG. 4 RELATION BETWEEN PRESSURE RATIO AND U_2/a_0 FOR $\gamma = 1.4$ (Eq. II(3))

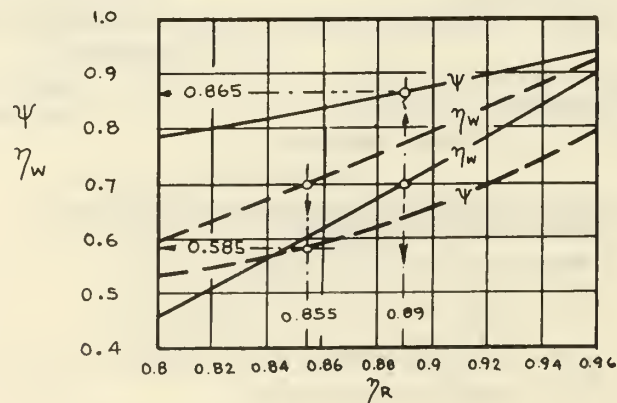


FIG. 5 RELATION BETWEEN ROTOR LOSS FORMULATIONS WITH η_R , η_w AND ψ (Eqs. 22 and 24)

$\alpha_2 = 60^\circ$ } $\beta_{10} = 70^\circ$, $R_{10}/R_2 = 0.7$, $\mu = 0.85$
 $\alpha_2 = 75^\circ$

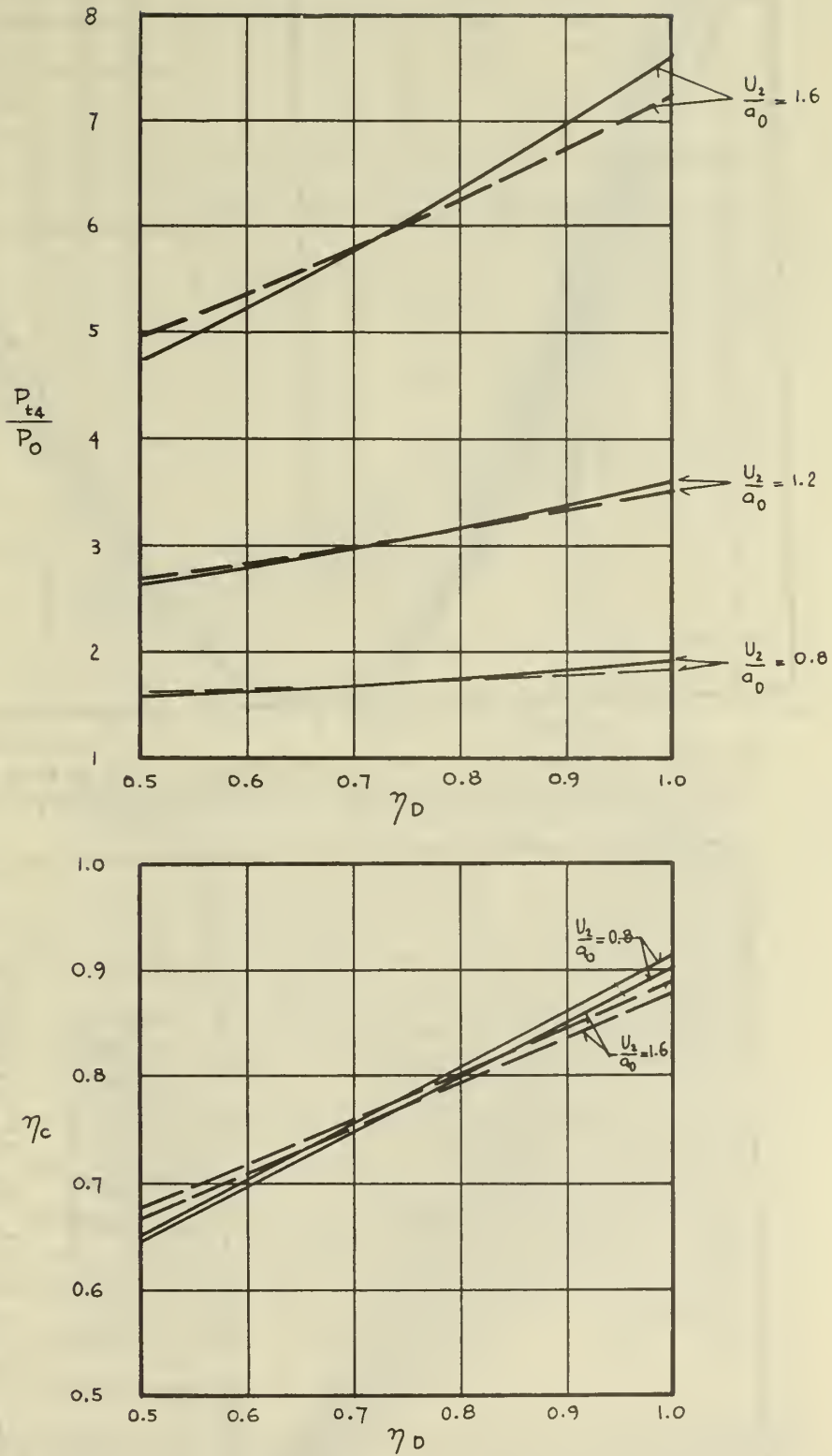


FIG.6 INFLUENCE OF DIFFUSOR EFFICIENCY η_D ON EFFICIENCY η_c AND PRESSURE RATIO P_{t4}/P_0 OF COMPRESSORS AT DIFFERENT SPEED RATIOS U_2/a_0

$\beta_{10} = 70^\circ$; $R_{10}/R_2 = 0.7$; $\lambda = v_4/v_2 = 0.2$
— $\alpha_2 = 60^\circ$; $\eta_w = 0.7$; $\eta_R = 0.89$; $\psi = 0.865$
— $\alpha_2 = 75^\circ$; $\eta_w = 0.7$; $\eta_R = 0.855$; $\psi = 0.585$

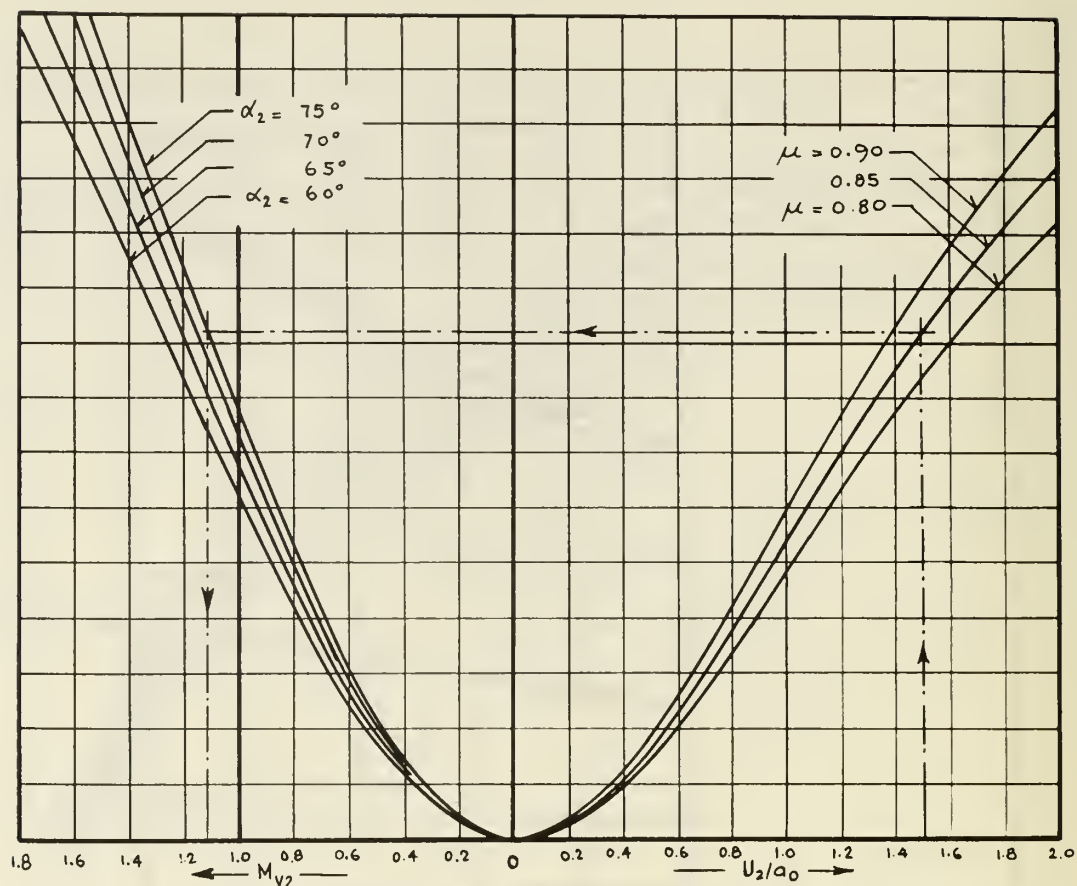


FIG.7 RELATION BETWEEN MACH NUMBER M_{V2} OF ABSOLUTE VELOCITY AT ROTOR DISCHARGE AND SPEED RATIO U_2/a_0 , FOR $\gamma = 1.4$ (Eq. II(6) of Table II)

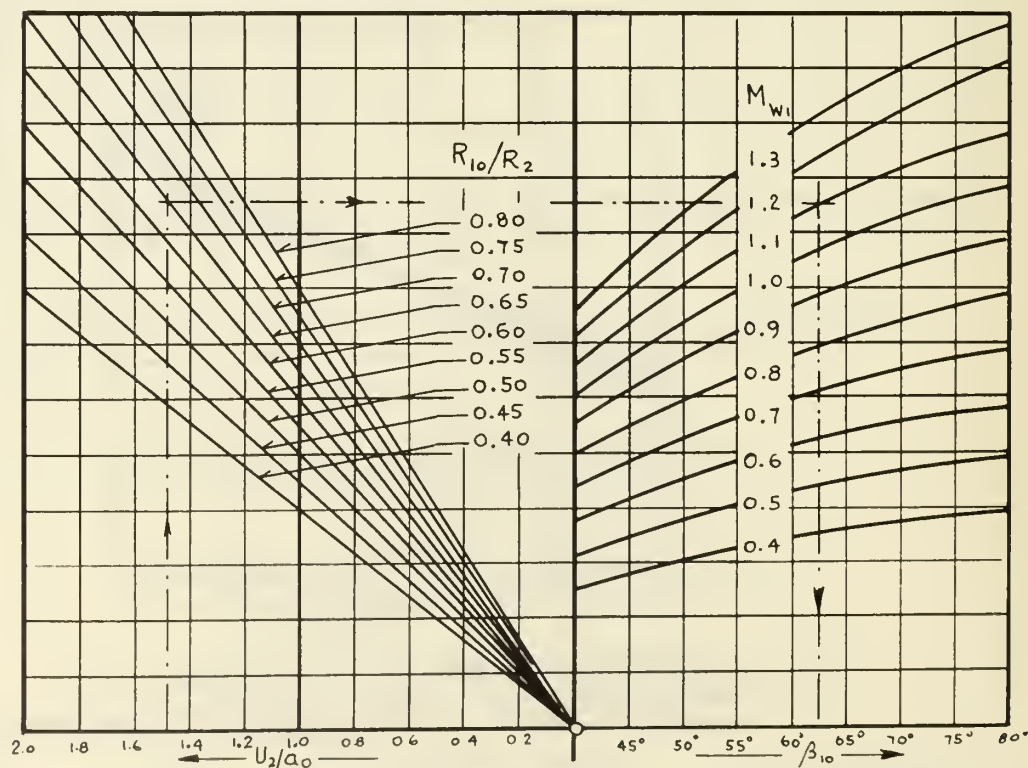


FIG.8 RELATION BETWEEN SPEED RATIO U_2/a_0 , RADIUS RATIO R_{10}/R_2 , VS. MACH NUMBER $M_{W1} = W_1/a_1$ AND RELATIVE FLOW ANGLE β_{10} AT OUTER RADIUS R_{10} OF COMPRESSOR INLET, FOR $\gamma = 1.4$. (Eq. II(4) of Table II)

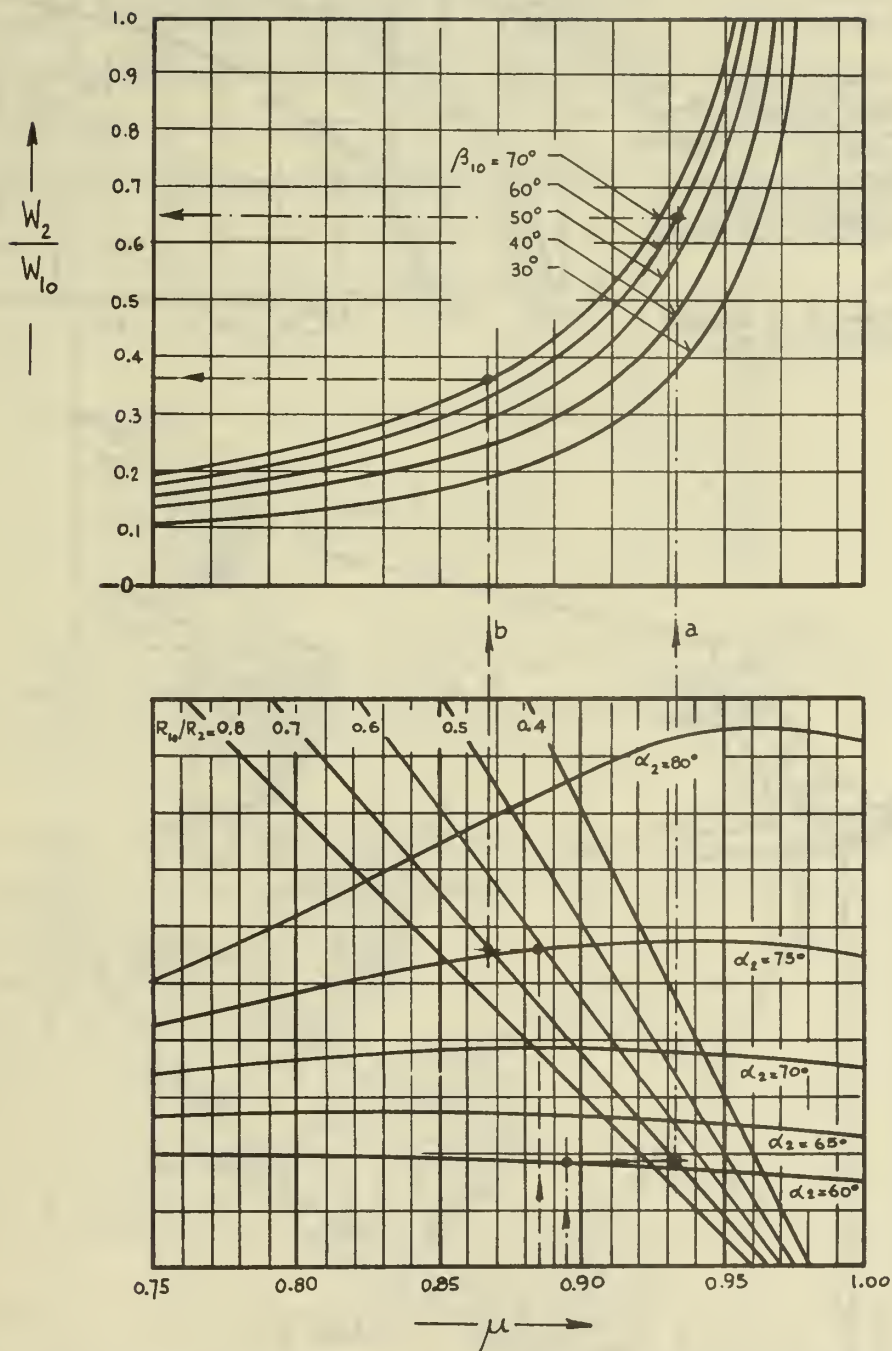


FIG.9 DIAGRAM REPRESENTING EQUATION II(5) OF TABLE II, SHOWING RELATIONSHIP BETWEEN DECELERATION RATIO W_2/W_{10} OF RELATIVE ROTOR VELOCITIES, RADIUS RATIO R_{10}/R_2 , RELATIVE INLET FLOW ANGLE β_{10} , ABSOLUTE ROTOR DISCHARGE ANGLE α_2 , AND SLIP FACTOR μ .

FIG. 10 MACH NUMBER M_{ix} OF
RELATIVE INLET VELOCITY AT
RADIUS R_{ix} FOR $M_{w1} = 1.3$ AT
OUTER RADIUS R_{10} OF WHEEL
INLET, AT DIFFERENT FLOW ANGLES
 β_{10} AT R_{10}

M_{V1} = Mach number of Absolute
Velocity V_1 at Inlet

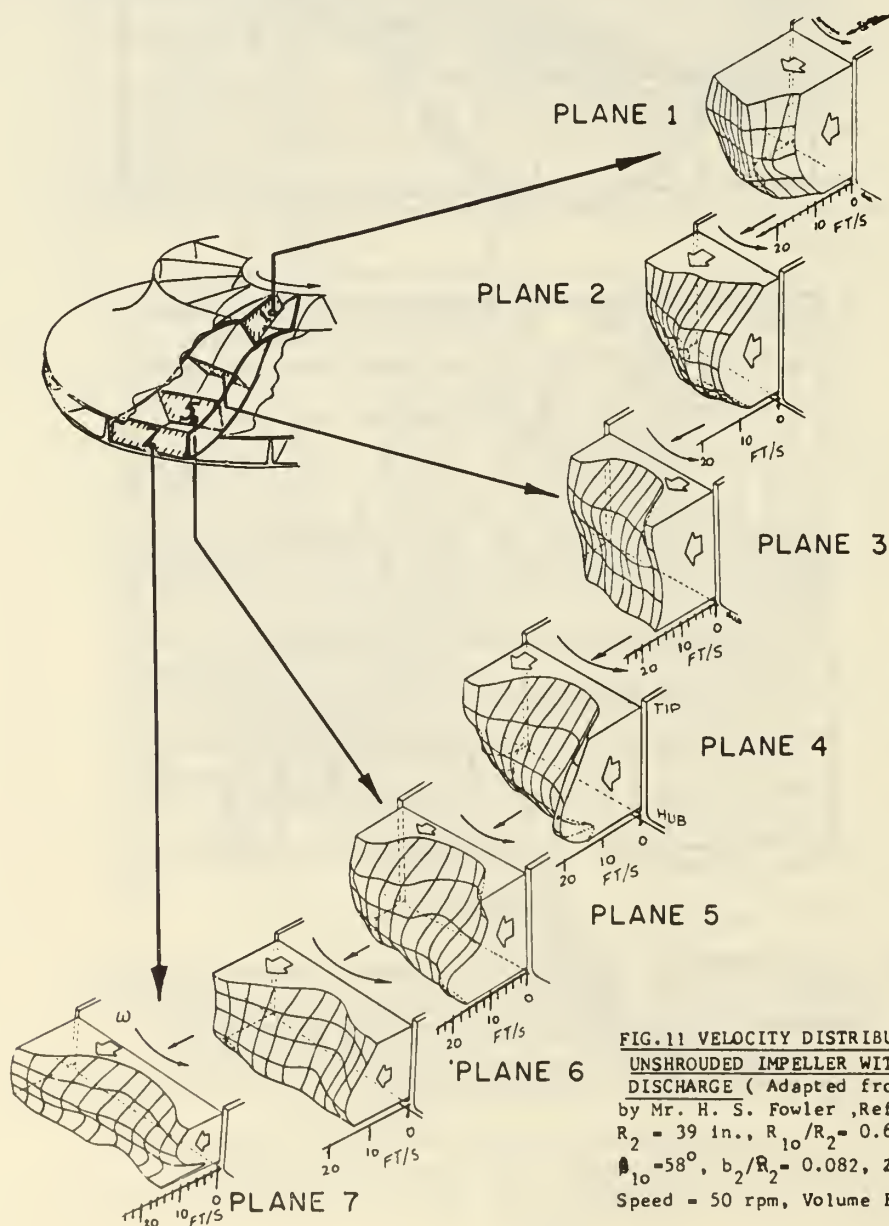
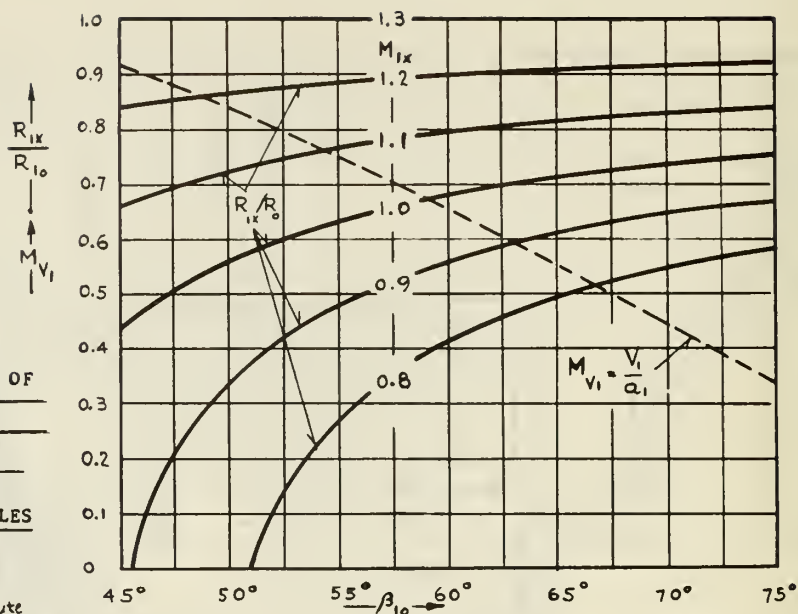


FIG. 11 VELOCITY DISTRIBUTIONS MEASURED IN
UNSHROUDED IMPELLER WITH RADIAL BLADES AT THE
DISCHARGE (Adapted from Personal Communication
by Mr. H. S. Fowler ,Refs.14 and 15)
 $R_2 = 39$ in., $R_{10}/R_2 = 0.629$, $R_{11}/R_{10} = 0.752$
 $\beta_{10} = 58^\circ$, $b_2/R_2 = 0.082$, $Z_R = 26$, $\delta_2/R_2 = 0.005$
Speed = 50 rpm, Volume Flow = $64.2 \text{ ft}^3/\text{s}$

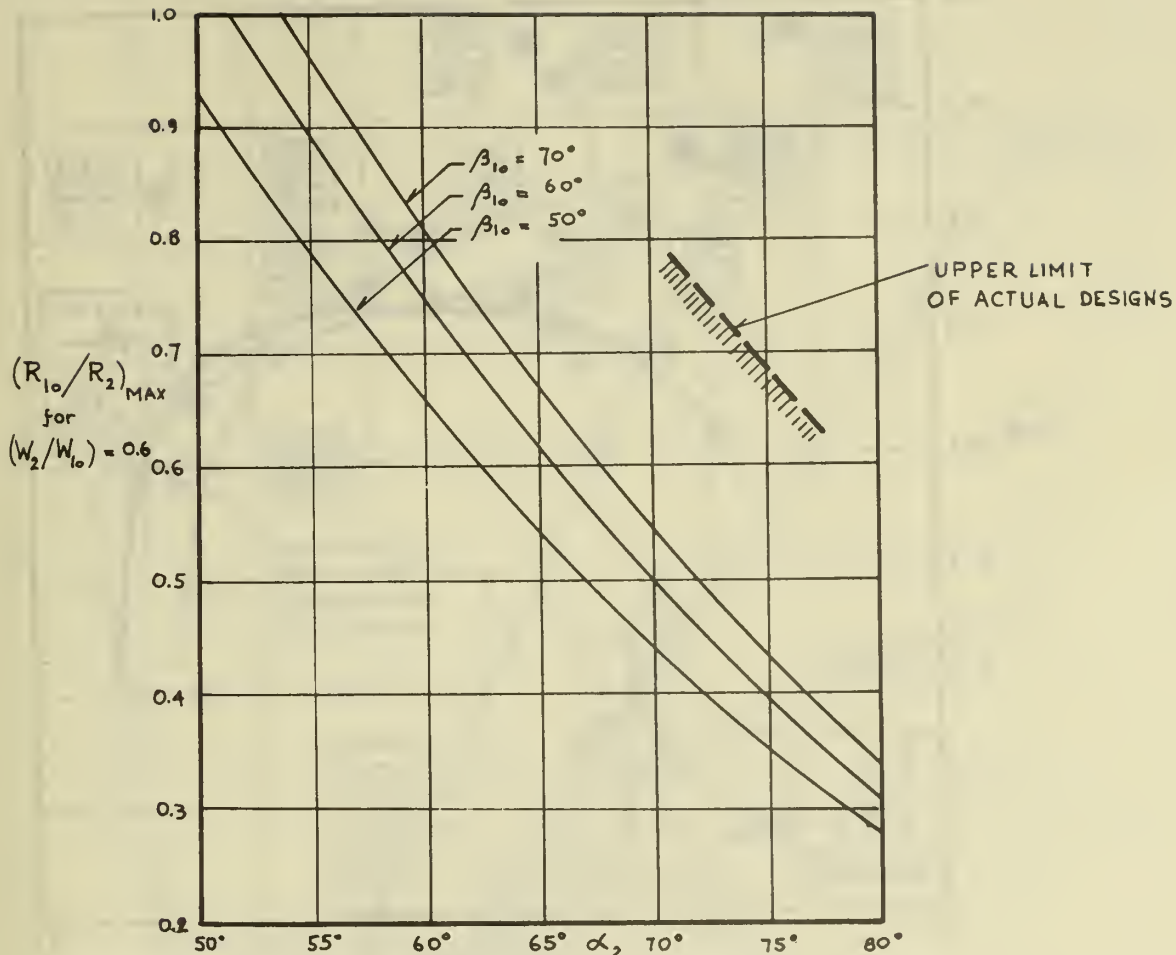


FIG.12 MAXIMUM POSSIBLE RADIUS RATIOS R_{10}/R_2 FOR A DECELERATION RATIO $W_2/W_{10} = 0.6$ FOR A SLIP FACTOR $\mu = 0.85$

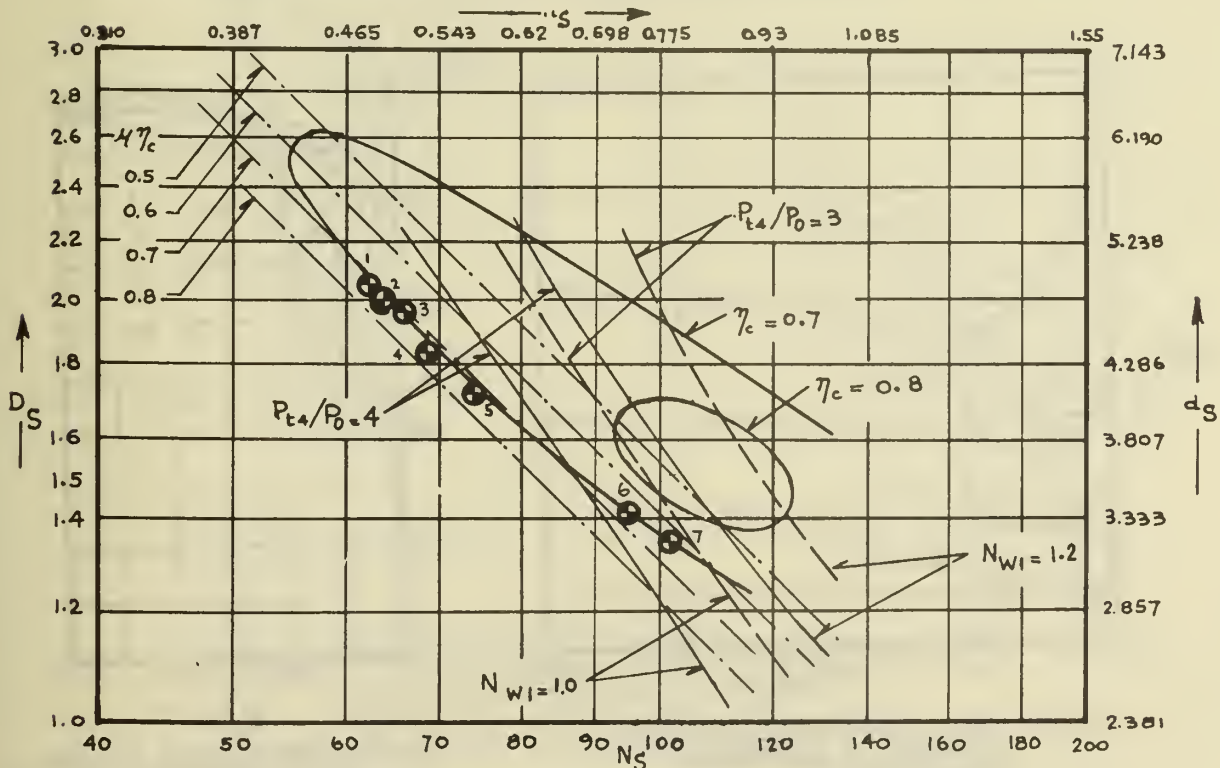


FIG.13 REPRESENTATION OF EQUATION $n_s d_s = 2 / (u \eta_c)^{1/2}$ OF EQ. III(10) WITH DESIGN DATA POINTS OF ACTUAL COMPRESSORS

(Other Curves adapted from Fig. 4 of Ref. 19)

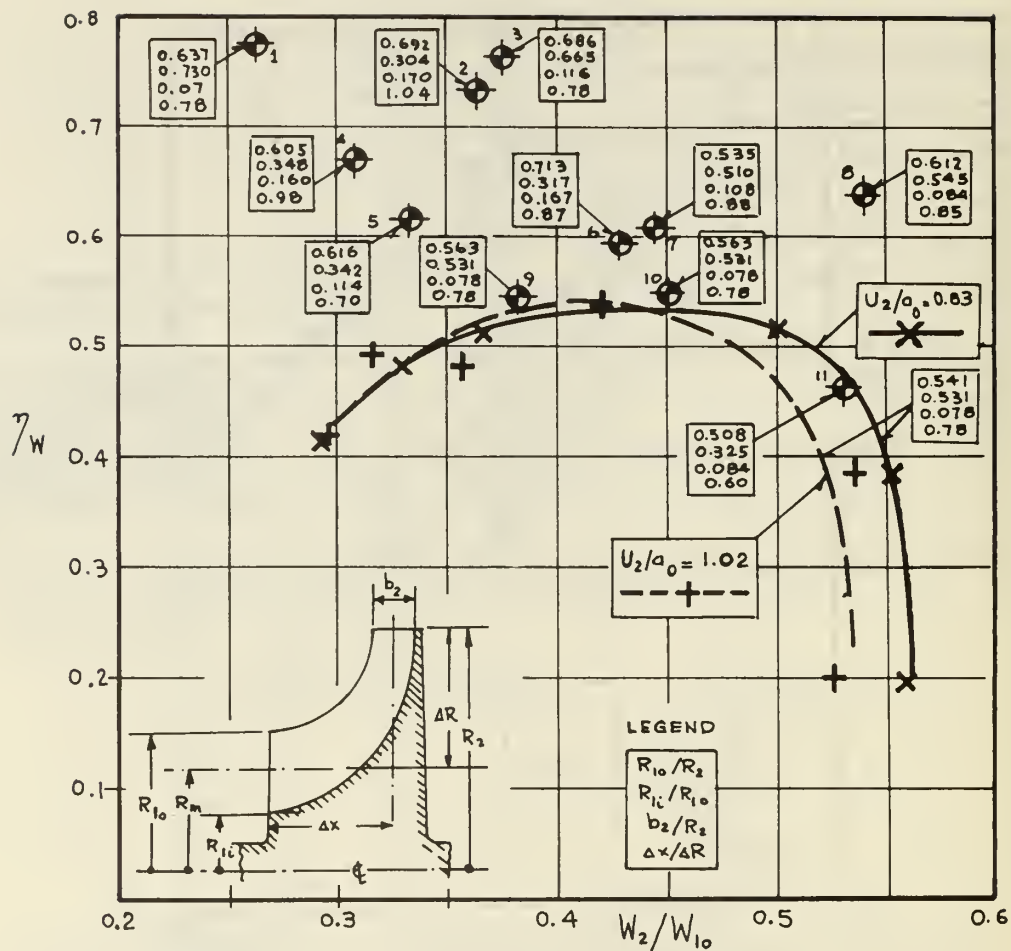


FIG. 14 WHEEL EFFICIENCY η_w AS FUNCTION OF THE DECELERATION RATIO W_2/W_{10} OF DIFFERENT RADIAL IMPELLERS

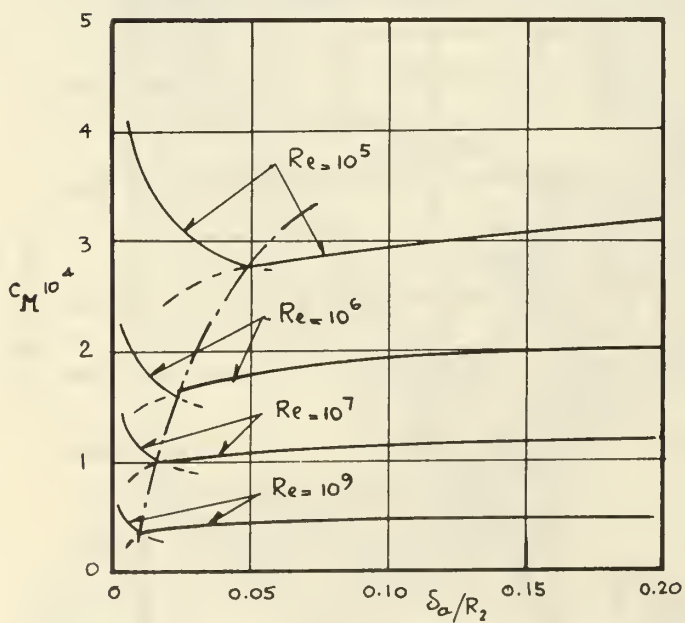


FIG. 15 DISK FRICTION MOMENT COEFFICIENT AS FUNCTION OF CLEARANCE AND REYNOLDS NUMBER

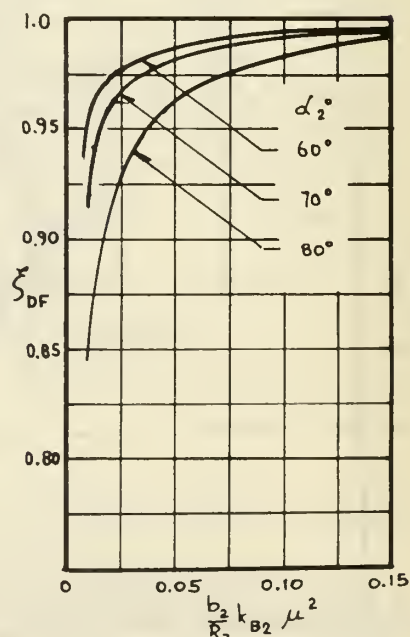


FIG. 16 INFLUENCE OF DISK FRICTION MOMENT ON COMPRESSOR EFFICIENCY

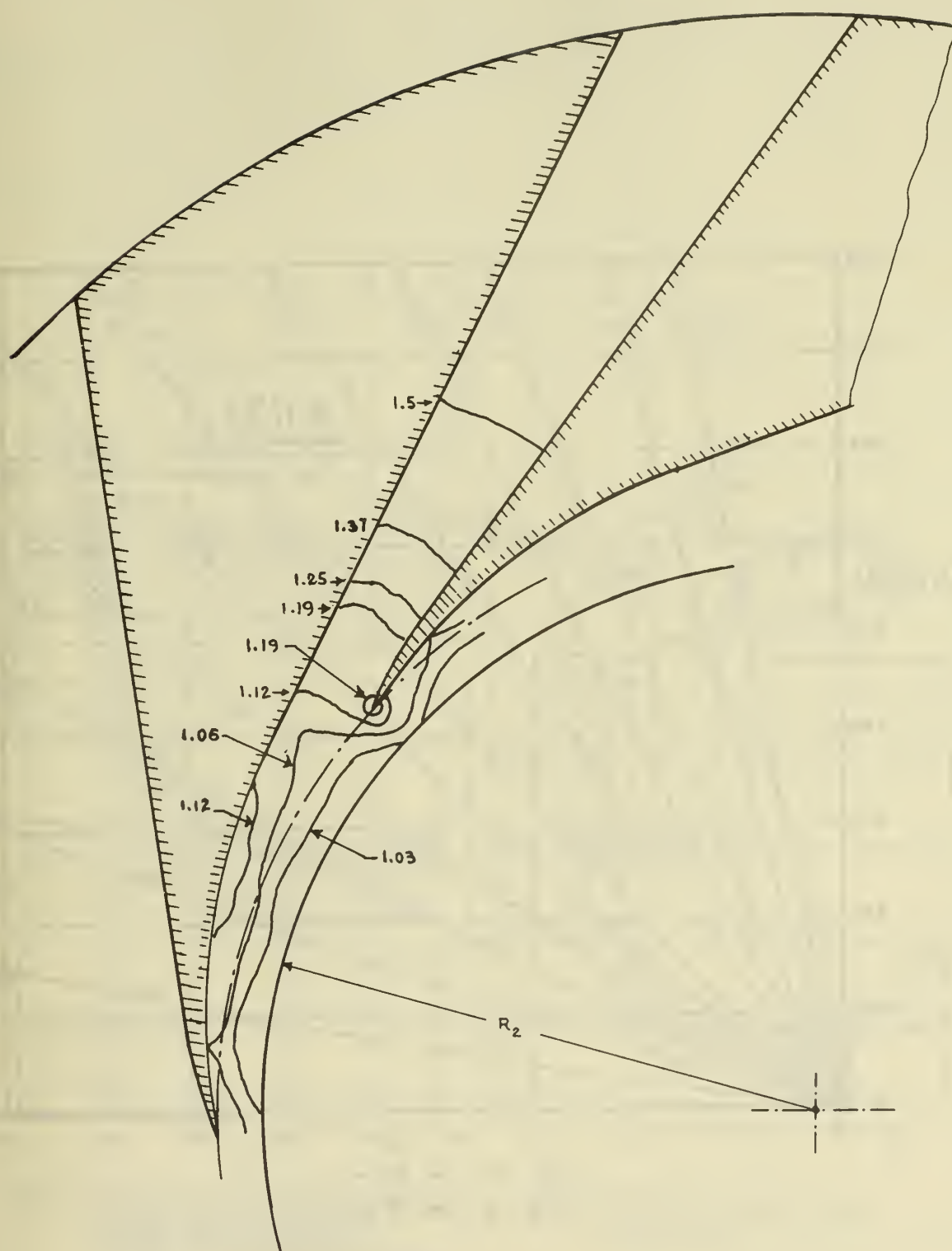


FIG. 17 TYPICAL DISTRIBUTION OF STATIC PRESSURES IN TRANSITION
SECTION AND DIFFUSER OF HIGH SPEED COMPRESSOR

(Numbers represent approximate ratios of static
pressures and average pressure p_2)

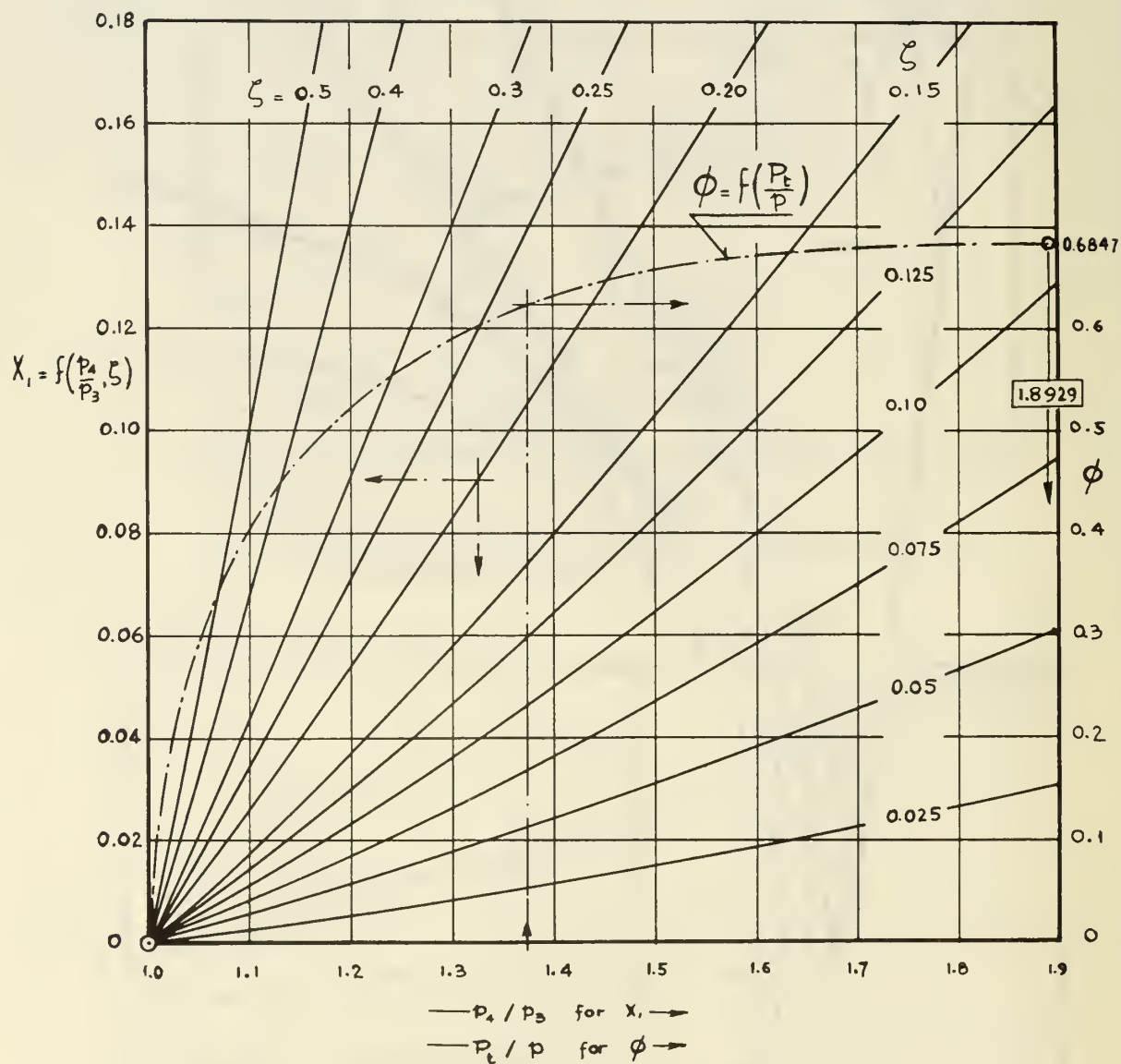


FIG.18 FUNCTION X_1 OF EQ.IV(16) OF TABLE IV FOR DIFFUSOR CALCULATION
AND DIMENSIONLESS FLOW FUNCTION OF EQ.IV(22) AND IV(29) OF TABLE IV

($\gamma = 1.4$)

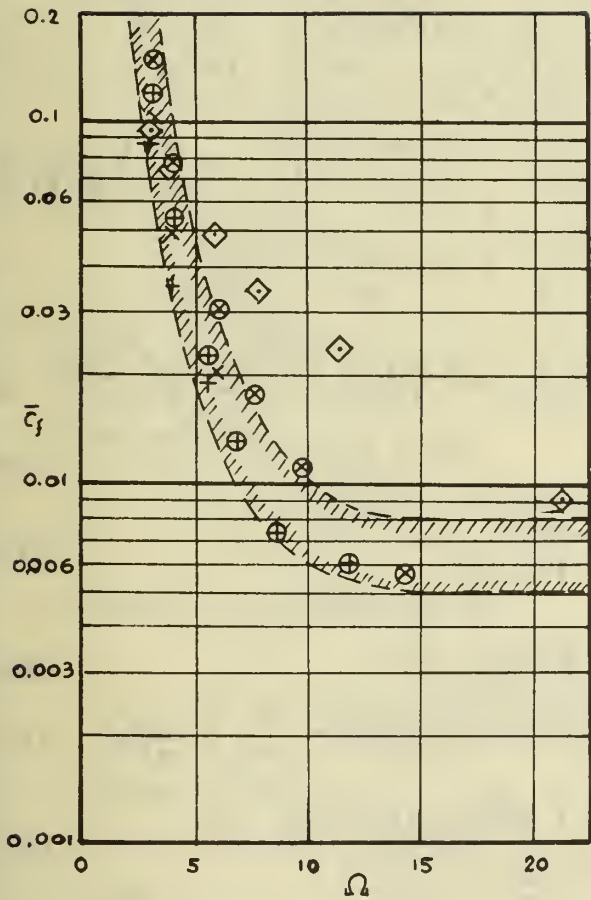


FIG.19 AVERAGE SKIN FRICTION COEFFICIENTS \bar{c}_f OBTAINED FROM TWO-DIMENSIONAL DIFFUSOR TEST DATA OF REF.27 AS FUNCTION OF THE DIFFUSOR SHAPE FACTOR Ω

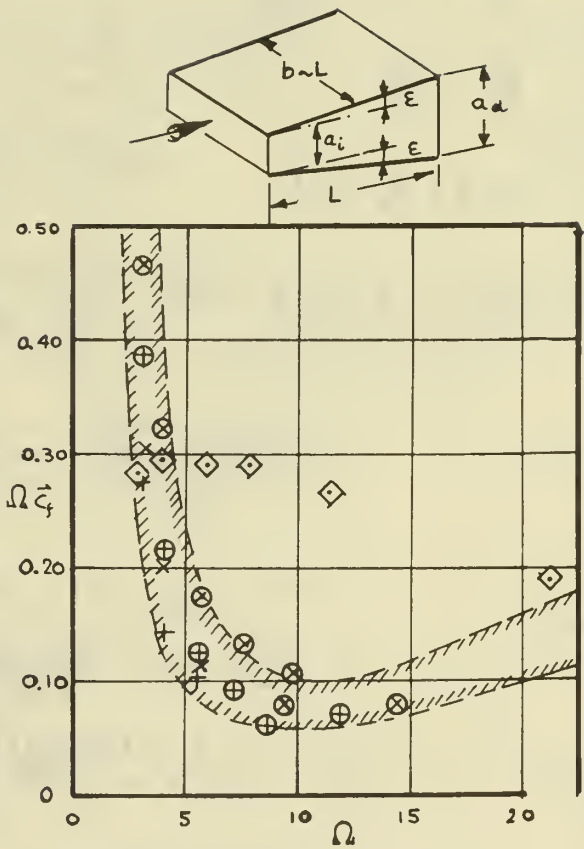


FIG.20 VALUES OF $\Omega \bar{c}_f$ FROM FIG.19 AS FUNCTION OF Ω

SYMBOLS IN FIGS. 19 AND 20:

- | | |
|--|--|
| \oplus $L/a_1 = 8$, $\delta^*/a_1 \approx 0.017$ | $+$ $L/a_1 = 8$, $\delta^*/a_1 \approx 0$ |
| \otimes $L/a_1 = 12$, $\delta^*/a_1 \approx 0.025$ | \times $L/a_1 = 12$, $\delta^*/a_1 \approx 0$ |
| \diamond $L/a_1 = 48$, $\delta^*/a_1 \approx 0.018$ | |
- δ^* = Displacement Thickness of Boundary Layer on Top and Bottom Wall

TABLE I FLOW PROPERTIES IN COMPRESSOR

(For Symbols see Figs. 1 and 2)

VELOCITIES

$$\frac{V_1}{U_2} = \frac{R_{10}}{R_2} \cot \beta_{10} \quad I(1) \quad \left| \quad \frac{W_{10}}{U_2} = \frac{R_{10}}{R_2} \frac{1}{\sin \beta_{10}} \quad I(2) \quad \right| \quad \frac{V_2}{U_2} = \frac{\mu}{\sin \alpha_2} \quad I(3) \quad \left| \quad \frac{W_2}{U_2} = \left[1 - 2\mu \left(1 - \frac{\mu}{2 \sin^2 \alpha_2} \right) \right]^{\frac{1}{2}} \quad I(4) \right.$$

$$\frac{V_{u2}}{U_2} = \mu \quad \frac{W_{u2}}{U_2} = 1 - \mu$$

$$\frac{V_{m2}}{U_2} = \mu \cot \alpha_2$$

$$V_4 = \lambda V_2 \quad W_2 = \psi W_{2is}$$

TEMPERATURES

$$\frac{T_{t1}}{T_0} = 1 \quad \frac{T_1}{T_0} = \frac{1}{1 + \frac{\gamma-1}{2} M_{w1}^2 \cos^2 \beta_{10}} = \frac{1 + \frac{\gamma-1}{2} \left(\frac{U_1}{a_0} \right)^2 \left(\frac{R_{10}}{R_2} \right)^2}{1 + \frac{\gamma-1}{2} M_{w1}^2} \quad I(5)$$

$$\frac{T_{t2}}{T_0} = 1 + (\gamma-1) \mu \left(\frac{U_2}{a_0} \right)^2 \quad I(6) \quad \frac{T_2}{T_0} = 1 + (\gamma-1) \mu \left(\frac{U_2}{a_0} \right)^2 \left[1 - \frac{\mu}{2 \sin^2 \alpha_2} \right] \quad I(7)$$

$$\frac{T_{t4}}{T_0} = \frac{T_{t2}}{T_0} \quad \frac{T_2'}{T_0} = 1 + (\gamma-1) \mu \left(\frac{U_2}{a_0} \right)^2 \left[\frac{1}{\psi^2} \left(1 - \frac{\mu}{2 \sin^2 \alpha_2} \right) - \frac{1}{2\mu} \left(\frac{1}{\psi^2} - 1 \right) \right] \quad I(8)$$

$$a_0 = \left[\gamma R_g T_0 \right]^{\frac{1}{2}} \quad \frac{T_4}{T_0} = 1 + (\gamma-1) \mu \left(\frac{U_2}{a_0} \right)^2 \left[1 - \frac{\lambda^2 \mu}{2 \sin^2 \alpha_2} \right] \quad I(9)$$

$$\frac{T_E}{T_0} = 1 + \frac{\gamma-1}{2} \left(\frac{U_2}{a_0} \right)^2 \quad I(10) \quad \frac{T_4'}{T_0} = 1 + (\gamma-1) \mu \left(\frac{U_2}{a_0} \right)^2 \left[1 - \frac{\mu}{2 \sin^2 \alpha_2} (1 - \gamma_D^*) \right] \quad I(11)$$

$$\gamma_D^* = \gamma_D (1 - \lambda^2) \quad I(12)$$

$$\frac{T_4''}{T_0} = \frac{(T_4'/T_0)(T_2'/T_0)}{T_2/T_0} = \frac{1 + (\gamma-1) \mu \left(\frac{U_2}{a_0} \right)^2 \left[\chi_1 + (\gamma-1) \mu \left(\frac{U_2}{a_0} \right)^2 \chi_2 \right]}{1 + (\gamma-1) \mu \left(\frac{U_2}{a_0} \right)^2 \left[1 - \frac{\mu}{2 \sin^2 \alpha_2} \right]} \quad I(13)$$

$$\chi_1 = \gamma_D^* - \frac{1}{2\mu} \left(\frac{1}{\psi^2} - 1 \right) + \left(1 - \frac{\mu}{2 \sin^2 \alpha_2} \right) \left(1 + \frac{1}{\psi^2} - \gamma_D^* \right) \quad I(14)$$

$$\chi_2 = \frac{\gamma_D^*}{2\mu} \left(1 - \frac{1}{\psi^2} \right) + \left(1 - \frac{\mu}{2 \sin^2 \alpha_2} \right) \left(\frac{\gamma_D^*}{\psi^2} - \frac{[1 - \gamma_D^*]}{2\mu} \left[\frac{1}{\psi^2} - 1 \right] \right) + \left(1 - \frac{\mu}{2 \sin^2 \alpha_2} \right) \left(\frac{1 - \gamma_D^*}{\psi^2} \right) \quad I(15)$$

$$\frac{\Delta T_{is}}{T_0} = \frac{T_4'' - T_0}{T_0} = \frac{(\gamma-1) \mu \left(\frac{U_2}{a_0} \right)^2 \left[\chi_1 - \left(1 - \frac{\mu}{2 \sin^2 \alpha_2} \right) + (\gamma-1) \mu \left(\frac{U_2}{a_0} \right)^2 \chi_2 \right]}{1 + (\gamma-1) \mu \left(\frac{U_2}{a_0} \right)^2 \left[1 - \frac{\mu}{2 \sin^2 \alpha_2} \right]} \quad I(16)$$

PRESSURES

$$\frac{P_{t2}'}{P_0} = (T_{t2}/T_0)^{\frac{\gamma}{\gamma-1}} \quad I(17) \quad \frac{P_1}{P_0} = (T_1/T_0)^{\frac{\gamma}{\gamma-1}} \quad I(18)$$

$$\frac{P_{t2}}{P_0} = \frac{P_2}{P_0} \frac{P_{t2}}{P_2} = \left[\frac{(T_2'/T_0)(T_{t2}/T_0)}{T_2/T_0} \right]^{\frac{\gamma}{\gamma-1}} \quad I(19) \quad \frac{P_2}{P_0} = (T_2'/T_0)^{\frac{\gamma}{\gamma-1}} \quad I(20)$$

$$\frac{P_{t4}}{P_0} = \frac{P_4}{P_0} = (T_4''/T_0)^{\frac{\gamma}{\gamma-1}} \quad I(21) \quad \frac{P_4}{P_2} = (T_4'/T_2)^{\frac{\gamma}{\gamma-1}} = \left(\frac{T_4'/T_0}{T_2/T_0} \right)^{\frac{\gamma}{\gamma-1}} \quad I(22)$$

$$\frac{P_{E1}}{P_0} = (T_E/T_0)^{\frac{\gamma}{\gamma-1}} \quad I(23) \quad \frac{P_{E2}}{P_0} = \frac{P_2}{P_0} \frac{P_{E2}}{P_2} = \left[\frac{(T_2'/T_0)(T_E/T_0)}{T_2/T_0} \right]^{\frac{\gamma}{\gamma-1}} \quad I(24)$$

TABLE II PERFORMANCE AND DESIGN PARAMETERS

$$\eta_c = \frac{\Delta T_{is}}{\Delta T_w} = \frac{X_1 - \left(1 - \frac{\mu}{2 \sin^2 \alpha_2}\right) + (\gamma - 1) \mu \left(\frac{U_2}{a_0}\right)^2 X_2}{1 + (\gamma - 1) \mu \left(\frac{U_2}{a_0}\right)^2 \left[1 - \frac{\mu}{2 \sin^2 \alpha_2}\right]} \quad \text{II (1)}$$

(X_1 and X_2 are given by Eqs. I(14) and I(15) of Table I)

$$r^* = \frac{T_2' - T_0}{\Delta T_{is}} = \frac{\frac{1}{\gamma^2} \left(1 - \frac{\mu}{2 \sin^2 \alpha_2}\right) - \frac{1}{2\mu} \left(\frac{1}{\gamma^2} - 1\right)}{\eta_c} \quad \text{II (2)}$$

$$\frac{U_2}{a_0} = \left[\frac{(P_{t4}/P_0) \frac{\gamma-1}{\gamma} - 1}{(\gamma-1) \mu \eta_c} \right]^{\frac{1}{2}} \quad \text{II (3)}$$

$$\frac{W_2}{W_{10}} = \frac{\left[1 - 2\mu \left(1 - \frac{\mu}{2 \sin^2 \alpha_2}\right)\right]^{\frac{1}{2}} \sin \beta_{10}}{(R_{10}/R_2)} \quad \text{II (5)}$$

$$\phi_1 = \frac{V_1}{U_2} = \frac{M_{w1} \cos \beta_{10}}{\frac{U_2}{a_0} \left[1 + \frac{\gamma-1}{2} M_{w1}^2 \cos^2 \beta_{10}\right]^{\frac{1}{2}}} \quad \text{II (7)}$$

$$\frac{R_{10}}{R_2} = \frac{M_{w1} \sin \beta_{10}}{\frac{U_2}{a_0} \left[1 + \frac{\gamma-1}{2} M_{w1}^2 \cos^2 \beta_{10}\right]^{\frac{1}{2}}} \quad \text{II (4)}$$

$$M_{v2} = \frac{V_2}{a_2} = \frac{\mu \frac{U_2}{a_0}}{\sin \alpha_2 \left[1 + (\gamma-1) \mu \left(\frac{U_2}{a_0}\right)^2 \left(1 - \frac{\mu}{2 \sin^2 \alpha_2}\right)\right]^{\frac{1}{2}}} \quad \text{II (6)}$$

$$\phi_2 = \frac{V_{m2}}{U_2} = \mu \cot \alpha_2 \quad \text{II (8)}$$

$$\pi R_2^2 \left[1 - \left(\frac{R_{1i}}{R_{10}}\right)^2\right] k_{B1} = \left(\frac{\dot{m} \sqrt{R_G T_0}}{P_0}\right) \left(\frac{U_2}{a_0}\right)^2 \frac{\left[1 + \frac{\gamma-1}{2} M_{w1}^2 \cos^2 \beta_{10}\right]^{\frac{3\gamma-1}{2(\gamma-1)}}}{\sqrt{\gamma} M_{w1}^3 \cos \beta_{10} \sin^2 \beta_{10}} \quad \text{II (9)}$$

$$\frac{\omega}{\left[1 - \left(\frac{R_{1i}}{R_{10}}\right)^2\right] k_{B1}} = \left[\frac{a_0 P_0}{\dot{m}}\right]^{\frac{1}{2}} \frac{\sin \beta_{10} \left[\pi \gamma \cos \beta_{10}\right]^{\frac{1}{2}}}{\left[1 + \frac{\gamma-1}{2} M_{w1}^2 \cos^2 \beta_{10}\right]^{\frac{3\gamma-1}{2(\gamma-1)}}} \quad \text{II (10)}$$

$$\left(\frac{b_2}{R_2}\right) k_{B2} = \left(\frac{\dot{m} \sqrt{R_G T_0}}{\pi R_2^2 P_0}\right) \frac{1 + (\gamma-1) \mu \left(\frac{U_2}{a_0}\right)^2 \left(1 - \frac{\mu}{2 \sin^2 \alpha_2}\right)}{2 \mu \sqrt{\gamma} \cot \alpha_2 \left(\frac{U_2}{a_0}\right) \left\{1 + (\gamma-1) \mu \left(\frac{U_2}{a_0}\right)^2 \left[\frac{1}{\gamma^2} \left(1 - \frac{\mu}{2 \sin^2 \alpha_2}\right) - \frac{1}{2\mu} \left(\frac{1}{\gamma^2} - 1\right)\right]\right\}} \frac{\gamma}{\gamma-1} \quad \text{II (11)}$$

Diffusor Exit Area A_4 :

$$A_4 k_{B4} = \left(\frac{\dot{m} \sqrt{R_G T_0}}{P_0}\right) \frac{\sin \alpha_2}{\lambda \mu \sqrt{\gamma} \left(\frac{U_2}{a_0}\right)} \frac{\left[1 + (\gamma-1) \mu \left(\frac{U_2}{a_0}\right)^2 \left(1 - \frac{\lambda^2 \mu}{2 \sin^2 \alpha_2}\right)\right]}{\left[1 + \eta_c (\gamma-1) \mu \left(\frac{U_2}{a_0}\right)^2\right] \frac{\gamma}{\gamma-1}} \quad \text{II (12)}$$

Diffusor Throat Area A_x if $M_{V2} > 1$:

$$A_x k_{Bx} = \frac{\left(\frac{\dot{m} \sqrt{R_G T_0}}{P_0}\right) \gamma \frac{\gamma}{\gamma-1}}{\phi_c \left(\frac{P_{tx}}{P_{t2}}\right) \left[1 + (\gamma-1) \mu \left(\frac{U_2}{a_0}\right)^2\right]^{\frac{\gamma+1}{2(\gamma-1)}}} \quad \text{II (13)}$$

where

$$\phi_c = \left\{ \frac{2\gamma}{\gamma-1} \left[\left(\frac{2}{\gamma+1}\right)^{\frac{2}{\gamma-1}} - \left(\frac{2}{\gamma+1}\right)^{\frac{\gamma+1}{\gamma-1}} \right] \right\}^{\frac{1}{2}} \quad \text{II (14)}$$

and

$$\gamma = \frac{T_2/T_0}{T_2'/T_0} = \frac{1 + (\gamma-1) \mu \left(\frac{U_2}{a_0}\right)^2 \left[1 - \frac{\mu}{2 \sin^2 \alpha_2}\right]}{1 + (\gamma-1) \mu \left(\frac{U_2}{a_0}\right)^2 \left[\frac{1}{\gamma^2} \left(1 - \frac{\mu}{2 \sin^2 \alpha_2}\right) - \frac{1}{2\mu} \left(\frac{1}{\gamma^2} - 1\right)\right]} \quad \text{II (15)}$$

Diffusor Throat Area A_x if $M_{V2} \leq 1$, and $V_x = \xi V_2$:

$$A_x k_{Bx} = \frac{\sin \alpha_2 \left(\frac{\dot{m} \sqrt{R_G T_0}}{P_0}\right) \gamma \frac{\gamma}{\gamma-1}}{\xi \mu \sqrt{\gamma} \left(\frac{U_2}{a_0}\right) \left(\frac{P_{tx}}{P_{t2}}\right) \left[1 + (\gamma-1) \mu \left(\frac{U_2}{a_0}\right)^2 \left(1 - \frac{\xi^2 \mu}{2 \sin^2 \alpha_2}\right)\right]^{\frac{1}{\gamma-1}}} \quad \text{II (16)}$$

TABLE III SPECIFIC SPEED RELATIONS

DEFINITIONS WITH ENGLISH UNITS

(see Refs. 18 and 19)

$$N_S = \frac{N Q_1^{1/2}}{H_{1s}^{3/4}} \quad \text{III(1)}$$

$$D_S = \frac{D H_{1s}^{1/4}}{Q_1^{1/2}} \quad \text{III(2)}$$

DEFINITIONS IN DIMENSIONLESS FORM

$$n_S = \frac{N_S}{129} = \frac{\omega Q_1^{1/2}}{(c_p \Delta T_{1s})^{3/4}} \quad \text{III(3)}$$

$$d_S = \frac{D_S}{0.42} = \frac{D (c_p \Delta T_{1s})^{1/4}}{Q_1^{1/2}} \quad \text{III(4)}$$

- N - Rotative Speed (rpm)
 ω - Angular Velocity (radians/s)
 Q_1 - Inlet Volume Flow Rate (cuft/s)
 $H_{1s} = g_o c_p \Delta T_{1s}$ - Isentropic Head (ft-lb/lbm)
 g_o - Gravitational Constant = 32.174 ft/s²
 c_p - Specific Heat at Constant Pressure ($\frac{\text{ft-lb}}{\text{slug, deg.R}}$)
 ΔT_{1s} - Isentropic Temperature Rise in Compressor (deg. R)
 D - Rotor Diameter (ft)

RELATIONS WITH SYMBOLS OF TABLES I AND II

$$\xi_1 = 1 - \left(\frac{R_{11}^2}{R_{10}^2} \right) \quad \text{III(5)}$$

$$Q_1 = \pi R_{10}^2 \xi_1 k_{B1} V_1$$

$$V_1 = U_{10} \cot \beta_{10}$$

$$c_p \Delta T_{1s} = \mu \eta_c U_2^2$$

$$\omega = U_2 / R_2$$

$$D = 2 R_2 = 2 U_2 / \omega$$

$$n_S^2 = \pi \left(\frac{R_{10}}{R_2} \right)^3 k_{B1} \frac{\cot \beta_{10} \xi_1}{(\mu \eta_c)^{3/2}} \quad \text{III(6)}$$

$$d_S^2 = \frac{4}{\pi} \frac{(\mu \eta_c)^{1/2}}{(R_{10}/R_2)^3 k_{B1} \cot \beta_{10} \xi_1} \quad \text{III(7)}$$

and

$$\xi_1 = \frac{n_S^2}{\pi} \frac{(\mu \eta_c)^{3/2} \tan \beta_{10}}{k_{B1} (R_{10}/R_2)^3} \quad \text{III(8)}$$

$$\xi_1 = \frac{4}{\pi d_S^2} \frac{(\mu \eta_c)^{1/2} \tan \beta_{10}}{k_{B1} (R_{10}/R_2)^3} \quad \text{III(9)}$$

Equating Eqs. 8 and 9:

$$n_S d_S = \frac{2}{(\mu \eta_c)^{1/2}} \quad \text{III(10)}$$

From Eq.8

$$\frac{R_{11}}{R_{10}} = \left[1 - \frac{n_S^2}{\pi} \frac{(\mu \eta_c)^{3/2} \tan \beta_{10}}{k_{B1} (R_{10}/R_2)^3} \right]^{1/2} \quad \text{III(11)}$$

EXAMPLE: For $\mu = 0.88$, $\eta_c = 0.83$, $k_{B1} = 0.85$, and $\beta_{10} = 68^\circ$, find R_{11}/R_{10} for different values of N_S for the two radius ratios $R_{10}/R_2 = 0.56$ and $R_{10}/R_2 = 0.70$

For $R_{10}/R_2 = 0.56$; from Eq.11

$$\frac{R_{11}}{R_{10}} = \left[1 - n_S^2 (3.288) \right]^{1/2} \quad \text{III(12)}$$

R_{11}/R_{10} is zero for $n_{S \text{ max}} = 0.552$, or $N_{S \text{ max}} = 71$
 For values of N_S lower than 71:

N_S	60	65	70
n_S	0.465	0.504	0.543
R_{11}/R_{10}	0.537	0.406	0.178

For $R_{10}/R_2 = 0.70$; from Eq.11

$$\frac{R_{11}}{R_{10}} = \left[1 - n_S^2 (1.683) \right]^{1/2} \quad \text{III(13)}$$

R_{11}/R_{10} is zero for $n_{S \text{ max}} = 0.771$, or $N_{S \text{ max}} = 99.4$
 For values of N_S lower than 99.4:

N_S	70	80	90	98
n_S	0.543	0.620	0.698	0.760
R_{11}/R_{10}	0.710	0.594	0.424	0.169

Relation between so-called Mach Number $N_{W1} = W_{10} / \sqrt{\frac{2\gamma}{\gamma+1} R_G T_0}$ and actual Mach Number $M_{W1} = W_{10} / a_1$:

$$N_{W1}^2 = \left[\frac{\gamma+1}{2} M_{W1}^2 \right] / \left[1 + \frac{\gamma-1}{2} M_{W1}^2 \cos^2 \beta_{10} \right] \quad \text{III(14)}$$

TABLE IV ANALYSIS OF FLOWS IN DIFFUSORS

ONE-DIMENSIONAL FLOW IN CHANNEL

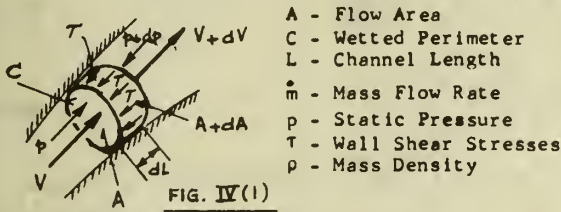


FIG. IV(1)

From Momentum Theorem:

$$\frac{1}{\rho} dp + d\left(\frac{V^2}{2}\right) = -\frac{T}{\rho} \frac{C}{A} dL$$

From Equation of Continuity:

$$\dot{m} = A \rho V$$

Derivation:

Eq. IV(4) into Eq. IV(1)

$$c_p dT - T ds + d\left(\frac{V^2}{2}\right) = -\frac{T}{\rho} \frac{C}{A} dL$$

$$d\left(c_p dT + \frac{V^2}{2}\right) - T ds = -\frac{T}{\rho} \frac{C}{A} dL$$

From Eq. 3

$$dT_t = 0 = d\left(T + \frac{V^2}{2c_p}\right)$$

$$T ds = \frac{T}{\rho} \frac{C}{A} dL$$

From Frictional Law with Eq. 2:

$$T = c_f \frac{\rho}{2} V^2 = \frac{c_f}{2} \frac{\dot{m}^2}{\rho A^2}$$

Into Eq. 10

$$T ds = \frac{c_f}{2} \frac{\dot{m}^2}{\rho^2 A^3} C dL$$

THERMODYNAMIC CONDITIONS

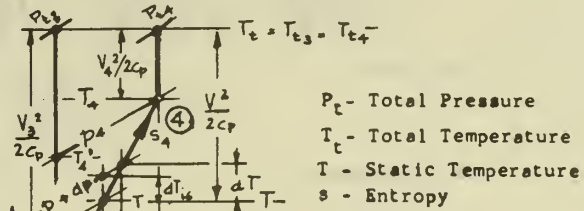


FIG. IV(2)

 P_t - Total Pressure T_t - Total Temperature T - Static Temperature s - Entropy η_p - Polytropic Efficiency $\zeta = 1 - \eta_p$ - Loss Coefficient

From Energy Equation:

$$T_t = T_{t3} = T_{t4} = T + \frac{V^2}{2c_p} = T_3 + \frac{V_3^2}{2c_p} = T_4 + \frac{V_4^2}{2c_p} \quad \text{IV (3)}$$

From First Law of Thermodynamics:

$$T ds = c_p dT - \frac{1}{\rho} dp = R_c \frac{T}{\gamma-1} d\left(\frac{p}{T}\right) - \frac{1}{\rho} dp \quad \text{IV (4)}$$

$$ds = R_g \left[\frac{\gamma}{\gamma-1} \frac{dT}{T} - \frac{dp}{p} \right] \quad \text{IV (5)}$$

For Adiabatic Polytropic Process

$$\eta_p = \frac{dT_{t3}}{dT} = \frac{T \left[\left(\frac{p+dp}{p} \right)^{\frac{\gamma}{\gamma-1}} - 1 \right]}{dT} = \frac{T}{dT} \frac{\gamma-1}{\gamma} \frac{dp}{p} \quad \text{IV (6)}$$

$$\frac{dT}{T} = \frac{\gamma-1}{\gamma p \gamma} \frac{dp}{p} \quad \text{IV (7)}$$

$$T = \text{constant} \quad p^{\frac{\gamma-1}{\gamma}} \quad \text{IV (8)}$$

$$\rho = \text{constant} \quad p^{1-\frac{\gamma-1}{\gamma}} \quad \text{IV (9)}$$

From Eqs. 5 and 7

$$\frac{ds}{R_g} = \left(\frac{1}{\eta_p} - 1 \right) \frac{dp}{p} = \frac{\zeta}{1-\zeta} \frac{dp}{p} \quad \text{IV (11)}$$

Dimensionless Referred Mass Flow Rate

$$\dot{m}_{r3} = \frac{\dot{m} \sqrt{R_g T_3}}{p_3 A_3} \quad \text{IV (14)}$$

PRINCIPAL EQUATION obtained from Eqs. 13 and 14, and $\rho = \frac{p}{R_g T}$

$$dX_1 = \frac{\rho p}{p_3 p_3} d\left(\frac{s}{R_g}\right) = \frac{c_f}{2} (\dot{m}_{r3})^2 \left(\frac{A_3}{A}\right)^3 \frac{C dL}{A_3} = \frac{c_f}{2} (\dot{m}_{r3})^2 d\Omega = dX_2 \quad \text{IV (15)}$$

$$X_1 = \int_3^4 dX_1 = \int_3^4 \frac{\rho p}{p_3 p_3} d\left(\frac{s}{R_g}\right) \quad \text{IV (16)}$$

With Eqs. 11 and 9

$$dX_1 = \left(\frac{1}{\eta_p} - 1 \right) \frac{\rho p}{p_3 p_3} \frac{dp}{p} = \left(\frac{1}{\eta_p} - 1 \right) \frac{\rho}{p_3} d\left(\frac{p}{p_3}\right)$$

$$dX_1 = \left(\frac{1}{\eta_p} - 1 \right) \left(\frac{p}{p_3} \right)^{1-\frac{\gamma-1}{\gamma}} d\left(\frac{p}{p_3}\right)$$

$$X_1 = \int_1^2 dX_1 = \frac{1}{2-\frac{\gamma-1}{\gamma}} \left[\left(\frac{p_2}{p_3} \right)^{2-\frac{\gamma-1}{\gamma}} - 1 \right]$$

and

$$X_1 = \frac{c_f \gamma}{\gamma+1-2\zeta\gamma} \left[\left(\frac{p_2}{p_3} \right)^{\frac{\gamma+1-2\zeta\gamma}{(1-\zeta)\gamma}} - 1 \right] \quad \text{IV (20)}$$

$$X_2 = \frac{1}{2} (\dot{m}_{r3})^2 \int_0^L \frac{c_f}{p} d\Omega = \frac{\zeta}{2} (\dot{m}_{r3})^2 \int_0^L d\Omega \quad \text{IV (17)}$$

$$X_2 = \frac{\zeta}{2} (\dot{m}_{r3})^2 \Omega \quad \text{IV (18)}$$

$$\Omega = \int_0^L \left(\frac{A_3}{A} \right)^3 \frac{C dL}{A_3} \quad \text{IV (19)}$$

 Ω will be denoted as Diffusor Shape Factor

From Eq. 20

$$\frac{p_2}{p_3} = \left[\frac{X_1 (\gamma+1-2\zeta\gamma)}{\zeta \gamma} + 1 \right]^{\frac{(1-\zeta)\gamma}{\gamma+1-2\zeta\gamma}} \quad \text{IV (21)}$$

TABLE IV (CONTD.) METHODS OF SOLUTION

For Effective Flow Area $A_3^* = k_{B3} A_3$ (k_{B3} = Blockage Factor, A_3 = Actual Area at Diffusor Inlet)

$$\frac{\dot{m} \sqrt{R_G T_{t3}}}{A_3^* P_{t3}} = \sqrt{\frac{2\gamma}{\gamma-1} \left[\left(\frac{p_3}{P_{t3}} \right)^{\frac{2}{\gamma}} - \left(\frac{p_3}{P_{t3}} \right)^{\frac{\gamma+1}{\gamma}} \right]} = \phi_3 = f\left(\frac{P_{t3}}{p_3}, \gamma\right) \quad \text{IV (22)}$$

From Eq. 14

$$\dot{m}_{r3} = \frac{\dot{m} \sqrt{R_G T_3}}{A_3^* p_3} = \phi_3 \sqrt{\frac{T_3}{P_{t3}}} \quad \text{IV (23)}$$

If p_3 is known,

$$\frac{T_3}{T_{t3}} = \left(\frac{p_3}{P_{t3}} \right)^{\frac{\gamma-1}{\gamma}} \quad \text{IV (25)}$$

Into Eq. 23

$$\dot{m}_{r3} = \phi_3 \left(\frac{P_{t3}}{p_3} \right)^{\frac{\gamma+1}{2\gamma}} \quad \text{IV (27)}$$

If $M_{V3} = V_3 / \sqrt{\gamma R_G T_3}$ is known, with $c_p = R_G \frac{\gamma}{\gamma-1}$,

$$\frac{T_{t3}}{T_3} = 1 + \frac{V_3^2}{2 c_p T_3} = 1 + \frac{\gamma-1}{2} \frac{V_3^2}{\gamma R_G T_3} = 1 + \frac{\gamma-1}{2} M_{V3}^2 \quad \text{IV (24)}$$

$$\frac{P_{t3}}{p_3} = \left[1 + \frac{\gamma-1}{2} M_{V3}^2 \right]^{\frac{\gamma}{\gamma-1}} \quad \text{IV (26)}$$

Into Eq. 23

$$\dot{m}_{r3} = \phi_3 \left[1 + \frac{\gamma-1}{2} M_{V3}^2 \right]^{\frac{\gamma+1}{2(\gamma-1)}} \quad \text{IV (28)}$$

For known Ω and \bar{C}_f , i.e. X_2 from Eq. 18, and $X_1 = X_2$, the Loss Coefficient ζ must be obtained with an iteration to satisfy the Equation of Continuity at Diffusor Discharge. For Effective Flow Area $A_4^* = k_{B4} A_4$ (k_{B4} = Blockage Factor, A_4 = Actual Diffusor Discharge Area), since $T_{t4} = T_{t3}$,

$$\frac{\dot{m} \sqrt{R_G T_{t3}}}{A_4^* P_{t4}} = \sqrt{\frac{2\gamma}{\gamma-1} \left[\left(\frac{p_4}{P_{t4}} \right)^{\frac{2}{\gamma}} - \left(\frac{p_4}{P_{t4}} \right)^{\frac{\gamma+1}{\gamma}} \right]} = \phi_4 = f\left(\frac{P_{t4}}{p_4}, \gamma\right) = \phi_3 \frac{A_3^*}{A_4^*} \frac{P_{t3}}{P_{t4}} \quad \text{IV (29)}$$

Since P_{t3}/P_{t4} is as yet unknown, it is not possible to determine P_{t4}/p_4 from function ϕ_4 to obtain $p_4/p_3 = (P_{t3}/p_3)/(P_{t4}/p_4)$. Additional relation is obtained by calculating entropy increase $\Delta s = s_4 - s_3$ for polytropic process from p_3 to p_4 with Eq. 11, and for T_t = constant from P_{t3} to P_{t4} with Eq. 5.

For Polytropic Process:

$$\frac{\Delta s}{R_G} = \frac{\zeta}{1-\zeta} \ln \left(\frac{p_4}{p_3} \right) = \ln \left[\left(\frac{p_4}{p_3} \right)^{\frac{\zeta}{1-\zeta}} \right] \quad \text{IV (30)}$$

Equating Eqs. 30 and 31

$$\frac{p_4}{p_3} = \left(\frac{P_{t3}}{P_{t4}} \right)^{\frac{1-\zeta}{\zeta}} \quad \text{IV (32)}$$

Along Line $T_{t3} = T_{t4}$ = Constant:

$$\frac{\Delta s}{R_G} = - \ln \left[\frac{P_{t4}}{P_{t3}} \right] = \ln \left[\frac{P_{t3}}{P_{t4}} \right] \quad \text{IV (31)}$$

$$\frac{P_{t3}}{P_{t4}} = \left(\frac{p_4}{p_3} \right)^{\frac{\zeta}{1-\zeta}} \quad \text{IV (33)}$$

With Eq. 33

$$\frac{P_{t4}}{p_4} = \left(\frac{P_{t4}}{p_4} \right) \left(\frac{P_{t3}}{p_3} \right) \left(\frac{p_3}{p_4} \right) = \frac{(P_{t3}/p_3)}{(P_{t3}/P_{t4})(p_4/p_3)} = \frac{(P_{t3}/p_3)}{\left(\frac{p_4}{p_3} \right)^{\frac{1}{1-\zeta}}} \quad \text{IV (34)}$$

ITERATION PROCEDURE

(1) For given values of Ω and \bar{C}_f calculate X_2 from Eq. 18 with Eq. 27 or 28. $X_1 = X_2$

(2) Choose initial value of ζ

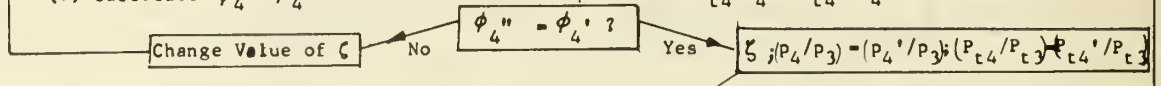
(3) Calculate $p_4/p_3 = p_4'/p_3$ by Eq. 21 for X_1 and ζ

(4) Calculate $P_{t3}/P_{t4} = P_{t3}'/P_{t4}'$ from Eq. 33 for p_4'/p_3

(5) Calculate $\phi_4' = \phi_3 (A_3^*/A_4^*) (P_{t3}'/P_{t4}')$ (Eq. 29)

(6) Calculate P_{t4}'/p_4' from Eq. 34 for p_4'/p_3

(7) Calculate $\phi_4 = \phi_4''$ from Flow Function (Eq. 29) for $P_{t4}/p_4 = P_{t4}'/p_4'$



Diffusor Efficiency η_{D3-4} between Stations (3) and (4)

$$\eta_{D3-4} = \frac{T_4' - T_3}{T_4 - T_3} = \frac{T_4'/T_3 - 1}{T_4/T_3 - 1} = \frac{(p_4/p_3)^{\frac{\gamma-1}{\gamma}} - 1}{(p_4/p_3)^{\frac{\gamma-1}{\gamma}} - 1}$$

With Eq. 8

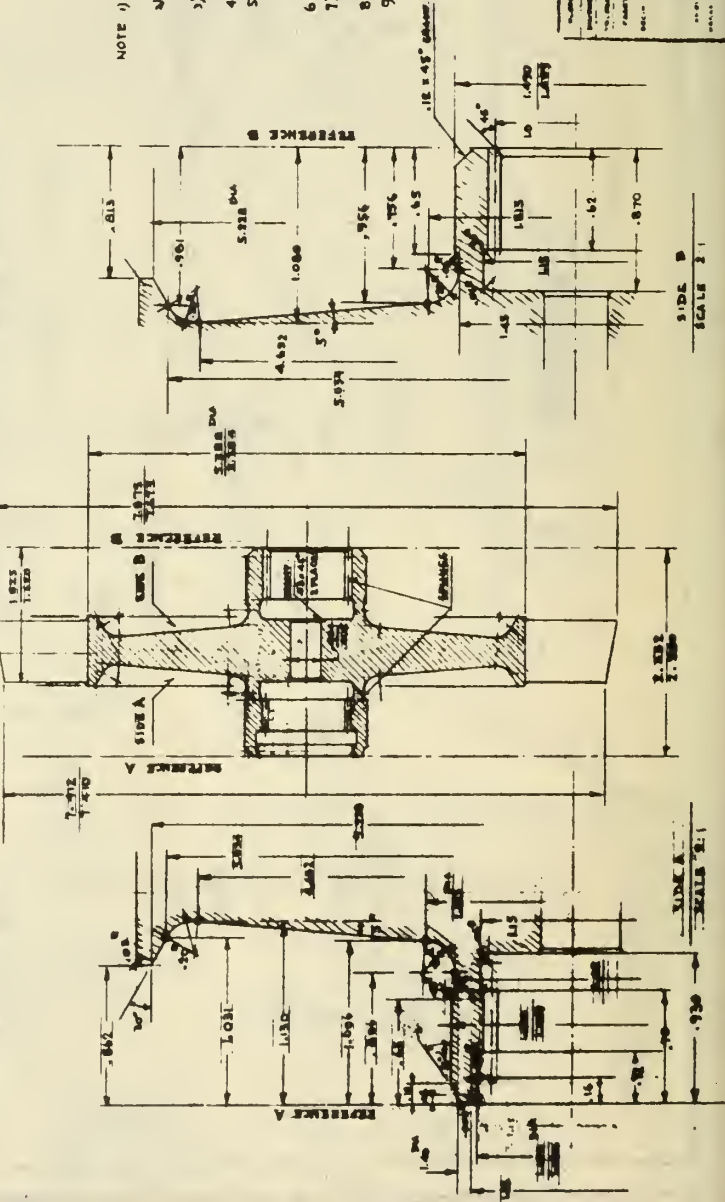
$$\eta_{D3-4} = \frac{(p_4/p_3)^{\frac{\gamma-1}{\gamma}} - 1}{(p_4/p_3)^{\frac{\gamma-1}{\gamma(1-\zeta)}} - 1} < (1 - \zeta) \quad \text{IV (35)}$$

APPENDIX B: MANUFACTURING DRAWINGS

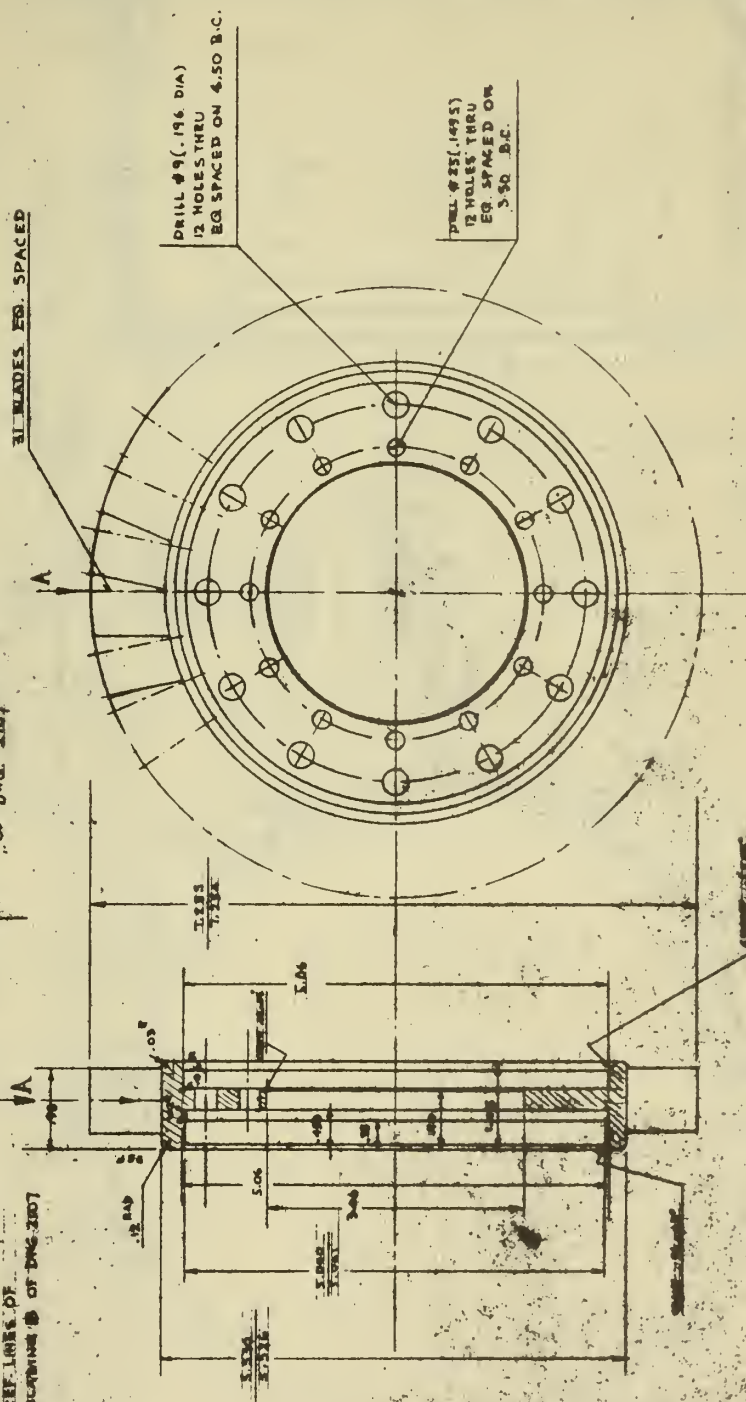
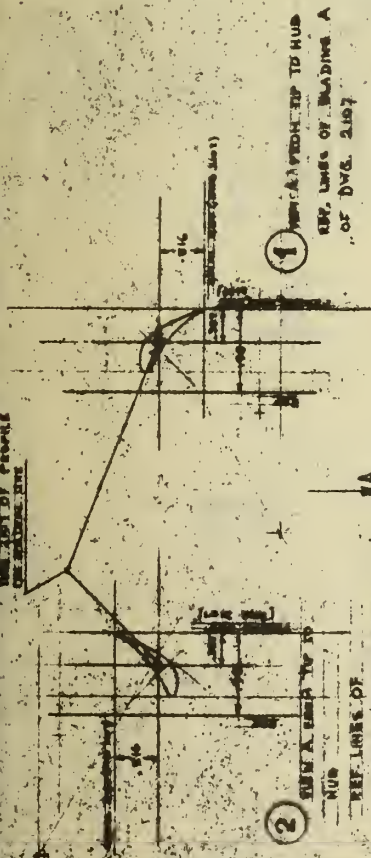
DATA FOR SPLINES ON SIDES ^a AND ^b (SCALE 5:1)
FILLET ROOT SIDE FIT, INVOLUTE INTERNAL SPLINE
(ASA B 5.15-1960)
NUMBER OF TEETH 20
PITCH 20/40
PRESSURE ANGLE 30°

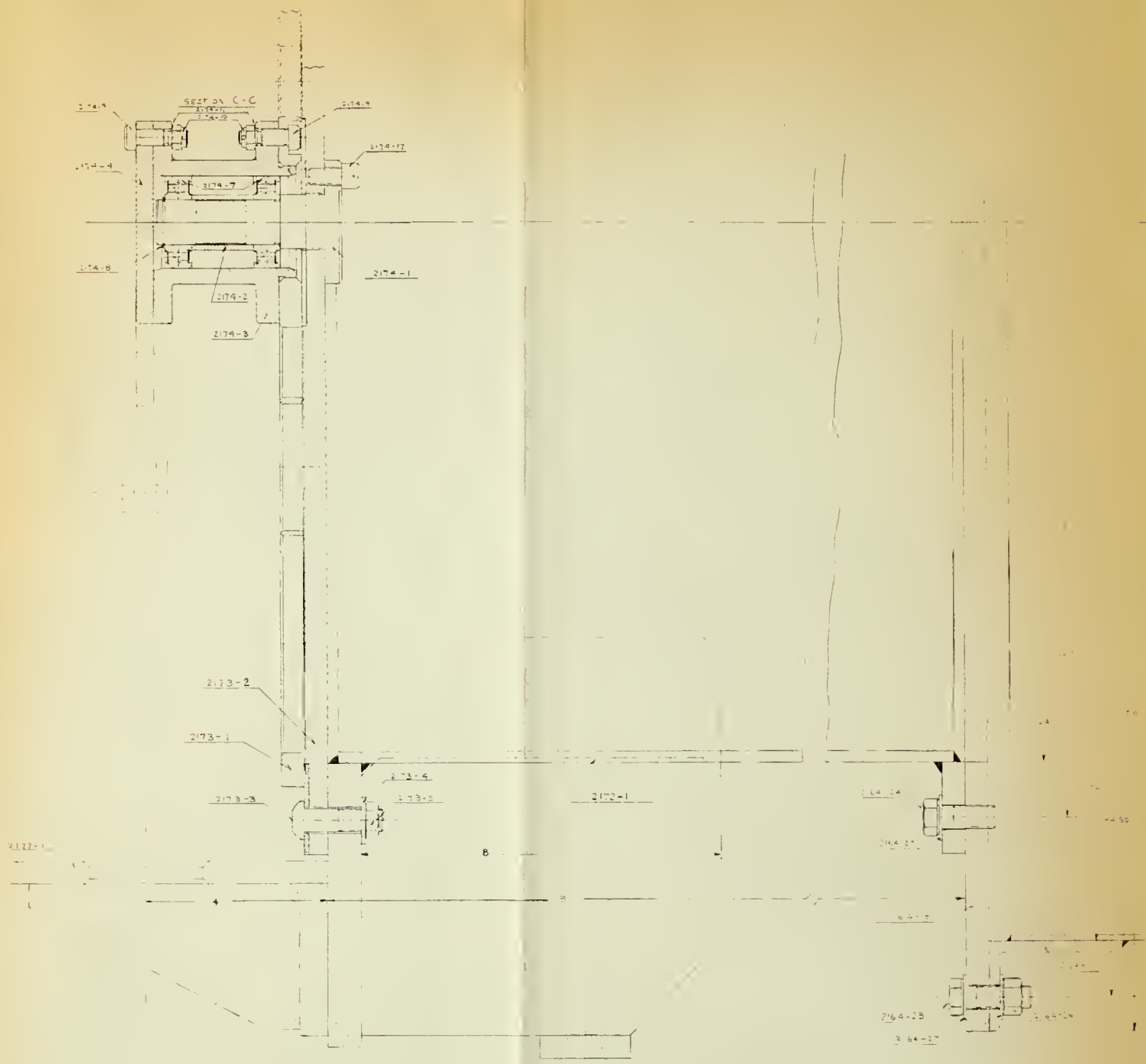
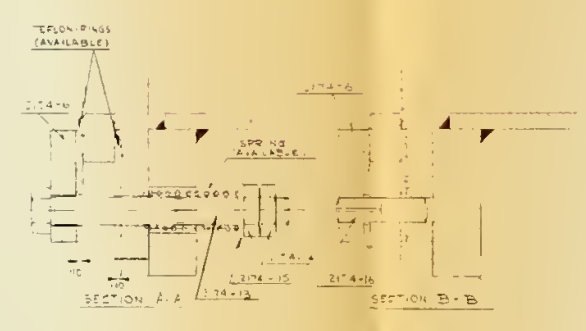
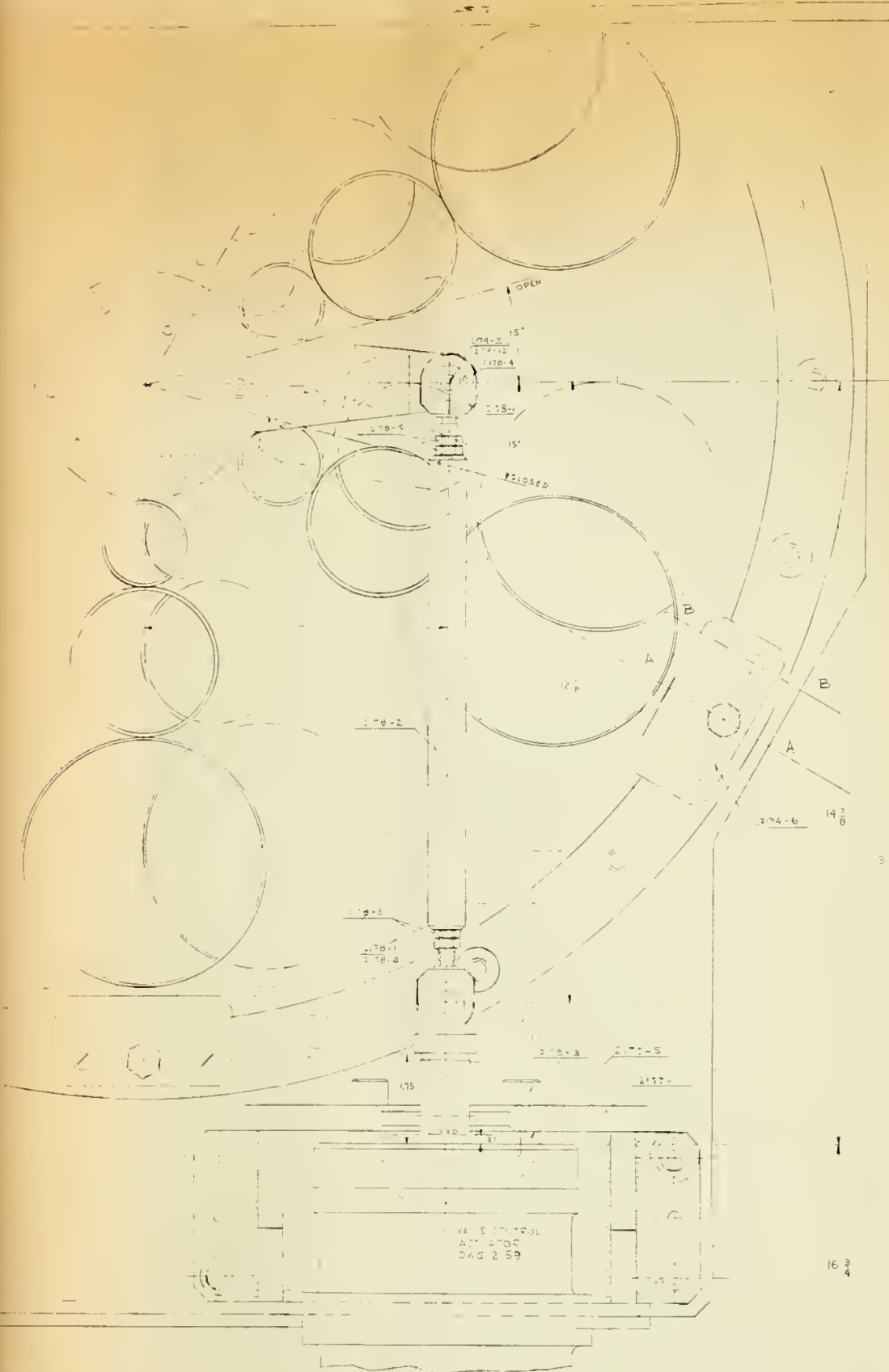
- 2109-2

2 VIEW C FROM TIP TO HUB OF ROTOR
REV. LINES IN ACCORDANCE
WITH BLADING B OF Dwg. 2407

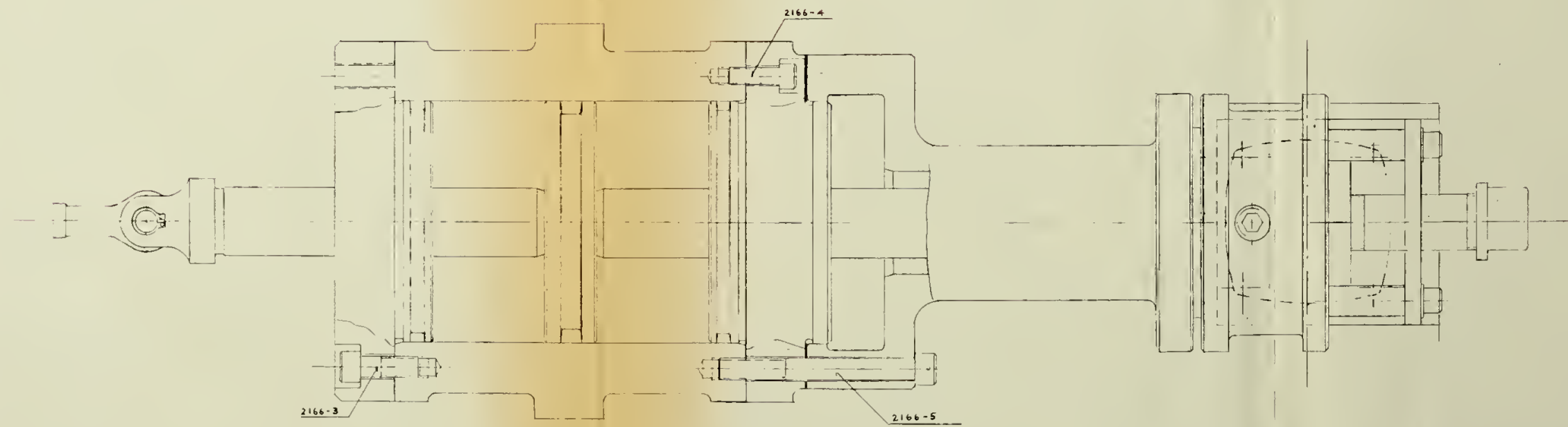
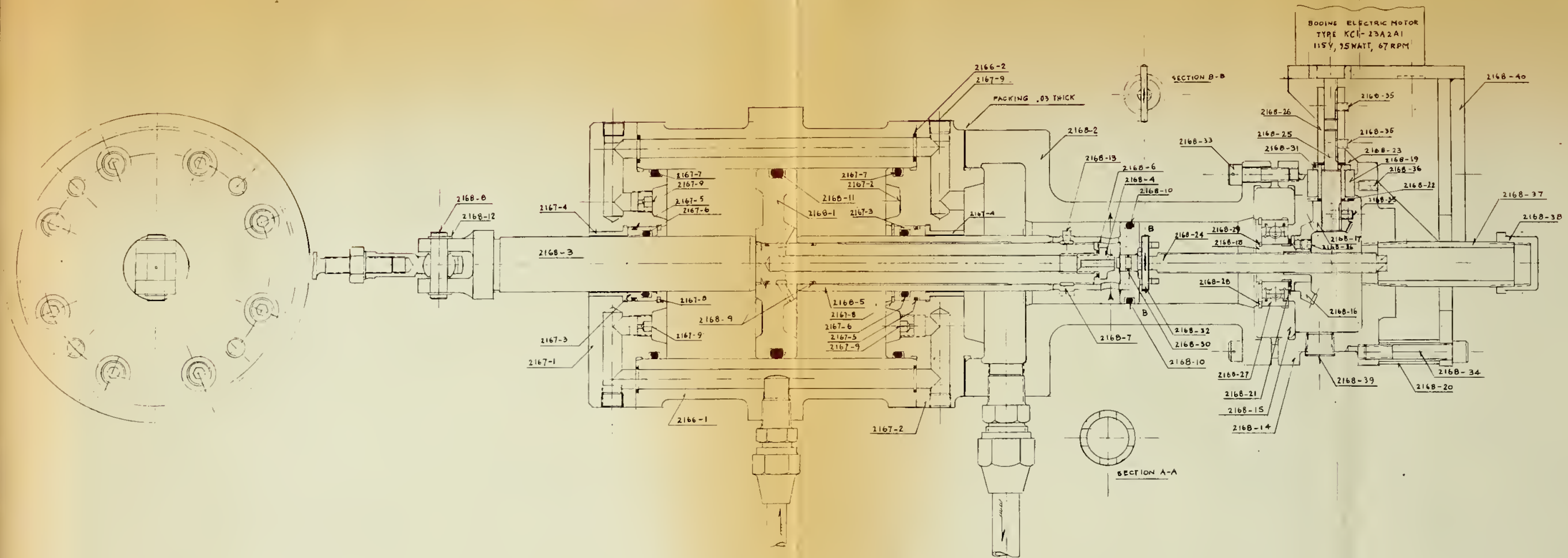
[illegible]

- NOTE 1) BOTH STATORS ARE IDENTICAL EXCEPT FOR THE ORIENTATION OF THE BLADES
- 2) BLADE PROFILES ARE THE SAME FROM HUB IN TIP AND HAVE NO TOW
- 3) PROFILE IS THE SAME FOR STATORS 1 AND 2 BUT ORIENTATION IS REVERSED
4. BETWEEN HUB AND PROFILE MUST BE A FILLET OF .003 RAD. AND AROUND PROFILE WITH INLETH TRANSITION
5. AFTER TOOL PATHS ON PROFILES
6. PROFILE COORDINATES ARE GIVEN IN DRAWING
- 7) THE SAME PROFILE IS USED FOR THE HOLLOW, PARTS 2100-1 AND 2100-2

[illegible]







UNLESS OTHERWISE STATED DIMENSIONS IN INCHES FRACTIONS DECIMALS ANGLES BREAK SHARP EDGES OFF DO NOT SCALE DRAWING	ITEM NO. REQ. # DES. LATION # MATERIAL NAVAL POSTGRADUATE SCHOOL DEPT. OF AERONAUTICS, TURBO PROPELLSION LABORATORY DRAWN M H VAVRA 5/14/70 CHECKED APPD USED ON 2158 SHEET 1 OF 1 SCALE FULL TRANSONIC COMPRESSOR TEST RIG CONTROL VALVE ACTUATOR 2159
---	--



24 HOLES $\frac{3}{16}$ EQ SPACED
ON $34\frac{1}{2}$ B.C., USE
PART 16 AS TEMPLATE

24 HOLES $\frac{3}{16}$ EQ SPACED
ON $34\frac{1}{2}$ B.C., USE
PART 17 AS TEMPLATE

INTERMEDIATE FILLET
WELD 2" x 2" ALL PARTS 5

SECTION C-C

SECTION D-D

DETAIL II (FULL SCALE)

DETAIL I (FULL SCALE)

FOR NOTES AND PARTS LIST SEE SHEET 2

UNLESS OTHERWISE STATED	ITEM NO.	REQ.	DESCRIPTION	MATERIAL
DIMENSIONS ARE IN INCHES				
TOLERANCES				
FRACTIONS	$\pm \frac{1}{16}$			
DECIMALS	$\pm .04$			
XXX	$\pm .02$			
ANGLES	$\pm \frac{1}{2}$			
BREAK SHARP EDGES ONLY				
DO NOT SCALE DRAWING				
NAVAL POSTGRADUATE SCHOOL DEPT. OF AERONAUTICS, TURBO-PROPULSION LABORATORY				
DRAWN M.H.V.V.R.A.		8/12/70	REV	USED ON 2160
CHECKED				SHEET 1 OF 2
APPD.				SCALE $\frac{1}{2}$ [3" PT]
INLET PLENUM			2164-1	



SECTION A-A

11560
.. 655
04
0.9
0.5
0.4

RECEIVED
INVESTIGATION DIVISION
FBI WASHINGTON
JAN 10 1968

TO DIRECTOR - FBI WASH DC
FROM SAC NEW YORK (100-157100)
SUBJECT: JAMES EARL RAY, AKA
MURDER OF MARTIN LUTHER KING, JR.
RE: NEW YORK TELETYPE TO BUREAU
JANUARY NINE LAST.

ENCLOSED FOR THE BUREAU ARE TWO COPIES
OF A LETTERHEAD MEMORANDUM DATED AND CAPTIONED AS ABOVE.

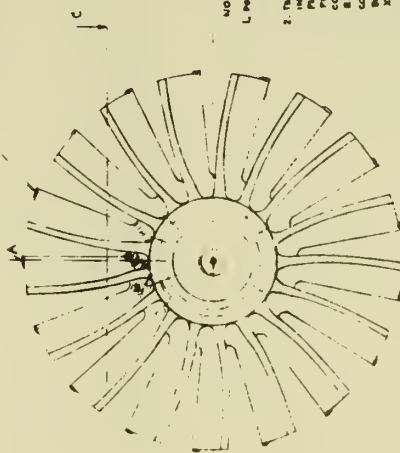
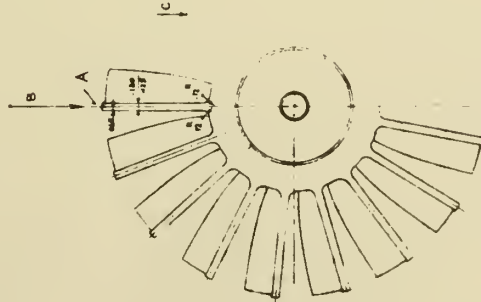
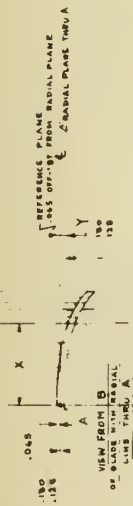
VERY TRULY YOURS,
WILLIAM F. MOHR
Special Agent in Charge

100-157100-100

3. SURFACES OF THE POLYMER IN SECTION
4. POLYMER SURFACES MUST BE PARALLEL AND SQUARE WITH SURFACES OF THE POLYMER IN SECTION



R	2.025	2.500	3.000	3.400	2.200	2.000	1.800	1.400	1.300	1.200	1.100
Z	0	0.18	0.15	0.47	0.70	1.02	1.44	2.00	2.84	3.75	4.80

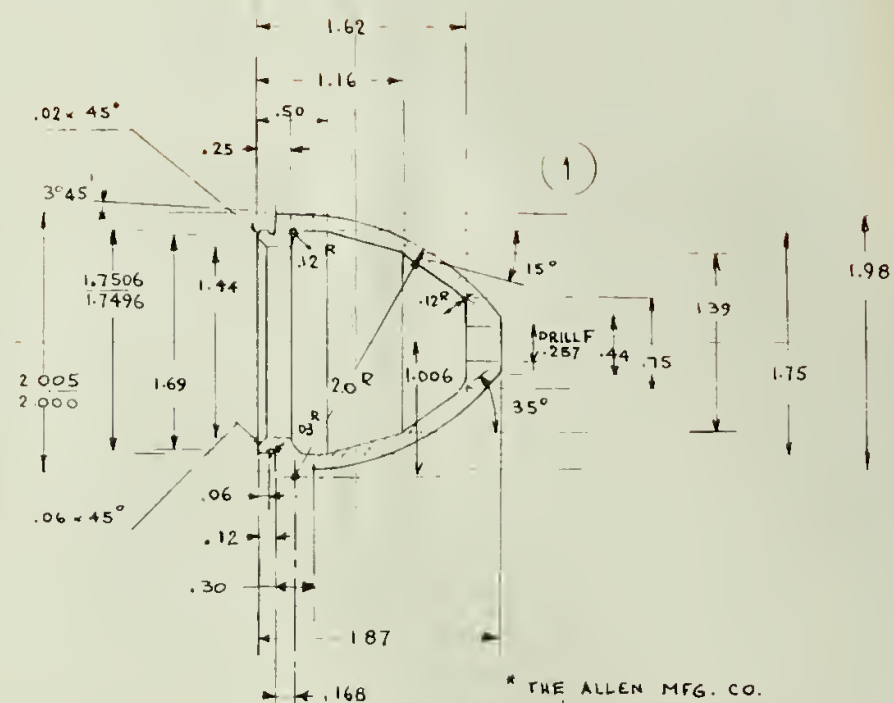


works

- [illegible]

[illegible]





DRILL AND REAM
HOLE $\frac{1.875}{.1903}$ ON .88 B.C.
2 PLACES EQ. SPACED

SECTION A-A

2

* THE ALLEN MFG. CO.

Technical drawing of a mechanical part, labeled (3). The drawing includes a side view on the left and a top view on the right.

Side View Dimensions:

- Top flange thickness: $.03 \times 45^\circ$
- Central hole diameter: $.50$
- Distance from center to edge: $.25$
- Distance from center to top flange: $.50$
- Total height: 1.12
- Bottom flange thickness: $.03$
- Bottom flange diameter: $.42$

Top View Dimensions:

- Hexagonal base diameter: $.50$
- Central hole diameter: $.03$
- Distance from center to edge: $.25$
- Distance from center to top flange: $.50$

Callouts:

- DRILL 23 (.154 DIA) THRU 2 PLACES
- DRILL 1 (.272 DIA) THRU TAP $\frac{3}{16}$ -24-UNF 2B

A technical drawing of a rectangular plate. The drawing includes the following text:

- PLATE ONE**
- DIMENSIONS**
- TENSILE STRENGTH**
- PRACTICE**
- 08 INCHES X 2**
- X = .01**
- X = .005**
- ANGLES**
- BREAK SHARP EDGES GOOD**
- DO NOT SCALE DRAWING**

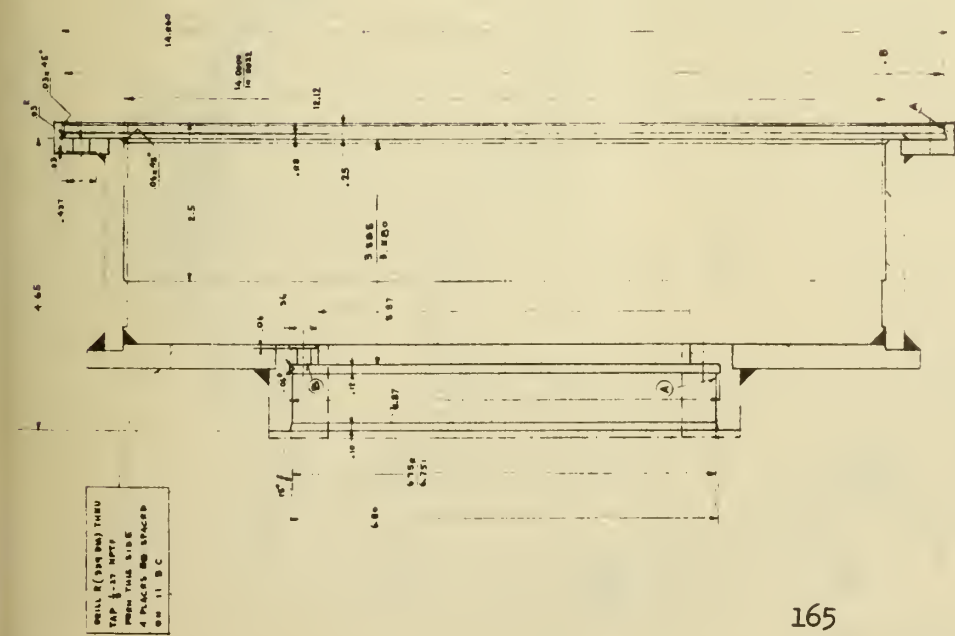
NAVAL POSTGRADUATE SCHOOL
DEPT. OF AERONAUTICS, 1100 FAY AVENUE, MONTEREY, CALIF. 94034

1042 M.H. VAVRA 11/5/70

1990 年 1 月

WHEEL ATTACHMENTS
HYBRID COMPRESSOR

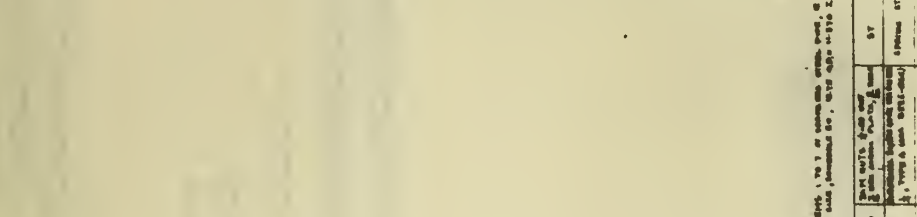
L5770N
 SHEET 1 OF 1
 SCALE FULL
 DWG NO.
 2205



- notes
1. SPACES (A) MUST BE CONCENTRIC WITHIN THE
 2. SPACES (B) MUST BE PARALLEL AND SQUARE WITH SPACES (A)

[illegible]

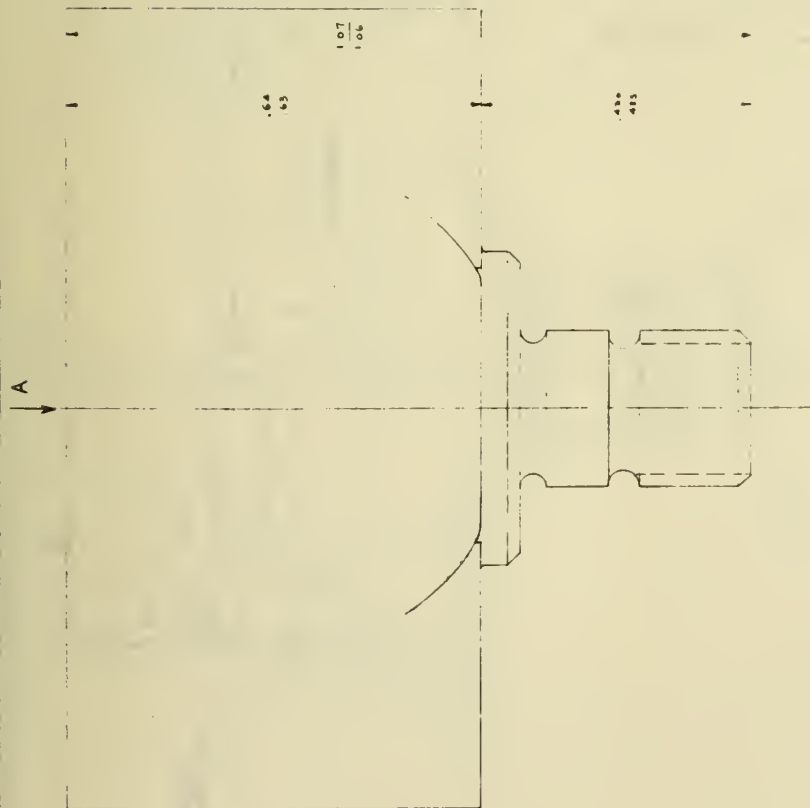
1	2	3	4	5	6	7	8	9	10	11	12	13	14	15	16	17	18	19	20	21	22	23	24	25	26	27	28	29	30	31	32	33	34	35	36	37	38	39	40	41	42	43	44	45	46	47	48	49	50	51	52	53	54	55	56	57	58	59	60	61	62	63	64	65	66	67	68	69	70	71	72	73	74	75	76	77	78	79	80	81	82	83	84	85	86	87	88	89	90	91	92	93	94	95	96	97	98	99	100
---	---	---	---	---	---	---	---	---	----	----	----	----	----	----	----	----	----	----	----	----	----	----	----	----	----	----	----	----	----	----	----	----	----	----	----	----	----	----	----	----	----	----	----	----	----	----	----	----	----	----	----	----	----	----	----	----	----	----	----	----	----	----	----	----	----	----	----	----	----	----	----	----	----	----	----	----	----	----	----	----	----	----	----	----	----	----	----	----	----	----	----	----	----	----	----	----	----	----	-----



11 72

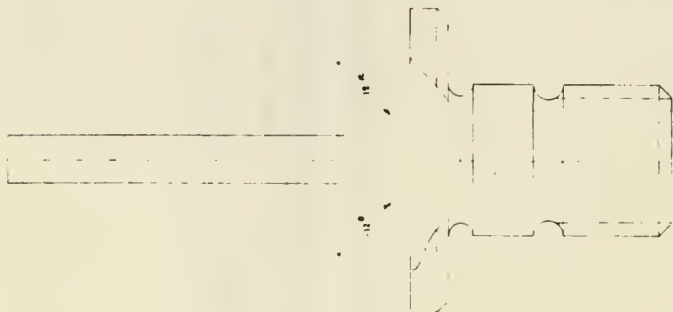
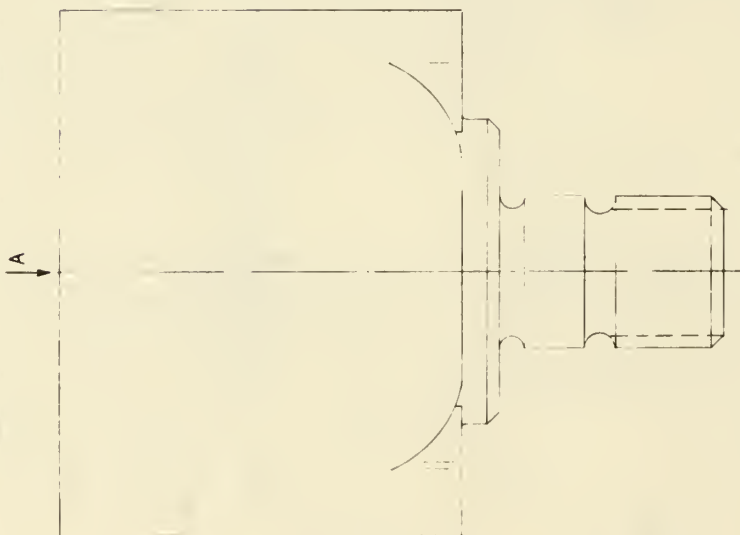
NOTE:
THESE CANNONS ONLY SOME OF
THE 80 RABBIT HOLES
IN MATHEOS $\frac{1142}{1161}$ AND
BE CONCENTRIC WITHIN
JEWELS WITH FACES (B)

33



PERFILS COMBINAIRE:

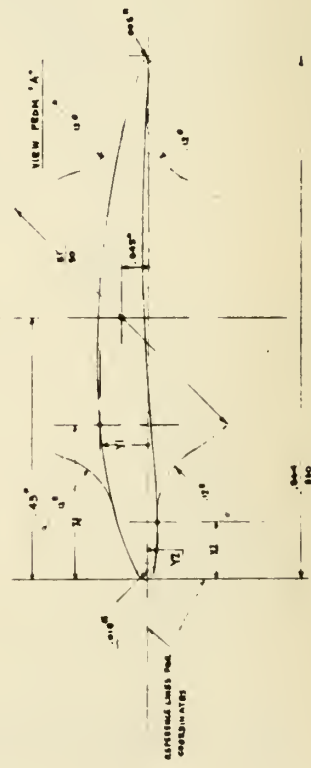
	X1	Y1	X2	Y2	X3	Y3	X4	Y4	X5	Y5	X6	Y6	X7	Y7	X8	Y8	X9	Y9	X10	Y10	X11	Y11	X12	Y12	X13	Y13	X14	Y14	X15	Y15	X16	Y16	X17	Y17	X18	Y18	X19	Y19	X20	Y20	X21	Y21	X22	Y22	X23	Y23	X24	Y24	X25	Y25	X26	Y26	X27	Y27	X28	Y28	X29	Y29	X30	Y30	X31	Y31	X32	Y32	X33	Y33	X34	Y34	X35	Y35	X36	Y36	X37	Y37	X38	Y38	X39	Y39	X40	Y40	X41	Y41	X42	Y42	X43	Y43	X44	Y44	X45	Y45	X46	Y46	X47	Y47	X48	Y48	X49	Y49	X50	Y50	X51	Y51	X52	Y52	X53	Y53	X54	Y54	X55	Y55	X56	Y56	X57	Y57	X58	Y58	X59	Y59	X60	Y60	X61	Y61	X62	Y62	X63	Y63	X64	Y64	X65	Y65	X66	Y66	X67	Y67	X68	Y68	X69	Y69	X70	Y70	X71	Y71	X72	Y72	X73	Y73	X74	Y74	X75	Y75	X76	Y76	X77	Y77	X78	Y78	X79	Y79	X80	Y80	X81	Y81	X82	Y82	X83	Y83	X84	Y84	X85	Y85	X86	Y86	X87	Y87	X88	Y88	X89	Y89	X90	Y90	X91	Y91	X92	Y92	X93	Y93	X94	Y94	X95	Y95	X96	Y96	X97	Y97	X98	Y98	X99	Y99	X100	Y100	X101	Y101	X102	Y102	X103	Y103	X104	Y104	X105	Y105	X106	Y106	X107	Y107	X108	Y108	X109	Y109	X110	Y110	X111	Y111	X112	Y112	X113	Y113	X114	Y114	X115	Y115	X116	Y116	X117	Y117	X118	Y118	X119	Y119	X120	Y120	X121	Y121	X122	Y122	X123	Y123	X124	Y124	X125	Y125	X126	Y126	X127	Y127	X128	Y128	X129	Y129	X130	Y130	X131	Y131	X132	Y132	X133	Y133	X134	Y134	X135	Y135	X136	Y136	X137	Y137	X138	Y138	X139	Y139	X140	Y140	X141	Y141	X142	Y142	X143	Y143	X144	Y144	X145	Y145	X146	Y146	X147	Y147	X148	Y148	X149	Y149	X150	Y150	X151	Y151	X152	Y152	X153	Y153	X154	Y154	X155	Y155	X156	Y156	X157	Y157	X158	Y158	X159	Y159	X160	Y160	X161	Y161	X162	Y162	X163	Y163	X164	Y164	X165	Y165	X166	Y166	X167	Y167	X168	Y168	X169	Y169	X170	Y170	X171	Y171	X172	Y172	X173	Y173	X174	Y174	X175	Y175	X176	Y176	X177	Y177	X178	Y178	X179	Y179	X180	Y180	X181	Y181	X182	Y182	X183	Y183	X184	Y184	X185	Y185	X186	Y186	X187	Y187	X188	Y188	X189	Y189	X190	Y190	X191	Y191	X192	Y192	X193	Y193	X194	Y194	X195	Y195	X196	Y196	X197	Y197	X198	Y198	X199	Y199	X200	Y200	X201	Y201	X202	Y202	X203	Y203	X204	Y204	X205	Y205	X206	Y206	X207	Y207	X208	Y208	X209	Y209	X210	Y210	X211	Y211	X212	Y212	X213	Y213	X214	Y214	X215	Y215	X216	Y216	X217	Y217	X218	Y218	X219	Y219	X220	Y220	X221	Y221	X222	Y222	X223	Y223	X224	Y224	X225	Y225	X226	Y226	X227	Y227	X228	Y228	X229	Y229	X230	Y230	X231	Y231	X232	Y232	X233	Y233	X234	Y234	X235	Y235	X236	Y236	X237	Y237	X238	Y238	X239	Y239	X240	Y240	X241	Y241	X242	Y242	X243	Y243	X244	Y244	X245	Y245	X246	Y246	X247	Y247	X248	Y248	X249	Y249	X250	Y250	X251	Y251	X252	Y252	X253	Y253	X254	Y254	X255	Y255	X256	Y256	X257	Y257	X258	Y258	X259	Y259	X260	Y260	X261	Y261	X262	Y262	X263	Y263	X264	Y264	X265	Y265	X266	Y266	X267	Y267	X268	Y268	X269	Y269	X270	Y270	X271	Y271	X272	Y272	X273	Y273	X274	Y274	X275	Y275	X276	Y276	X277	Y277	X278	Y278	X279	Y279	X280	Y280	X281	Y281	X282	Y282	X283	Y283	X284	Y284	X285	Y285	X286	Y286	X287	Y287	X288	Y288	X289	Y289	X290	Y290	X291	Y291	X292	Y292	X293	Y293	X294	Y294	X295	Y295	X296	Y296	X297	Y297	X298	Y298	X299	Y299	X300	Y300	X301	Y301	X302	Y302	X303	Y303	X304	Y304	X305	Y305	X306	Y306	X307	Y307	X308	Y308	X309	Y309	X310	Y310	X311	Y311	X312	Y312	X313	Y313	X314	Y314	X315	Y315	X316	Y316	X317	Y317	X318	Y318	X319	Y319	X320	Y320	X321	Y321	X322	Y322	X323	Y323	X324	Y324	X325	Y325	X326	Y326
--	----	----	----	----	----	----	----	----	----	----	----	----	----	----	----	----	----	----	-----	-----	-----	-----	-----	-----	-----	-----	-----	-----	-----	-----	-----	-----	-----	-----	-----	-----	-----	-----	-----	-----	-----	-----	-----	-----	-----	-----	-----	-----	-----	-----	-----	-----	-----	-----	-----	-----	-----	-----	-----	-----	-----	-----	-----	-----	-----	-----	-----	-----	-----	-----	-----	-----	-----	-----	-----	-----	-----	-----	-----	-----	-----	-----	-----	-----	-----	-----	-----	-----	-----	-----	-----	-----	-----	-----	-----	-----	-----	-----	-----	-----	-----	-----	-----	-----	-----	-----	-----	-----	-----	-----	-----	-----	-----	-----	-----	-----	-----	-----	-----	-----	-----	-----	-----	-----	-----	-----	-----	-----	-----	-----	-----	-----	-----	-----	-----	-----	-----	-----	-----	-----	-----	-----	-----	-----	-----	-----	-----	-----	-----	-----	-----	-----	-----	-----	-----	-----	-----	-----	-----	-----	-----	-----	-----	-----	-----	-----	-----	-----	-----	-----	-----	-----	-----	-----	-----	-----	-----	-----	-----	-----	-----	-----	-----	-----	-----	-----	-----	-----	-----	-----	-----	-----	-----	-----	-----	-----	-----	-----	------	------	------	------	------	------	------	------	------	------	------	------	------	------	------	------	------	------	------	------	------	------	------	------	------	------	------	------	------	------	------	------	------	------	------	------	------	------	------	------	------	------	------	------	------	------	------	------	------	------	------	------	------	------	------	------	------	------	------	------	------	------	------	------	------	------	------	------	------	------	------	------	------	------	------	------	------	------	------	------	------	------	------	------	------	------	------	------	------	------	------	------	------	------	------	------	------	------	------	------	------	------	------	------	------	------	------	------	------	------	------	------	------	------	------	------	------	------	------	------	------	------	------	------	------	------	------	------	------	------	------	------	------	------	------	------	------	------	------	------	------	------	------	------	------	------	------	------	------	------	------	------	------	------	------	------	------	------	------	------	------	------	------	------	------	------	------	------	------	------	------	------	------	------	------	------	------	------	------	------	------	------	------	------	------	------	------	------	------	------	------	------	------	------	------	------	------	------	------	------	------	------	------	------	------	------	------	------	------	------	------	------	------	------	------	------	------	------	------	------	------	------	------	------	------	------	------	------	------	------	------	------	------	------	------	------	------	------	------	------	------	------	------	------	------	------	------	------	------	------	------	------	------	------	------	------	------	------	------	------	------	------	------	------	------	------	------	------	------	------	------	------	------	------	------	------	------	------	------	------	------	------	------	------	------	------	------	------	------	------	------	------	------	------	------	------	------	------	------	------	------	------	------	------	------	------	------	------	------	------	------	------	------	------	------	------	------	------	------	------	------	------	------	------	------	------	------	------	------	------	------	------	------	------	------	------	------	------	------	------	------	------	------	------	------	------	------	------	------	------	------	------	------	------	------	------	------	------	------	------	------	------	------	------	------	------	------	------	------	------	------	------	------	------	------	------	------	------	------	------	------	------	------	------	------	------	------	------	------	------	------	------	------	------	------	------	------	------	------	------	------	------	------	------	------	------	------	------	------	------	------	------	------	------	------	------	------	------	------	------	------	------	------	------	------	------	------	------	------	------	------	------	------	------	------	------	------	------	------	------	------	------	------	------	------	------	------	------	------	------	------	------	------	------



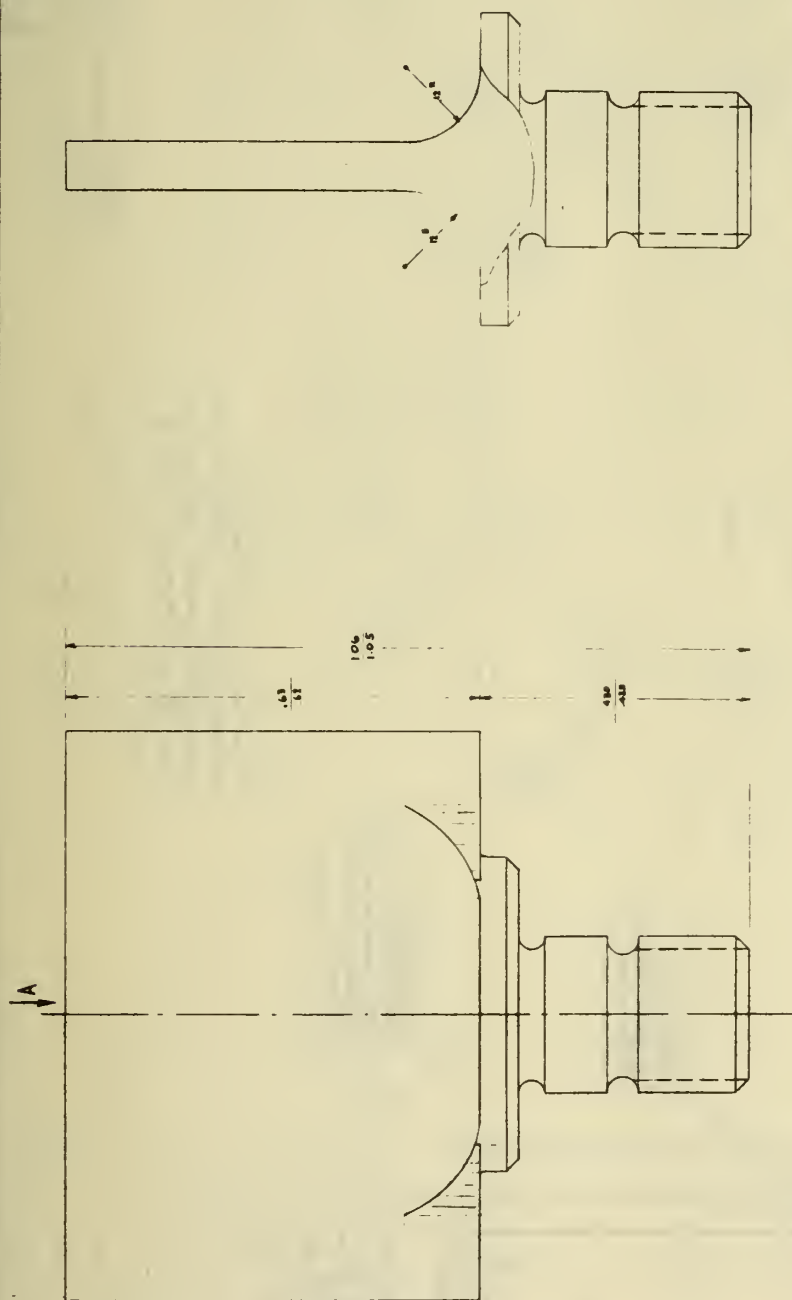
Profile coordinates

Convex side	X1	0	100	200	300	400	500	600	700	800	900	1000	1100	1200	1300	1400	1500	1600	1700	1800	1900	2000	2100	2200	2300	2400	2500	2600	2700	2800	2900	3000	3100	3200	3300	3400	3500	3600	3700	3800	3900	4000	4100	4200	4300	4400	4500	4600	4700	4800	4900	5000	5100	5200	5300	5400	5500	5600	5700	5800	5900	6000	6100	6200	6300	6400	6500	6600	6700	6800	6900	7000	7100	7200	7300	7400	7500	7600	7700	7800	7900	8000	8100	8200	8300	8400	8500	8600	8700	8800	8900	9000	9100	9200	9300	9400	9500	9600	9700	9800	9900	10000
Concave side	X2	0	100	200	300	400	500	600	700	800	900	1000	1100	1200	1300	1400	1500	1600	1700	1800	1900	2000	2100	2200	2300	2400	2500	2600	2700	2800	2900	3000	3100	3200	3300	3400	3500	3600	3700	3800	3900	4000	4100	4200	4300	4400	4500	4600	4700	4800	4900	5000	5100	5200	5300	5400	5500	5600	5700	5800	5900	6000	6100	6200	6300	6400	6500	6600	6700	6800	6900	7000	7100	7200	7300	7400	7500	7600	7700	7800	7900	8000	8100	8200	8300	8400	8500	8600	8700	8800	8900	9000	9100	9200	9300	9400	9500	9600	9700	9800	9900	10000

1. COORDINATE Y2 AS SHOWN IN SLIDES IS NEGATIVE
2. DISTANCES 0.45" AND 4.5" ARE NOT CRITICAL BUT SHOULD BE EQUAL FOR ALL BLADES
3. FOR MISSING DIMENSIONS SEE DWG 2210-1
4. FOR 0.15" PILETS BETWEEN BASE AND PROFILE SEE NOTE 3 OF DWG 2210-1
5. VIEW FROM "A" IS A VIEW FROM THE BLADE TIP TO THE BASE WITH 81/60 DIA

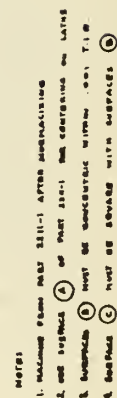


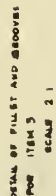
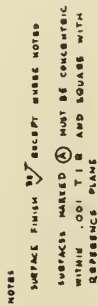
3		4		5		6		7		8		9		10		11		12		13		14		15		16		17		18		19		20		21		22		23		24		25		26		27		28		29		30		31		32		33		34		35		36		37		38		39		40		41		42		43		44		45		46		47		48		49		50		51		52		53		54		55		56		57		58		59		60		61		62		63		64		65		66		67		68		69		70		71		72		73		74		75		76		77		78		79		80		81		82		83		84		85		86		87		88		89		90		91		92		93		94		95		96		97		98		99		100	
3		4		5		6		7		8		9		10		11		12		13		14		15		16		17		18		19		20		21		22		23		24		25		26		27		28		29		30		31		32		33		34		35		36		37		38		39		40		41		42		43		44		45		46		47		48		49		50		51		52		53		54		55		56		57		58		59		60		61		62		63		64		65		66		67		68		69		70		71		72		73		74		75		76		77		78		79		80		81		82		83		84		85		86		87		88		89		90		91		92		93		94		95		96		97		98		99		100	

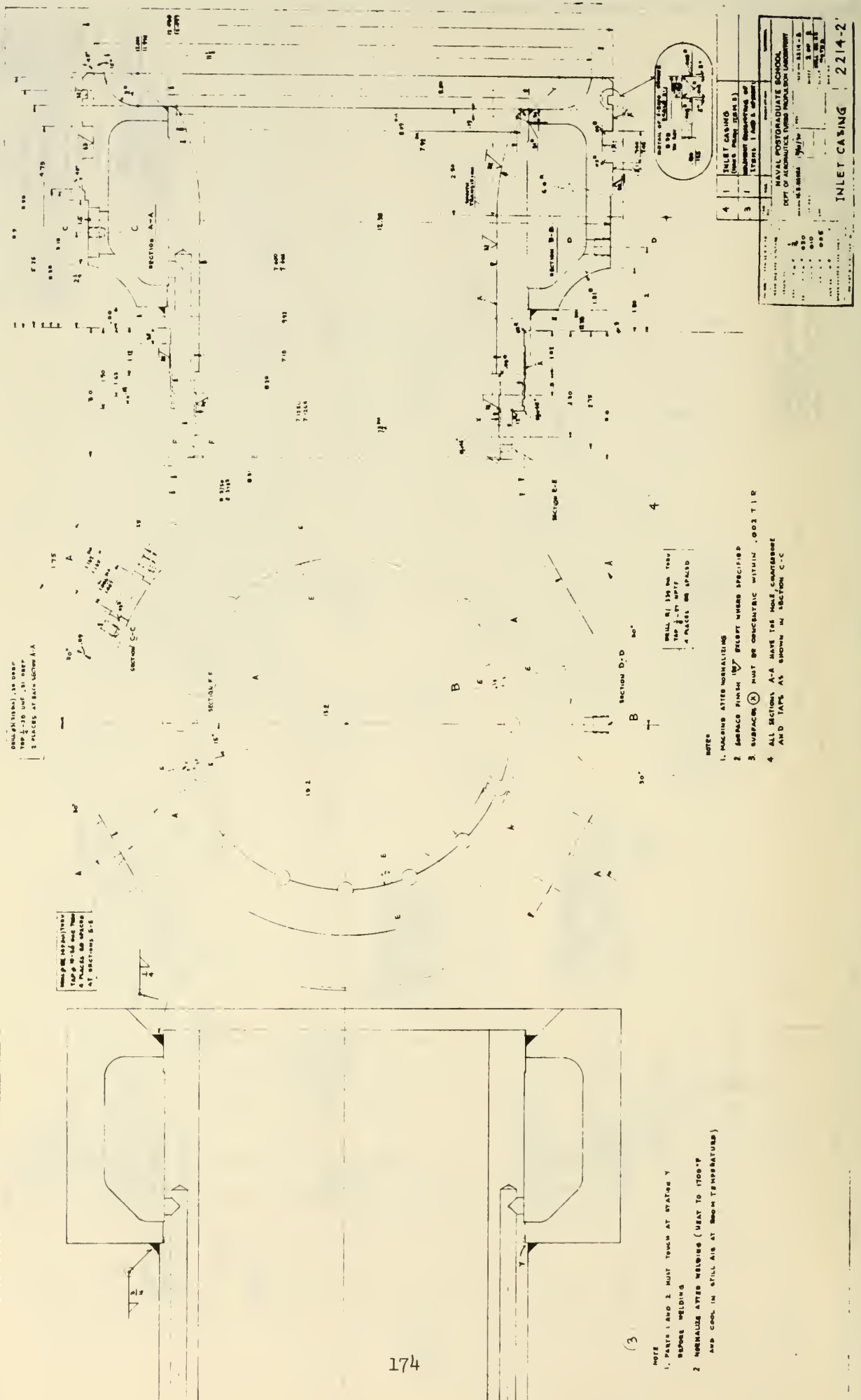


PROFILE COORDINATES

GROUP	FILE	0	101	102	103	104	105	106	107	108	109	110	111	112	113	114	115	116	117	118	119	120	121	122	123	124	125	126	127	128	129	130	131	132	133	134	135	136	137	138	139	140	141	142	143	144	145	146	147	148	149	150	151	152	153	154	155	156	157	158	159	160	161	162	163	164	165	166	167	168	169	170	171	172	173	174	175	176	177	178	179	180	181	182	183	184	185	186	187	188	189	190	191	192	193	194	195	196	197	198	199	200	201	202	203	204	205	206	207	208	209	210	211	212	213	214	215	216	217	218	219	220	221	222	223	224	225	226	227	228	229	230	231	232	233	234	235	236	237	238	239	240	241	242	243	244	245	246	247	248	249	250	251	252	253	254	255	256	257	258	259	260	261	262	263	264	265	266	267	268	269	270	271	272	273	274	275	276	277	278	279	280	281	282	283	284	285	286	287	288	289	290	291	292	293	294	295	296	297	298	299	300	301	302	303	304	305	306	307	308	309	310	311	312	313	314	315	316	317	318	319	320	321	322	323	324	325	326	327	328	329	330	331	332	333	334	335	336	337	338	339	340	341	342	343	344	345	346	347	348	349	350	351	352	353	354	355	356	357	358	359	360	361	362	363	364	365	366	367	368	369	370	371	372	373	374	375	376	377	378	379	380	381	382	383	384	385	386	387	388	389	390	391	392	393	394	395	396	397	398	399	400	401	402	403	404	405	406	407	408	409	410	411	412	413	414	415	416	417	418	419	420	421	422	423	424	425	426	427	428	429	430	431	432	433	434	435	436	437	438	439	440	441	442	443	444	445	446	447	448	449	450	451	452	453	454	455	456	457	458	459	460	461	462	463	464	465	466	467	468	469	470	471	472	473	474	475	476	477	478	479	480	481	482	483	484	485	486	487	488	489	490	491	492	493	494	495	496	497	498	499	500	501	502	503	504	505	506	507	508	509	510	511	512	513	514	515	516	517	518	519	520	521	522	523	524	525	526	527	528	529	530	531	532	533	534	535	536	537	538	539	540	541	542	543	544	545	546	547	548	549	550	551	552	553	554	555	556	557	558	559	560	561	562	563	564	565	566	567	568	569	570	571	572	573	574	575	576	577	578	579	580	581	582	583	584	585	586	587	588	589	590	591	592	593	594	595	596	597	598	599	600	601	602	603	604	605	606	607	608	609	610	611	612	613	614	615	616	617	618	619	620	621	622	623	624	625	626	627	628	629	630	631	632	633	634	635	636	637	638	639	640	641	642	643	644	645	646	647	648	649	650	651	652	653	654	655	656	657	658	659	660	661	662	663	664	665	666	667	668	669	670	671	672	673	674	675	676	677	678	679	680	681	682	683	684	685	686	687	688	689	690	691	692	693	694	695	696	697	698	699	700	701	702	703	704	705	706	707	708	709	710	711	712	713	714	715	716	717	718	719	720	721	722	723	724	725	726	727	728	729	730	731	732	733	734	735	736	737	738	739	740	741	742	743	744	745	746	747	748	749	750	751	752	753	754	755	756	757	758	759	760	761	762	763	764	765	766	767	768	769	770	771	772	773	774	775	776	777	778	779	780	781	782	783	784	785	786	787	788	789	790	791	792	793	794	795	796	797	798	799	800	801	802	803	804	805	806	807	808	809	810	811	812	813	814	815	816	817	818	819	820	821	822	823	824	825	826	827	828	829	830	831	832	833	834	835	836	837	838	839	840	841	842	843	844	845	846	847	848	849	850	851	852	853	854	855	856	857	858	859	860	861	862	863	864	865	866	867	868	869	870	871	872	873	874	875	876	877	878	879	880	881	882	883	884	885	886	887	888	889	890	891	892	893	894	895	896	897	898	899	900	901	902	903	904	905	906	907	908	909	910	911	912	913	914	915	916	917	918	919	920	921	922	923	924	925	926	927	928	929	930	931	932	933	934	935	936	937	938	939	940	941	942	943	944	945	946	947	948	949	950	951	952	953	954	955	956	957	958	959	960	961	962	963	964	965	966	967	968	969	970	971	972	973	974	975	976	977	978	979	980	981	982	983	984	985	986	987	988	989	990	991	992	993	994	995	996	997	998	999	1000	1001	1002	1003	1004	1005	1006	1007	1008	1009	1010	1011	1012	1013	1014	1015	1016	1017	1018	1019	1020	1021	1022	1023	1024	1025	1026	1027	1028	1029	1030	1031	1032	1033	1034	1035	1036	1037	1038	1039	1040	1041	1042	1043	1044	1045	1046	1047	1048	1049	1050	1051	1052	1053	1054	1055	1056	1057	1058	1059	1060	1061	1062	1063	1064	1065	1066	1067	1068	1069	1070	1071	1072	1073	1074	1075	1076	1077	1078	1079	1080	1081	1082	1083	1084	1085	1086	1087	1088	1089	1090	1091	1092	1093	1094	1095	1096	1097	1098	1099	1100	1101	1102	1103	1104	1105	1106	1107	1108	1109	1110	1111	1112	1113	1114	1115	1116	1117	1118	1119	1120	1121	1122	1123	1124	1125	1126	1127	1128	1129	1130	1131	1132	1133	1134	1135	1136	1137	1138	1139	1140	1141	1142	1143	1144	1145	1146	1147	1148	1149	1150	1151	1152	1153	1154	1155	1156	1157	1158	1159	1160	1161	1162	1163	1164	1165	1166	1167	1168	1169	1170	1171	1172	1173	1174	1175	1176	1177	1178	1179	1180	1181	1182	1183	1184	1185	1186	1187	1188	1189	1190	1191	1192	1193	1194	1195	1196	1197	1198	1199	1200	1201	1202	1203	1204	1205	1206	1207	1208	1209	1210	1211	1212	1213	1214	1215	1216	1217	1218	1219	1220	1221	1222	1223	1224	1225	1226	1227	1228	1229	1230	1231	1232	1233	1234	1235	1236	1237	1238	1239	1240	1241	1242	1243	1244	1245	1246	1247	1248	1249	1250	1251	1252	1253	1254	1255	1256	1257	1258	1259	1260	1261	1262	1263	1264	1265	1266	1267	1268	1269	1270	1271	1272	1273	1274	1275	1276	1277	1278	1279	1280	1281	1282	1283	1284	1285	1286	1287	1288	1289	1290	1291	1292	1293	1294	1295	1296	1297	1298	1299	1300	1301	1302	1303	1304	1305	1306	1307	1308	1309	1310	1311	1312	1313	1314	1315	1316	1317	1318	1319	1320	1321	1322	1323	1324	1325	1326	1327	1328	1329	1330	1331	1332	1333	1334	1335	1336	1337	1338	1339	1340	1341	1342	1343	1344	1345	1346	1347	1348	1349	1350	1351	1352	1353	1354	1355	1356	1357	1358	1359	1360	1361	1362	1363	1364	1365	1366	1367	1368	1369	1370	1371	1372	1373	1374	1375	1376	1377	1378	1379	1380	1381	1382	1383	1384	1385	1386	1387	1388	1389	1390	1391	1392	1393	1394	1395	1396	1397	1398	1399	1400	1401	1402	1403	1404	1405	1406	1407	1408	1409	1410	1411	1412	1413	1414	1415	1416	1417	1418	1419	1420	1421	1422	1423	1424	1425	1426	1427	1428	1429	1430	1431	1432	1433	1434	1435	1436	1437	1438	1439	1440	1441	1442	1443	1444	1445	1446	1447	1448	1449	1450	1451	1452	1453	1454	1455	1456	1457	1458	1459	1460	1461	1462	1463	1464	1465	1466	1467	1468	1469	1470	1471	1472	1473	1474	1475	1476	1477	1478	1479	1480	1481	1482	1483	1484	1485	1486	1487	1488	1489	1490	1491	1492	1493	1494	1495	1496	1497	1498	1499	1500	1501	1502	1503	1504	1505	1506	1507	1508	1509	1510	1511	1512	1513	1514	1515	1516	1517	1518	1519	1520	1521	1522	1523	1524	1525	1526	1527	1528	1529	1530	1531	1532	1533	1534	1535	1536	1537	1538	1539	1540	1541	1542	1543	1544	1545	1546	1547	
-------	------	---	-----	-----	-----	-----	-----	-----	-----	-----	-----	-----	-----	-----	-----	-----	-----	-----	-----	-----	-----	-----	-----	-----	-----	-----	-----	-----	-----	-----	-----	-----	-----	-----	-----	-----	-----	-----	-----	-----	-----	-----	-----	-----	-----	-----	-----	-----	-----	-----	-----	-----	-----	-----	-----	-----	-----	-----	-----	-----	-----	-----	-----	-----	-----	-----	-----	-----	-----	-----	-----	-----	-----	-----	-----	-----	-----	-----	-----	-----	-----	-----	-----	-----	-----	-----	-----	-----	-----	-----	-----	-----	-----	-----	-----	-----	-----	-----	-----	-----	-----	-----	-----	-----	-----	-----	-----	-----	-----	-----	-----	-----	-----	-----	-----	-----	-----	-----	-----	-----	-----	-----	-----	-----	-----	-----	-----	-----	-----	-----	-----	-----	-----	-----	-----	-----	-----	-----	-----	-----	-----	-----	-----	-----	-----	-----	-----	-----	-----	-----	-----	-----	-----	-----	-----	-----	-----	-----	-----	-----	-----	-----	-----	-----	-----	-----	-----	-----	-----	-----	-----	-----	-----	-----	-----	-----	-----	-----	-----	-----	-----	-----	-----	-----	-----	-----	-----	-----	-----	-----	-----	-----	-----	-----	-----	-----	-----	-----	-----	-----	-----	-----	-----	-----	-----	-----	-----	-----	-----	-----	-----	-----	-----	-----	-----	-----	-----	-----	-----	-----	-----	-----	-----	-----	-----	-----	-----	-----	-----	-----	-----	-----	-----	-----	-----	-----	-----	-----	-----	-----	-----	-----	-----	-----	-----	-----	-----	-----	-----	-----	-----	-----	-----	-----	-----	-----	-----	-----	-----	-----	-----	-----	-----	-----	-----	-----	-----	-----	-----	-----	-----	-----	-----	-----	-----	-----	-----	-----	-----	-----	-----	-----	-----	-----	-----	-----	-----	-----	-----	-----	-----	-----	-----	-----	-----	-----	-----	-----	-----	-----	-----	-----	-----	-----	-----	-----	-----	-----	-----	-----	-----	-----	-----	-----	-----	-----	-----	-----	-----	-----	-----	-----	-----	-----	-----	-----	-----	-----	-----	-----	-----	-----	-----	-----	-----	-----	-----	-----	-----	-----	-----	-----	-----	-----	-----	-----	-----	-----	-----	-----	-----	-----	-----	-----	-----	-----	-----	-----	-----	-----	-----	-----	-----	-----	-----	-----	-----	-----	-----	-----	-----	-----	-----	-----	-----	-----	-----	-----	-----	-----	-----	-----	-----	-----	-----	-----	-----	-----	-----	-----	-----	-----	-----	-----	-----	-----	-----	-----	-----	-----	-----	-----	-----	-----	-----	-----	-----	-----	-----	-----	-----	-----	-----	-----	-----	-----	-----	-----	-----	-----	-----	-----	-----	-----	-----	-----	-----	-----	-----	-----	-----	-----	-----	-----	-----	-----	-----	-----	-----	-----	-----	-----	-----	-----	-----	-----	-----	-----	-----	-----	-----	-----	-----	-----	-----	-----	-----	-----	-----	-----	-----	-----	-----	-----	-----	-----	-----	-----	-----	-----	-----	-----	-----	-----	-----	-----	-----	-----	-----	-----	-----	-----	-----	-----	-----	-----	-----	-----	-----	-----	-----	-----	-----	-----	-----	-----	-----	-----	-----	-----	-----	-----	-----	-----	-----	-----	-----	-----	-----	-----	-----	-----	-----	-----	-----	-----	-----	-----	-----	-----	-----	-----	-----	-----	-----	-----	-----	-----	-----	-----	-----	-----	-----	-----	-----	-----	-----	-----	-----	-----	-----	-----	-----	-----	-----	-----	-----	-----	-----	-----	-----	-----	-----	-----	-----	-----	-----	-----	-----	-----	-----	-----	-----	-----	-----	-----	-----	-----	-----	-----	-----	-----	-----	-----	-----	-----	-----	-----	-----	-----	-----	-----	-----	-----	-----	-----	-----	-----	-----	-----	-----	-----	-----	-----	-----	-----	-----	-----	-----	-----	-----	-----	-----	-----	-----	-----	-----	-----	-----	-----	-----	-----	-----	-----	-----	-----	-----	-----	-----	-----	-----	-----	-----	-----	-----	-----	-----	-----	-----	-----	-----	-----	-----	-----	-----	-----	-----	-----	-----	-----	-----	-----	-----	-----	-----	-----	-----	-----	-----	-----	-----	-----	-----	-----	-----	-----	-----	-----	-----	-----	-----	-----	-----	-----	-----	-----	-----	-----	-----	-----	-----	-----	-----	-----	-----	-----	-----	-----	-----	-----	-----	-----	-----	-----	-----	-----	-----	-----	-----	-----	-----	-----	-----	-----	-----	-----	-----	-----	-----	-----	-----	-----	-----	-----	-----	-----	-----	-----	-----	-----	-----	-----	-----	-----	-----	-----	-----	-----	-----	-----	-----	-----	-----	-----	-----	-----	-----	-----	-----	-----	-----	-----	-----	-----	-----	-----	-----	-----	-----	-----	-----	-----	-----	-----	-----	-----	-----	-----	-----	-----	-----	-----	-----	-----	-----	-----	-----	-----	-----	-----	-----	-----	-----	-----	-----	-----	-----	-----	-----	-----	-----	-----	-----	-----	-----	-----	-----	-----	-----	-----	-----	-----	-----	-----	-----	-----	-----	-----	-----	-----	-----	-----	-----	-----	-----	-----	-----	-----	-----	-----	-----	-----	-----	-----	-----	-----	-----	-----	-----	-----	-----	-----	-----	-----	-----	-----	-----	-----	-----	-----	-----	-----	-----	-----	-----	-----	-----	-----	-----	-----	-----	-----	-----	-----	-----	-----	-----	-----	-----	-----	-----	-----	-----	-----	-----	-----	-----	-----	-----	-----	-----	-----	-----	-----	-----	-----	-----	-----	-----	-----	-----	-----	-----	-----	-----	-----	-----	-----	-----	-----	-----	-----	-----	-----	-----	-----	-----	-----	-----	-----	-----	-----	-----	-----	-----	-----	-----	-----	-----	-----	-----	-----	-----	-----	-----	-----	-----	-----	-----	-----	-----	------	------	------	------	------	------	------	------	------	------	------	------	------	------	------	------	------	------	------	------	------	------	------	------	------	------	------	------	------	------	------	------	------	------	------	------	------	------	------	------	------	------	------	------	------	------	------	------	------	------	------	------	------	------	------	------	------	------	------	------	------	------	------	------	------	------	------	------	------	------	------	------	------	------	------	------	------	------	------	------	------	------	------	------	------	------	------	------	------	------	------	------	------	------	------	------	------	------	------	------	------	------	------	------	------	------	------	------	------	------	------	------	------	------	------	------	------	------	------	------	------	------	------	------	------	------	------	------	------	------	------	------	------	------	------	------	------	------	------	------	------	------	------	------	------	------	------	------	------	------	------	------	------	------	------	------	------	------	------	------	------	------	------	------	------	------	------	------	------	------	------	------	------	------	------	------	------	------	------	------	------	------	------	------	------	------	------	------	------	------	------	------	------	------	------	------	------	------	------	------	------	------	------	------	------	------	------	------	------	------	------	------	------	------	------	------	------	------	------	------	------	------	------	------	------	------	------	------	------	------	------	------	------	------	------	------	------	------	------	------	------	------	------	------	------	------	------	------	------	------	------	------	------	------	------	------	------	------	------	------	------	------	------	------	------	------	------	------	------	------	------	------	------	------	------	------	------	------	------	------	------	------	------	------	------	------	------	------	------	------	------	------	------	------	------	------	------	------	------	------	------	------	------	------	------	------	------	------	------	------	------	------	------	------	------	------	------	------	------	------	------	------	------	------	------	------	------	------	------	------	------	------	------	------	------	------	------	------	------	------	------	------	------	------	------	------	------	------	------	------	------	------	------	------	------	------	------	------	------	------	------	------	------	------	------	------	------	------	------	------	------	------	------	------	------	------	------	------	------	------	------	------	------	------	------	------	------	------	------	------	------	------	------	------	------	------	------	------	------	------	------	------	------	------	------	------	------	------	------	------	------	------	------	------	------	------	------	------	------	------	------	------	------	------	------	------	------	------	------	------	------	------	------	------	------	------	------	------	------	------	------	------	------	------	------	------	------	------	------	------	------	------	------	------	------	------	------	------	------	------	------	------	------	------	------	------	------	------	------	------	------	------	------	------	------	------	------	------	------	------	------	------	------	------	------	------	------	------	------	------	------	------	------	------	------	------	------	------	------	------	------	------	------	------	------	------	------	------	------	------	------	------	------	------	------	------	------	------	------	------	------	------	------	------	------	------	------	------	------	------	------	------	------	------	------	------	------	------	------	------	------	------	------	------	------	------	------	------	--

[illegible]

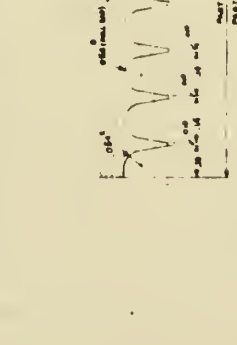
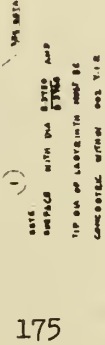
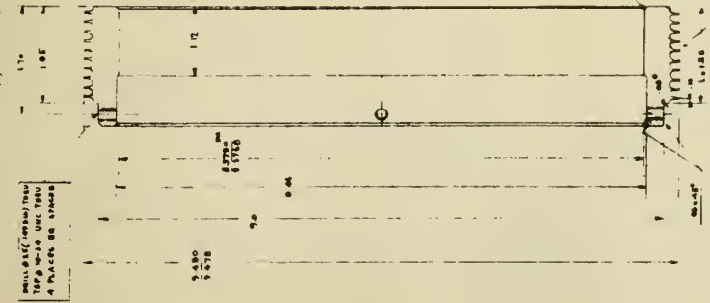
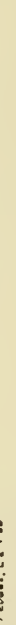
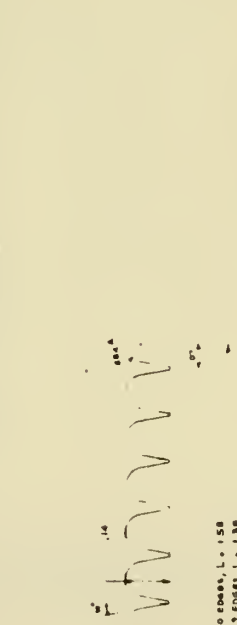
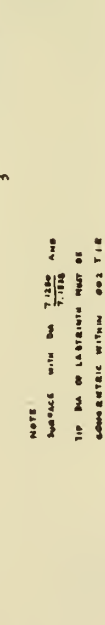
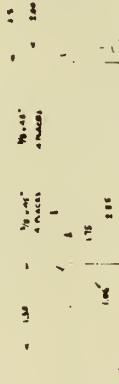
[illegible]





NOTES

MAKE FROM A151 434L
 1. STROKE 9/16" IN. 2. 1/2" DIA. 3. 1/2" DIA. 4. 1/2" DIA.
 AND PLAYS 1/16" 1/16" 1/16" ON SURFACE FROM
 151ST AND TEMPER AT 1000°F
 153 GRIND (BUCKELL C39) HARDENES
 1. SMOOTH TRANSITION AT A BETWEEN
 PILET 12" AND PLAT WITHOUT TOOL



Age					Category					Person					Sex					Address					Notes																																																																																																																																																																																																																																																																																																																																																																																																																																																																																																																																																																																																																																																																																																																																																																																																																																																																																																																																																																																																																																																																																																																																																																																																																																																																																																																																																																																																																																																																						
15	4	John Smith	M	123 Main St.	12/15/45	16	5	Mary Jones	F	456 Oak St.	12/16/45	17	6	Robert Brown	M	789 Pine St.	12/17/45	18	7	Elizabeth White	F	101 Elm St.	12/18/45	19	8	William Black	M	202 Maple St.	12/19/45	20	9	Patricia Green	F	303 Cedar St.	12/20/45	21	10	James Hall	M	404 Birch St.	12/21/45	22	11	Barbara King	F	505 Walnut St.	12/22/45	23	12	Richard Lee	M	606 Cherry St.	12/23/45	24	13	Susan Scott	F	707 Hickory St.	12/24/45	25	14	Thomas Young	M	808 Poplar St.	12/25/45	26	15	Jane Adams	F	909 Ash St.	12/26/45	27	16	Michael Baker	M	1010 Magnolia St.	12/27/45	28	17	Linda Clark	F	1111 Sycamore St.	12/28/45	29	18	David Evans	M	1212 Dogwood St.	12/29/45	30	19	Karen Foster	F	1313 Redwood St.	12/30/45	31	20	Christopher Gibson	M	1414 Cypress St.	12/31/45	32	21	Alicia Harper	F	1515 Juniper St.	1/1/46	33	22	Benjamin Hill	M	1616 Fir St.	1/2/46	34	23	Christina Ives	F	1717 Laurel St.	1/3/46	35	24	Gregory King	M	1818 Birch St.	1/4/46	36	25	Helen Lee	F	1919 Elm St.	1/5/46	37	26	Isaac Miller	M	2020 Maple St.	1/6/46	38	27	Jessica Moore	F	2121 Oak St.	1/7/46	39	28	Jonathan Nelson	M	2222 Pine St.	1/8/46	40	29	Kathleen Olsen	F	2323 Cedar St.	1/9/46	41	30	Kevin Parker	M	2424 Birch St.	1/10/46	42	31	Laura Quinn	F	2525 Walnut St.	1/11/46	43	32	Matthew Reed	M	2626 Cherry St.	1/12/46	44	33	Nancy Scott	F	2727 Hickory St.	1/13/46	45	34	Oliver Taylor	M	2828 Poplar St.	1/14/46	46	35	Pamela Vance	F	2929 Ash St.	1/15/46	47	36	Quinn Webb	M	3030 Magnolia St.	1/16/46	48	37	Rachel White	F	3131 Sycamore St.	1/17/46	49	38	Samuel Young	M	3232 Dogwood St.	1/18/46	50	39	Tina Zane	F	3333 Redwood St.	1/19/46	51	40	Victor Adams	M	3434 Cypress St.	1/20/46	52	41	Wendy Baker	F	3535 Juniper St.	1/21/46	53	42	Xavier Clark	M	3636 Fir St.	1/22/46	54	43	Yvonne Evans	F	3737 Laurel St.	1/23/46	55	44	Zoe Foster	F	3838 Birch St.	1/24/46	56	45	Adam Gibson	M	3939 Elm St.	1/25/46	57	46	Beth Hall	F	4040 Maple St.	1/26/46	58	47	Carl Ives	M	4141 Oak St.	1/27/46	59	48	Dana King	F	4242 Pine St.	1/28/46	60	49	Ethan Lee	M	4343 Cedar St.	1/29/46	61	50	Fiona Miller	F	4444 Birch St.	1/30/46	62	51	Gavin Nelson	M	4545 Walnut St.	1/31/46	63	52	Hannah Olsen	F	4646 Cherry St.	2/1/46	64	53	Ian Parker	M	4747 Hickory St.	2/2/46	65	54	Jasmine Quinn	F	4848 Poplar St.	2/3/46	66	55	Kyle Reed	M	4949 Ash St.	2/4/46	67	56	Liam Scott	M	5050 Magnolia St.	2/5/46	68	57	Mia Taylor	F	5151 Sycamore St.	2/6/46	69	58	Noah Vance	M	5252 Dogwood St.	2/7/46	70	59	Olivia Webb	F	5353 Redwood St.	2/8/46	71	60	Peter White	M	5454 Cypress St.	2/9/46	72	61	Quinn Young	M	5555 Juniper St.	2/10/46	73	62	Rachel Zane	F	5656 Fir St.	2/11/46	74	63	Samuel Adams	M	5757 Laurel St.	2/12/46	75	64	Tina Baker	F	5858 Birch St.	2/13/46	76	65	Umar Clark	M	5959 Elm St.	2/14/46	77	66	Vivian Evans	F	6060 Maple St.	2/15/46	78	67	Walter Foster	M	6161 Oak St.	2/16/46	79	68	Xavier Gibson	M	6262 Pine St.	2/17/46	80	69	Yvonne Harper	F	6363 Cedar St.	2/18/46	81	70	Zoe Ives	F	6464 Birch St.	2/19/46	82	71	Adam King	M	6565 Walnut St.	2/20/46	83	72	Beth Lee	F	6666 Cherry St.	2/21/46	84	73	Carl Miller	M	6767 Hickory St.	2/22/46	85	74	Dana Nelson	F	6868 Poplar St.	2/23/46	86	75	Ethan Olsen	M	6969 Ash St.	2/24/46	87	76	Fiona Scott	F	7070 Magnolia St.	2/25/46	88	77	Gavin Taylor	M	7171 Sycamore St.	2/26/46	89	78	Hannah Vance	F	7272 Dogwood St.	2/27/46	90	79	Ian Webb	M	7373 Redwood St.	2/28/46	91	80	Jasmine White	F	7474 Cypress St.	2/29/46	92	81	Kyle Young	M	7575 Juniper St.	2/30/46	93	82	Liam Zane	M	7676 Fir St.	3/1/46	94	83	Mia Adams	F	7777 Laurel St.	3/2/46	95	84	Noah Baker	M	7878 Birch St.	3/3/46	96	85	Olivia Clark	F	7979 Elm St.	3/4/46	97	86	Peter Evans	M	8080 Maple St.	3/5/46	98	87	Quinn Foster	F	8181 Oak St.	3/6/46	99	88	Rachel Gibson	F	8282 Pine St.	3/7/46	100	89	Samuel Harper	M	8383 Cedar St.	3/8/46	101	90	Tina Ives	F	8484 Birch St.	3/9/46	102	91	Victor King	M	8585 Walnut St.	3/10/46	103	92	Wendy Lee	F	8686 Cherry St.	3/11/46	104	93	Xavier Miller	M	8787 Hickory St.	3/12/46	105	94	Yvonne Nelson	F	8888 Poplar St.	3/13/46	106	95	Zoe Olsen	F	8989 Ash St.	3/14/46	107	96	Adam Scott	M	9090 Magnolia St.	3/15/46	108	97	Beth Taylor	F	9191 Sycamore St.	3/16/46	109	98	Carl Vance	M	9292 Dogwood St.	3/17/46	110	99	Dana Webb	F	9393 Redwood St.	3/18/46	111	100	Ethan White	M	9494 Cypress St.	3/19/46	112	101	Fiona Young	F	9595 Juniper St.	3/20/46	113	102	Gavin Zane	M	9696 Fir St.	3/21/46	114	103	Hannah Adams	F	9797 Laurel St.	3/22/46	115	104	Ian Baker	M	9898 Birch St.	3/23/46	116	105	Jasmine Clark	F	9999 Elm St.	3/24/46	117	106	Kyle Evans	M	10000 Maple St.	3/25/46	118	107	Liam Foster	M	10101 Oak St.	3/26/46	119	108	Mia Gibson	F	10202 Pine St.	3/27/46	120	109	Noah Harper	M	10303 Cedar St.	3/28/46	121	110	Olivia Ives	F	10404 Birch St.	3/29/46	122	111	Peter King	M	10505 Walnut St.	3/30/46	123	112	Quinn Lee	F	10606 Cherry St.	3/31/46	124	113	Rachel Miller	F	10707 Hickory St.	4/1/46	125	114	Samuel Nelson	M	10808 Poplar St.	4/2/46	126	115	Tina Olsen	F	10909 Ash St.	4/3/46	127	116	Victor Scott	M	11010 Magnolia St.	4/4/46	128	117	Wendy Taylor	F	11111 Sycamore St.	4/5/46	129	118	Xavier Vance	M	11212 Dogwood St.	4/6/46	130	119	Yvonne Webb	F	11313 Redwood St.	4/7/46	131	120	Zoe White	F	11414 Cypress St.	4/8/46	132	121	Adam Young	M	11515 Juniper St.	4/9/46	133	122	Beth Zane	F	11616 Fir St.	4/10/46	134	123	Carl Adams	M	11717 Laurel St.	4/11/46	135	124	Dana Baker	F	11818 Birch St.	4/12/46	136	125	Ethan Clark	M	11919 Elm St.	4/13/46	137	126	Fiona Evans	F	12020 Maple St.	4/14/46	138	127	Gavin Foster	M	12121 Oak St.	4/15/46	139	128	Hannah Gibson	F	12222 Pine St.	4/16/46	140	129	Ian Harper	M	12323 Cedar St.	4/17/46	141	130	Jasmine Ives	F	12424 Birch St.	4/18/46	142	131	Kyle King	M	12525 Walnut St.	4/19/46	143	132	Liam Lee	M	12626 Cherry St.	4/20/46	144	133	Mia Miller	F	12727 Hickory St.	4/21/46	145	134	Noah Nelson	M	12828 Poplar St.	4/22/46	146	135	Olivia Olsen	F	12929 Ash St.	4/23/46	147	136	Peter Scott	M	13030 Magnolia St.	4/24/46	148	137	Quinn Taylor	F	13131 Sycamore St.	4/25/46	149	138	Rachel Vance	F	13232 Dogwood St.	4/26/46	150	139	Samuel Webb	M	13333 Redwood St.	4/27/46	151	140	Tina White	F	13434 Cypress St.	4/28/46	152	141	Victor Young	M	13535 Juniper St.	4/29/46	153	142	Wendy Zane	F	13636 Fir St.	4/30/46	154	143	Xavier Adams	M	13737 Laurel St.	5/1/46	155	144	Yvonne Baker	F	13838 Birch St.	5/2/46	156	145	Zoe Clark	F	13939 Elm St.	5/3/46	157	146	Adam Evans	M	14040 Maple St.	5/4/46	158	147	Beth Foster	F	14141 Oak St.	5/5/46	159	148	Carl Gibson	M	14242 Pine St.	5/6/46	160	149	Dana Harper	F	14343 Cedar St.	5/7/46	161	150	Ethan Ives	M	14444 Birch St.	5/8/46	162	151	Fiona King	F	14545 Walnut St.	5/9/46	163	152	Gavin Lee	M	14646 Cherry St.	5/10/46	164	153	Hannah Miller	F	14747 Hickory St.	5/11/46	165	154	Ian Nelson	M	14848 Poplar St.	5/12/46	166	155	Jasmine Olsen	F	14949 Ash St.	5/13/46	167	156	Kyle Scott	M	15050 Magnolia St.	5/14/46	168	157	Liam Taylor	M	15151 Sycamore St.	5/15/46	169	158	Mia Vance	F	15252 Dogwood St.	5/16/46	170	159	Noah Webb	M	15353 Redwood St.	5/17/46	171	160	Olivia White	F	15454 Cypress St.	5/18/46	172	161	Peter Young	M	15555 Juniper St.	5/19/46	173	162	Quinn Zane	F	15656 Fir St.	5/20/46	174	163	Rachel Adams	F	15757 Laurel St.	5/21/46	175	164	Samuel Baker	M	15858 Birch St.	5/22/46	176	165	Tina Clark	F	15959 Elm St.	5/23/46	177	166	Victor Evans	M	16060 Maple St.	5/24/46	178	167	Wendy Foster	F	16161 Oak St.	5/25/46	179	168	Xavier Gibson	M	16262 Pine St.	5/26/46	180	169	Yvonne Harper	F	16363 Cedar St.	5/27/46	181	170	Zoe Ives	F	16464 Birch St.	5/28/46	182	171	Adam King	M	16565 Walnut St.	5/29/46	183	172	Beth Lee	F	16666 Cherry St.	5/30/46	184	173	Carl Miller	M	16767 Hickory St.	5/31/46	185	174	Dana Nelson	F	16868 Poplar St.	6/1/46	186	175	Ethan Olsen	M	16969 Ash St.	6/2/46	187	176	Fiona Scott	F	17070 Magnolia St.	6/3/46	188	177	Gavin Taylor	M	17171 Sycamore St.	6/4/46	189	178	Hannah Vance	F	17272 Dogwood St.	6/5/46	190	179	Ian Webb	M	17373 Redwood St.	6/6/46	191	180	Jasmine White	F	17474 Cypress St.	6/7/46	192	181	Kyle Young	M	17575 Juniper St.	6/8/46	193	182	Liam Zane	M	17676 Fir St.	6/9/46	194	183	Mia Adams	F	17777 Laurel St.	6/10/46	195	184	Noah Baker	M	17878 Birch St.	6/11/46	196	185	Olivia Clark	F	17979 Elm St.	6/12/46	197	186	Peter Evans	M	18080 Maple St.	6/13/46	198	187	Quinn Foster	F	18181 Oak St.	6/14/46	199	188	Rachel Gibson	F	18282 Pine St.	6/15/46	200	189	Samuel Harper	M	18383 Cedar St.	6/16/46	201	190	Tina Ives	F	18484 Birch St.	6/17/46	202	191	Victor King	M	18585 Walnut St.	6/18/46	203	192	Wendy Lee	F	18686 Cherry St.	6/19/46	204	193	Xavier Miller	M	18787 Hickory St.	6/20/46	205	194	Yvonne Nelson	F	18888 Poplar St.	6/21/46	206	195	Zoe Olsen	F	18989 Ash St.	6/22/46	207	196	Adam Scott	M	19090 Magnolia St.	6/23/46	208	197	Beth Taylor	F	19191 Sycamore St.	6/24/46	209	198	Carl Vance	M	19292 Dogwood St.	6/25/46	210	199	Dana Webb	F	19393 Redwood St.	6/26/46	211	200	Ethan White	M	19494 Cypress St.	6/27/46	212	201	Fiona Young	F	19595 Juniper St.	6/28/46	213	202	Gavin Zane	M	19696 Fir St.	6/29/46	214	203	Hannah Adams	F	19797 Laurel St.	6/30/46	215	204	Ian Baker	M	19898 Birch St.	7/1/46	216	205	Jasmine Clark	F	19999 Elm St.	7/2/46	217	206	Kyle Evans	M	20000 Maple St.	7/3/46	218	207	Liam Foster	M	20101 Oak St.	7/4/46	219	208	Mia Gibson	F	20202 Pine St.	7/5/46	220	209	Noah Harper	M	20303 Cedar St.	7/6/46	221	210	Olivia Ives	F	20404 Birch St.	7/7/46	222	211	Peter King	M	20505 Walnut St.	7/8/46	223	212	Quinn Lee	F	20606 Cherry St.	7/9/46	224	213	Rachel Miller	F	20707 Hickory St.	7/10/46	225	214	Samuel Nelson	M	20808 Poplar St.	7/11/46	226	215	Tina Olsen	F	20909 Ash St.	7/12/46	227	216	Victor Scott	M	21010 Magnolia St.	7/13/46	228	217	Wendy Taylor	F	21111 Sycamore St.	7/14/46	229	218	Xavier Vance	M	21212 Dogwood St.	7/15/46	230	219	Yvonne Webb	F	21313 Redwood St.	7/16/46	231	220	Zoe White	F	21414 Cypress St.	7/17/46	232	221	Adam Young	M	21515 Juniper St.	7/18/46	233	222	Beth Zane	F	21616 Fir St.	7/19/46	234	223	Carl Adams	M	21717 Laurel St.	7/20/46	235	224	Dana Baker	F	21818 Birch St.	7/21/46	236	225	Ethan Clark	M	21919 Elm St.	7/22/46	237	226	Fiona Evans	F	22020 Maple St.	7/23/46	238	227	Gavin Foster	M	22121 Oak St.	7/24/46	239	228	Hannah Gibson	F	22222 Pine St.	7/25/46	240	229	Ian Harper	M	22323 Cedar St.	7/26/46	241	230	Jasmine Ives	F	22424 Birch St.	7/27/46	242	231	Kyle King	M	22525 Walnut St.	7/28/46	243	232	Liam Lee	M	22626 Cherry St.	7/29/46	244	233	Mia Miller	F	22727 Hickory St.	7/30/46	245	234	Noah Nelson	M	22828 Poplar St.	7/31/46	246	235	Olivia Olsen	F	22929 Ash St.	8/1/46	247	236	Peter Scott	M	23030 Magnolia St.	8/2/46	248	237	Quinn Taylor	F	23131 Sycamore St.	8/3/46	249	238	Rachel Vance	F	23232 Dogwood St.	8/4/46	250	239	Samuel Webb	M	23333 Redwood St.	8/5/46	251	240	Tina White	F	23434 Cypress St.	8/6/46	252	241	Victor Young	M	23535 Juniper St.	8/7/46	253	242	Wendy Zane	F	23636 Fir St.	8/8/46	254	243	Xavier Adams	M	23737 Laurel St.	8/9/46

[illegible]



DRILL .531 DIA THRU
16 HOLES EQ SPACED
WITHIN .010 ON
22.00 B.C.

SECTION C-C
DRILL X(.397 DIA) THRU
C'BORE .68 DIA, .44 DEEP
4 PLACES ON 22.00 B.C.
AT SECTIONS C-C

8 FINS EQ. SPACED
WELD BOTH SIDES
2 PLACES AT
EACH FIN

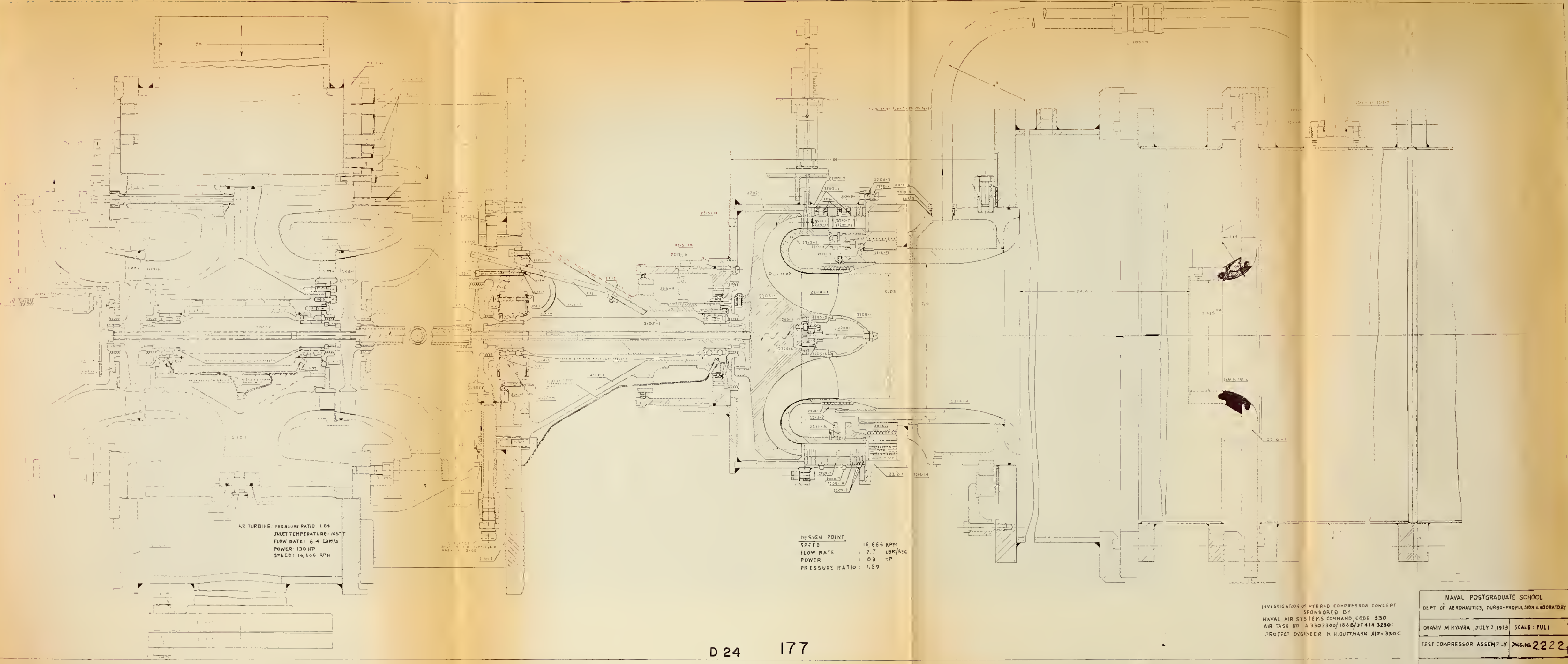
DRILL R(.339 DIA) .44 DEEP
DRILL .062 DIA THRU
TAP 1/8-27 NPTF
4 PLACES EQ. SPACED

- 1
- NOTES
1. WELDED TYPE CONSTRUCTION WITH THRU WELDS AS INDICATED.
 2. BEFORE MACHINING SURFACES WITH ∇ NORMALIZE WELOMENT (HEAT TO 1700°F AND COOL IN STILL AIR AT ROOM TEMPERATURE)
 3. SURFACES MARKED (X) MUST BE CONCENTRIC WITHIN .010 T.I.R. AND SQUARE WITH SURFACE (Y)
 4. BORE WITH $\frac{5.375}{5.380}$ MUST HAVE MINIMUM POSSIBLE TAPER

4	8	FINS $1\frac{1}{2} \times \frac{1}{2}$ THICK $\times 3.20$ LG	H.R. STEEL FLAT M 1020
3	1	SEAMLESS STEEL PIPE, 6" NOM. DOUBLE EXTRA STRONG, 6.625 OD WALL $\times \frac{1}{8}$ LG	ASTM - A 53
2	1	PLATE 24 OD $\times 1$ THICK	ASTM - A 36
1	1	NOZZLE (MACHINE FROM WELD- MENT OF ITEMS 2, 3 AND 4)	
NAVAL POSTGRADUATE SCHOOL DEPT. OF AERONAUTICS, TURBO PROPULSION LABORATORY GRANN M.H. VAVRA 11/15/70 REV CHECKED APPD NOZZLE FRAME USED ON SHEET 1 OF 1 SCALE HALF OR AS NOTED DWG NO. 2216			

1 IN. PER INCH DRAWING
DIM. IN. UNLESS NOTED
TOLERANCES
FRACTIONS $\pm \frac{1}{32}$
DECIMALS $\pm .03$
X = $\pm .01$
XXX = $\pm .005$
ANGLES \pm
BREAK SHARP EDGES 00SR
DO NOT SCALE DRAWING





AIR TURBINE: PRESSURE RATIO: 1.64
 INLET TEMPERATURE: 105°F
 FLOW RATE: 6.4 LBM/S
 POWER: 130 HP
 SPEED: 14,666 RPM

DESIGN POINT
 SPEED : 16,666 RPM
 FLOW RATE : 2.7 LBM/SEC
 POWER : 83 HP
 PRESSURE RATIO: 1.59

INVESTIGATION OF HYBRID COMPRESSOR CONCEPT
 SPONSORED BY
 NAVAL AIR SYSTEMS COMMAND, CODE 330
 AIR TASK NO. A 330330a/186B/3F414 32301
 PROJECT ENGINEER: K. H. GUTTMANN, AIR-330C

NAVAL POSTGRADUATE SCHOOL DEPT. OF AERONAUTICS, TURBO-PROPULSION LABORATORY	
DRAWN: M. HYVRA, JULY 7, 1973	SCALE: FULL
TEST COMPRESSOR ASSEMBLY	DWG. NO. 2222



ROTATING
THROTTLE VALVE (DWG 2158)

AMBIENT AIR

INLET PLENUM (DWG 2164-1)

INVESTIGATION OF HYBRID COMPRESSOR CONCEPT
SPONSORED BY
NAVAL AIR SYSTEMS COMMAND
AIR TASK: A330330 0/1868/3F41432301
PROJECT ENGINEER K H GUTTMANN, AIR-330C

NAVAL POSTGRADUATE SCHOOL TURBO-PROPULSION LAB, DEPT OF AERONAUTICS	
DRAWN: M H VAVRA, JULY 9, 1973	SCALE: 1/10
INSTALLATION OF HYBRID COMPRESSOR TEST RIG IN CELL 2 OF TURBO-PROPULSION LAB	DWG 2223

THROTTLE
ACTUATOR
(DWG 2159)

ELECTRIC SERVO MOTOR

REMOTE CONTROLLED
BUTTERFLY VALVE

BLAST SHIELD

FOUNDATION (DWG 2155)

TURBINE INLET PIPE
(DWG 2136)

TURBINE EXHAUST

EMERGENCY BYPASS VALVE
(DWG 2148)

TO ATMOSPHERE

REMOTE CONTROLLED
BUTTERFLY VALVE

22"
(MIN)

12'-4"
(MAX)

28'-0"

HYBRID COMPRESSOR (DWG 2222)

FLOW NOZZLE

36"

84"

74"



APPENDIX C

LOSSES IN RADIAL COMPRESSOR WHEELS

The flows in rotors of radial machines are greatly influenced by Coriolis and centripetal accelerations and are difficult to analyze even if viscous effects are ignored. The prediction of the losses in radial impellers constitutes an even more difficult task because of the complex three-dimensional nature of the real flow through such wheels which makes it impossible to apply conventional boundary layer theories or to use loss data for stationary channels or diffusers. At off-design operating conditions the prediction of the flow losses with theoretical means is nearly impossible because of local flow separations that occur in the wheels.

A more detailed discussion on losses in impellers of centrifugal compressors is given in paragraph 5 of Appendix A which also emphasizes the need for more and better experimental data. At present only a limited amount of such data is available in the open literature, for instance in Ref. 2 and Ref. 10. Although not directly applicable to the special rotor of the Hybrid compressor the test data of these references are evaluated in the following to obtain indications how the rotor losses are influenced by the different design parameters.

Reference 10 will be discussed first because it gives the losses in a particular rotor with specified dimensions which is shown in Fig. 12. Hence its pertinent geometrical characteristics are:

$$R_{10}/R_2 = 0.541$$

$$R_{1i}/R_2 = 0.287$$

$$b_2/R_2 = 0.078$$

The blade angle at R_{10} is given as 57° .

Figure 13 shows the so-called polytropic impeller efficiency η_{RP} , which is defined in Ref. 11, as a function of β_{10} , U_2/a_0 and the Mach number M_{W1} of the relative velocity W_{10} at the inducer tip radius R_{10} . Figure 13 is an exact reproduction of Fig. 4 of Ref. 10, but with the symbols of this report. The dashed parts of the curves for $\eta_{RP} = \text{constant}$ are extrapolations by the writer. It is noticeable from Fig. 13 that the best rotor performance is obtained for positive incidence angles of about 9° if blockage because of the blade thickness is ignored. Reference 10 states that the inducer blades have a parabolic mean camber line and that their thickness is about 3% of the arc length of the camber line. Figure 14 gives the relations to determine the arc length m of a parabolic blade with axial length L and inlet blade angle β_B . From Fig. 12 there is $L = 19.5$ mm, and for $\beta_B = 57^\circ$, $m = 21.51$ mm. Hence the blade thickness t is equal to $(0.03)(21.51) = 0.64$ mm. In accordance with Eqs. 7 and 8, the flow angle β_{10}' of Fig. 3b is

$$\tan \beta_{10}' = \tan \beta_{10} \left(\frac{s}{s - t/\cos \beta_B} \right) \quad C(1)$$

For 20 rotor blades, and with the dimensions of Fig. 12,

$$s = \pi(97.4)/20 = 15.30 \text{ mm}$$

and for $t = 0.64$ mm, $\beta_B = 57^\circ$,

$$\tan \beta_{10}' = \tan \beta_{10} (0.923)$$

In Fig. 13 the angles β_{10}' of this relation are shown on a special horizontal scale that is labeled β_{10}' . Hence if the blockage due to the thickness of the blades is taken into account, the optimum incidence angle i' defined by Fig. 3b is still about $+7^\circ$, which is at variance with

the findings of Ref. 2 (see Fig. 24) where it is shown that incidence angles of about zero at the inducer inlet give the best rotor performance. The same conclusion is made in Ref. 12 on the basis of past experience.

The parametric curves $M_{W1} = \text{constant}$ of Fig. 13 were transposed from Fig. 4 of Ref. 10 also. In the following it will be shown that these curves give data that are redundant since M_{W1} is known if U_2/a_0 , β_{10} , and R_{10}/R_2 are known. Reference 10 defines M_{W1} as the Mach number of the relative velocity W_{10} at R_{10} . Independent of whether the absolute velocity V_1 at the inducer inlet is constant or changing along the radius R_1 ,

$$M_{W1} = \frac{W_{10}}{a_1} = \frac{\omega R_{10}}{\sin \beta_{10}} = \frac{U_2}{R_2} R_{10} \frac{1}{\sin \beta_{10}} \quad C(2)$$

The quantity a_1 is the velocity of sound of the flow at R_{10} where the static temperature is T_{10} . Now, with

$$M_{V1} = \frac{V_{10}}{a_1} = \frac{W_{10} \cos \beta_{10}}{a_1} = M_{W1} \cos \beta_{10}$$

and

$$\frac{a_0}{a_1} = \sqrt{\frac{T_0}{T_{10}}} = \left[1 + \frac{\gamma-1}{2} M_{V1}^2 \right]^{\frac{1}{2}}$$

there is

$$M_{W1} = \frac{U_2}{a_0} \frac{R_{10}}{R_2} \frac{1}{\sin \beta_{10}} \left[1 + \frac{\gamma-1}{2} M_{W1}^2 \cos^2 \beta_{10} \right]^{\frac{1}{2}}$$

and

$$M_{wl} = \frac{(U_2/a_0) (R_{10}/R_2)}{\left[\sin^2 \beta_{10} - \frac{\gamma-1}{2} \cos^2 \beta_{10} (U_2/a_0)^2 (R_{10}/R_2)^2 \right]^{\frac{1}{2}}} \quad C(3)$$

This relation could have been derived directly from Eq. A II(4) but it has been developed here to show that it holds for arbitrary distributions of V_1 vs. R_1 and not only for uniform inlet velocities ahead of the rotor. Equation C(3) can be modified to obtain the angle β_{10} as a function of U_2/a_0 and M_{wl} , or

$$\sin \beta_{10} = (U_2/a_0) (R_{10}/R_2) \sqrt{\frac{1/M_{wl}^2 + \frac{\gamma-1}{2}}{1 + \frac{\gamma-1}{2} (U_2/a_0)^2 (R_{10}/R_2)^2}} \quad C(4)$$

At point A of Fig. 13 the curve $M_{wl} = 0.6$ intersects the line $U_2/a_0 = 0.9$ at an angle β_{10} of 66.5° , giving $i = 66.5 - 57 = 9.5^\circ$. However for $R_{10}/R_2 = 0.541$ of the rotor of Fig. 12, $U_2/a_0 = 0.9$, $M_{wl} = 0.6$, and $\gamma = 1.4$, Eq. C(4) gives a flow angle

$$\beta_{10} = 55.2^\circ$$

so that the incidence angle without blockage is -1.8° instead of $+9.5^\circ$. Figure 15 has been obtained by calculating the angles $\beta_{10} = \beta_{10}^*$ from Eq. C(4) with the values of U_2/a_0 along the curves $M_{wl} = \text{constant}$ of Fig. 13 that pertain to particular efficiencies η_{RP} . Through the points thus obtained, which are marked by circles in Fig. 15, a new set of curves $\eta_{RP} = \text{constant}$ has been drawn. In Eq. C(4) the value of R_{10}/R_2 has been taken as 0.541 in accordance with the rotor dimensions of Fig. 12.

Figure 15 shows that the incidence angles are greatly reduced and that their values for optimum efficiencies become smaller with increasing ratios U_2/a_0 .

If Fig. 15 is correct; that is, if the relationship between M_{w1} , U_2/a_0 , and η_{RP} in Fig. 13 is valid, but if the flow angles β_{10} given in this figure are in error, the resulting incidence angles are more in line with experience. Then the argumentation in Ref. 10 based on its Fig. 5, which is presented as Fig. 16 in this report, namely, that positive incidence angles are necessary to obtain favorable velocity distributions along the inducer blades, would be without substance. The curves of Fig. 16 were obtained theoretically by neglecting blade thickness, compressibility and friction. It is very doubtful, however, whether velocity distributions similar to those shown in Fig. 16 occur along the actual inducer blades, not only because effects of blade thickness and leading edge shape were ignored, but primarily because the inducer was treated as a stationary cascade whose flow is not influenced by the impeller downstream of it. Hence no account is taken of Coriolis and centripetal accelerations and the fact that the inducer and impeller blades adjoin at the inducer discharge and form continuous blade surfaces from rotor inlet to rotor discharge. Hence at the station where the inducer and impeller blades join, the velocities on either side of a blade will differ and not be equal as Fig. 16 shows.

It will be tried to support the relationship presented in Fig. 15 by additional data of Ref. 10, namely, those given by its Fig. 3 which are presented here in Fig. 17. This figure shows the polytropic efficiency of the rotor of Fig. 12 at $U_2/a_0 = 0.83$ for three different diffusers.

It is evident from Fig. 18 that the rotor performance is almost independent of the diffuser configurations, although the latter influences the range of operation of the compressor.

The rotor efficiencies of Fig. 17 are given as functions of the flow coefficient φ_1 , defined by

$$\varphi_1 = \frac{Q_1}{U_2 R_2^2} \quad c(5)$$

where Q_1 is the volume flow rate at the inducer inlet. Because of the curved walls of the inlet duct ahead of the inducer of Fig. 12 the absolute velocity V_1 will vary from the inner radius R_{1i} to the outer radius R_{1o} of the inlet eye. Let \bar{V}_1 be the average velocity at the inducer inlet such that

$$Q_1 = A_1 k_{B1} \bar{V}_1 \quad c(6)$$

where

$$A_1 = \pi R_{1o}^2 \left[1 - \left(\frac{R_{1i}}{R_{1o}} \right)^2 \right]$$

k_{B1} is the blockage factor at station (1). Then, from Eqs. C(5) and C(6)

$$\frac{\bar{V}_1}{a_0} = \frac{\varphi_1}{k_{B1}} \left(\frac{U_2}{a_0} \right) \left(\frac{R_2}{R_{1o}} \right)^2 \frac{1}{\pi \left[1 - (R_{1i}/R_{1o})^2 \right]} \quad c(7)$$

The weight flow rate \dot{w} through the compressor is

$$\dot{w} = Q_1 \frac{\bar{p}_1}{R_G \bar{T}_1} = \varphi_1 U_2 R_2^2 \frac{(\bar{p}_1/P_0) P_0}{R_G (\bar{T}_1/T_0) T_0} \quad c(8)$$

\bar{p}_1, \bar{T}_1 are the flow properties at the radius \bar{R}_1 where the velocity \bar{V}_1 occurs. Then, for an isentropic process from P_0, T_0 to \bar{p}_1, \bar{T}_1 ,

$$\frac{\bar{p}_1/P_0}{\bar{T}_1/T_0} = (\bar{T}_1/T_0)^{1/(\gamma-1)} \quad C(9)$$

and, since

$$\bar{V}_1^2 = 2g c_p (T_0 - \bar{T}_1) = \frac{2}{\gamma-1} a_0^2 \left[1 - \frac{\bar{T}_1}{T_0} \right]$$

or

$$\frac{\bar{T}_1}{T_0} = 1 - \frac{\gamma-1}{2} \left(\frac{\bar{V}_1}{a_0} \right)^2 \quad C(10)$$

the dimensionless mass flow rate $(\dot{m})^*$ of Eq. 66 becomes

$$(\dot{m})^* = \frac{(\dot{w}/g) \sqrt{g R_G T_0}}{\pi R_2^2 P_0} = \frac{\varphi_1}{\pi} \left(\frac{U_2}{a_0} \right) \sqrt{\gamma} \left[1 - \frac{\gamma-1}{2} \left(\frac{\bar{V}_1}{a_0} \right)^2 \right]^{1/(\gamma-1)} \quad C(11)$$

Since by Eq. C(7) the ratio (\bar{V}_1/a_0) is a function of φ_1 and (U_2/a_0) for known impeller dimensions, the dimensionless mass flow rate $(\dot{m})^*$ can be determined for assumed blockage factors k_{Bl} .

The change of V_1 along R_1 can be determined approximately by assuming that the curvatures k_m of the generatrices of the axisymmetric stream surfaces at the inducer inlet vary linearly from k_{mi} at R_{1i} to k_{mo} at R_{1o} , where k_{mi} and k_{mo} are the curvatures of the meridional contours at these radii. In accordance with Eq. 11 (122) of Ref. 5

$$V_1 = V_{1i} e^{-\int_0^n k_m dn} \quad C(12)$$

where $n = R_l - R_{li}$, and V_{li} is the velocity at R_{li} . As shown in Art. 3.3 of Ref. 5 the curvatures k_m in Eq. C(12) for the channel of Fig. 12 must be introduced as negative values. The assumed linear variation of k_m is given by

$$k_m = k_{mi} + \frac{k_{mo} - k_{mi}}{R_{lo} - R_{li}} (R_l - R_{li}) \quad C(13)$$

and the integral of Eq. C(12) becomes

$$- \int_0^n k_m \, dn = R_2 k_{mi} \left(\frac{R_l}{R_2} - \frac{R_{li}}{R_2} \right) + \frac{R_2 k_{mo} - R_2 k_{mi}}{2 \left(\frac{R_{lo}}{R_2} - \frac{R_{li}}{R_2} \right)} \left(\frac{R_l}{R_2} - \frac{R_{li}}{R_2} \right)^2 \quad C(14)$$

On examining Fig. 12 it can be noticed that the rotor drawing presented in Ref. 10 is not to scale. From the measured distances of the figure the radius ratios R_{lo}/R_2 and R_{li}/R_2 are about 0.59 and 0.275, instead of 0.541 and 0.287 in accordance with the dimensions of Fig. 12. Because of this situation it is not possible to determine the radii of curvature of the meridian contours at R_{li} and R_{lo} from Fig. 12 with graphical means. Although the approach explained in the following is speculative it is believed that it gives a sufficiently good approximation for k_{mi} and k_{mo} . It is based on the assumption that the meridian contours of the rotor are curves with the equation $r/a = \theta^{-b}$ in polar coordinates. As shown in Fig. 18 and explained in Program No. 110 of Appendix D, such curves have zero curvature at a point P_0 given by r_0/a and θ_0 for any value of b between zero and unity. For angles θ larger than θ_0 the curvatures increase smoothly to reach a maximum value of k_m at point P_m where the tangent to the curve is perpendicular to that at P_0 .

The writer has investigated a large number of curves and believes that those with $r/a = \theta^{-b}$ have the smallest curvature k_m at P_m for a given ratio y_0/x_0 of the coordinates of Fig. 18. Three-dimensional flow analyses indicate that smoothly changing curvatures k of the meridian contours of a channel and small values of k produce small changes of the velocities across the width of the channel and along the flow paths. In addition to satisfying these conditions it is seen from Fig. 20 also that contours with $r/a = \theta^{-b}$ establish flow channels that look very much like those of high-performance radial impellers. The inner or hub contour is supposed to be located between station P_0 and P_m of Fig. 20. For this curve

$$y_0/x_0 = \frac{180 - 51.7}{2(44.5)} = 1.4416$$

From Fig. 12 it is apparent that the tip contour does not have zero curvature at the outer rotor diameter of 180 mm, but that it is curved to the diameter where the axial width of the diffuser is 7 mm. It can be seen from Ref. 10 that this diameter is 215 mm. Hence, in accordance with Fig. 20 the tip contour is supposed to extend from P_m' to P_0' having

$$y_0'/x_0' = \frac{215 - 97.4}{2(37.5)} = 1.5680$$

The points P_0 and P_0' correspond to station P_0 of Fig. 18 so that the curvatures of the meridian at these locations are zero.

Since no direct solution of the problem of establishing the exponent b in $r/a = \theta^{-b}$ for given ratios y_0/x_0 is possible, the Calculator Program No. 110 of Appendix D has been established to obtain this relationship with an iterative process. Figure 19 shows b as function of y_0/x_0

and gives the maximum curvature k_m at station P_m of Fig. 18 by the dimensionless quantity $x_0 k_m$. From Fig. 19 for the hub contour

$$k_m = k_{mi} = \frac{(1.174)}{44.5} = (2.638)(10^{-2}) \text{ mm}^{-1}$$

so that the radius of curvature R_{ci} is

$$R_{ci} = \frac{1}{k_{mi}} = 37.90 \text{ mm}$$

For the tip contour

$$k_m' = k_{mo} = \frac{1.232}{37.5} = (3.285)(10^{-2}) \text{ mm}^{-1}$$

or

$$R_{co} = \frac{1}{k_{mo}} = 30.44 \text{ mm}$$

The exponents b were found to be 0.2552 for the inner and 0.3525 for the outer contour. They were used to establish the coordinates of the meridian contours of Fig. 20.

The calculated curvatures k_{mi} and k_{mo} introduced into Eq. C(14) give

$$-\int_0^n k_m \, dn = -0.6815 + 2.3747 \frac{R_1}{R_2} + 1.1456 \left(\frac{R_1}{R_2} - 0.287 \right)^2 \quad C(15)$$

From Eqs. C(12) and C(15) for $R_1/R_2 = R_{1o}/R_2 = 0.541$

$$\frac{V_{1o}}{V_{1i}} = e^{0.67712} = 1.9682$$

or

$$\frac{V_1}{a_0} = \frac{V_{10}}{a_0} (0.5081) e^{-\int_0^n k_m dn} = \frac{V_{10}}{a_0} X \quad C(16)$$

Thus, for chosen values of V_{10}/a_0 the ratios V_1/a_0 at the different radii R_1 are known, and it is possible to determine the corresponding weight flow rates by

$$\dot{w} = k_{B1} \int_{R_{1i}}^{R_{10}} 2 \pi R_1 V_1 \frac{p_1}{R_G T_1} dR_1$$

or

$$\dot{w} = 2 \pi R_2^2 k_{B1} \frac{p_0}{T_0} \frac{a_0}{R_G} \int_{R_{1i}/R_2}^{R_{10}/R_2} \frac{R_1}{R_2} \frac{V_1}{a_0} \frac{p_1/p_0}{T_1/T_0} d\left(\frac{R_1}{R_2}\right)$$

Similar to Eqs. C(9) and C(10)

$$\frac{p_1/p_0}{T_1/T_0} = \left[1 - \frac{\gamma-1}{2} \left(\frac{V_1}{a_0} \right)^2 \right]^{1/(\gamma-1)}$$

Then, since $R_{1i}/R_2 = 0.287$ and $R_{10}/R_2 = 0.541$, the dimensionless mass flow rate $(\dot{m})^*$ of Eq. C(11) is obtained also from

$$(\dot{m})^* = 2 k_{B1} \sqrt{\gamma} \left(\frac{V_{10}}{a_0} \right) \int_{0.287}^{0.541} \left(\frac{R_1}{R_2} \right) X \left[1 - \frac{\gamma-1}{2} \left(\frac{V_{10}}{a_0} X \right)^2 \right]^{1/(\gamma-1)} d\left(\frac{R_1}{R_2}\right) \quad C(17)$$

where X is defined by Eq. 16.

With Eqs. C(11) and C(17) the flow coefficient φ_1 can be related to V_{10}/a_0 by determining \bar{V}_1/a_0 from Eq. C(7) for particular values of φ_1 and calculating $(\dot{m})^*$ by Eq. C(11). Then, that ratio V_{10}/a_0 has to be established which,

introduced in Eq. C(16) and used in Eq. C(17), gives the same value of $(\dot{m})^*$. Since the same blockage factor k_{Bl} is used in both calculating procedures, its influence on the relationship between φ_1 and V_{10}/a_0 is small, and a constant value $k_{Bl} = 0.97$ will be assumed. For the ratios V_{10}/a_0 thus determined, the flow angle β_{10} at R_{10} is given by

$$\tan \beta_{10} = \frac{\omega R_{10}}{V_{10}} = \frac{(U_2/a_0) (R_{10}/R_2)}{(V_{10}/a_0)} = \frac{0.44903}{(V_{10}/a_0)} \quad C(18)$$

The rotor efficiencies η_{PR} of Fig. 17 which hold for $U_2/a_0 = 0.83$ can therefore be related to the flow angle β_{10} at the tip of the inducer. With the calculated data it is possible also to establish the Mach number M_{W1} at the inducer tip radius by means of Eq. C(3). For $\gamma = 1.4$

$$M_{W1} = \frac{0.44903}{\left[\sin^2 \beta_{10} - (0.2) (0.44903)^2 \cos^2 \beta_{10} \right]^{\frac{1}{2}}} \quad C(19)$$

These calculations have been performed on a Monroe 1655 Calculator. In particular, the evaluation of Eq. C(17) for the velocity ratios of Eq. C(16) has been carried out with Program No. 108 of Appendix D. Figure 21 shows the dimensionless mass flow rate $(\dot{m})^*$ as functions of φ_1 and of V_{10}/a_0 . The relationship $(\dot{m})^* = f_1(\varphi_1)$ has been obtained from Eqs. C(11) and C(10), and $(\dot{m})^* = f_3(V_{10}/a_0)$ is the result of the calculations with Program No. 108. Whereas $f_1(\varphi_1)$ depends solely on the rotor dimensions which are given by Fig. 12, the accuracy of the function $f_3(V_{10}/a_0)$ depends on how well the assumed stream surface curvatures correspond to reality.

Figure 21 also shows the rotor efficiency η_{RP} as function of φ_1 . This curve has been obtained from the test data of Fig. 17, and represents the best estimate of a continuous curve that can be drawn through all the test points between $\varphi_1 \approx 0.11$ and $\varphi_1 \approx 0.275$. With this composite diagram the flow functions φ_1 can be determined for chosen ratios V_{10}/a_0 , since corresponding values must have the same dimensionless mass flow rate $(\dot{m})^*$. Hence, as shown in Fig. 21, it is also possible to obtain η_{RP} as a function of V_{10}/a_0 . Moreover, since by Eq. C(18) the relationship between the flow angle β_{10} and V_{10}/a_0 is known for the velocity distribution of Eq. C(16), the rotor efficiency η_{RP} is obtained as function of the angle β_{10} at the speed ratio $U_2/a_0 = 0.83$ for which the data of Fig. 17 hold. Moreover, Eq. C(19) establishes the Mach number M_{W1} for different flow angles β_{10} . The data thus obtained are marked by circles in Fig. 22. It can be seen that the maximum rotor efficiency occurs at a flow angle of about 55° ; that is, at an incidence angle i of about -2° . The data points marked by crosses in Fig. 22 are from Fig. 15 for $U_2/a_0 = 0.83$. Both curves of η_{RP} have the same maximum at about the same flow angle, but the efficiencies from Fig. 15 decrease more rapidly with flow angle on either side of the maximum than the data from Fig. 21. Figure 15 was obtained from the data of Ref. 10, shown in Fig. 13, by determining the flow angle (β_{10}^*) with Eq. C(4) on assuming that U_2/a_0 and M_{W1} of Fig. 13 are correct and that the rotor dimensions are those given by Fig. 12. In spite of the much smaller range of rotor efficiency with inlet flow angle which the data from Fig. 15 exhibit, it is remarkable how well the Mach numbers M_{W1} of the two approaches of Fig. 22 coincide.

For purposes of discussion the curves of η_{PR} and M_{WL} obtained from Fig. 21 are compared in Fig. 23 with the data of Fig. 13 at $U_2/a_0 = 0.83$ which are marked by crosses, and which represent the original values given by Ref. 10. It must be noted, however, that in Fig. 23 the curves from Fig. 13 are plotted against a scale marked β_{10}^{**} which is shifted by about 12° with respect to the horizontal scale β_{10} that holds for the data from Fig. 21. This shift has been chosen such that the two curves for η_{RP} coincide as closely as possible.

The conclusions that can be drawn from the preceeding analyses are:

- (1) The curves of Fig. 13 are not consistent because, for the rotor dimensions of Fig. 12, the flow angles β_{10} must be different than those of Fig. 13 if the velocity ratios U_2/a_0 and the Mach numbers M_{WL} of this figure are assumed to be correct, and doubt exists whether optimum efficiencies are reached at incidence angle i of about $+9^\circ$.
- (2) If the curves of Fig. 13 are plotted against the flow angle β_{10}^* , obtained from Eq. C(4) to establish the correct relationship between U_2/a_0 and M_{WL} , the resulting curves of Fig. 15 give optimum incidence angle i of about -2° .
- (3) If other original values of Ref. 10 for $U_2/a_0 = 0.83$, presented in Fig. 17, are analyzed with the best possible procedure, the optimum incidence angle i is also about -2° but, as shown in Fig. 22, the range in which the flow angle can vary for a specified off-design efficiency is about twice that of the curves of Fig. 15 described in point (2) above. However, the inlet Mach numbers M_{WL} of the two approaches lie on the same curve.

- (4) If the relations computed from Fig. 17 are compared with the original results of Fig. 13, it is seen from Fig. 23 that the two curves $\eta_{RP} = f(\beta_{10})$ at $U_2/a_0 = 0.83$ can be made to coincide only if the flow angles of Fig. 13 are reduced by about 12° . In this case, however, different inlet Mach numbers M_{WL} occur.
- (5) The discrepancies in the data from Ref. 10 make it inadvisable to use Fig. 13 with reduced flow angles, or Fig. 15, where the range of flow angle for given off-design efficiency is very much smaller than that derived from Fig. 17.
- (6) It is not believed that the design criteria of Ref. 10 have general applicability. The inconsistencies in the data could be due to non-uniform inlet velocity distributions because of the shape of the inlet duct and its supporting fins. It is possible also that the flow angle measurements are in error or that the dimensions of the rotor are different from those given by Fig. 12.

Test data of radial compressor wheels are presented also in Ref. 2. The curves of Fig. 23b of Ref. 2 are redrawn in Fig. 24 of this report in a somewhat modified form, and with U_2/a_0 instead of with $U_2/\sqrt{T_0}$ as parameter. There is, in metric units for air,

$$\frac{U_2}{a_0} = \frac{U_2}{\sqrt{\gamma R_G g T_0}} = \frac{U_2}{\sqrt{T_0}} \frac{4.9874}{100}$$

for:

$$\gamma = 1.4$$

$$R_G = R/M = 847.83/28.964 = 29.272 \text{ (m}^2/\text{°K)}$$

$$g = 9.81 \text{ (m/s}^2\text{)}$$

The incidence angle i' of Fig. 24 equals

$$i' = \beta_{10}' - \beta_{Bo}$$

where β_{10}' is the flow angle at R_{10} obtained from Eq. C(1) by taking account of the blockage due to the inducer blade thickness, and β_{Bo} is the inducer blade angle at R_{10} . Reference 2 does not give the dimensions and the inducer blade angles of the rotor for which Fig. 24 has been established. Hence Mach number M_{WL} and peripheral speed ratio U_2/a_0 cannot be related to each other by, say, Eq. C(3). Point D of Fig. 25, which gives the curves of Fig. 24 also corresponds to the design point of the Hybrid impeller with $M_{WL} = 0.4842$; $i' \cong +0.5^\circ$, and $U_2/a_0 = 0.7156$. It can be noticed that for these values of M_{WL} and i' the parameter U_2/a_0 of Figs. 24 and 25 is very nearly equal to 0.7156. It was decided, therefore, to ignore the curves $U_2/a_0 = \text{constant}$ in Fig. 24 for the off-design performance calculations of the Hybrid compressor and to assume that $r_e = \eta_R/\eta_{RMAX}$ is only depending on M_{WL} and i' , not only because of the limited information given in Ref. 2 but also because these two quantities seem to be the most important variables that affect the rotor efficiency. The curve labeled "Max. Flow Rate" in Fig. 24 appears to represent the limit at which stable operation is possible, probably because of the flow separations that occur on the pressure, or concave, sides of the inducer blades at these negative incidence angles. The surge limit of Fig. 24 is that which occurs if a non-bladed diffuser is arranged after the impeller. Hence, for bladed diffusers, compressor surge may be initiated by separations in the diffuser at incidence angles i' smaller than those of Fig. 24.

APPENDIX D
CALCULATING PROGRAMS
FOR
MONROE MODEL 1655/56
ELECTRIC PROGRAMMABLE DISPLAY CALCULATOR
WITH
CARD READER CR-1
AND
MONROE MODEL 1880-22
SCIENTIFIC PROGRAMMABLE PRINTING CALCULATOR

PROGRAM No. 102

MONROE CALCULATOR 1655 WITH CARD READER CR-1

Description

Program 102 calculates the dimensionless flow rate of a radial compressor from the conditions at the impeller discharge. From Eq. II (11) of Ref. (a)*,

$$\phi_2 = \frac{\dot{w} \sqrt{(R_G/g) T_0}}{P_0 A_2 k_{B2}} = \mu \sqrt{\gamma} \cot \alpha_2 \left(\frac{U_2}{a_0} \right) \frac{P_2/P_0}{T_2/T_0}$$

where:

\dot{w} = weight flow rate (lbm/s)

R_G = gas constant (ft-lb/(lbm, °R))

g = 32.174 (ft/s²)

T_0 = total temperature ahead of rotor (°R)

P_0 = total pressure ahead of rotor (psia)

$A_2 = 2\pi R_2 b_2$ = rotor discharge area (in.²)

k_{B2} = restriction factor (-)

$A_1 = \pi (R_{1o}^2 - R_{1i}^2)$ = rotor inlet area (in.²)

k_{B1} = restriction factor (-)

μ = slip factor (-)

$\gamma = c_p/c_v$ (-)

α_2 = absolute flow angle at rotor discharge (°)

U_2 = peripheral rotor speed (ft/s)

$a_0 = \sqrt{g \gamma R_G T_0}$

 *(a) Vavra, M. H., "Basic Elements for Advanced Design of Radial Flow Compressors," in AGARD-LS-39-70, "Advanced Compressors," Techn. Editing & Reprod. Ltd; London 1970.

p_2 = static pressure out rotor discharge (psia)

T_2 = static temperature at rotor discharge ($^{\circ}\text{R}$)

From Eqs. I(20) and I(8) of Ref. (a)

$$\frac{p_2}{p_0} = (T_2'/T_0)^{\gamma(\gamma-1)}$$

$$\frac{T_2'}{T} = 1 + (\gamma-1) \mu \left(\frac{U_2}{a_0} \right)^2 \left[\frac{1}{\psi^2} \left(1 - \frac{\mu}{2 \sin^2 \alpha_2} \right) - \frac{1}{2\mu} \left(\frac{1}{\psi^2} - 1 \right) \right]$$

From Eq. I(7) of Ref. (a)

$$\frac{T_2}{T_0} = 1 + (\gamma-1) \mu \left(\frac{U_2}{a_0} \right)^2 \left(1 - \frac{\mu}{2 \sin^2 \alpha_2} \right)$$

The velocity coefficient

$$\psi = \frac{W_2}{W_{2 \text{ is}}}$$

establishes the rotor loss in accordance with Ref. (a).

The following quantities will be used during the calculations:

$$A = 1 - \frac{\mu}{2 \sin^2 \alpha_2}$$

$$B = \frac{1}{2\mu} \left(\frac{1}{\psi^2} - 1 \right)$$

$$C = (\gamma-1) \mu \left(\frac{U_2}{a_0} \right)^2$$

$$D = \mu \sqrt{\gamma} \cot \alpha_2 \left(\frac{U_2}{a_0} \right)$$

Then

$$T_2'/T_0 = F = 1 + C \left(\frac{1}{\psi^2} A - B \right)$$

$$p_2/p_0 = F^{\gamma/(\gamma-1)}$$

$$T_2/T_0 = 1 + C A$$

$$\Phi_2 = D \frac{(p_2/p_0)}{(T_2/T_0)}$$

$$X = \Phi_2 A_2 k_{B2} = \frac{\dot{w} \sqrt{(R_G/g) T_0}}{P_0}$$

$$\Phi_1 = \frac{X}{A_1 k_{B1}} = \frac{\dot{w} \sqrt{(R_G/g) T_0}}{P_0 A_1 k_{B1}}$$

The flow function Φ_1 will be used in program No. 103 to establish the ratios p_1/p_0 and T_1/T_0 . The area $A_1 = \pi (R_{1o}^2 - R_{1i}^2)$ must be introduced in square inches.

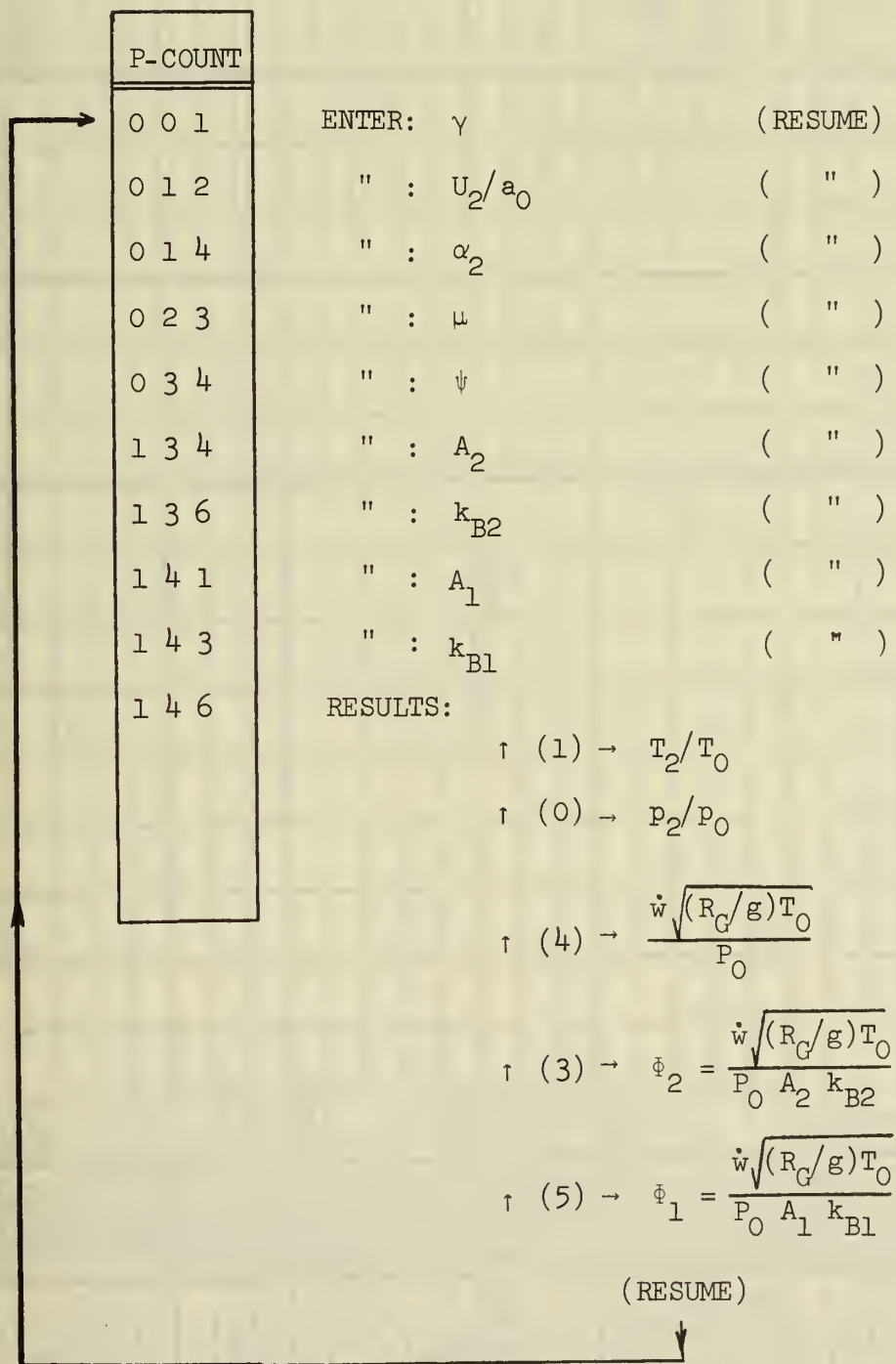
Enclosures: Operating Instructions (1 page)
Program Listing (4 pages)

OPERATING INSTRUCTIONS PROGRAM No. 102

MONROE CALCULATOR 1655/6 WITH CARD READER CR-1

Set-Up: (RESET); (TO(0)); Depress (LOAD); Read Cards 1-3

Release (LOAD); (TO(0)); Depress (P); (RESUME)



BR PT	ADDRESS P COUNT	COMMAND	CODE	REGISTERS																NOTES
				E	A	M	0	1	2	3	4	5	6	7	8	9	X	Y	Z	
0	0 0 0	HALT	4 0 1	Y															ENTER: γ	
	1	STR(2)	4 4 1	Y					γ											
	2	-	0 6 2																	
	3	1	0 0 1																	
	4	\div	0 7 2	$\gamma-1$																
	5	RCL(2)	4 6 1	γ																
	6	=	0 2 0	$\frac{\gamma-1}{\gamma}$																
	0 7	INV	0 5 4	$\frac{\gamma}{\gamma-1}$																
	1 0	STR(0)	4 5 7																	
	1 1	HALT	4 0 1																ENTER: U_2/a_0	
	2	STR(6)	4 4 5											U_2/a_0						
	1 3	HALT	4 0 1	α_2															ENTER: α_2	
	4	SIN/COS	0 4 0	$\sin \alpha_2$																
	5	x	0 7 0																	
	6	=	0 2 0	$\sin^2 \alpha_2$									$\sin^2 \alpha_2$							
	1 7	STR(5)	4 4 4																	
1	2 0	INV	0 5 4	$\sin^2 \alpha_2$																
	1	x	0 7 0																	
	2 2	HALT	4 0 1	μ															ENTER: μ	
	3	STR(4)	4 4 3	μ								μ								
	4	\div	0 7 2	$\frac{\mu}{\sin^2 \alpha_2}$																
	5	2	0 0 2	$\frac{\mu}{2 \sin^2 \alpha_2}$																
	6	-	0 6 2																	
	2 7	1	0 0 1																	
	3 0	=	0 2 0	-A																
	1	CHSGN	0 1 3	A																
	2	STR(3)	4 4 2						A											
	3 3	HALT	4 0 1	ψ															ENTER: ψ	
	4	INV	0 5 4	$1/\psi$																
	5	x	0 7 0																	
	6	-	0 6 2	$1/\psi^2$																
	3 7	STR(7)	4 4 6														$1/\psi^2$			

BR PT	ADDRESS P COUNT	COMMAND	CODE	REGISTERS													NOTES		
				E	A	M	0	1	2	3	4	5	6	7	8	9		X	Y
4	1 0 0	x	0 7 0				P_2/P_0	C	γ	A	μ	$\sin^2 \alpha_2$	U_2/a_0						
	1 1 0	RCL(3)	4 6 2	A															
	2	+	0 6 0	CA															
	3	1	0 0 1																
	4	=	0 2 0	T_2/T_0															
	5	STR(1)	4 4 0					T_2/T_0											
	6	1	0 0 1																
	1 0 7	-	0 6 2																
	1 1 0	RCL(5)	4 6 4	$\sin^2 \alpha_2$															
	1	\div	0 7 2	$\cos^2 \alpha_2$															
	2	RCL(5)	4 6 4	$\sin^2 \alpha_2$															
	3	x	0 7 0	$\cot^2 \alpha_2$															
	4	RCL(2)	4 6 1	γ															
	5	=	0 2 0	$\gamma \cot^2 \alpha_2$															
	6	$\sqrt{\quad}$	0 5 6	$\sqrt{\gamma \cot^2 \alpha_2}$															
	1 1 7	x	0 7 0																
5	1 2 0	RCL(6)	4 6 5	U_2/a_0															
	1	x	0 7 0																
	2	RCL(4)	4 6 3	μ															
	3	x	0 7 0																
	4	I	0 0 1																
	5	x	0 7 0	D															
	6	RCL(0)	4 7 7	P_2/P_0															
	1 2 7	\div	0 7 2																
	1 3 0	RCL(1)	4 6 0	T_2/T_0															
	1	x	0 7 0	Φ_2															
	2	STR(3)	4 4 2																
	1 3 3	HALT	4 0 1	A_2															
	4	x	0 7 0																
	1 3 5	HALT	4 0 1	K_{B2}															
	6	\div	0 7 2	X															
	1 3 7	STR(4)	4 4 3								X								
				E	A	M	0	1	2	3	4	5	6	7	8	9	X	Y	Z

ENTER: A_2

ENTER: K_{B2}

[illegible]

PROGRAM No. 103

MONROE CALCULATOR 1655/6 WITH CARD READER CR-1

Description

Program 103 deals with the flow of a perfect gas with $\gamma = c_p/c_v = \text{constant}$ that passes through a given area A . Because of boundary layers the effective flow area is supposed to be $k_B A$. The total pressure P_t and the total temperature T_t of the flow are known. To be determined is the average static pressure p that exists at the flow area $k_B A$. The equation of continuity can be expressed by a dimensionless flow function Φ where

$$\Phi = \sqrt{\frac{2\gamma}{\gamma-1} \left[\left(\frac{p}{P_t} \right)^{2/\gamma} - \left(\frac{p}{P_t} \right)^{(\gamma+1)/\gamma} \right]}$$

where

$$\Phi = \frac{\dot{w} \sqrt{(R_G/g) T_t}}{k_B A P_t} = \frac{\dot{m} \sqrt{g R_G T_t}}{k_B A P_t}$$

There are:

\dot{w} = weight flow rate (lbm/s)

\dot{m} = mass flow rate (slug/s)

R_G = gas constant (ft-lb/(lbm, °R))

$g = 32.174$ (ft/s²)

$k_B A$ = effective cross-sectional area of channel where static pressure p occurs

P_t, p (psia)

T_t (°R)

A (in.²)

Figure D 103 shows a plot of Φ vs. $r = p/P_t$. At the critical pressure ratio r_c the function $\Phi = \Phi_c$ has a maximum, hence no solutions occur if

Φ is larger than Φ_c . There are:

$$r_c = \left(\frac{2}{\gamma + 1} \right)^{\gamma/(\gamma-1)} = \left[\left(\frac{2}{\gamma + 1} \right)^{1/(\gamma-1)} \right]^{\gamma}$$

and

$$\Phi_c = \sqrt{\frac{2\gamma}{\gamma + 1}} \left(\frac{2}{\gamma + 1} \right)^{1/(\gamma-1)}$$

If Φ is smaller than Φ_c two solutions of $r = p/P_t$ are obtained, say, r_I if the velocity at the area A is subsonic, and r_{II} if the flow is supersonic. These pressure ratios must be obtained with an iterative process, by assuming a value of r , say r_i , and verifying whether the corresponding value Φ_i equals the specified flow function Φ .

The following quantities are used in the calculations

$$E1 = 2/\gamma$$

$$E2 = (\gamma+1)/\gamma$$

$$A = 2\gamma/(\gamma-1)$$

$$B = \left(\frac{2}{\gamma + 1} \right)^{1/(\gamma-1)}$$

$$C = \sqrt{\frac{2\gamma}{\gamma + 1}} = \sqrt{\frac{2}{E2}}$$

With,

$$r = p/P_t$$

there are:

$$\Phi = \sqrt{A(r^{E1} - r^{E2})}$$

$$r_c = (p/P_t)_c = B^{\gamma}$$

$$\Phi_c = C B$$

Enclosures: Fig. D(103)

Operating Instruction (1 page)

Program Listing (3 pages)

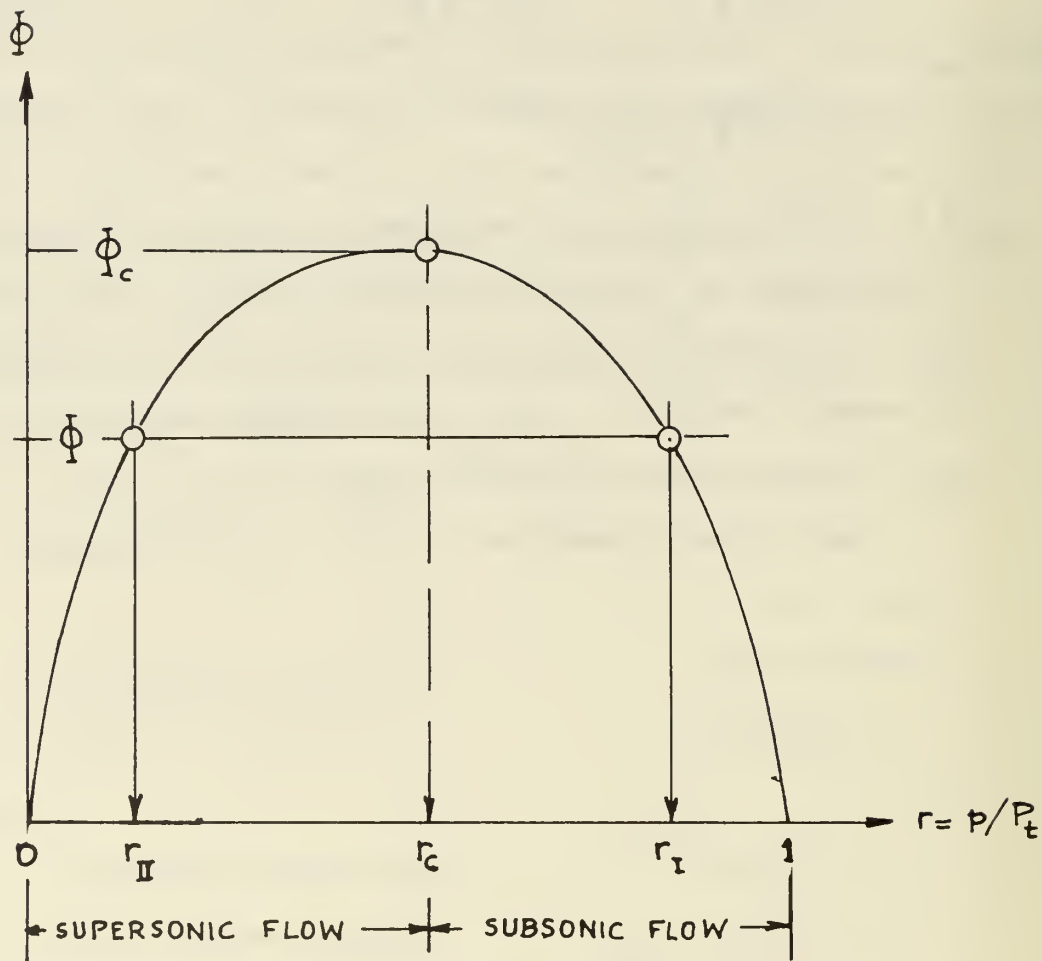


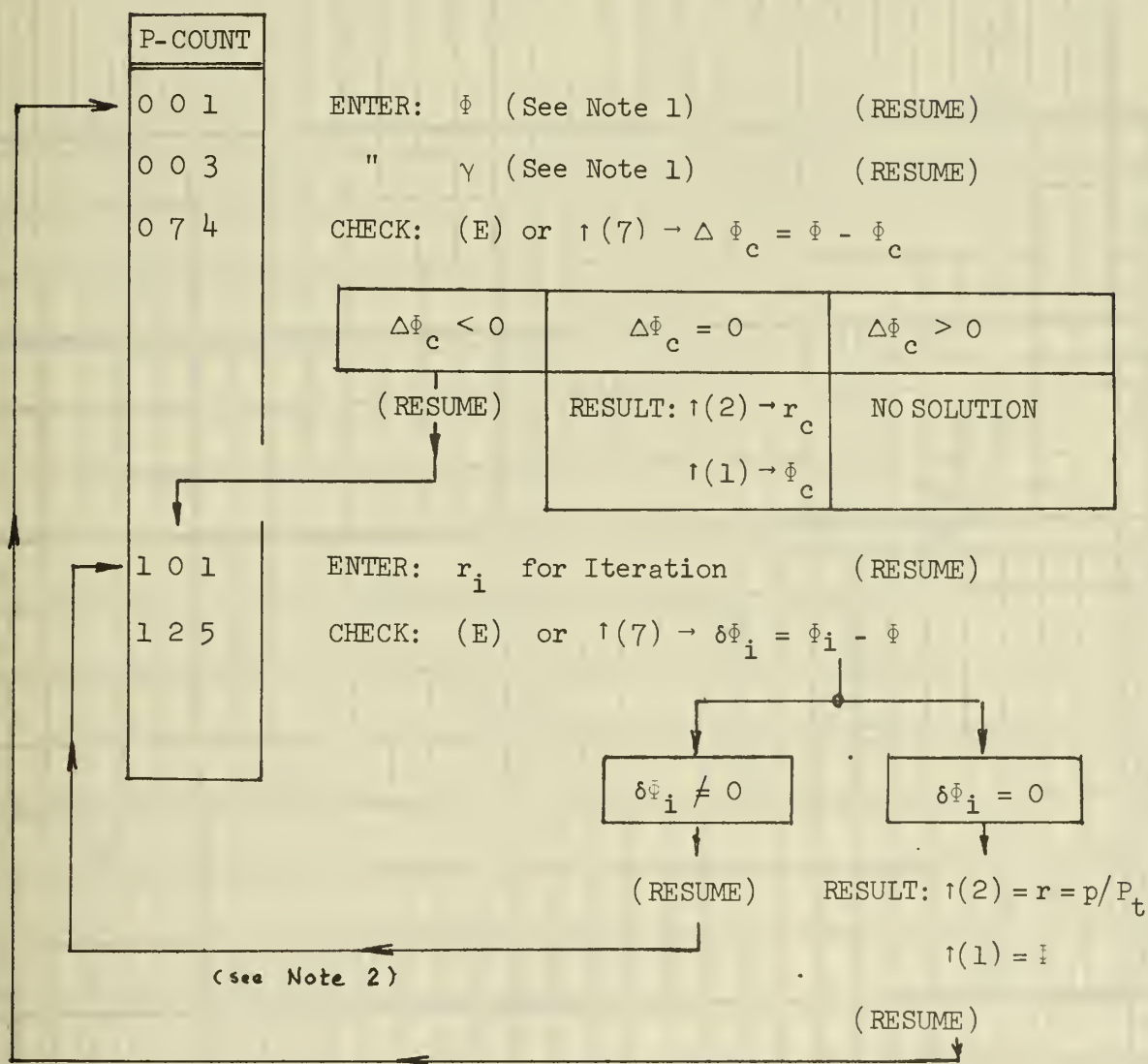
FIG. D(103) ISENTROPIC FLOW FUNCTION Φ

OPERATING INSTRUCTIONS PROGRAM No. 103

MONROE CALCULATOR 1655/6 WITH CARD READER CR-1

Set-Up: (RESET); (TO(0)); Depress (LOAD); Read Cards 1-3

Release (LOAD); (TO(0)); Depress (P); (RESUME)



Note 1: If Program 103 is used immediately after Program 102:

Enter at P-Count 1: $\uparrow(5)$ for Φ

Enter at P-Count 3: $\uparrow(1)$ for γ

Note 2: Change of r_i (Reg. 2) to r_{i+1} for next iteration:

	SUBSONIC FLOW	SUPERSONIC FLOW
$\delta \Phi_i > 0$	$r_{i+1} > r_i$	$r_{i+1} < r_i$
$\delta \Phi_i < 0$	$r_{i+1} < r_i$	$r_{i+1} > r_i$

BR PT		ADDRESS P COUNT		COMMAND	CODE	E	A	M	0	1	2	3	4	5	6	7	8	9	X	Y	Z	NOTES
0	0	0	0	HALT	4 0 1	Φ																ENTER: $\Phi[f(5) \text{ of No. 102}]$
			1	STR(1)	4 4 0					Φ												
0	0	2		HALT	4 0 1	γ																
		3		STR(6)	4 4 5	γ																
		4		+	0 6 0										γ							
		5		1	0 0 1																	
		6		\div	0 7 2	$\gamma+1$																
0	0	7		2	0 0 2																	
		1	0	=	0 2 0	$\frac{\gamma+1}{2}$																
		1		INV	0 5 4	$\frac{2}{\gamma+1}$																
		2		STR(5)	4 4 4																	
		3		x	0 7 0																	
		4		RCL(6)	4 6 5	γ																
		5		=	0 2 0	$\frac{2\gamma}{\gamma+1}$																
		6		$\sqrt{\quad}$	0 5 6	C																
		1	7	STR(4)	4 4 3								C									
		2	0	RCL(6)	4 6 5	γ																
		1		—	0 6 2																	
		2		1	0 0 1																	
		3		=	0 2 0	$\gamma-1$																
		4		INV	0 5 4	$\frac{1}{\gamma-1}$																
		5		STR(3)	4 4 2																	
		6		RCL(5)	4 6 4	$\frac{2}{\gamma+1}$																
		2	7	a^x	0 7 4																	
		3	0	RCL(3)	4 6 2	$\frac{1}{\gamma-1}$																
		1		x	0 7 0	B																
		2		STR(2)	4 4 1						B											
		3		RCL(4)	4 6 3	C																
		4		=	0 2 0	Φ_c																
		5		STR(0)	4 5 7																	
		6		RCL(2)	4 6 1	B																
		3	7	a^x	0 7 4																	

208

1

BR PT	ADDRESS P COUNT	COMMAND	CODE	REGISTERS													NOTES			
				E	A	M	0	1	2	3	4	5	6	7	8	9		X	Y	Z
2	0 4	0 RCL(6)	4 6 5	Y			Φ_c	Φ	B	$\frac{1}{Y-1}$	C	$\frac{2}{X+1}$	Y							
		1 =	0 2 0	r_c					r_c											
		2 STR(2)	4 4 1																	
		3 RCL(3)	4 6 2	$\frac{1}{Y-1}$																
		4 x	0 7 0																	
		5 RCL(6)	4 6 5	Y																
		6 x	0 7 0																	
	4 7	2	0 0 2																	
	5 0	=	0 2 0	A																
		1 STR(5)	4 4 4									A								
		2	0 0 2																	
		3 ÷	0 7 2																	
		4 RCL(6)	4 6 5	Y																
		5 =	0 2 0	E1																
		6 STR(4)	4 4 3								E1									
	5 7	RCL(6)	4 6 5	Y																
	6 0	+	0 6 0																	
		1	0 0 1																	
		2 ÷	0 7 2	$Y+1$																
		3 RCL(6)	4 6 5	Y																
		4 =	0 2 0	E2																
		5 STR(3)	4 4 2							E2										
		6 RCL(1)	4 6 0	Φ																
	6 7	-	0 6 2																	
	7 0	RCL(0)	4 7 7	Φ_c																
		1 =	0 2 0	$\Phi-\Phi_c$																
		2 STR(7)	4 4 6																	
	7 3	HALT	4 0 1	$\Phi-\Phi_c$			Φ_c		r_c					$\Phi-\Phi_c$						
		4 0	0																	
		5 0	0																	
		6 0	0																	
		7 0	0																	
				E	A	M	0	1	2	3	4	5	6	7	8	9	X	Y	Z	

209

3

CHECK: $\Phi-\Phi_c = ?$

CHECK: $\Phi-\Phi_c = ?$

BR PT	ADDRESS P COUNT	COMMAND	CODE	REGISTERS																NOTES
				E	A	M	0	1	2	3	4	5	6	7	8	9	X	Y	Z	
4	1 0 0	HALT	4 0 1	r_c			Φ_c	Φ	r_c	E2	E1	A	γ							ENTER: r_c for iteration
		1 STR(2)	4 4 1	r_c					r_c											
		2 a^*	0 7 4																	
		3 RCL(3)	4 6 2	E2																
		4 =	0 2 0	r_c E2																
		5 STR(0)	4 5 7				r_c E2													
		6 RCL(2)	4 6 1	r_c																
	1 0 7	a^*	0 7 4																	
	1 1 0	RCL(4)	4 6 3	E1																
		1 —	0 6 2	r_c E1																
		2 RCL(0)	4 7 7	r_c E2																
		3 X	0 7 0																	
		4 RCL(5)	4 6 4	A																
		5 =	0 2 0																	
		6 $\sqrt{\quad}$	0 5 6	Φ_c																
	1 1 7	STR(0)	4 5 7				Φ_c													
	1 2 0	—	0 6 2																	
		1 RCL(1)	4 6 0	Φ																
		2 =	0 2 0	$\Phi_c - \Phi$																
		3 STR(7)	4 4 6																	
	1 2 4	HALT	4 0 1	$\Phi_c - \Phi$			Φ_c	Φ	r_c	E2	E1	A	γ	$\Phi_c - \Phi$	$\Phi_c - \Phi$					
		5 SFSNS	5 2 3																	
		6 SKF1	5 4 0																	
	1 2 7	JUMP 00	6 0 0																	
	1 3 0	TO(0)	7 4 0																	
		1																		
		2																		
		3																		
		4																		
		5																		
		6																		
		7																		
				E	A	M	0	1	2	3	4	5	6	7	8	9	X	Y	Z	

CHECK: $\Phi_c = \Phi$?
 Depr.(SENSE) if $\Phi_c = \Phi$

MONROE CALCULATOR 1055/1056 WITH CARD READER CR-1

Description

This program can be used to determine the flow properties at the inlet of a radial compressor rotor provided the absolute velocity V_1 at this station is axial and uniform. The following quantities must be known:

$$\phi_1 = \frac{\dot{w} \sqrt{(R_G/g) T_0}}{P_0 A_1 k_{B1}} = \frac{\dot{m} \sqrt{R_G g T_0}}{P_0 A_1 k_{B1}} = \text{dimensionless flow function}$$

p_1/P_0 = ratio of static and total pressure at inlet

U_2/a_0 = speed ratio

R_{10}/R_2 = ratio of outer radius at inlet and outer rotor radius

$\gamma = c_p/c_v$ = specific heat ratio

The program determines:

T_1/T_0 = ratio of static and total temperatures at inlet

V_1/a_0 = ratio of absolute velocity at inlet and velocity of sound at T_0

W_{10}/a_0 = ratio of relative velocity at R_{10} and velocity of sound at T_0

β_{10} = relative flow angle at R_{10}

$M_{W1} = W_{10}/a_1$ = Mach number of W_{10}

Symbols:

\dot{w} = weight flow rate (lbm/s)

\dot{m} = mass flow rate (slug/s)

R_G = gas constant (ft-lb/(lbm, °R)

$g = 32.174$ (ft/s²)

T_0 = total inlet temperature (°R)

P_0 = total inlet pressure (psia)

$A_1 = \pi (R_{10}^2 - R_{1i}^2)$ = area of inlet eye of rotor (in.²)

k_{Bl} = restriction factor (-)

p_1 = static pressure at inlet (psia)

T_1 = static temperature at inlet ($^{\circ}R$)

U_2 = peripheral rotor speed at outer radius R_2 (ft/s)

$$a_0 = \sqrt{g \gamma R_G T_0} \quad (\text{ft/s})$$

R_{1i} = inner radius at inlet eye (in.)

R_{1o} = outer radius at inlet eye (in.)

R_2 = outer radius of impeller (in.)

Although English units are used in the above list, the program can be used for any consistent system of units.

Derivations:

$$T_1/T_0 = (p_1/P_0)^{(\gamma-1)/\gamma}$$

$$\dot{w} = A_1 k_{Bl} V_1 \frac{p_1}{R_G T_1} = A_1 k_{Bl} \frac{V_1}{a_0} \frac{(p_1/P_0)}{(T_1/T_0)} \frac{\sqrt{g \gamma R_G T_0}}{R_G} \frac{P_0}{T_0}$$

or

$$\phi_1 = \sqrt{\gamma} \frac{V_1}{a_0} \frac{(p_1/P_0)}{(T_1/T_0)}$$

and

$$\frac{V_1}{a_0} = \frac{\phi_1}{\sqrt{\gamma}} \frac{T_1/T_0}{(p_1/P_0)}$$

The peripheral speed U_{1o} at R_{1o} is

$$U_{1o} = (R_{1o}/R_2) U_2$$

For axial entry

$$W_{1o}^2 = V_1^2 + U_{1o}^2$$

$$\tan \beta_{1o} = U_{1o}/V_1$$

Thus

$$\frac{W_{10}}{a_0} = \sqrt{\left(\frac{V_1}{a_0}\right)^2 + \left(\frac{U_2}{a_0}\right)^2 \left(\frac{R_{10}}{R_2}\right)^2}$$

$$\tan \beta_{10} = \frac{(R_{10}/R_2)(U_2/a_0)}{(V_1/a_0)}$$

and

$$M_{W1} = \frac{W_{10}}{a_1} = \frac{W_{10}}{a_0} \frac{a_0}{a_1} = \frac{W_{10}/a_0}{\sqrt{T_1/T_0}}$$

The flow angle β_{10}' , by taking account of the blade thickness, is

$$\tan \beta_{10}' = \left(1 - \frac{t_u}{s}\right) \tan \beta_{10} = k \tan \beta_{10}$$

where

$$t_u = \frac{t}{\cos \beta_B}$$

$$s = \frac{2\pi R_{10}}{Z_R}$$

where:

t = actual blade thickness at R_{10}

β_B = blade inlet angle at R_{10}

Z_R = number of rotor blade

Also

$$\cot \beta_{10}' = \frac{(V_1/a_0)/k}{(R_{10}/R_2)(U_2/a_0)}$$

with

$$k = 1 - \frac{t Z_R}{\cos \beta_B 2\pi R_{10}}$$

If β_B is the blade angle at R_{10} , the incidence angle i' is

$$i' = \beta_{10}' - \beta_B$$

Enclosures: Operating Instructions (1 page)
Program Listing (3 pages)

OPERATING INSTRUCTIONS PROGRAM No. 104

MONROE CALCULATOR 1655/6 WITH CARD READER CR-1

Set-Up: (RESET); (TO(0)); Depress (LOAD); Read Cards 1-2

Release (LOAD); (TO(0)); Depress (P); (RESUME)

P-COUNT	
0 0 1	ENTER: Φ_1 (see note) (RESUME)
0 0 3	" p_1/p_0 (see note) (")
0 0 5	" γ (")
0 3 6	" U_2/a_0 (")
0 4 0	" R_{10}/R_2 (")
0 6 7	" k (")
0 7 6	" β_B (")
1 0 1	RESULTS: $\uparrow (4) \rightarrow (T_1/T_0)$
	$\uparrow (3) \rightarrow (v_1/a_0)$
	$\uparrow (2) \rightarrow (w_{10}/a_0)$
	$\uparrow (1) \rightarrow \beta_{10} (^{\circ})$
	$\uparrow (0) \rightarrow \beta'_{10} (^{\circ})$
	$\uparrow (5) \rightarrow M_{w1}$
	$\uparrow (7) \rightarrow i'(^{\circ})$
	(RESUME)

Note: If Program 104 is used immediately after Program 103, enter:

at P-Count 001: $\uparrow (1)$ to obtain Φ ,

at P-Count 003: $\uparrow (2)$ to obtain p_1/p_0

BR PT	ADDRESS P COUNT	COMMAND	CODE	REGISTERS																NOTES
				E	A	M	0	1	2	3	4	5	6	7	8	9	X	Y	Z	
0	0	0	0																	ENTER: Φ_1 [1(1) of PROG. 103]
	0	0	1																	
	0	0	2																	ENTER: P_1/P_0 [1(2) of PROG. 103]
	0	0	3																	
	0	0	4																	ENTER: γ [1(6) of PROG. 103]
	0	0	5																	
	0	0	6																	
	0	0	7																	
	1	0	0																	
	1	0	1																	
	1	0	2																	
	1	0	3																	
	1	0	4																	
	1	0	5																	
	1	0	6																	
	1	0	7																	
	1	0	8																	
	1	0	9																	
	1	0	10																	
	1	0	11																	
	1	0	12																	
	1	0	13																	
	1	0	14																	
	1	0	15																	
	1	0	16																	
	1	0	17																	
	1	0	18																	
	1	0	19																	
	1	0	20																	
	1	0	21																	
	1	0	22																	
	1	0	23																	
	1	0	24																	
	1	0	25																	
	1	0	26																	
	1	0	27																	
	1	0	28																	
	1	0	29																	
	1	0	30																	
	1	0	31																	
	1	0	32																	
	1	0	33																	
	1	0	34																	
	1	0	35																	
	1	0	36																	
	1	0	37																	
	1	0	38																	
	1	0	39																	
	1	0	40																	
	1	0	41																	
	1	0	42																	
	1	0	43																	
	1	0	44																	
	1	0	45																	
	1	0	46																	
	1	0	47																	
	1	0	48																	
	1	0	49																	
	1	0	50																	
	1	0	51																	
	1	0	52																	
	1	0	53																	
	1	0	54																	
	1	0	55																	
	1	0	56																	
	1	0	57																	
	1	0	58																	
	1	0	59																	
	1	0	60																	
	1	0	61																	
	1	0	62																	
	1	0	63																	
	1	0	64																	
	1	0	65																	
	1	0	66																	
	1	0	67																	
	1	0	68																	
	1	0	69																	
	1	0	70																	
	1	0	71																	
	1	0	72																	
	1	0	73																	
	1	0	74																	
	1	0	75																	
	1	0	76																	
	1	0	77																	
	1	0	78																	
	1	0	79																	
	1	0	80																	
	1	0	81																	
	1	0	82																	
	1	0	83																	
	1	0	84																	
	1	0	85																	
	1	0	86																	
	1	0	87																	
	1	0	88																	
	1	0	89																	
	1	0	90																	
	1	0	91																	
	1	0	92																	
	1	0	93																	
	1	0	94																	
	1																			

BR PT	ADDRESS P COUNT	COMMAND	CODE	REGISTERS																NOTES
				E	A	M	0	1	2	3	4	5	6	7	8	9	X	Y	Z	
2	0	4	0	C								V_1/a_0	T_1/T_0	P/P_0	Φ_1	$(V_1/a_0)^2$				$C = (U_2/d_0)(R_{10}/R_2)$
	1	STR(0)	0 7 0	C																
	2	+	0 6 0	C^2																
	3	RCL(7)	4 6 6	$(V_1/a_0)^2$																
	4	=	0 2 0	$(W_1/a_0)^2$																
	5	$\sqrt{\quad}$	0 5 6	W_1/a_0																
	6	STR(2)	4 4 1							W_1/a_0										
	4	RCL(3)	4 6 2	V_1/a_0																
	5	X	0 7 6																	
	1	RCL(0)	4 7 7																	
	2	=	0 2 0	β_{10}^*																
	3	$R \rightarrow$	0 4 6	β_{10}^0						β_{10}										
	4	STR(1)	4 4 0							β_{10}										
	5	RCL(4)	4 6 3	T_1/T_0																
	6	$\sqrt{\quad}$	0 5 6	$\sqrt{T_1/T_0}$																
	5	\div	0 7 2																	
3	6	RCL(2)	4 6 1	W_1/a_0																
	1	=	0 2 0	$1/M_{W1}$																
	2	INV	0 5 4	M_{W1}										M_{W1}						
	3	STR(5)	4 4 4																	
	4	RCL(3)	4 6 2	V_1/a_0																
	5	\div	0 7 2																	
	6	HALT	4 0 1	K																ENTER: K
	6	X	0 7 6	$K V_1/d_0$																
	7	RCL(0)	4 7 7	C																
	1	=	0 2 0	β_{10}^*																
	2	$R \rightarrow$	0 4 6	β_{10}^0																
	3	STR(0)	4 5 7	β_{10}^0																
	4	-	0 6 2																	
	7	HALT	4 0 1	β_B																ENTER: β_B
	6	=	0 2 0	i'																
	7	STR(7)	4 4 6																	

ENTER: K

ENTER: β_B

217

Description

In Ref. (a)* the so-called adiabatic rotor efficiency η_R of a radial compressor wheel is related to the wheel efficiency η_W and to the velocity ratio

$$\Psi = \frac{W_2}{W_{2is}}$$

which is a convenient measure to express the rotor losses for performance calculations.

From Eq. a(21); that is, Eq. (21) of Ref. (a),

$$\Psi = \frac{W_2/W_{10}}{\left[1 - \eta_W + \eta_W(W_2/W_{10})^2\right]^{\frac{1}{2}}}$$

From Eq. a(27)

$$\eta_W = \frac{\eta_R - C}{1 - C}$$

where, from Eq. a(25),

$$C = \frac{1 - (R_{10}/R_2)^2}{(R_{10}/R_2)^2 \cot^2 \beta_{10} + 2\mu (1 - \mu/[2 \sin^2 \alpha_2])}$$

From Eq. II(5) of Ref. (a)

$$\frac{W_2}{W_{10}} = \frac{\left[1 - 2\mu (1 - \mu/[2 \sin^2 \alpha_2])\right]^{\frac{1}{2}} \sin \beta_{10}}{R_{10}/R_2}$$

*See page 1 of Program 102

The following quantities are supposed to be known:

R_{10}/R_2 = ratio of outer radius at impeller inlet and impeller exit radius

α_2 = absolute flow angle at impeller exit

μ = impeller slip factor

β_{10} = relative flow angle at outer radius at impeller inlet

η_R = adiabatic rotor efficiency [see Eq. a(12)]

To be determined are:

η_W = wheel efficiency [see Eq. a(15)]

W_2/W_{10} = ratio of relative velocity at impeller exit and relative velocity at outer radius at impeller inlet

$\Psi = W_2/W_{2is}$ = ratio of actual and isentropic relative velocities at impeller exit

The following quantities are used for the calculations

$$A = 2\mu \left(1 - \frac{\mu}{2 \sin^2 \alpha_2} \right)$$

$$B = \sqrt{1 - A}$$

Then

$$C = \frac{1 - (R_{10}/R_2)^2}{(R_{10}/R_2)^2 \cot^2 \beta_{10} + A} = \frac{D}{E}$$

$$W_2/W_{10} = \frac{B \sin \beta_{10}}{R_{10}/R_2}$$

$$F = \left[1 - \eta_W + \eta_W (W_2/W_{10})^2 \right]^{\frac{1}{2}}$$

$$\Psi = \frac{W_2/W_{10}}{F}$$

Enclosures: Operating Procedure (1 page)

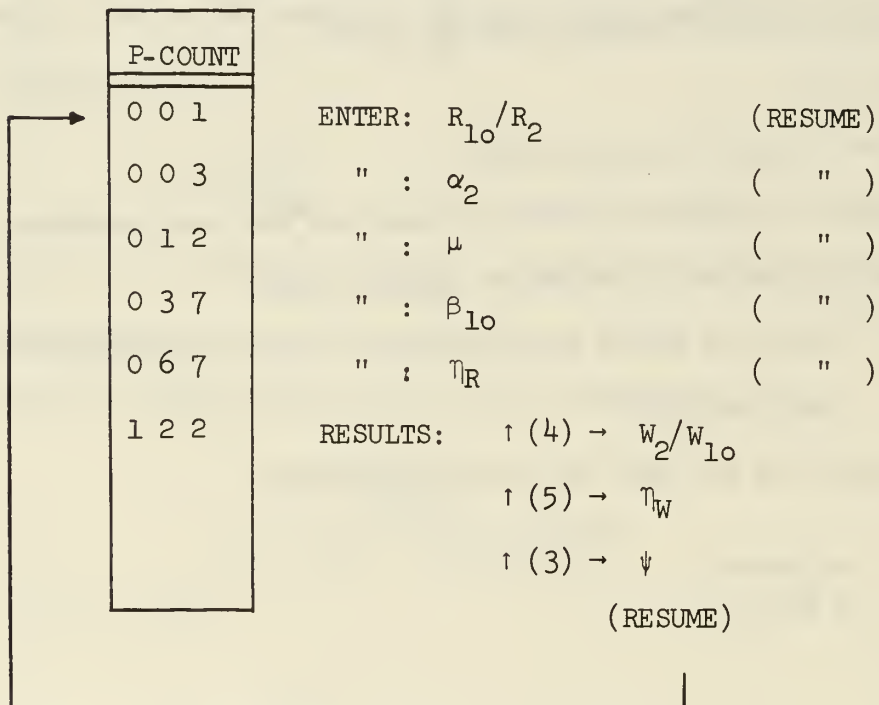
Program Listing (3 pages)

OPERATING INSTRUCTIONS PROGRAM No. 105

MONROE CALCULATOR 1655/6 WITH CARD READER CR-1

Set-Up: (RESET); (TO(0)); Depress (LOAD); Read Cards 1-3

Release (LOAD); (TO(0)); Depress (P); (RESUME)



BR PT	ADDRESS P COUNT	COMMAND	CODE	REGISTERS																NOTES
				E	A	M	0	1	2	3	4	5	6	7	8	9	X	Y	Z	
0	0	0	0	4	0	1														ENTER: R_{10}/R_2
			1	STR(6)	4	4	5													
	0	0	2	HALT	4	0	1													ENTER: α_2
		3	SIN/COS	0	4	0														
		4	X	0	7	0														
		5	X	0	7	0														
		6	2	0	0	2														
	0	0	7	=	0	2	0													
		1	0	STR(1)	4	4	0													
	0	1	1	HALT	4	0	1													
		2	STR(2)	4	4	1														ENTER: μ
		3	\div	0	7	2														
		4	RCL(1)	4	6	0														
		5	-	0	6	2														
		6	1	0	0	1														
		1	7	X	0	7	0													
	1	0	2	2	0	0	2													
		1		X	0	7	0													
		2	RCL(2)	4	6	1														
		3	+	0	6	0														
		4	1	0	0	1														
		5	-	0	6	2														
		6	STR(1)	4	4	0														
		2	7	1	0	0	1													
		3	=	0	2	0														
		1	CHSGN	0	1	3														
		2	STR(2)	4	4	1														
		3	RCL(1)	4	6	0														
		4	$\sqrt{\quad}$	0	5	6														
		5	STR(1)	4	4	0														
	0	3	6	HALT	4	0	1													ENTER: β_{10}
		3	7	SIN/COS	0	4	0													
					E	A	M	0	1	2	3	4	5	6	7	8	9	X	Y	Z

[illegible]

[illegible]

Description

This program is used to determine the flow properties at the discharge of a radial compressor wheel with the following equations of Ref. (a)*.

$$\text{Eq. I (6): } \frac{T_{t2}}{T_0} = 1 + (\gamma-1) \mu \left(\frac{U_2}{a_0} \right)^2$$

$$\text{Eq. I (7): } \frac{T_2}{T_0} = 1 + (\gamma-1) \mu \left(\frac{U_2}{a_0} \right)^2 \left[1 - \frac{\mu}{2 \sin^2 \alpha_2} \right]$$

$$\text{Eq. I (8): } \frac{T_2'}{T_0} = 1 + (\gamma-1) \mu \left(\frac{U_2}{a_0} \right)^2 \left[\frac{1}{\psi^2} \left(1 - \frac{\mu}{2 \sin^2 \alpha_2} \right) - \frac{1}{2\mu} \left(\frac{1}{\psi^2} - 1 \right) \right]$$

$$\text{Eq. I(20): } \frac{p_2}{p_0} = \left(\frac{T_2'}{T_0} \right)^{\gamma/(\gamma-1)}$$

$$\text{Eq. I(19): } \frac{p_{t2}}{p_0} = \left(\frac{p_2}{p_0} \right) \left(\frac{T_{t2}/T_0}{T_2/T_0} \right)^{\gamma/(\gamma-1)}$$

$$\text{Eq. II(6): } M_{v2} = \frac{\mu U_2/a_0}{\sin \alpha_2 \sqrt{T_2/T_0}}$$

Input data are:

$$\frac{U_2}{a_0} = \frac{\text{peripheral speed of impeller at discharge}}{\text{velocity of sound at total inlet temperature } T_0}$$

α_2 = absolute flow angle at impeller exit

μ = rotor slip factor

* See page 1 of Program 102

$$\gamma = c_p / c_v$$

$$\Psi = W_2 / W_{2is} = \text{velocity ratio}$$

The calculated values are :

$$T_0 = \text{total temperature at impeller inlet}$$

$$P_0 = \text{total pressure at impeller inlet}$$

$$T_2 = \text{static temperature at impeller exit}$$

$$p_2 = \text{static pressure at impeller exit}$$

$$T_{t2} = \text{total temperature at impeller exit}$$

$$P_{t2} = \text{total pressure at impeller exit}$$

$$M_{V2} = \text{Mach number of absolute velocity } V_2 \text{ at impeller}$$

$$\text{exit} = V_2 / \sqrt{g \gamma R_G T_2}$$

The following quantities are established during the calculations

$$A = (\gamma - 1) \mu \left(\frac{U_2}{a_0} \right)^2$$

$$B = 1 - \frac{\mu}{2 \sin^2 \alpha_2}$$

$$C = \frac{1}{2\mu} \left(\frac{1}{\Psi^2} - 1 \right)$$

$$D = \frac{\mu^2 (U_2 / a_0)^2}{\sin^2 \alpha_2}$$

$$E = \gamma / (\gamma - 1)$$

Then:

$$\frac{T_{t2}}{T_0} = 1 + A$$

$$\frac{T_2}{T_0} = 1 + AB$$

$$\frac{T_2'}{T_0} = 1 + \left[A \frac{1}{\psi^2} B - C \right]$$

$$M_{V2} = \sqrt{\frac{D}{T_2/T_0}}$$

Enclosures: Operating Instructions (1 page)

Program Listing (3 pages)

OPERATING INSTRUCTIONS PROGRAM No. 106

MONROE CALCULATOR 1655/6 WITH CARD READER CR-1

Set-Up: (RESET); (TO(0)); Depress (LOAD); Read Cards 1-3

Release (LOAD); (TO(0)); Depress (P); (RESUME)

P-COUNT		
0 0 1	ENTER: U_2/a_0	(RESUME)
0 0 5	" : α_2	(")
0 1 2	" : γ	(")
0 2 0	" : μ	(")
0 4 5	" : ψ	(")
1 3 7	RESULTS: $\uparrow (1) \rightarrow T_{t2}/T_0$	
	$\uparrow (2) \rightarrow P_{t2}/P_0$	
	$\uparrow (3) \rightarrow T_2/T_0$	
	$\uparrow (4) \rightarrow p_2/P_0$	
	$\uparrow (5) \rightarrow M_{V2}$	
	(RESUME)	

Note: N-switch must be in "Down" position.

BR PT	ADDRESS P COUNT	COMMAND	CODE	REGISTERS																NOTES																																																																																																																																																																																																																																																																																																																																																																																																																																																																																																																																																																																																																																																																																																																																																																																																																																																																																																																																																																																																																																																																																																																																																																																																																																																																																																																																																								
				E	A	M	0	1	2	3	4	5	6	7	8	9	X	Y	Z																																																																																																																																																																																																																																																																																																																																																																																																																																																																																																																																																																																																																																																																																																																																																																																																																																																																																																																																																																																																																																																																																																																																																																																																																																																																																																																																																									
0	0	0	0	HALT	4	0	1																																																																																																																																																																																																																																																																																																																																																																																																																																																																																																																																																																																																																																																																																																																																																																																																																																																																																																																																																																																																																																																																																																																																																																																																																																																																																																																																																																					</

BR PT	ADDRESS P COUNT	COMMAND	CODE	REGISTERS																NOTES
				E	A	M	0	1	2	3	4	5	6	7	8	9	X	Y	Z	
2	040	f	001					A	E					$\sin^2 \alpha_2 (U_2/a_0)^2$	γ	$\gamma-1$	μ			
	1	=	020	-B																
	2	CHSGN	013	B																
	3	STR(3)	442							B										
0	4	HALT	401	ψ																ENTER: ψ
	5	INV	054	$1/\psi$																
	6	x	070																	
	7	-	062	$1/\psi^2$																
0	50	STR(7)	446												$1/\psi^2$					
	1	1	001																	
	2	\div	072	$1/t^2-1$																
	3	2	002																	
	4	\div	072																	
	5	RCL(9)	470	μ																
	6	=	020	C							C									
	7	STR(4)	443																	
3	060	RCL(9)	470	μ																
	1	x	070																	
	2	x	070	μ^2																
	3	RCL(6)	465	$(U_2/a_0)^2$																
	4	\div	072																	
	5	RCL(5)	464	$\sin \alpha_2$																
	6	=	020	D																
	7	STR(5)	444											D						
0	70	RCL(7)	466	$1/t^2$																
	1	x	070																	
	2	RCL(3)	462	B																
	3	-	062																	
	4	RCL(4)	463	C																
	5	x	070																	
	6	RCL(1)	460	A																
0	77	+	060																	
				E	A	M	0	1	2	3	4	5	6	7	8	9	X	Y	Z	

PROGRAM NO. 108

MONROE CALCULATOR 1655 WITH CARD READER CR-1

Description

This program calculates Eq. C(17) of Appendix C.

$$(\dot{m})^* = 2k_{B1} \sqrt{\gamma} \int_{0.287}^{0.541} \left(\frac{R_1}{R_2} \right) X \left(\frac{V_{10}}{a_0} \right) \left[1 - \frac{\gamma-1}{2} \left(X \frac{V_{10}}{a_0} \right)^2 \right]^{1/(\gamma-1)} d \left(\frac{R_1}{R_2} \right)$$

where $X = \frac{V_1/a_0}{V_{10}/a_0}$

For five equal increments of R_1/R_2 between 0.287 and 0.541 the ratio X can be calculated from Eqs. C(15) and C(16). The following table gives the data that have to be entered in the program in the order required, starting from $i = 0$. The quantity z_i is used in the process of integration.

i	0	1	2	3	4	5
X_i	0.5081	0.5749	0.6544	0.7493	0.8631	1.0
$(R_1/R_2)_i$	0.287	0.3378	0.3886	0.4394	0.4902	0.541
z_i	2	1	1	1	1	2

With $\Delta(R_1/R_2) = (0.541 - 0.287)/5 = 0.0508$ and

$$N_i = \left(\frac{R_1}{R_2} \right)_i X_i \left[\frac{V_{10}}{a_0} \right] \left[1 - \frac{\gamma-1}{2} \left(X_i \frac{V_{10}}{a_0} \right)^2 \right]^{1/(\gamma-1)}$$

there is with the trapezoidal method of integration

$$\int_{0.287}^{0.541} = \left(N_0/2 + N_1 + N_2 + N_3 + N_4 + N_5/2 \right) \Delta \left(\frac{R_1}{R_2} \right)$$

or

$$S = \int_{0.287}^{0.541} = 0.0508 \sum_{i=0}^5 N_i/z_i$$

Hence

$$(m)^* = 2k_{B1} \sqrt{\gamma} S$$

Further, from Eq. C(18)

$$\cot \beta_{10} = \frac{V_{10}/a_0}{(U_2/a_0) (R_{10}/R_2)} = \frac{V_{10}/a_0}{0.44903}$$

From Eq. C(19)

$$M_{W1} = \frac{0.44903}{\left[\sin^2 \beta_{10} - \frac{\gamma-1}{2} (0.44903)^2 \cos^2 \beta_{10} \right]^{\frac{1}{2}}}$$

The program can be used for different values of γ , k_{B1} , U_2/a_0 and R_{10}/R_2 .

It can be adapted also to integrations with more than five equal increments between R_{1i}/R_2 and R_{10}/R_2 . In this case the increment $\Delta(R_1/R_2)$ must be entered in addresses 75 to 103 (octal).

Enclosures: Operating Instruction (1 page)

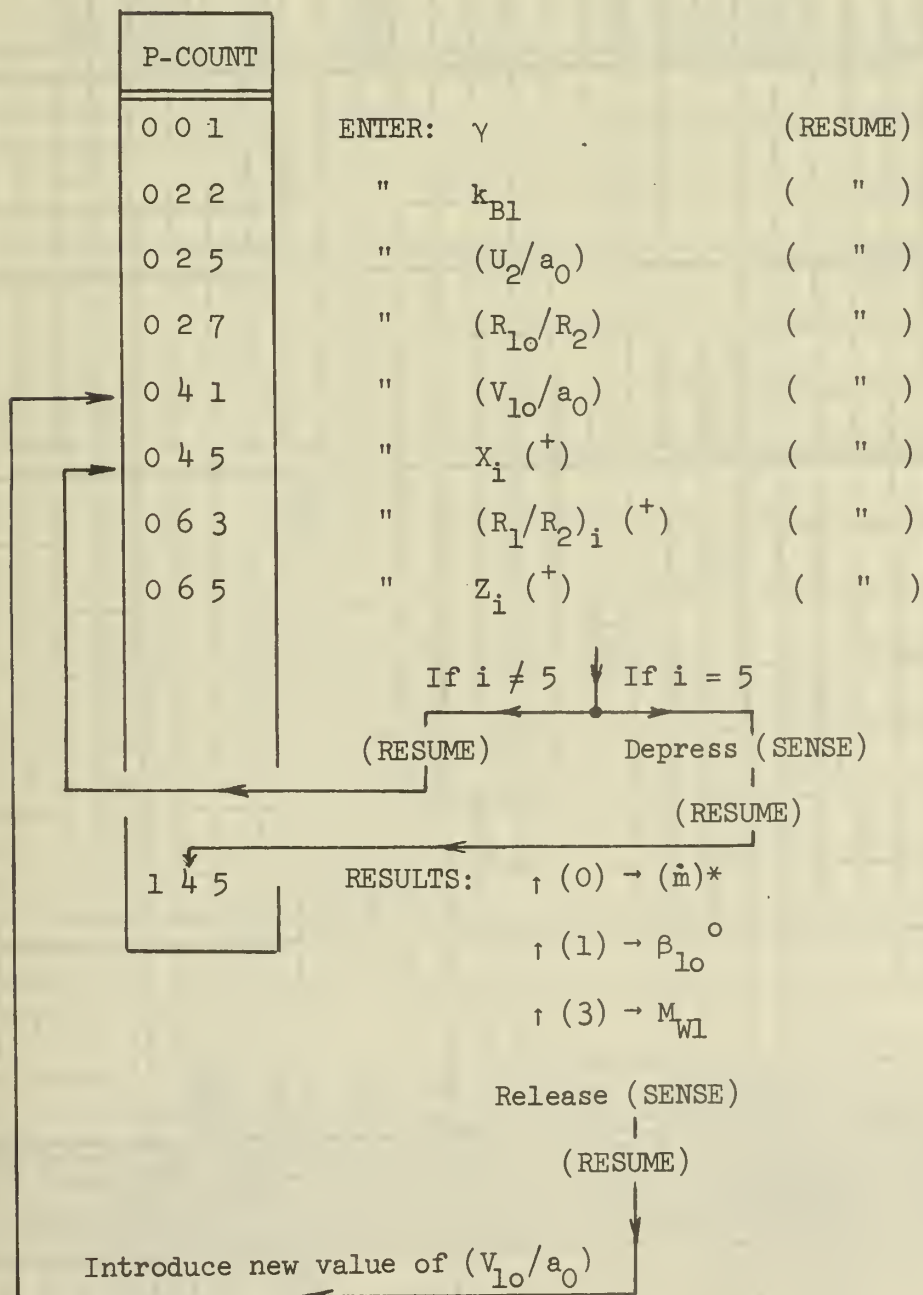
Program Listing (4 pages)

OPERATING INSTRUCTIONS PROGRAM No. 108

MONROE CALCULATOR 1655/6 WITH CARD READER CR-1

Set-Up: (RESET); (TO(0)); Depress (LOAD); Read Cards 1-4;

Release (LOAD); (TO(0)); Depress (P); (RESUME)



(⁺) Enter val. with equal indices i of Table on p. 1 of Program
 Descripti sequentially for $i = 0, 1, 2, 3, 4, 5$.

BR PT	ADDRESS P COUNT	COMMAND	CODE	REGISTERS																NOTES
				E	A	M	0	1	2	3	4	5	6	7	8	9	X	Y	Z	
0	0	0	0	Y																ENTER: γ
	1	STR(1)	4 4 0	Y				γ												
	2	-	0 6 2																	
	3	1	0 0 1																	
	4	\div	0 7 2	$\gamma-1$																
	5	STR(2)	4 4 1						$\gamma-1$											
	6	2	0 0 2																	
	0 7	=	0 2 0	$\gamma-1$																
	1 0	STR(5)	4 4 4									$\frac{\gamma-1}{2}$								
	1	RCL(2)	4 6 1	$\gamma-1$																
	2	INV	0 5 4	$\frac{1}{\gamma-1}$																
	3	STR(4)	4 4 3								$\frac{1}{\gamma-1}$									
	4	RCL(1)	4 6 0	γ																
	5	$\sqrt{\quad}$	0 5 6	$\sqrt{\gamma}$																
	6	x	0 7 0																	
	1 7	2	0 0 2																	
	2 0	x	0 7 0	$2\sqrt{\gamma}$																
	2 1	HALT	4 0 1	k																ENTER: $k_{B1} = k$
	2	=	0 2 0	$2k\sqrt{\gamma}$																
	3	STR(6)	4 4 5											$2k\sqrt{\gamma}$						
	2 4	HALT	4 0 1	U_2/a_0																ENTER: U_2/a_0
	5	x	0 7 0																	
	2 6	HALT	4 0 1	R_{10}/R_2																ENTER: R_{10}/R_2
	2 7	=	0 2 0	b																$b = (U_2/a_0)/(R_{10}/R_2)$
	3 0	STR(2)	4 4 1						b											
	1	0	0 0 0																	
	2	0	0 0 0																	
	3	0	0 0 0																	
	4	0	0 0 0																	
	5	0	0 0 0																	
	6	0	0 0 0																	
	3 7	STR(0)	4 5 7				0	γ	b		$\frac{1}{\gamma-1}$	$\frac{\gamma-1}{2}$	$2k\sqrt{\gamma}$							Clears (0)

BR PT	ADDRESS P COUNT	COMMAND	CODE	REGISTERS													NOTES			
				E	A	M	0	1	2	3	4	5	6	7	8	9		X	Y	Z
2	0 4 0	HALT	4 0 1	v			0	y	b											ENTER: $(V_{10}/a_0) = v$
	4 2	RCL(1)	4 6 0	v				v												
	3	x	0 7 0																	
	4 4	HALT	4 0 1	X_i																ENTER: $(X_i); i=0 \rightarrow 5, 1$
	5	x	0 7 0	vX_i																
	6	STR(3)	4 4 2																	
	4 7	x	0 7 0	$(vX_i)^2$																
	5 0	RCL(5)	4 6 4	$\frac{y-1}{2}$																
	1	=	0 2 0	c_i																$c_i = \frac{y-1}{2} (vX_i)^2$
	2	CHSGN	0 1 3	$-c_i$																
	3	+	0 6 0																	
	4	1	0 0 1																	
	5	Q^x	0 7 4	$1-c_i$																
	6	RCL(4)	4 6 3	$\frac{1}{y-1}$																
	5 7	x	0 7 0	g_i																$g_i = (1 - c_i)^{1/(r-1)}$
	6 0	RCL(3)	4 6 2	vX_i																
	1	x	0 7 0																	
	6 2	HALT	4 0 1	$(R_i/R_2)_i$																ENTER: $(R_i/R_2)_i; i=0 \rightarrow 5, 1$
	3	\div	0 7 2	N_i																
	6 4	HALT	4 0 1	z_i																
	5	+	0 6 0	N_i/z_i																
	6	RCL(0)	4 7 7	\bullet																$\bullet \sum (N_i/z_i)$
	6 7	=	0 2 0	\odot																$\odot \sum (N_i/z_i)$
	7 0	STR(0)	4 5 7	\odot																
	1	SFSNS	5 2 3																	
	2	SKFI	5 4 0																	
	3	JUMP 42	6 4 2																	
	4	x	0 7 0	$\sum (N_i/z_i)$																
	7 5	.	0 1 2																	
	7 6	0	0 0 0																	
	7 7	5	0 0 5																	$\Delta R/R_2 = .050800$

BR ADDRESS PTIP COUNT	COMMAND	CODE	REGISTERS										NOTES					
			E	A	M	0	1	2	3	4	5	6	7	8	9	X	Y	Z
6 1 4 0	x	0 7 0				$(\dot{m})^*$	β_{10}°	b	$\sin \beta_{10}$	$\frac{1}{Y-1}$	$\frac{Y-1}{2}$	$2k\sqrt{8}$						
1 1 4 1	RCL(2)	4 6 1	b															
2 1 4 2	=	0 2 0	M_{W1}															
3 1 4 3	STR(3)	4 4 2							M_{W1}									
1 1 4 4	HALT	4 0 1				$(\dot{m})^*$	β_{10}°		M_{W1}									RESULTS
5 1 4 5	0	0 0 0																Clears (0)
6 1 4 6	STR(0)	4 5 7																To repeat with new Value γ_{10}/Q_0
1 1 4 7	TO(2)	7 4 2																
0 1 4 0																		
1 1 4 1																		
2 1 4 2																		
3 1 4 3																		
4 1 4 4																		
5 1 4 5																		
6 1 4 6																		
7 1 4 7																		
0 1 4 0																		
1 1 4 1																		
2 1 4 2																		
3 1 4 3																		
4 1 4 4																		
5 1 4 5																		
6 1 4 6																		
7 1 4 7																		
0 1 4 0			E	A	M	0	1	2	3	4	5	6	7	8	9	X	Y	Z

MONROE CALCULATOR 1655 WITH CARD READER CR-1

Description

This program calculates the flow conditions after an axial row of blades for known entrance conditions. Figure D(109)1 shows such a cascade located between station (e) and station (d). It is assumed that the conditions at the mean radii R_{me} and R_{md} , at entrance and discharge, respectively, are representative of the average flow properties ahead of and after the cascade. The effective flow area at station (e) is taken as

$$A_e k_{Be} = 2\pi R_{me} h_e k_{Be}$$

where k_{Be} is a blockage factor that takes account of the boundary layers at the inner and outer wall contours. Similarly, at discharge station (d)

$$A_d k_{Bd} = 2\pi R_{md} h_d k_{Bd}$$

Figure D(109)2 shows a diffuser cascade of a subsonic axial compressor where the flow angle is reduced from α_e to α_d . Figure D(109)4 shows a stator of a turbine blading where the subsonic velocity V_e ahead of the row is accelerated to a supersonic velocity V_d because of the converging-diverging area change of the flow channel. Figures D(109)3 and 5 represent the flow processes in the bladings of Fig. D(109)2 and 4, respectively in entropy diagrams, by assuming that the processes are adiabatic and that the fluids have constant specific heat ratios γ . In general, from the equation of continuity

$$A_e k_{Be} \rho_e V_e \cos \alpha_e = A_d k_{Bd} \rho_d V_d \cos \alpha_d$$

With ρ_e and ρ_d from

$$\rho = p / g R_G T$$

and the Mach numbers M_e and M_d from

$$M = V / \sqrt{g \gamma R_G T}$$

there is

$$M_d = \frac{A_e k_{Be}}{A_d k_{Bd}} \frac{\cos \alpha_e}{\cos \alpha_d} \frac{p_e}{\sqrt{T_e}} M_e \frac{\sqrt{T_d}}{p_d}$$

To obtain dimensionless relations the static pressure p and the static temperatures T will be taken as multiples of the constants P_0 and T_0 , respectively. Then

$$M_d = K \frac{\sqrt{T_d/T_0}}{(p_d/P_0)} \quad D109(1)$$

where

$$K = \frac{A_e k_{Be} \cos \alpha_e}{A_d k_{Bd} \cos \alpha_d} M_e \frac{p_e/P_0}{\sqrt{T_e/T_0}} \quad D109(2)$$

The dimensionless quantity K is known from the cascade geometry and the inlet conditions. It is assumed that the ratios P_{te}/P_0 , T_{te}/T_0 and the Mach number M_e are known, where P_{te} and T_{te} are the total pressure and the total temperature at station (e). Then, from

$$T_{te} = T_e \left[1 + \frac{\gamma-1}{2} M_e^2 \right]$$

and

$$P_{te} = p_e \left[1 + \frac{\gamma-1}{2} M_e^2 \right]^{\gamma/(\gamma-1)}$$

there are

$$\frac{T_e}{T_0} = \frac{T_{t2}/T_0}{1 + \frac{\gamma-1}{2} M_e^2} \quad D109(3)$$

and

$$\frac{p_e}{P_0} = \frac{P_{te}/P_0}{\left[1 + \frac{\gamma-1}{2} M_e^2\right]^{\gamma/(\gamma-1)}} \quad D109(4)$$

These quantities establish the value of K of Eq. 2, if the flow areas, the blockage factors, and the flow angles at stations (e) and (d) are known.

Since $T_{td} = T_{te}$ for an adiabatic process, there is similar to Eq. 3

$$\frac{T_d}{T_0} = \frac{T_{te}/T_0}{1 + \frac{\gamma-1}{2} M_d^2} \quad D109(5)$$

The losses in the row of the blade are expressed by the total pressure loss coefficient Y_t defined by

$$Y_t = \frac{P_{te} - P_{td}}{P_{te} - p_e} \quad D109(6)$$

Hence

$$\frac{P_{td}}{P_0} = \frac{P_{te}}{P_0} - Y_t \left(\frac{P_{te}}{P_0} - \frac{p_e}{P_0} \right) \quad D109(7)$$

and, similar to Eq. 4,

$$\frac{p_d}{P_0} = \frac{P_{td}/P_0}{\left[1 + \frac{\gamma-1}{2} M_d^2\right]^{\gamma/(\gamma-1)}} \quad D109(8)$$

Because of the above exponential expression it is not possible to obtain a closed solution for M_d by substituting Eqs. 5 and 8 into Eq. 1. It is necessary to choose a particular value $M_d = M_d^*$, which is used to determine

T_d/T_0 and p_d/P_0 by Eqs. 5 and 8. These values are introduced into Eq. 1., and M_d^* must be iterated until the result of Eq. 1 equals M_d^* . For given flow conditions at station (e) there always occur two solutions, one for which M_d is subsonic, the other for which M_d is supersonic.

All input data are dimensionless with the exception of the cross-sectional areas A_e and A_d . The dimensions of these areas are arbitrary but the units for A_e and A_d must be equal. As seen from the operating instructions, the calculated ratios p_e/P_0 and T_e/T_0 must be read before the iteration for M_d . If the condition $M_d = M_d^*$ has been satisfied, the final results are obtained by depressing the (SENSE) switch.

The velocity V_d after the cascade is

$$V_d = M_d a_0 \sqrt{\frac{T_d}{T_0}}$$

where a_0 is the velocity of sound corresponding to T_0 . The velocity V_d is obtained with the keyboard operation

$$\uparrow (8) \sqrt{x} \uparrow (0) x (\text{Value of } a_0) =$$

at P-Count 173.

Enclosures: Figure D(109)

Operating Instruction (1 page)

Program Listing (4 pages)

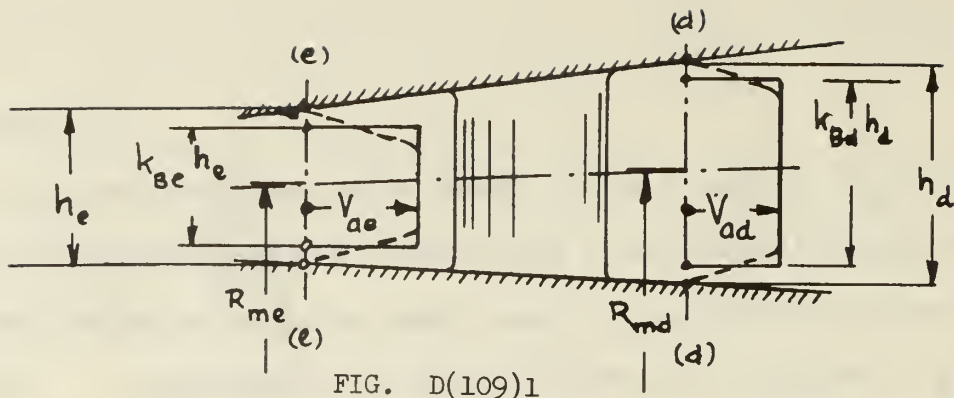


FIG. D(109)1

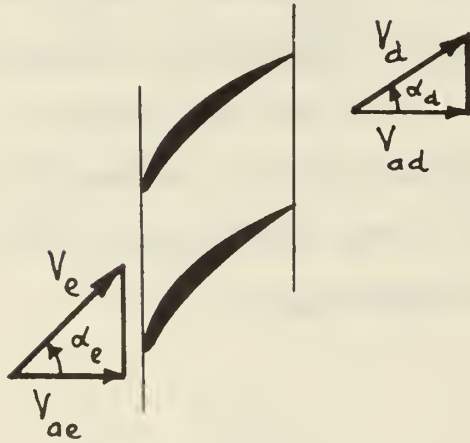


FIG. D(109)2

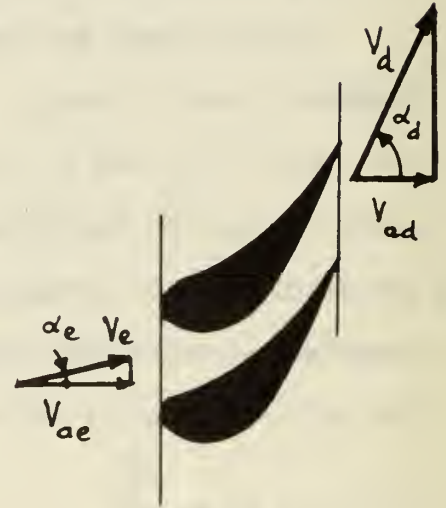


FIG. D(109)4

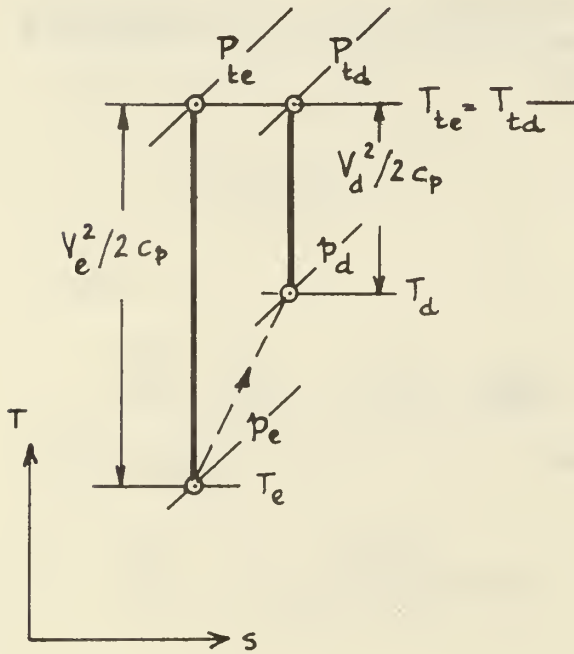


FIG. D(109)3

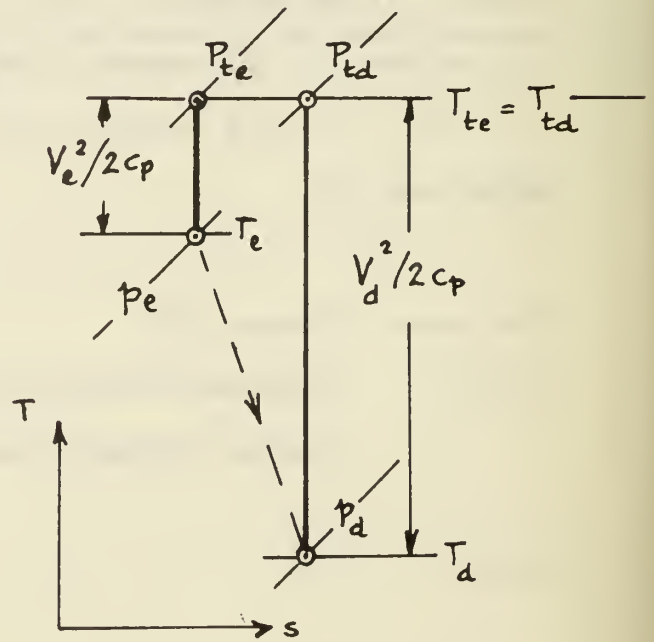


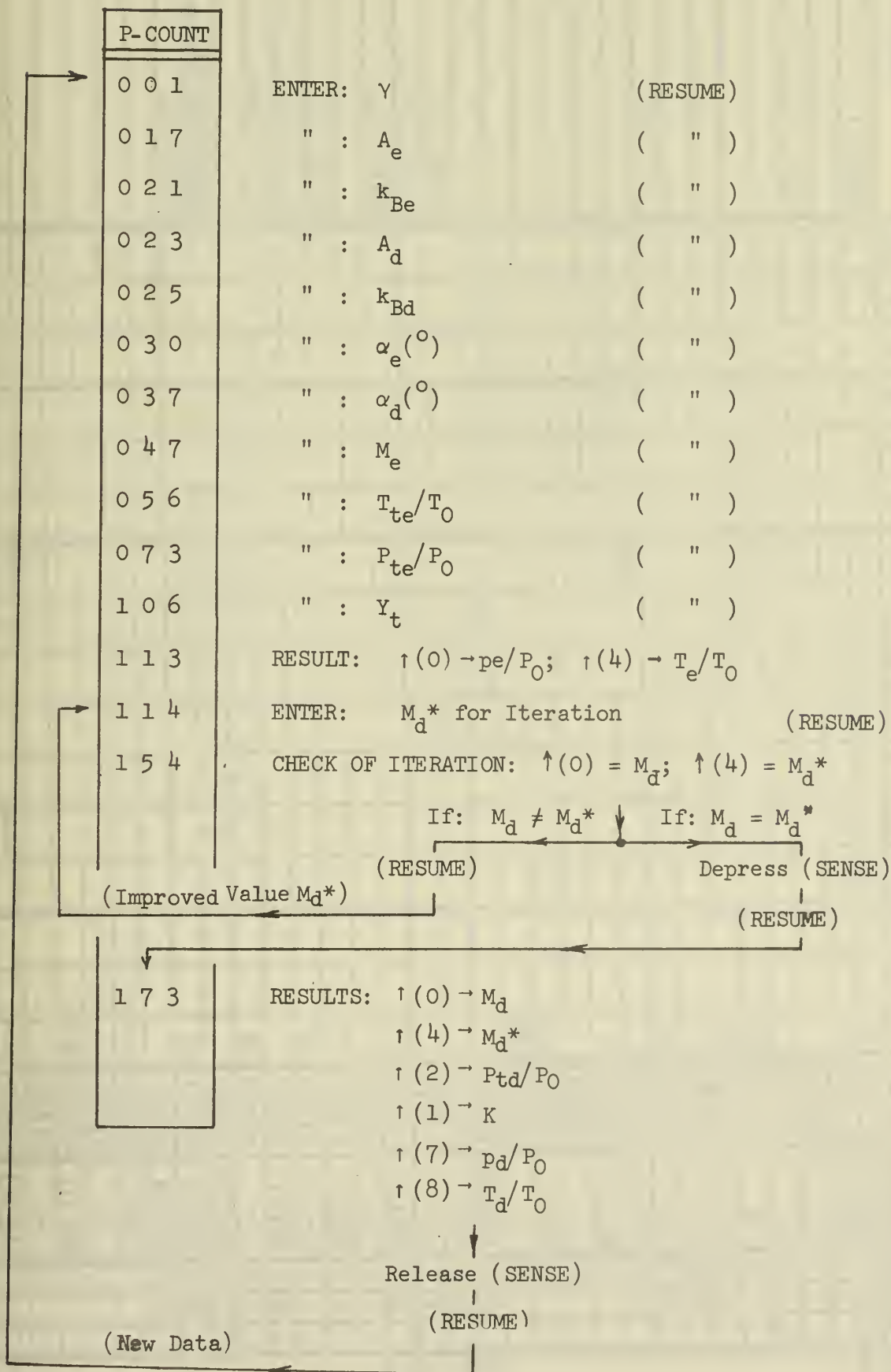
FIG. D(109)5

FIG. D(109) FLOW THROUGH CASCADE

MONROE CALCULATOR 1655 WITH CARD READER CR-1

Set-Up: (RESET); (TO(0)); Depress (LOAD); Read Cards 1-4

Release (LOAD); (TO(0)); Depress (P); (RESUME)



BR PT	ADDRESS COUNT	COMMAND	CODE	REGISTERS																NOTES
				E	A	M	0	1	2	3	4	5	6	7	8	9	X	Y	Z	
0	0	0	0	Y																ENTER: Y
	1	STR(1)	4 4 0					Y												
	2	-	0 6 2																	
	3	1	0 0 1																	
	4	÷	0 7 2	Y-1																
	5	STR(2)	4 4 1	Y-1					Y-1											
	6	2	0 0 2																	
	7	=	0 2 0	$\frac{Y-1}{2}$																
	10	STR(6)	4 4 5											$\frac{Y-1}{2}$						
	11	RCL(1)	4 6 0	Y																
	2	÷	0 7 2																	
	3	RCL(2)	4 6 1	Y-1																
	4	=	0 2 0	$\frac{Y}{Y-1}$																
	15	STR(5)	4 4 4																	
	16	HALT	4 0 1																	ENTER: A _e
	17	X	0 7 0																	ENTER: k _{be}
1	20	HALT	4 0 1																	ENTER: A _d
	1	÷	0 7 2																	ENTER: k _{BD}
2	2	HALT	4 0 1																	
3	3	÷	0 7 2																	
2	4	HALT	4 0 1																	
5	5	=	0 2 0	B																
6	6	STR(1)	4 4 0					B												$B = (A_e k_{be}) / (A_d k_{BD})$
2	7	HALT	4 0 1	α _e																ENTER: α _e
3	0	SIN/cos	0 4 0																	
1	1	2.FUNCT	0 3 6	cos α _e																
2	2	X	0 7 0																	
3	3	RCL(1)	4 6 0	B																
4	4	=	0 2 0																	
5	5	STR(1)	4 4 0					B cos α _e												
6	6	HALT	4 0 1	α _d																ENTER: α _d
3	3	3	3																	

BR PT	ADDRESS P COUNT	COMMAND	CODE	REGISTERS													NOTES			
				E	A	M	0	1	2	3	4	5	6	7	8	9		X	Y	Z
2	4	2.FUNCT	0 3 6																	
	1	÷	0 7 2																	
	2	RCL(1)	4 6 0																	
	3	=	0 2 0																	
	4	INV	0 5 4																	
	5	X	0 7 0																	
	4	HALT	4 0 1																	
	4	STR(2)	4 4 1																	
	5	=	0 2 0																	
	1	STR(1)	4 4 0																	
	2	RCL(2)	4 6 1																	
	3	TO(6)	7 4 6																	
	4	X	0 7 0																	
	5	HALT	4 0 1																	
	6	STR(3)	4 4 2																	
	5	=	0 2 0																	
	6	STR(4)	4 4 3																	
	1	√	0 5 6																	
	2	INV	0 5 4																	
	3	X	0 7 0																	
	4	RCL(1)	4 6 0																	
	5	=	0 2 0																	
	6	STR(1)	4 4 0																	
	6	RCL(2)	4 6 1																	
	7	TO(7)	7 4 7																	
	1	X	0 7 0																	
	7	HALT	4 0 1																	
	3	STR(2)	4 4 1																	
	4	X	0 7 0																	
	5	STR(0)	4 5 7																	
	6	RCL(1)	4 6 0																	
	7	=	0 2 0																	

245

3

ENTER: M_e

$C = \frac{A_e \cdot h_{BC} \cdot \cos \alpha_e}{A_d \cdot k_{BD} \cdot \cos \alpha_d} M_e$

ENTER: T_{te}/T_0

$C' = C / \sqrt{T_{te}/T_0}$

ENTER: P_{te}/P_0

BR PT	ADDRESS COUNT	COMMAND	CODE	REGISTERS																NOTES
				E	A	M	0	1	2	3	4	5	6	7	8	9	X	Y	Z	
4	1	0	0	1	0	0	0	1	1	1	1	1	1	1	1	1	1	1	1	
	1	0	1	1	0	0	0	0	0	0	0	0	0	0	0	0	0	0	0	
	2		2	0	0	0	0	0	0	0	0	0	0	0	0	0	0	0	0	
	3	RCL(2)	4	6	1															
	4	X	0	7	0															
	1	0	5	HALT	4	0	1													ENTER: Y_c
	6	+	0	6	0															
	1	0	7	RCL(2)	4	6	1													
	1	1	0	=	0	2	0													
	1	STR(2)	4	4	1															
	1	1	2	HALT	4	0	1													RESULTS: $N(0) \rightarrow P_c/P_0; \dot{q}(4) \rightarrow Y_{T0}$
	1	1	3	HALT	4	0	1													ENTER: M_d^* for Iteration
	1	1	4	STR(4)	4	4	3													
	5	To(7)	7	4	7															
	6	X	0	7	0															
	1	1	7	RCL(2)	4	6	1													
	5	=	0	2	0															
	1	STR(7)	4	4	6															
	2	INV	0	5	4															
	3	X	0	7	0															
	4	RCL(1)	4	6	0															
	5	=	0	2	0															
	6	STR(0)	4	5	7															
	1	2	7	RCL(4)	4	6	3													
	1	3	0	To(6)	7	4	6													
	1	1	1	X	0	7	0													
	2	RCL(3)	4	6	2															
	3	=	0	2	0															
	4	STR(8)	4	4	7															
	5	V	0	5	6															
	6	X	0	7	0															
	1	3	7	JUMP	50	6	5	0												

Description

The curve of Fig. D(110) has the characteristics that its curvature k at the point P_0 is zero and that k increases gradually with increasing angle θ . To be found is that curve which has the angle $\delta_m = \pi/2$ between the tangents of the curve at P_0 and P_m such that particular distances x_0/a and y_0/a are obtained. For

$$r/a = \theta^{-b} \quad 110(1)$$

there is *

$$\tan \Psi = -\frac{\theta}{b} \quad 110(2)$$

For $0 < b < 1$ there is $\pi/2 < \Psi < \pi$ and since

$$\mathcal{V} = \Psi - \pi/2$$

one obtains

$$\cot \mathcal{V} = -\tan(\Psi - \pi/2) = \theta/b \quad 110(3)$$

and

$$\sin \mathcal{V} = \sqrt{\frac{1}{1 + (\theta/b)^2}} \quad 110(4)$$

where

$$0 < \mathcal{V} < \pi/2$$

The curvature k at $P(r/a, \theta)$ is

$$k = \frac{1 - b(1-b)/\theta^2}{a\theta^{-b} [1 + (b/\theta)^2]^{3/2}} \quad 110(5)$$

*Vavra, M. H., "Aerothermodynamics and Flow in Turbomachines," pp. 293/298, John Wiley & Sons, New York, 1960.

At $P_0 (r_0/a, \theta_0)$ the curvature k_0 is zero, hence, by Eq. 5

$$\theta_0 = \sqrt{b(1-b)} \quad 110(6)$$

From Eq. 1

$$\frac{r_0}{a} = \theta_0^{-b} = [b(1-b)]^{-\frac{b}{2}} \quad 110(7)$$

and from Eq. 4

$$\vartheta_0 = \sin^{-1} \sqrt{\frac{1}{1 + (\theta_0/b)^2}} \quad 110(8)$$

From Fig. D(110) for $P(r/a, \theta)$

$$\delta = (\theta + \vartheta) - (\theta_0 + \vartheta_0) = E - E_0$$

and for $P_m \left(\frac{r_m}{a}, \theta_m \right)$, where $\delta_m = \pi/2$,

$$\delta_m = \frac{\pi}{2} = (\theta_m + \vartheta_m) - (\theta_0 + \vartheta_0) = E_m - E_0 \quad 110(9)$$

where, according to Eq. 4

$$\vartheta_m = \sin^{-1} \sqrt{\frac{1}{1 + (\theta_m/b)^2}} \quad 110(10)$$

From Fig. D(110) the coordinates x_0/a and y_0/a are

$$\frac{x_0}{a} = \frac{r_0}{a} \cos \vartheta_0 - \frac{r_m}{a} \sin \vartheta_m \quad 110(11)$$

$$\frac{y_0}{a} = \frac{r_0}{a} \sin \vartheta_0 + \frac{r_m}{a} \cos \vartheta_m \quad 110(12)$$

From Eq. 3

$$\frac{b}{\theta} = \tan \vartheta$$

Hence

$$1 + (b/\theta)^2 = 1 + \tan^2 \psi = \frac{1}{\cos^2 \psi}$$

Introduced into Eq. 5, with Eqs. 1 and 6,

$$a k = \frac{1 - (\theta_o/\theta)^2}{r/a} \cos^3 \psi \quad 110(13)$$

Hence at P_m the curvature k_m is obtained from

$$a k_m = \frac{1 - (\theta_o/\theta_m)^2}{r_m/a} \cos^3 \psi_m \quad 110(14)$$

It is not possible to calculate the parameters of a curve with $\delta_m = \pi/2$ that has a given ratio y_o/x_o with a closed solution. It is necessary to choose a value of b which establishes θ_o , r_o/a and ψ_o . Then the angle θ_m must be varied until $\delta_m = 90^\circ$ by Eq. 9. With θ_m , the quantities r_m/a and ψ_m are obtained from Eqs. 1 and 10. Then the coordinates x_o/a and y_o/a of Eqs. 11 and 12 establish the ratio y_o/x_o . If this ratio differs from that of the desired curve the quantity b must be varied until agreement is reached

From Eqs. 11 and 14 it is possible also to express the curvature k_m as a multiple of $1/x_o$ or

$$k_m x_o = (a k_m) (x_o/a) \quad 110(15)$$

Enclosures: Figure D(110)

Operating Instruction (1 page)

Program Listing (4 pages)

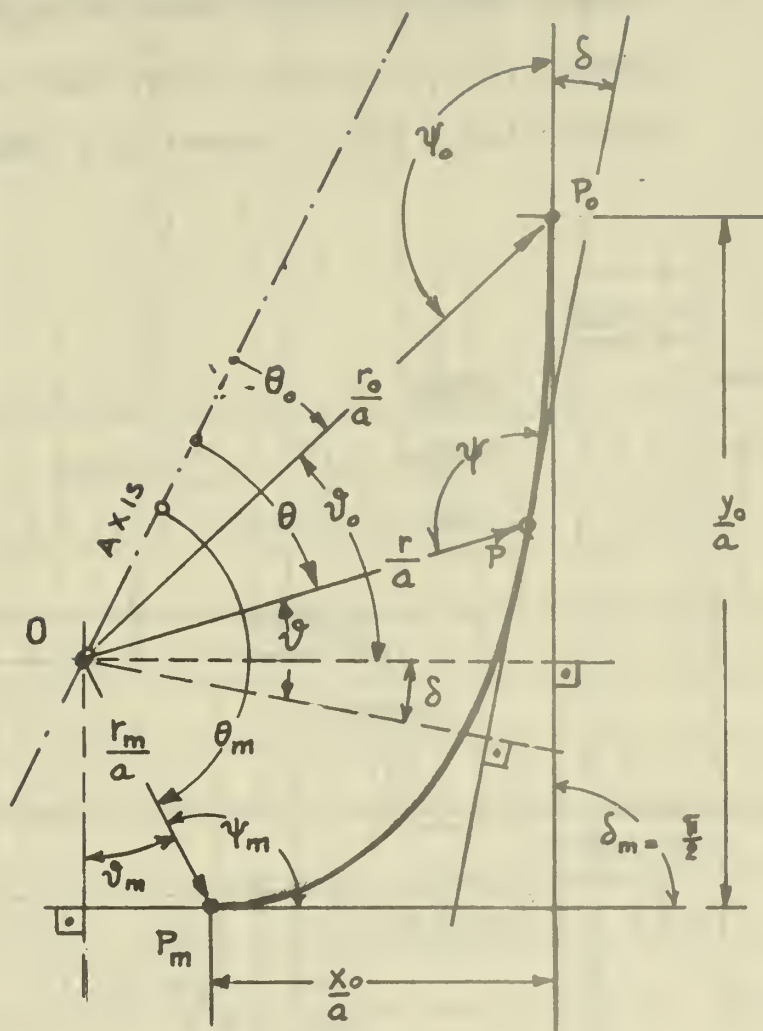


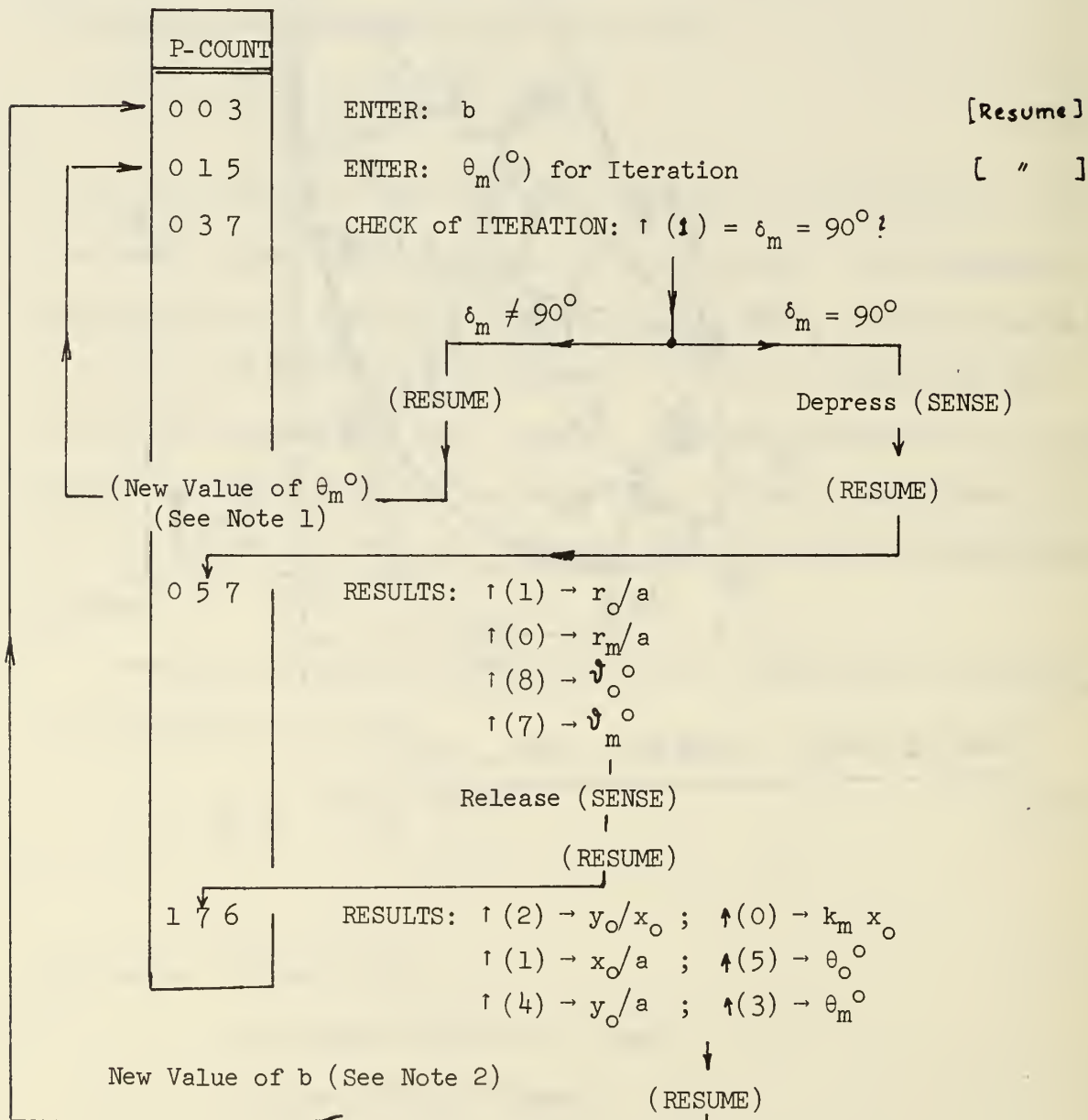
FIG. D(110) CURVE $r/a = \theta^{-b}$

OPERATING INSTRUCTIONS PROGRAM No. 110

MONROE CALCULATOR 1655/6 WITH CARD READER CR-1

Set-Up: (RESET); (TO(0)); Depress (LOAD); Read Cards 1-4

Release (LOAD); TO(0)); Depress (P); (RESUME)



Note 1: $\delta_m < 90^{\circ} \rightarrow$ Increase θ_m ; $\delta_m > 90^{\circ} \rightarrow$ Decrease θ_m

Note 2: To increase $y_0/x_0 \rightarrow$ Increase b

To decrease $y_0/x_0 \rightarrow$ Decrease b

BR PT	ADDRESS P COUNT	COMMAND	CODE	REGISTERS													NOTES			
				E	A	M	0	1	2	3	4	5	6	7	8	9		X	Y	Z
0	000	1	001	1																
		-	062																	
	02	HALT	401	b																ENTER: b
	3	STR(6)	445												b					
	4	X	070	1-b																
	5	RCL(6)	465	b																
	6	=	020	b(1-b)																
	07	V	056	θ_0^R																
	10	STR(5)	444	θ_0^R										θ_0^R						
	1	TO(7)	747	$\sin \theta_0^R$																
	2	\sin^2/\cos^2	042	\hat{v}_0^R										\hat{v}_0^R						
	3	STR(4)	443																	
	14	HALT	401	θ_m^0																ENTER: $\theta_m^0 (0 \leq \theta_m \leq 180^\circ)$
	5	\sin/\cos	040																	
	6	2FUNCT	036	$\cos \theta_m^0$																
	17	\sin^2/\cos^2	042																	
1	20	2FUNCT	036	θ_m^R																
	1	STR(3)	442	θ_m^R									θ_m^R							
	2	TO(7)	747	$\sin \theta_m^R$																
	3	\sin^2/\cos^2	042	\hat{v}_m^R																
	4	STR(2)	441	\hat{v}_m^R									\hat{v}_m^R							
	5	+	060																	
	6	RCL(3)	462	θ_m^R																
	27	-	062																	
	30	RCL(5)	464	θ_0^R																
	1	-	062																	
	2	RCL(4)	463	\hat{v}_0^R																
	3	=	020	δ_m^R																
	4	$R \rightarrow$	046	δ_m^0																$\delta_m = \hat{v}_m + \theta_m - (\theta_0 + \theta_0)$
	5	STR(1)	440																	CHECK: $\delta_m = 90^\circ$? If true: [SENSE]
	36	HALT	401																	
	37	SFSNS	523																	

BR PT	ADDRESS P COUNT	COMMAND	CODE	REGISTERS																NOTES																																																																																																																																																																																																																																																																																																																																																																																																																																																																																																																																																																																																																																																																																																																																																																																																																																																																																																																																																																																																																																																																																																																																																																																																																																																																																																																																																																							
				E	A	M	0	1	2	3	4	5	6	7	8	9	X	Y	Z																																																																																																																																																																																																																																																																																																																																																																																																																																																																																																																																																																																																																																																																																																																																																																																																																																																																																																																																																																																																																																																																																																																																																																																																																																																																																																																																																																								
2	0	4	0	SKFI	5	4	0																																																																																																																																																																																																																																																																																																																																																																																																																																																																																																																																																																																																																																																																																																																																																																																																																																																																																																																																																																																																																																																																																																																																																																																																																																																																																																																																																																																				</

BR PT	ADDRESS P COUNT	COMMAND	CODE	REGISTERS													NOTES																																																																																																																																																																																																																																																																																																																																																																																																																																																																																																																																																																																																																																																																																																																																																																																																																																																																																																																																																																																																																																																																																																																																																																																																																																																																																																																																																													
				E	A	M	0	1	2	3	4	5	6	7	8	9		X	Y	Z																																																																																																																																																																																																																																																																																																																																																																																																																																																																																																																																																																																																																																																																																																																																																																																																																																																																																																																																																																																																																																																																																																																																																																																																																																																																																																																																																										
4	1	0	0	RCL(1)	4	6	0																																																																																																																																																																																																																																																																																																																																																																																																																																																																																																																																																																																																																																																																																																																																																																																																																																																																																																																																																																																																																																																																																																																																																																																																																																																																																																																																																																							

$$Y = (1 - (\theta_s / \theta_m)^2) / (r_m / a)$$

BR PT	ADDRESS P COUNT	COMMAND	CODE	REGISTERS																NOTES
				E	A	M	0	1	2	3	4	5	6	7	8	9	X	Y	Z	
6	140	d^x	074	θ																
	1	RCL(6)	465	b										b						SUBROUTINE: $r/a = \theta^{-b}$
	2	=	020	θ^b																
	3	INV	054	θ^{-b}																
	4	RCLP	557	r/a																
	145	RCL(1)	460	x_0/a				x_0/a	θ_m^R	θ_m^R	y_0/a	θ_0^R	b							
	6	=	020	$x_0 k_m$																
	147	STR(0)	457				$x_0 k_m$													
	150	RCL(4)	463	y_0/a																
	1	\div	072																	
	2	RCL(1)	460	x_0/a																
	3	=	020	y_0/x_0																
	4	STR(2)	441					y_0/x_0												
	5	RCL(5)	464	θ_0^R																
	6	$R \rightarrow$	046	θ_0°																
	157	JUMP 71	671																	
7	160	\div	072	θ										b						
	1	RCL(6)	465	b																
	2	x	070	θ/b																
	3	+	060	$(\theta/b)^2$																
	4	1	001																	
	5	=	020	$(1+(\theta/b)^2)^3$																
	6	$\sqrt{\quad}$	056																	
	167	INV	054	$\sin \theta$																
	170	RCLP	557																	
	171	STR(5)	444	θ_0°				$x_0 k_m$	y_0/x_0	θ_m^R	y_0/a	θ_0°	b							
	2	RCL(3)	462	θ_m^R																
	3	$R \rightarrow$	046	θ_m°																
	4	STR(3)	442						θ_m°											
	175	HALT	401					$x_0 k_m$	y_0/x_0	θ_m°	y_0/a	θ_0°	b							RESULTS: $\frac{y_0}{x_0} = \frac{y_0}{a} \cdot \frac{x_0}{a} \cdot \frac{x_0 k_m}{a} \cdot \theta_0^\circ \cdot \theta_m^\circ$
	6	TO(0)	740																	
	7																			

Description

Program 517 calculates the conditions after the diffuser, the honeycomb flow straightener, and the discharge duct of the Hybrid compressor. Details of these calculations are given in Section III.3 of "Hybrid Compressor Design Report." The compressor is supposed to operate as an exhaustor such that the static pressure (p_6) at the compressor discharge is 14.7 psia. The total temperature at the impeller inlet (T_0) is taken to be 520°R. Basic data to be used in the program are the conditions after the rotor obtained by the method described in Section III.2 of "Hybrid Compressor Design Report."

Both diffuser rows are considered as a unit and it is assumed that the flow angle α_4 after the second diffuser blade row is constant, equal to 21°. The program contains program 109, described in Appendix D, which by an iterative procedure establishes the Mach number $M_{V4} = M_4$ of the flow after the diffuser with losses that are a multiple of its design pressure loss coefficient.

After calculating the diffuser performance program 517 determines the overall compressor performance in accordance with Section III.4. Examples of print-outs are given in Tables XI and XII of the aforementioned report.

Enclosures: Operating Instructions (1 page)

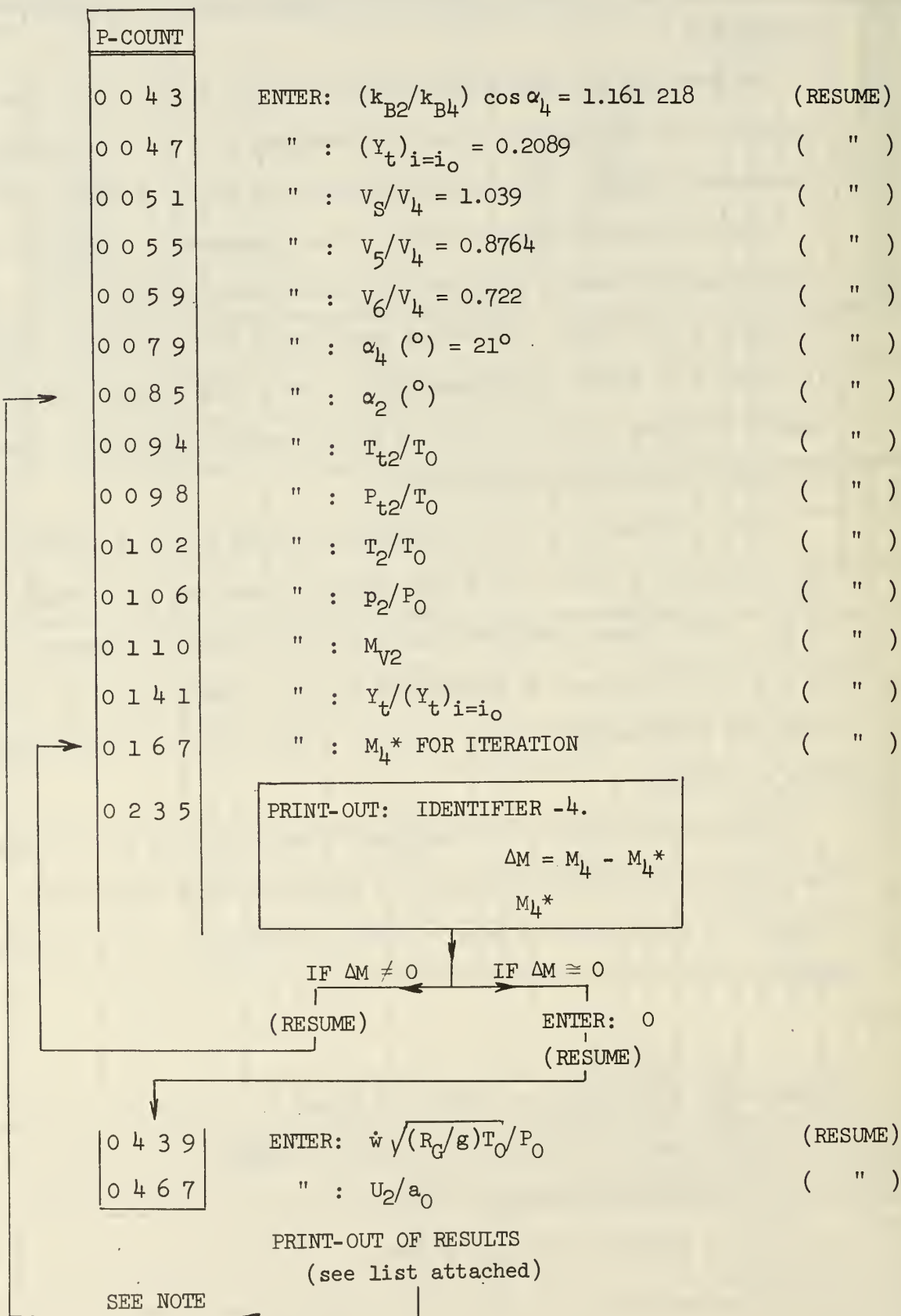
List of Print-Out of Results (1 page) .

Program Listing (12 pages)

Main Data Storage (1 page)

MONROE CALCULATOR 1880-22

Set-Up: Read 2 Magnetic Cards starting at Branch Point 00



NOTE: After "Print-out of Results" the program automatically returns to P-Count 0085 for new data.

PROGRAM 517

MONROE CALCULATOR 1880-22

LIST OF PRINT-OUT OF RESULTS:

.

$$U_2/a_0$$

$$\alpha_2 \quad (^\circ)$$

$$P_{t4}/P_0$$

$$p_4/P_0$$

$$T_4/T_0$$

$$M_{V4} = M_4$$

$$V_4/a_0$$

$$P_{t4}'/P_0$$

$$p_4'/P_0$$

$$P_{t4}''/P_0$$

$$p_4''/P_0$$

$$P_{t5}/P_0$$

$$P_{t6}/P_0$$

$$p_6/P_0$$

$$P_0 \quad (\text{psia})$$

$$\dot{w} \quad (\text{lbm/s})$$

$$\text{HP} \quad (\text{HP})$$

$$N \quad (\text{rpm})$$

$$\eta_T \quad (-)$$

.

STEP	SOURCE	SYMBOL	COMMAND	COMMENTS	ENTER	STORE	PRINT
0	Q	0	2				
		1	9				
		2	.				
		3	3				
		4	6				
		5	4				
		6	0				
		7	7				
		8	7	$E = \sqrt{(R_0/q) T_0}$			
		9	↓ () ()				
0	Q	0	2				
		1	0	x		E → 20	
		2	1				
		3	7				
		4	6				
		5	.				
		6	5				
		7	4	$F = R_0 (r/(r-1)) T_0 / 550$			
		8	↓ () ()				
		9	2				
0	2	0	1	x		F → 21	
		1	2				
		2	3				
		3	2				
		4	9				
		5	0				
		6	.				
		7	2				
		8	1				
		9	↓ () ()	$G = a_0 720 / (\pi D_L)$			
0	3	0	2				
		1	2			G → 22	
		2	/				
		3	/				
		4	/				
		5	/	NO OP.			
		6	/				
		7	/				
		8	/				
		9	/				
0	4	0	SET D.P.				
		1	4				
		2	HALT	ENTER: $C = \frac{k_{B2}}{k_{B1}} \cos \alpha_1 = 1.16 \pm 2.18$	C		
		3	↓ () ()				
		4	0				
		5	0			C → 00	
		6	HALT	ENTER: $(Y_t)_i = i_0 = 0.2089 = Y_{t0}$	Y_{t0}		
		7	↓ () ()				
		8	0				
		9	1			$Y_{t0} \rightarrow 01$	

STEP	SYMBOL	COMMAND	COMMENTS	ENTER	STORE	PRINT
05	0	HALT	ENTER: $V_5/V_4 = 1.039$	V_5/V_4		
	1	$\downarrow () ()$				
	2	0				
	3	2			$V_5/V_4 \rightarrow 02$	
	4	HALT	ENTER: $V_5/V_4 = 0.8764$	V_5/V_4		
	5	$\downarrow () ()$			$V_5/V_4 \rightarrow 03$	
	6	0				
	7	3				
	8	HALT	ENTER: $V_6/V_4 = 0.722$	V_6/V_4		
	9	$\downarrow () ()$				
06	0	0				
	1	4			$V_6/V_4 \rightarrow 04$	
	2	.				
	3	4	$x-1$			
	4	\div				
	5	1				
	6	.				
	7	4	x			
	8	=	$(x-1)/x$			
	9	$\downarrow () ()$				
07	0	0				
	1	5			$x-1 \rightarrow 05$	
	2	3				
	3	.				
	4	5	$x/(x-1)$			
	5	$\downarrow () ()$				
	6	0			$x/(x-1) \rightarrow 06$	
	7	6				
	8	HALT	ENTER: $\alpha_4 = 21$	α_4		
	9	$\downarrow () ()$				
08	0	0				
	1	7			$\alpha_4 \rightarrow 07$	
	2	+	IND/SYMB \uparrow SYMBOL. ADDRESS +			
	3	+	\downarrow			
	4	HALT	ENTER: α_2	α_2		
	5	$\downarrow () ()$				
	6	2				
	7	9			$\alpha_2 \rightarrow 29$	
	8	SIN/COS				
	9	2NDFUNC	$\cos \alpha_2$			
09	0	$\downarrow () ()$				
	1	1			$\cos \alpha_2 \rightarrow 10$	
	2	0				
	3	HALT	ENTER: T_{t2}/T_0	T_{t2}/T_0		
	4	$\downarrow () ()$				
	5	1				
	6	1			$T_{t2}/T_0 \rightarrow 11$	
	7	HALT	ENTER: P_{t2}/P_0	P_{t2}/P_0		
	8	$\downarrow () ()$				
	9	1				

STEP	SYMBOL	COMMAND	COMMENTS	ENTER	STORE	PRINT
1 0 0		2			$P_2/P_0 \rightarrow 12$	
1		HALT	ENTER: T_2/T_0	T_2/T_0		
2		$\downarrow()()$				
3		1				
4		3			$T_2/T_0 \rightarrow 13$	
5		HALT	ENTER: P_2/P_0	P_2/P_0		
6		$\downarrow()()$				
7		1				
8		4			$P_2/P_0 \rightarrow 14$	
9		HALT	ENTER: $M_{V2} = M_2$	M_{V2}		
1 1 0		$\downarrow()()$				
1		1				
2		5			$M_2 \rightarrow 15$	
3		$\uparrow()()$				
4		1				
5		3	T_2/T_0			
6		$\sqrt{\quad}$	$\sqrt{T_2/T_0}$			
7		$1/x$	$1/\sqrt{T_2/T_0}$			
8		x				
9		$\uparrow()()$				
1 2 0		1				
1		5	M_2			
2		x				
3		$\uparrow()()$				
4		1				
5		4	P_2/P_0			
6		x				
7		$\uparrow()()$				
8		1				
9		0	$\cos \alpha_2$			
1 3 0		x				
1		$\uparrow()()$				
2		0				
3		0	C			
4		=	K			
5		$\downarrow()()$				
6		0				
7		8			$K \rightarrow 08$	
8		/	\uparrow NO OP			
9		/				
1 4 0		HALT	ENTER: Y_t / Y_{t0}	Y_t / Y_{t0}		
1		x				
2		$\uparrow()()$				
3		0				
4		1	Y_{t0}			
5		CHSGN	$-Y_{t0}$			
6		x				
7		(
8		$\uparrow()()$				
9		1				

STEP	SYMBOL	COMMAND	COMMENTS	ENTER	STORE	PRINT
1 5 0		2	P_{t2}/P_0			
1		-				
2		$\uparrow()()$				
3		1				
4		4	P_2/P_0			
5)				
6		+				
7		$\uparrow()()$				
8		1				
9		2	P_{t2}/P_0			
1 6 0		=	P_{t4}/P_0			
1		$\downarrow()()$				
2		3				
3		0			$P_{t4}/P_0 \rightarrow 40$	
4	X	IND/SYMB	1 SYMBOL. ADDRESS X			
5		X				
6		HALT	ENTER: M_4^* FOR ITERATION OF M_4	M_4^*		
7		$\downarrow()()$				
8		1				
9		6			$M_4^* \rightarrow 16$	
1 7 0		X				
1		X	M_4^{*2}			
2		.				
3		2	$(\gamma-1)/2$			
4		+				
5		1				
6		a^x	$1 + \frac{\gamma-1}{2} M_4^{*2} = A1$			
7		$\downarrow()()$				
8		1				
9		7			$A1 \rightarrow 17$	
1 8 0		$\uparrow()()$				
1		0				
2		6	$k/(\gamma-1) = 3.5$			
3		=	$(1 + \frac{\gamma-1}{2} M_4^{*2})^{3.5} =$			
4		$1/x$				
5		X				
6		$\uparrow()()$				
7		1				
8		0	P_{t4}/P_0			
9		=	P_4/P_0			
1 9 0		$\downarrow()()$				
1		1				
2		1			$P_4/P_0 \rightarrow 31$	
3		$\uparrow()()$				
4		1				
5		1	T_{t2}/T_0			
6		\div				
7		$\uparrow()()$				
8		1				
9		7	A1			

STEP	SYMBOL	COMMAND	COMMENTS	ENTER	STORE	PRINT
2 0	0	=	T_4/T_0			
	1	$\downarrow () ()$				
	2	3				
	3	2			$T_4/T_0 \rightarrow 22$	
	4	$\sqrt{\quad}$	$\sqrt{T_4/T_0}$			
	5	\div				
	6	$\uparrow () ()$				
	7	3				
	8	1	p_4/P_0			
	9	x				
2 1	0	$\uparrow () ()$				
	1	0				
	2	8	K			
	3	=	M_4			
	4	$\downarrow () ()$				
	5	3				
	6	3			$M_4 \rightarrow 33$	
	7	-				
	8	$\uparrow () ()$				
	9	1				
2 2	0	6	M_4^*			
	1	=	$\Delta M = M_4 - M_4^*$			
	2	$\downarrow ()$				
	3	0			$\Delta M \rightarrow 0$	
	4	4	\uparrow PRINT IDENTIFIER - 4.			
	5	CHSGN	\downarrow			
	6	EC 177				-4.
	7	$\uparrow ()$				
	8	0	ΔM			
	9	PRINT A				ΔM
2 3	0	$\uparrow () ()$				
	1	1				
	2	6	M_4^*			
	3	PRINT A				M_4^*
	4	HALT	IF $\Delta M \leq 0$; ENTER: 0			
	5	JUMP	\uparrow			
	6	=	GO TO S.A. \div IF $\Delta M = 0$			
	7	IND/SYMB	\downarrow			
	8	\div				
	9	JUMP	\uparrow GO TO S.A. X IF $\Delta M \neq 0$ FOR			
2 4	0	IND/SYMB	BETTER APPROXIMATION OF M_4			
	1	x	\downarrow			
	2	\div	\uparrow SYMBOL. ADDRESS \div			
	3	\div	\downarrow			
	4	$\uparrow () ()$				
	5	3				
	6	2	T_4/T_0			
	7	$\sqrt{\quad}$	$\sqrt{T_4/T_0}$			
	8	x				
	9	$\uparrow () ()$				

STEP	SYMBOL	COMMAND	COMMENTS	ENTER	STORE	PRINT
2 5 0		3				
1		3	M_4			
2		x	V_4/a_0			
3		$\downarrow()$				
4		3				
5		4			$V_4/a_0 \rightarrow 34$	
6		(
7		$\uparrow()$				
8		0				
9		7	α_4			
2 6 0		SIN/COS				
1)	$\sin \alpha_4$			
2		x	$(V_4/a_0) \sin \alpha_4$			
3		x	$[(V_4/a_0) \sin \alpha_4]^2$			
4		.				
5		2	$(x-1)/2$			
6		+				
7		$\uparrow()$				
8		3				
9		2	T_4/T_0			
2 7 0		=	T_4^*/T_0			
1		$1/x$	T_0/T_4^*			
2		x				
3		$\uparrow()$				
4		1				
5		1	T_{t2}/T_0			
6		a^x	$(T_{t2}/T_0)(T_0/T_4^*)$			
7		$\uparrow()$				
8		0				
9		6	$x/(x-1) = 3.5$			
2 8 0		x				
1		$\uparrow()$				
2		3				
3		1	P_4/P_0			
4		=	P_{t4}^*/P_0			
5		$\downarrow()$				
6		3				
7		5			$\frac{P_{t4}^*}{P_0} \rightarrow 35$	
8		$\uparrow()$				
9		3				
2 9 0		4	V_4/a_0			
1		x				
2		$\uparrow()$				
3		0				
4		2	$V_5/V_4 = 1.039$			
5		x	V_5/a_0			
6		x	$(V_5/a_0)^2$			
7		.				
8		2	$(x-1)/2 = .2$			
9		CHSGN	$-.2$			

STEP	SYMBOL	COMMAND	COMMENTS	ENTER	STORE	PRINT
3 0 0		+				
1		$\uparrow()()$				
2		1				
3		1	T_{t2}/T_0			
4		\div	T_{t4}'/T_0			
5		$\uparrow()()$				
6		1				
7		1	T_{t2}/T_0			
8		a^*				
9		$\uparrow()()$				
3 1 0		0				
1		6	$\gamma/(\gamma-1) = 3.5$			
2		x				
3		$\uparrow()()$				
4		3				
5		5	P_{t4}'/P_0			
6		x	P_{t4}'/P_0			
7		$\downarrow()()$				
8		3				
9		6			$P_{t4}' \rightarrow 36$	
3 2 0		/	NO OP		P_0	
1		.				
2		3				
3		+	$.3 (P_{t4}'/P_0)$			
4		(
5		.				
6		7				
7		x				
8		$\uparrow()()$				
9		3				
3 3 0		5	P_{t4}'/P_0			
1)	$.7 (P_{t4}'/P_0)$			
2		\div	P_{t4}''/P_0			
3		$\downarrow()()$				
4		3				
5		7			$P_{t4}'' \rightarrow 37$	
6		$\uparrow()()$			P_0	
7		3				
8		5	P_{t4}'/P_0			
9		x				
3 4 0		$\uparrow()()$				
1		3				
2		6	P_{t4}'/P_0			
3		=	P_{t4}''/P_0			
4		$\downarrow()()$				
5		3				
6		8			$P_{t4}'' \rightarrow 38$	
7		$\uparrow()()$			P_0	
8		3				
9		4	V_4/Q_0			

STEP	SYMBOL	COMMAND	COMMENTS	ENTER	STORE	PRINT
350		X				
1		f()()				
2		0				
3		3	$V_5/V_4 = 0.8764$			
4		X	V_5/a_0			
5		X	$(V_5/a_0)^2$			
6		.				
7		2	$(\gamma-1)/2$			
8		CHSGN	- .2			
9		+				
360		f()()				
1		1				
2		1	T_{t2}/T_0			
3		=	T_5/T_0			
4		1/x	T_0/T_5			
5		X				
6		f()()				
7		1				
8		1	T_{t2}/T_0			
9		a ^x	T_{t2}/T_5			
370		f()()				
1		0				
2		6	$b/(\gamma-1) = 3.5$			
3		X				
4		f()()				
5		3				
6		8	p_4''/P_0			
7		X	P_{t5}/P_0			
8		↓()()				
9		3				
380		9			$P_{t5} \rightarrow 39$	
1		.			P_0	
2		6	0.6			
3		+	$0.6 (P_{t5}/P_0)$			
4		(
5		f()()				
6		3				
7		8	p_4''/P_0			
8		X				
9		.				
390		4				
1)				
2		=	P_{t6}/P_0			
3		↓()()				
4		4				
5		0			$P_{t6} \rightarrow 40$	
6		f()()			P_0	
7		3				
8		4	V_4/a_0			
9		X				

STEP	SYMBOL	COMMAND	COMMENTS	ENTER	STORE	PRINT
4 0	0	↑() ()				
	1	0				
	2	4	$V_6/V_4 = .722$			
	3	x	V_6/q_0			
	4	x	$(V_6/q_0)^2$			
	5	.				
	6	2	$(k-1)/2 = .2$			
	7	CHSGN	- .2			
	8	+				
	9	↑() ()				
4 1	0	1				
	1	1	T_{t2}/T_0			
	2	÷	T_6/T_0			
	3	↑() ()				
	4	1				
	5	1	T_{t2}/T_0			
	6	a ^x	T_6/T_{t2}			
	7	↑() ()				
	8	0				
	9	6	$\gamma/(\gamma-1) = 3.5$			
4 2	0	x				
	1	↑() ()				
	2	4				
	3	0	P_{t6}/P_0			
	4	=	P_6/P_0			
	5	↓() ()				
	6	4				
	7	1				$\frac{P_6}{P_0} \rightarrow 41$
	8	1/x	P_0/P_6			
	9	x				
4 3	0	1				
	1	4	$P_{ATM} = 14.7 \text{ psia}$			
	2	.				
	3	7				
	4	=	$P_0 \text{ (psia)}$			
	5	↓() ()				
	6	4				
	7	2				$P_0 \rightarrow 42$
	8	HALT	ENTER: $X = \dot{w} \sqrt{(R/g) T_0} / P_0$	X		
	9	x				
4 4	0	↑() ()				
	1	4				
	2	2	P_0			
	3	÷				
	4	↑() ()				
	5	2				
	6	0	E			
	7	x	$\dot{w} \text{ (lbm/s)}$			
	8	↓() ()				
	9	4				

STEP	SYMBOL	COMMAND	COMMENTS	ENTER	STORE	PRINT
4 5	0	3			$\dot{W} \rightarrow 43$	
	1	(
	2	$\uparrow()()$				
	3	1				
	4	1	T_{t2}/T_0			
	5	-				
	6	1				
	7)	$(T_{t2}/T_0) - 1$			
	8	x				
	9	$\uparrow()()$				
4 6	0	2				
	1	1	F			
	2	=	HP			
	3	$\downarrow()()$				
	4	4				
	5	4			HP $\rightarrow 44$	
	6	HALT	ENTER: U_2/a_0	U_2/a_0		
	7	$\downarrow()()$				
	8	2				
	9	8			$U_1 \rightarrow 28$	
4 7	0	x			a_0	
	1	$\uparrow()()$				
	2	2				
	3	2	G			
	4	=	N (rpm			
	5	$\downarrow()()$				
	6	4				
	7	5			N $\rightarrow 45$	
	8	$\uparrow()()$				
	9	3				
4 8	0	0	P_{t4}/P_0			
	1	a^x				
	2	$\uparrow()()$				
	3	0				
	4	5	$(\gamma-1)/\gamma = .4/1.4$			
	5	-	$(P_{t4}/P_0)^{\gamma-1/\gamma}$			
	6	1	$r-1$			
	7	\div	$(P_{t4}/P_{t0})^{\frac{r-1}{\gamma}} - 1$			
	8	(
	9	$\uparrow()()$				
4 9	0	1				
	1	1	T_{t2}/T_0			
	2	-				
	3	1				
	4)	$(T_{t2}/T_0) - 1$			
	5	=	η_T			
	6	$\downarrow()()$				
	7	4				
	8	6			$\eta_T \rightarrow 46$	
	9	EC 176	PRINT LINE OF DOTS		

STEP	SYMBOL	COMMAND	COMMENTS	ENTER	STORE	PRINT
500		2	↑			
1		8	SET-UP POINTER 28 (FIRST REG.			
2		↓ ()	TO BE PRINTED & STR. 49			
3		.				
4		↓ () ()				
5		4				
6		9	↓			
7	PRINT A	IND/SYMB	↑ SYMBOL. ADDRESS "PRINT A"			
8		PRINT A	↓			
9		↑ () ()	↑ RCL ACC. TO POINTER			
510		IND/SYMB	↓			
1		PRINT A				DATA
2		SET D.P	↑ SET DEC. POINT TO 4			
3		4	↓			
4		1	↑			
5		↑ () ()	ADD 1 TO POINTER, STR 49			
6		+	AND SET UP NEW POINTER			
7		4				
8		9				
9		↓ () ()				
520		4				
1		9				
2		↓ ()				
3		.				
4		-				
5		4				
6		5				
7		=	NEW POINTER - 45			
8		BRANCH	↑ IF NEW POINTER = 45, I.E. IF N			
9		=	IS TO BE PRINTED SET DP TO ZERO			
530		IND/SYMB	WITH S.R. Φ			
1		Φ	↓			
2		↑ () ()				
3		4				
4		9	NEW POINTER			
5		-				
6		4				
7		7				
8		=	NEW POINTER - 47			
9		JUMP	↑			
540		=	GO TO S.A. \checkmark IF NEW POINTER			
1		IND/SYMB	= 47, OR DO NOT PRINT			
2		\checkmark	↓			
3		JUMP	↑ GO TO S.A. "PRINT A" IF NEW			
4		IND/SYMB	POINTER ≤ 46			
5		PRINT A	↓			
6	\checkmark	IND/SYMB	↑ SYMBOL. ADDRESS \checkmark			
7		\checkmark	↓			
8	EC	176	PRINT LINE OF DOTS		
9		JUMP	↑			

STEP	SYMBOL	COMMAND	COMMENTS	ENTER	STORE	PRINT
550		IND/SYMB	JUMP TO S.A. ADD. + TO			
1		+	PROCESS NEW DATO			
2	Φ	IND/SYMB	SUBROUTINE Φ SETS D.POINT TO 0			
3		Φ	FOR PRINTING OF N			
4		SET D.P				
5		0				
6		RESUME	V			
7						
8						
9						
560						
1						
2						
3						
4						
5						
6						
7						
8						
9						
0						
1						
2						
3						
4						
5						
6						
7						
8						
9						
0						
1						
2						
3						
4						
5						
6						
7						
8						
9						
0						
1						
2						
3						
4						
5						
6						
7						
8						
9						

REGISTER	CONTENTS 1	CONTENTS 2	CONTENTS 3
0 0	$C = (k_{B2}/k_{B4})/\cos 21^\circ = 1.16$	2 18	
1	$\gamma_{t0} = .2089$		
2	$V_5/V_4 = 1.039$		
3	$V_5/V_4 = .8764$		
4	$V_6/V_4 = .722$		
5	$(\gamma-1)/\gamma = .4/1.4$		
6	$\gamma/(\gamma-1) = 1.4/.4 = 3.5$		
7	$\alpha_4 = 21^\circ$		
8	K		
9			
1 0	$\cos \alpha_2$		
1	T_{t2}/T_0		
2	P_{t2}/P_0		
3	T_2/T_0		
4	p_2/P_0		
5	$M_{y2} = M_2$		
6	M_4^*		
7	$A1 = 1 + [(\gamma-1)/2] M_4^{*2}$		
8			
9			
2 0	$E = 29.364 077$		
1	$F = 176.54$		
2	$G = 23290.21$		
3			
4			
5			
6			
7			
8	U_2/a_0	PRINT-OUT OF INPUT	
9	α_2		
3 0	P_{t4}/P_0		
1	p_4/P_0		
2	T_4/T_0		
3	M_4	LINE UP	
4	V_4/a_0	OF CALCULATED DATA	
5	P_{t4}'/P_0	FOR PRINTING.	
6	p_4'/P_0		
7	P_{t4}''/P_0		
8	p_4''/P_0		
9	P_{t5}/P_0		
4 0	P_{t6}/P_0		
1	p_6/P_0		
2	P_0 (psia)		
3	\dot{w} (lbm/s)		
4	HP		
5	N (rpm)		
6	γ_T		
7			
8			
9	POINTER		

DISTRIBUTION LIST

	<u>No. of Copies</u>
1. Defense Documentation Center Cameron Station Alexandria, Virginia 22314	12
2. Library Code 0212 Naval Postgraduate School Monterey, California 93940	2
3. Superintendent Naval Postgraduate School Monterey, California 93940	1
4. Provost Code 02 Naval Postgraduate School Monterey, California 93940	1
5. Dean of Research Code 023 Naval Postgraduate School Monterey, California 93940	1
6. Chairman Department of Aeronautics Code 57 Naval Postgraduate School Monterey, California 93940	1
7. Turbo-Propulsion Laboratory Department of Aeronautics Naval Postgraduate School Monterey, California 93940	5
8. Commanding Officer Naval Air Systems Command Navy Department Washington, D. C. 20360	1
9. Asst. Commander for Research & Technology Naval Air Systems Command Navy Department Washington, D. C. 20360	1

10. Dr. Frank Tanczos 1
Code 03
Naval Air Systems Command
Navy Department
Washington, D. C. 20360
11. Mr. I. Silver 1
Code 03B
Naval Air Systems Command
Navy Department
Washington, D. C. 20360
12. Dr. Edward S. Lamar 1
Chief Scientist, AIR-03C
Naval Air Systems Command
Navy Department
Washington, D. C. 20360
13. Dr. H. J. Mueller 1
Research Administrator
Code 310A
Naval Air Systems Command
Navy Department
Washington, D. C. 20360
14. Mr. E. A. Lichtman 1
Naval Air Systems Command
Code 330
Navy Department
Washington, D. C. 20360
15. Mr. Karl H. Guttman 2
Code 330C
Naval Air Systems Command
Navy Department
Washington, D. C. 20360
16. Rear Admiral C. O. Holmquist, USN 1
Chief of Naval Research
Office of Naval Research
Arlington, Virginia 22218
17. Commanding Officer 6
Naval Air Propulsion Test Center
Attn: Mr. E. Stawski
Trenton, New Jersey 08628
18. Mr. Eric Lister 1
R & T Division
Naval Air Propulsion Test Center
Trenton, New Jersey 08628

19. Mr. Elmer G. Johnson 1
Director, Fluid Dynamics Facilities
Research Laboratories (ARL)
Wright-Patterson AFB, Ohio 45433
20. Mr. R. A. Langworthy 1
Army Aviation Materiel Laboratories
Department of the Army
Fort Eustis, Virginia 23604
21. National Aeronautics and Space Administration 1
Lewis Research Center (Library)
2100 Brookpark Road
Cleveland, Ohio 44135
22. Prof Dr. Ing. Karl Bammert 1
Institut fuer Stroemungsmaschinen
Technische Hochschule Hannover
3 Hannover, Germany
23. Prof M. Berchtold 1
Institut fuer Thermodynamik
Eidg. Technische Hochschule
Sonneggstr. 3
8006 Zurich
Switzerland
24. Dr. V. Beglinger 1
Manager of Development
Brown Boveri-Sulzer Turbomachinery Ltd
Ch-8023 Zurich
Switzerland
25. Library 1
AiResearch Mfg. Corporation
Division of Garrett Corporation
402 South 36th Street
Phoenix, Arizona 85034
26. CAG Library 1
The Boeing Company
Seattle, Washington 98124
27. Prof Jacques Chauvin 1
von Karman Institute
Chaussee de Waterloo 72
1640 Rhode-Saint-Genese
Belgium
28. Mr. Jean Fabri 1
ONERA
29, Ave. de al Division Leclerc
92 Chatillon
Franch

29. Dr. Robert Goulard 1
Director, Project SQUID
Jet Propulsion Center
Purdue University
Lafayette, Indiana 47907
30. Dr. Robert E. Henderson 1
Director of Research
Detroit Diesel Allison Division
General Motors
P. O. Box 894
Indianapolis, Indiana 46206
31. Dr. B. Lakshminarayana 1
Professor of Aerospace Engineering
The Pennsylvania State University
233 Hammond Building
University Park, Pennsylvania 16802
32. Library 1
General Electric Company
Aircraft Engine Technology Division
DTO Mail Drop H43
Cincinnati, Ohio 45215
33. Library 1
Pratt and Whitney Aircraft
Post Office Box 2691
West Palm Beach, Florida 33402
34. Library 1
Pratt and Whitney Aircraft
East Hartford, Connecticut 06108
35. Prof Dr. Ing. H. Marcinowski 1
Institut fuer Stroemungsmaschinen
Universitaet (T. H.) Karlsruhe
Karlsruhe, Germany
36. Prof Gordon C. Oates 1
Department of Aeronautics and Astronautics
University of Washington
Seattle, Washington 98105
37. Dr. Bruce A. Reese 1
Director, Jet Propulsion Center
School of Mechanical Engineering
Purdue University
Lafayette, Indiana 47907
38. Dr. W. Schlachter 1
Brown, Boveri-Sulzer Turbomachinery Ltd
Dept. TDE
Escher Wyss Platz
CH-8023 Zurich
Switzerland

39. Prof Dr. Ing. H. Schlichting 1
Institut fuer Stroemungsmechanik
Technische Hochschule Braunschweig
Bienroder Weg 3
93 Braunschweig, Germany
40. Dr. George K. Serovy 1
Professor of Mechanical Engineering
208 Mechanical Engineering Building
Iowa State University
Ames, Iowa 50010
41. Dr. J. Surugue 1
Director, Energie et Propulsion
ONERA
29 Ave. de la Division Leclerc
92 Chatillon
France
42. Dr. W. Tabakoff 1
Professor, Department of Aerospace Engineering
University of Cincinnati
Cincinnati, Ohio 45221
43. Prof Dr. W. Traupel 1
Institut fur Thermische Turbomaschinen
Eidg, Technische Hochschule
Sonneggstr. 3
8006 Zurich
Switzerland
44. Dr. Arthur J. Wennerstrom 1
Chairman, ASME Turbomachinery Committee
ARL/LF
Wright-Patterson AFB
Dayton, Ohio 45433

REPORT DOCUMENTATION PAGE		READ INSTRUCTIONS BEFORE COMPLETING FORM
1. REPORT NUMBER NPS-57Va73071A	2. GOVT ACCESSION NO.	3. RECIPIENT'S CATALOG NUMBER
4. TITLE (and Subtitle) Design Report of Hybrid Compressor and Associated Test Rig		5. TYPE OF REPORT & PERIOD COVERED Final Report to July 1973
7. AUTHOR(s) Michael H. Vavra		6. PERFORMING ORG. REPORT NUMBER
9. PERFORMING ORGANIZATION NAME AND ADDRESS Department of Aeronautics Naval Postgraduate School Monterey, Calif 93940		8. CONTRACT OR GRANT NUMBER(s) Airtask No. A3303300/186B/3F41432301
11. CONTROLLING OFFICE NAME AND ADDRESS Naval Air Systems Command AIR 330C Washington, D. C. 20360		10. PROGRAM ELEMENT, PROJECT, TASK AREA & WORK UNIT NUMBERS N.A.
14. MONITORING AGENCY NAME & ADDRESS (if different from Controlling Office)		12. REPORT DATE July 1973
		13. NUMBER OF PAGES 279
		15. SECURITY CLASS. (of this report) Unclassified
		15a. DECLASSIFICATION/DOWNGRADING SCHEDULE
16. DISTRIBUTION STATEMENT (of this Report) Approved for public release and sale; distribution unlimited.		
17. DISTRIBUTION STATEMENT (of the abstract entered in Block 20, if different from Report)		
18. SUPPLEMENTARY NOTES		
19. KEY WORDS (Continue on reverse side if necessary and identify by block number) Hybrid compressor concept. Aerodynamic Design Design- and Off-Design Performance Losses in Radial Compressor Wheels <u>Performance of Drive Air Turbine</u>		
20. ABSTRACT (Continue on reverse side if necessary and identify by block number) This report presents the aerodynamic calculations and describes the mechanical features of a test rig that has been designed at the Turbopropulsion Laboratory, Department of Aeronautics, for research work on a special type of centrifugal compressor. This so-called Hybrid compressor consists of a centrifugal rotor with 180° flow deflection in the meridional plane followed by an axial flow diffuser. The report establishes a method to predict the off-design performance of the subject compressor, which can be applied also to conventional centrifugal compressors. Extensive use is made of modern programmable calculators, and		

Item 19 continued:

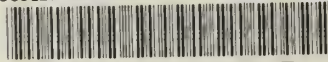
Description of Test Rig
Torque Measurement
Programs for Programmable Calculators

Item 20 continued:

programs are presented to show the effectiveness of these tools in engineering endeavors.

U158642

DUDLEY KNOX LIBRARY - RESEARCH REPORTS



5 6853 01060501 7

1115864